# Development of antisense/antigene agents based on synthetic oligonucleotides to inhibit extended-spectrum β-lactamases and restore antibiotic sensitivity in resistant bacterial pathogens

John Benedict Readman

Royal Holloway, University of London

A thesis submitted for the degree of Doctor of Philosophy

## Declaration of Authorship

I, John Benedict Readman, hereby declare that this thesis and the work presented in it is entirely my own. Where I have consulted the work of others, this is always clearly stated.

Signed:

Date:

## Abstract

Increasingly prevalent are strains of bacteria that have a reduced susceptibility to multiple antibiotics, often leaving few therapeutic treatment options for bacterial infections. Extended spectrum β-lactamases confer resistance to β-lactam antibiotics and have been observed in a wide range of bacterial species.

Synthetic antisense oligonucleotide analogues have been shown to specifically inhibit the translation of targeted bacterial genes and enable the possibility of the restoration of antibiotic sensitivity of resistant bacteria by the targeted inhibition of proteins responsible for reduced susceptibility, such as β-lactamases, thereby restoring antimicrobial efficacy.

The current study designed and developed antisense oligomers to target CTX-M-group 1 extended-spectrum β-lactamase mRNA and inhibit enzyme expression via ribosomal hindrance. Expression plasmids harbouring *bla*$_{\text{CTX-M-15}}$ cloned from field isolates were constructed for gene expression inhibition studies. Two assays for the quantification of β-lactamase activity were developed. Antisense oligomers significantly inhibited CTX-M-15 β-lactamase activity by 92 - 100% ($P < 0.001$) in a cell-free translation-transcription coupled system. An atypically permeable cell-wall mutant *E. coli* strain was transformed with expression plasmids harbouring *bla*$_{\text{CTX-M-15}}$ to yield a resistant phenotype, and in cell growth inhibition assays sensitivity to cefotaxime was significantly increased. Antisense oligomers covalently attached to a cell-penetrating peptide significantly ($P < 0.05$) increased sensitivity to cefotaxime in clinical isolates in a dose dependent manner.

A novel synthetic antisense oligomer delivery vehicle based on a 3D tetrahedral DNA structure was also developed and evaluated - a significant increase ($P < 0.001$) in the sensitivity of field and clinical isolates to cefotaxime was observed in a dose dependent manner.

The current study has demonstrated the efficacy of targeted synthetic antisense oligomers in partially restoring cefotaxime sensitivity in previously resistant clinical *E. coli* isolates, and demonstrated the efficacy of a novel vector able to deliver antisense oligomers into bacteria.

## Table of Contents

## List of Figures

## List of Tables

## Abbreviations

| | |
|---|---|
| µg | Microgram |
| µg/ml | Micrograms per millilitre |
| µM | Micromolar |
| aa | Amino acid |
| AMX | Amoxicillin |
| AMC | Amoxicillin‑Clavulanic Acid |
| AMP | Ampicillin |
| bp | Base pairs |
| BSA | Bovine serum albumin |
| C | Cytosine |
| CFU | Colony forming unit |
| CFP | Cefoperazone |
| CLA | Clavulanic Acid |
| CTX | Cefotaxime |
| CAZ | Ceftazidime |
| CRO | Ceftriaxone |
| Da | Dalton |
| DNA | Deoxyribose nucleic acid |
| dNTP | Deoxyribonucleotide triphosphate |
| E. | Escherichia |
| EDTA | Ethylenediaminetetraacetic acid |
| g | Gravity |
| FITC | Fluorescein isothiocyanate |
| G | Guanine |
| g | Gram |

| | |
|---|---|
| HPA | Health Protection Agency |
| KAN | Kanamycin |
| kb | Kilo−base |
| kDa | Kilodalton |
| kg | Kilogram |
| L | Litre |
| LB | Lysogeny broth (often referred to as Luria-Bertani) |
| LPS | Lipopolysaccharide |
| M | Molar |
| MCS | Multi cloning site |
| MeOH | Methanol |
| -mer | part (from Greek *meros*) |
| mg | Milligram |
| MHB | Meuller‑Hinton Broth |
| MIC | Minimum inhibitory concentration |
| min | Minutes |
| ml | Millilitre |
| mM | Millimolar |
| mol | Mole |
| MW | Molecular weight |
| ng | Nanogram |
| nm | Nanometre |
| nt | Nucleotide |
| O.D. | Optical density |
| PBS | Phosphate buffered saline |
| PCR | Polymerase chain reaction |
| PIP | Piperacillin |

| | |
|---|---|
| RNA | Ribonucleic acid |
| rpm | Revolutions per minute |
| SAM | Ampicillin‑Sulbactam |
| SDM | Site‑directed mutagenesis |
| SUL | Sulbactam |
| TAE | TRIS‑acetate EDTA |
| TBE | TRIS‑borate EDTA |
| TE | TRIS‑EDTA |
| TET | Tetracycline |
| TRIS | Tris (hydroxymethyl) aminomethane |
| TZB | Tazobactam |
| TZP | Piperacillin‑Tazobactam |
| UV | Ultraviolet |
| vol | Volume |
| w/v | Weight/volume |

## Acknowledgments

I would like to thank Professor George Dickson and Dr Nick Coldham for giving me the opportunity to undertake this study and for their constant and outstanding support, guidance, advice and encouragement throughout the duration of this project.

Thanks and appreciation also to the researchers at Royal Holloway and the Animal Health and Veterinary Laboratories Agency who provided me with support, expert advice and guidance when needed.

Thanks also to Charlotte Austin for support, proofreading and discussions of new ideas.

## Dedication

This work is dedicated to the memory of my father

and to my mother, whose support made this possible.

# Chapter 1. Introduction

## 1.1. Bacteria

Bacteria are among the earliest forms of life known to have evolved, with evidence having been found to support the possibility of bacteria-like prokaryotic life existing up to 3.2 - 3.4 billion years ago [1, 2]. Prokaryotes are highly diverse with an unknown number of species, and by many measurable criteria – biomass, population size, ecological diversity, age – could be considered the most successful organisms that have ever evolved. They are highly adaptable and able to rapidly evolve to survive in changing or hostile environments. One of the most important reasons for their success would appear to be this adaptability – being a single celled organism with a rapid replication time of as little as 20 minutes between generations, evolution and adaptation to a new or changing environment can occur much faster than more complex multicellular life forms.

Bacteria are ubiquitous in every known environment on earth, and can survive in the harshest of environments. They also live in, and on, other organisms, sometimes forming a symbiotic relationship for mutual benefit – bacterial cells in and on the human body outnumber host cells by up to 10:1 [3]. The majority of bacterial species inhabiting the human body are commensal, or beneficial to the host, however, those that have a negative impact on the health of the host can cause serious life threatening infections.

### 1.1.1. Bacterial infections

Pathogenic bacteria are the causes of some of the most virulent infections and conditions that afflict humans. The severity of human bacterial infections range from

minor non life-threatening infections such as, for example, a campylobacter gastrointestinal infection, to life threatening infections such as tuberculosis or anthrax.

### 1.1.2. *Escherichia coli*

*Escherichia coli* (*E. coli*) is a non-sporulating rod-shaped gram-negative bacterium whose principle environmental habitat is the bowels of endothermic organisms (humans for example) as part of their typical gut flora [4, 5]. It is an archetypal member of the family *Enterobacteriaceae*, with a diverse range of genetically variable species [6]. In most cases, *E. coli* is neutral or beneficial to its host organism, for example by the inhibition of colonisation by other, potentially pathogenic, bacteria [7]. Pathogenic *E. coli* strains however, can cause conditions from the relatively mild, such as gastroenteritis or urinary tract infections, to more severe such as haemolytic-uremic syndrome [8]. *E. coli* is a well-characterised organism; its reproduction rate of as little as 20 minutes between generations, the ability to grow in a diverse range of pressure, temperature [9] and culture media, and an abundance of non-pathogenic strains, have made it an ideal model organism for biological research.

## 1.2. Antibiotics

Antibiotics are therapeutic antimicrobial agents which are able either to kill or inhibit growth of bacteria, and are often the first line of defence against bacterial infection. Although the antibiotic era is generally regarded as having begun in the early 20$^{th}$ century with the discovery and subsequent synthesis and commercialisation of active antimicrobial compounds, there is evidence of human exposure to, or use of, antibiotics from much earlier times. Tetracycline traces, for example, have been identified in human remains dating to 350 – 500 CE from ancient Sudanese Nubia [10] and from Roman period human skeletons [11].

The sulphonamides were the first chemotherapeutic agents to be used systemically against bacterial infections. Synthesised in 1932, the drug named Prontosil, showed no in vitro activity against streptococci, but had a strong effect in streptococcus infections in mice [12]. Prontosil was later discovered to be a pro-drug which broke down to release the active compound sulphanilamide [13]. This discovery led to the later development of many sulphonamide derivatives.

Alexander Fleming is credited with the accidental discovery of penicillin in 1928 when observing the antimicrobial properties of the fungus *Penicillium rubens* [14]. Whilst earlier researchers such as Sir John Scott Burdon-Sanderson (1870) [15], Joseph Lister (1871), William Roberts (1874), Louis Pasteur (1877), Vincenzo Tiberio (1895) [16], Ernest Duchesne (1897), and Andre Gratia [17] and Sara Dath (1920s) had all previously reported antibiotic activity associated with *Penicillium* and other fungi, they were unable to isolate or describe the active antimicrobial agent. The advent of antibiotics heralded a new era in medication and were regarded, and referred to, as miracle drugs.

In the years immediately following the introduction of the first antibiotics, there was a period of rapid discovery and development of new classes of antibiotics including: the aminoglycosides discovered in 1943, tetracyclines in 1944, the chloramphenicols in 1946, macrolides in 1948, rifamycins in 1957 and quinolones in 1961 [18]. These classes of antibiotics all had different spectra of activity and mechanisms of action, some, for example, acting to inhibit cell wall synthesis and others that were ribosomal inhibitors. With this rapidly expanding range of antibiotics, bacterial infections were no longer regarded as a serious threat and research was prioritised towards the perceived greater, and more profitable, threats of such conditions as cancer, viral infections and

heart disease. The risk of resistance arising to antibiotics appeared remote, despite resistance to each new antibiotic being observed to emerge around the same time, or in some cases before, their introduction into therapeutic usage. Partly due to research priority focussed elsewhere, especially on more profitable conditions requiring long term drug administration, such as cancer, the discovery and introduction of new antibiotics slowed to a near standstill after 1986 [18]. As resistance continued to increase and evolve, previously effective antibiotics became obsolete and their use discontinued. The streptogramins (1998) and oxazolidinones (2000) were the first new classes of antibiotics approved for use since 1968 [18].

New effective antimicrobial agents have become urgently needed - since 2000 only 2 first-in-class antibiotics have been introduced; fidaxomicin and bedaquiline [19]. With a renewed sense of urgency and funding, new approaches to discovering and developing antimicrobial agents have shown promise. In 2015, Ling *et al.* developed methods to enable the culturing of soil-dwelling bacteria that were previously considered unculturable. This has directly led to the discovery and characterisation of a lipid-binding antibiotic (teixobactin) active against gram-positive bacteria [20]. An estimated 99% of soil-dwelling bacteria cannot be lab-cultured. With the new methods now available to culture these bacteria, the possibility of the discovery of many more new antibiotics now exists.

### 1.1.3. β-Lactam antibiotics

β-Lactam antibiotics are the most widespread and commonly prescribed class of antibiotics worldwide – measured by sales they represented approximately 65% of the global antibiotic market in 2003 [21]. They are a broad class of antibiotics characterised by the presence of a four-membered cyclic amide (lactam) ring (Figure 1-1).

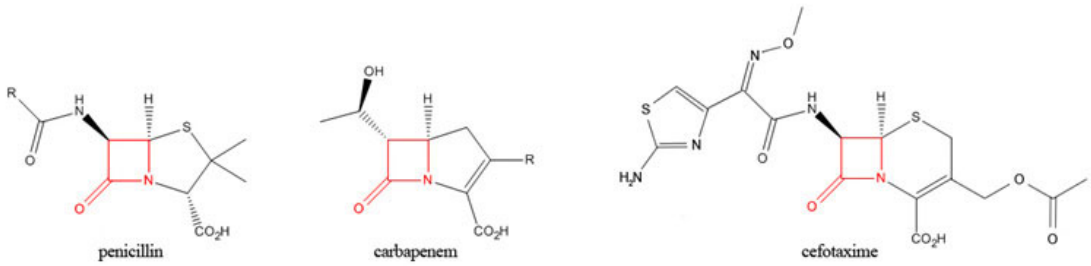


Figure 1-1. Structures of example β-lactam antibiotics.
The β-lactam ring is shown in red [22].

An essential component for bacterial structural integrity (with a few exceptions, such as members of the order of *Mycoplasmatales*, which lack a cell wall [23]) is the peptidoglycan layer. This layer consists of glycan strands cross linked by short peptides forming a rigid structural layer, either surrounding the lipid membrane in the case of gram-positive bacteria, or sandwiched between the inner and outer lipid membranes in the case of gram-negative bacteria [24]. This is an essential component without which the bacterium would be unable to withstand internal osmotic pressure. β-Lactam antibiotics inhibit transpeptidases, the enzymes responsible for catalysing the reaction that forms the bonds between peptidoglycan sugar-amino acid molecules. These enzymes are also known as penicillin binding proteins because of their high affinity for penicillin. β-Lactam antibiotics bind irreversibly to the active site in the transpeptidases, resulting in their irreversible inactivation and the inability to form the cross-links in the peptidoglycan layer [25]. Inhibition of the synthesis of this layer ultimately leads to the lysis of the bacterial cell, and its death.

The earliest β-lactam antibiotics, the penicillins, were mainly effective against gram-positive bacteria, but later generations have shown increased activity against gram-negative bacteria [26].

#### 1.1.3.1. Cephalosporins

Originally isolated from the fungus *Acremonium,* formerly known as *Cephalosporium* [27], cephalosporins are a sub-class of β-lactam antibiotics. They are grouped into chronological generations defined by their spectrums of activity, although this is a loose grouping which can vary between countries. Generally, each newer generation of cephalosporin exhibits greater activity against gram-negative bacteria. First generation cephalosporins showed activity against both gram-negative and gram-positive bacteria. Second generation cephalosporins exhibited less activity against gram-positive bacteria than first generation cephalosporins, but a greater activity against gram-negative bacteria. Members of the group of third generation cephalosporins showed decreased activity against gram-positive, but an increased broad spectrum of activity against gram-negative bacteria.

### 1.2. Bacterial antibiotic resistance

*"The first rule of antibiotics is try not to use them, and the second rule is try not to use too many of them." - Paul Marino, The ICU Book 2007 [28]*

Resistance to antibiotics is of global concern to the health of many animal species, including human. The evolution and dissemination of antibiotic resistance mechanisms in bacteria, which renders certain antibiotics ineffective, is currently proceeding at a pace that outstrips the speed of development of new antimicrobial agents. This has the potential to result in a situation where there are few treatment options for bacterial infections. Margaret Chan, director-general of the World Health Organisation, stated in 2012: "A post-antibiotic era means, in effect, an end to modern medicine as we know it. Things as common as strep throat or a child's scratched knee could once again kill" [29].

In 2014 an estimated 50,000 people died from antimicrobial resistant infections in Europe and the US, and 700,000 worldwide [30]. The Centres for Disease Control and Prevention (CDC) estimated that in 2013 at least 2 million people in the US were infected with resistant bacteria and fungi, responsible for at least 23,000 deaths [31].

In 2013 Professor Dame Sally Davies, Chief Medical Officer for England, warned of a post antibiotic era within 20 years that could lead to deaths from routine infections that are currently treated with antibiotics [32]. The journal Nature also drew attention to the major causative factors of over prescription of antibiotics to humans and to the widespread use in livestock [33]. The European Society of Clinical Microbiology and Infectious Disease (ESCMID) warned that without additional spending on drug development, more than 1 million human deaths in Europe could be attributable to drug resistant bacteria by 2025 [34]. UK Prime Minister David Cameron in 2014 further elevated the concern highlighting the "market failure" of a period of 25 years with no new classes of antibiotics being developed, and the concern regarding the overuse of antibiotics worldwide. In late 2015 the first observation of a plasmid-mediated resistance mechanism to polymixin, one of the 'drugs of last resort', was reported in *Enterobacteriaceae* in China [35]. After the observation in China, this mechanism of resistance was detected in the UK by the Animal and Plant Health Agency in bacteria found on three pig farms [36].

In addition to the global threat to health arising from antimicrobial resistance, there is inevitably an economic impact and financial burden of antimicrobial resistant bacteria – more expensive therapies are required and the duration of illnesses and hospital stays are usually increased. Difficult to assess, one review, by Smith and Coast in 2013 [37], of the available research into the economics of bacterial resistance found that the

highest estimate of the cost of bacterial resistance in the US was an annual additional $55 billion, which included additional healthcare costs and estimated costs of lost productivity [38]. In 2014 a study on the global economic effects of antimicrobial resistance estimated that the current rate of growth of resistance would lead to a reduction of world gross domestic product, resulting in a cumulative loss by 2050 of between $2.1 trillion (low rate of spread of resistance) to $124.5 trillion (worst case scenario of no effective antibiotics) [39].

A review panel to analyse the key areas of the antimicrobial resistance problem was commissioned in 2014 [40]. The implication of the appointment of an economist to chair this review could suggest the perception of the antibiotic resistance problem is more related to market forces than an understanding of the biology and complexity of evolutionary resistance mechanisms. Indeed, there is a prevalent attitude, an overconfidence that science can deal with any problem, if given enough financial incentive, and perhaps this overconfidence has led to a seeming lack of urgency in addressing this situation.

Antibiotic resistance in previously sensitive bacteria can arise through mutation, and/or through the acquisition of pre-existing resistance gene(s). Often borne on plasmids and closely associated with transposable elements, resistance genes spread rapidly in the presence of sub-lethal antibiotic concentrations [41]. The CDC estimates that up to 50% of antibiotics prescribed for people are 'not needed or are not optimally effective' and 'much of antibiotic use in animals is unnecessary and inappropriate' [31]. For example, Yezli and Li (2012) found that in China the overuse of antibiotics was widespread and endemic due, in part, to financial incentives for health care professionals to prescribe drugs [42]. One study found that greater than 98% of patients from one Chinese hospital

were prescribed antibiotics for the common cold [43]. The same study also noted that the problem of bacterial resistance was not widely recognised, with many health practitioners suggesting the cause of antibiotic ineffectiveness was due to resistance within the patient rather than the bacterium. A study of antimicrobial medicines in emerging countries, such as India, found a proportion (6%) were of substandard and sub-therapeutic quality, contributing to the spread of antimicrobial resistance [44].

A commonly criticised example of inappropriate, non-therapeutic use of antibiotics in food animals is the routine administering of antibiotics solely to promote growth. This practice originated in the 1950s when the effect of non-medicinal low dose antibiotics on growth was noted, although the cause or mechanism for this effect still remains unclear. This practice was restricted in the European Union from 2006 [45].

This situation of the exposure of bacteria to antibiotics, often in insufficient doses, is the ideal environment for resistance to evolve, develop and spread. Systems of antibiotic stewardship are regularly recommended by overseeing bodies to curtail excessive practices and slow the advance of resistance [31, 32, 46].

When antibiotics were first introduced and widely used in the 1950s, the prevailing consensus of opinion was that resistance in bacteria was unlikely to arise to such an extent to cause a significant threat to its therapeutic use, as it was believed that the required mutations would be complex, specific and unlikely to occur rapidly enough [47]. It was regarded that medical science had all but won the battle against such infections. This was obviously a premature and optimistic sentiment as the potential for the rapid acquisition and dissemination of beneficial mutations, and the mobility of genetic elements was unknown at that time [47].

The transfer of resistance genes between bacterial cells allows the rapid spread of beneficial traits between bacteria. Usually borne on plasmids, these genes can be highly mobile and rapidly deployed to negate antibiotic action.

As the current rate of development of new antimicrobials would appear to be slower than the rate of bacteria developing and spreading resistance, alternative approaches to the treatment of bacterial infections would be highly desirable [48].

### 1.2.1. Overview of bacterial antibiotic resistance mechanisms of action

Bacterial defence mechanisms against antimicrobial agents are ancient and diverse, and multiple resistance mechanisms exist for each class of antibiotic. The major commonly found and described mechanisms of action of reducing bacterial susceptibility to antibiotics are the enzymatic inactivation of the detrimental antibiotic, antibiotic target alteration, alternative metabolic pathways circumventing the ones affected by the antibiotic and a reduction of drug accumulation either through efflux or a decrease in cell permeability [49-52]. A brief summary of the most common resistance mechanisms of action follows:

#### 1.2.1.1. Enzymatic inactivation of antibiotics

A major mechanism of antibiotic susceptibility reduction amongst pathogenic bacteria is the production of an enzyme by a bacterium to inactivate an antibiotic [53]. Examples of this would include resistance to β-lactam antibiotics through the production of β-lactamases which inactivate and degrade β-lactam antibiotics by hydrolysis; β-lactamase is discussed in greater detail in section 1.2.2. A second example of enzymatic antibiotic inactivation is the transfer of chemical groups to exposed or vulnerable sites on the antibiotic, rendering it ineffective due to steric hindrance [53,

54]. Enzymes exhibiting this type of modification include aminoglycoside-modifying enzymes, which confer resistance to aminoglycoside antibiotics.

#### 1.2.1.2. Antibiotic resistance by target alteration

Bacterial resistance mediated by alteration of the target site of the antibiotic is another commonly found resistance mechanism [53]. Often as a result of spontaneous mutation(s), recombination events or the acquisition of exogenous gene(s) encoding the targets of an antibiotic, an altered enzyme can be produced with a lower affinity for the antibiotic, resulting in a phenotype of reduced susceptibility [55, 56]. One example of this is resistance to rifamycins, which interact with RNA polymerase. As these antibiotics do not bind at the RNA polymerase active site, and hence are not analogues of its substrate, it is believed that altered target-mediated resistance develops more readily [55]. Amino acid alterations in the region of RNA polymerase targeted by rifamycin antibiotics have been found in a range of different rifampicin-resistant isolates [57, 58].

#### 1.2.1.3. Reduction of intracellular antibiotic accumulation by increased efflux or decreased permeability

To reduce susceptibility to certain drugs, bacterial efflux pumps can remove antibiotics by actively transporting them out of the cell [52]. Efflux mechanisms specific to a particular drug are generally encoded by plasmids and often associated with mobile elements and other drug resistance genes, in contrast to multi-drug efflux mechanisms which are often highly conserved and mostly chromosome encoded [52]. Active efflux of antibiotics was first described as a mechanism of action of tetracycline resistance in *E. coli* in 1980 [59]. Since the initial observation of efflux-mediated tetracycline resistance many more efflux-mediated class-specific and multidrug antibiotic resistance

mechanisms have been identified [52]. Gram negative bacteria are able to reduce susceptibility to porin-mediated antibiotics with the adaptation of outer membrane pores. Changes in the number of, and/or specific function of outer membrane pores can lead to a reduction in the amount of small hydrophilic antibiotic crossing the membrane and can lead to a reduction in susceptibility to multiple antibiotics [60, 61]. Charrel *et al*. identified, from a panel of 80 β-lactam resistant clinical isolates, 23 that had an atypical porin content [62].

### 1.2.2. β-Lactamase

Resistance to β-lactam antibiotics is mainly acquired in bacteria by the production of a β-lactamase enzyme [63] which inactivates β-lactam antibiotics. The first β-lactamase to be discovered and described was penecillinase in 1940 - before penicillin had even entered into widespread medicinal use [64]. Driven by mutation and selective pressure from antibiotic exposure, bacteria have evolved and acquired new, more efficient and wider spectrum β-lactamases to match the development of β-lactam antibiotics.

Thought to be an ancient class of enzymes, first evolving around 2 billion years ago [65], β-lactamases bind to, and hydrolyse the β-lactam ring at the core of a β-lactam antibiotic. In a two-step, intermediate forming reaction, the β-lactam antibiotic is rendered unable to interact and inactivate penicillin-binding proteins [66].

β-Lactamases have been grouped and classified by different methods and two classification systems are most currently commonly used. The Ambler molecular classification system groups β-lactamases into four categories, A, B, C and D based on their amino acid sequence, and thus their evolutionary relationships. Groups A, C and D contain serine residues near their active sites, while the class B β-lactamases are the metallo β-lactamases that contain a metal ion ($Zn^{+}$) [67]. Some problems exist with this

system as new enzymes are discovered or evolve differences and have features of multiple classes, or share no features. All the serine-based β-lactamases share structural similarity suggesting either a common ancestor or convergent evolution, but little sequence identity at the molecular level [68].

Bush, Jacoby and Medeiros classified β-lactamases according to their functional characteristics [69]. Their numbered classification system grouped β-lactamases on the basis of their preferred substrates and inhibitor profiles. Group 1 β-lactamases in this system include cephalosporinases, group 2, the largest grouping which is further refined into subgroups, includes extended-spectrum cephalosporinases and serine carbapenemases, group 3 includes the metallo-β-lactamases [70].

#### 1.2.2.1. Extended-spectrum β-lactamases

Adaptations and mutations have led to an increasing array of β-lactamases with widening spectrums and resistance ability. First described in enterobacteria 1983 by Knothe *et. al*., extended-spectrum β-lactamases (ESBLs) confer resistance to expanded-spectrum cephalosporins [71]. Originally discovered in *Klebsiella pneumonia,* ESBLs are now widespread in many bacterial species, including *E. coli*.

β-lactamases, such as metallo β-lactamases, have evolved that are able to inactivate a wide range of β-lactam antibiotics, including some carbapenems, leaving few treatment options [46].

#### 1.2.2.2. CTX-M extended-spectrum β-lactamases

In 1990, gram-negative bacteria with a higher level of resistance to cefotaxime (CTX) than to ceftazidime were reported by Bauernfeind *et al.* (1990). They were designated CTX-M-1 due to their high level of resistance to cefotaxime (CTX), and first observed

in Munich [41]. CTX-M-type β-lactamases, classified in group 2be in the Bush *et al.* classification system [69] and Ambler class A [67], are a group of rapidly spreading ESBLs, both geographically and in range of clinical bacteria, and are now the dominant family, especially prevalent in such bacteria as *E. coli* and *K. pneumoniae* [72]. Sharing less than 40% amino acid identity [73], they appear to have a separate evolutionary history from other β-lactamases such as TEM and SHV, with which they share similar activity, and were originally found in *K. cryocrescens* [41]. They represent a present and growing threat to human health.

The CTX-M β-lactamases are often carried on large plasmids of around 100 kb, which also frequently harbour other antibiotic resistance genes including other β-lactamase types, and resistance to other antibiotics [74]. These plasmids are often highly mobile and transmissible, and many harbour addiction systems which seem likely to ensure their persistence and continued propagation even when released from antibiotic selective pressure [74]. Genes encoding CTX-M β-lactamases are frequently associated with the insertion sequences IS26 and IS*Ecp*1 [75-79]. The presence of upstream insertion sequences are often accompanied by downstream sequences similar to the inverted right repeat of IS*Ecp*1, which suggest mobility by transposition events [47, 80]. IS*Ecp*1 also has been shown to harbour at least one promoter sequence which drives or enhances the expression of $bla_{\text{CTX-M}}$ [76, 81, 82].

The CTX-M family have been grouped into 5 different subclasses, with members of each group sharing greater than 94% amino acid identity [41, 83]. They are clustered into groups CTX-M: -1, -2, -8, -9 and -25 [41], the group being designated with the name of the first member of that group to be described.

Particularly widespread in Europe and the US is the β-lactamase CTX-M-15, a member of group 1, conferring resistance to 3rd generation cephalosporin antibiotics.

## 1.3. Methods of tackling resistance to β-lactam antibiotics

As bacteria acquire resistance to specific antibiotics, the therapeutic solution has been to treat the infection with an alternative antibiotic, often a newer generation antibiotic with a broader spectrum of activity. As antibiotic resistance becomes increasingly prevalent, and with a finite arsenal of antibiotics available, this approach is not a long term viability. Either a constant stream of new antibiotics are required to be developed or discovered at the same, or faster pace, than resistance develops, or alternative antimicrobial therapeutics need to be researched.

### 1.3.1. β-Lactamase inhibitors

Inhibition of β-lactamase is a proven therapeutic method of tackling bacteria with reduced susceptibility to β-lactam antibiotics [84]. This approach allows for the continued use of a β-lactam antibiotic after bacteria have evolved resistance strategies against it.

Novel synthetic β-lactamase inhibitors have been shown to enhance the activity of certain antibiotics. Avibactam, a synthetic β-lactamase inhibitor, for example, was observed to have a synergistic effect with ceftazidime against many resistant species [85]. Zhang *et al.* (2014) reported the effective anti-β-lactamase activity of charged metallopolymers which inhibited β-lactamase and also attacked the bacterial cell wall [86]. Other chemical agents, such as heterobicyclic compounds [87], have also shown inhibitory activity against β-lactamase. Other β-lactamase inhibitors, such as Merck's

relebactam for use in combination with imipenem/cilastatin, are currently in development [88].

#### 1.3.1.1. Clavulanic acid, sulbactam and tazobactam

Clavulanic acid, sulbactam and tazobactam, are suicide competitive β-lactamase inhibitors. Clavulanic acid contains a penicillin-like β-lactam ring core structure, making it a β-lactamase substrate. First described and named in 1977, clavulanic acid was isolated from *Streptomyces clavuligerus* [89]. It was found to have little antimicrobial activity alone, but MICs of ampicillin and cephaloridine were reduced when used in combination against β-lactamase producing strains of *S. aureus, K. aerogenes, P. mirabilis,* and *E. coli* [26, 89, 90]. Clavulanic acid inactivates β-lactamase by covalently binding to the active serine residue in the enzyme which causes a conformational change in the clavulanic acid to increase its reactivity. This in turn, reacts with another residue in the β-lactamase active site causing the enzyme to become inactive [91]. The combination of amoxicillin and clavulanic acid has been branded under the trade name Augmentin and prescribed to treat bacterial infections that are resistant to amoxicillin. This antibiotic/inhibitor combination is active against many strains of resistant bacteria [92]. Some adverse effects of therapeutic uses of clavulanic acid in human patients such as cholestatic jaundice and acute hepatitis have been reported [93]. In addition to these limitations, resistance to the amoxicillin/clavulanic acid combination have been observed to have evolved [26, 94]

Sulbactam is a synthetic β-lactamase inhibitor which, like clavulanic acid, contains a penicillin-like β-lactam ring structure. Whilst having reportedly low antimicrobial properties alone, sulbactam shows direct activity against *Bacteroides* and *Acinetobacter* species [95]. When used alone, sulbactam was found to exhibit some bactericidal

properties against *bla*$_{\text{CTX-M-15}}$ producing *E. coli* (this study) – the concentration required for complete growth inhibition was lower for sulbactam alone than it was for cefotaxime alone. When used in conjunction with cefotaxime, it was found to have a synergistic effect. It is currently clinically co-administered with ampicillin and cefoperazone in the US and UK, to restore the activity of these antibiotics against bacteria with reduced susceptibility [96].

Tazobactam also shares a β-lactam ring core structural similarity with β-lactam antibiotics [91], and clinically it is currently combined with piperacillin. When the properties of tazobactam were investigated in the current study, it was found to exhibit weak antibiotic activity when a clinical isolate expressing *bla*$_{\text{CTX-M-15}}$ was treated with tazobactam in the absence of cefotaxime, but a strong synergistic effect was observed when combined with cefotaxime.

Whilst the current range of β-lactamase inhibitors have proved successful in broadening the spectrum of activity of certain antibiotics and combating β-lactamase mediated resistance [91], there are limitations and drawbacks associated with their widespread use. The metabolism of drugs can create stable or transient intermediate chemical species, breakdown products, or other metabolites which can be highly reactive, with the potential for off-target unwanted interactions with other cellular molecules [97]. Drugs which form covalent bonds with other molecules as a part of their mechanism of action have been a particular cause of concern for this reason [97]. The three β-lactamase inhibitors in clinical use, clavulanic acid, sulbactam and tazobactam, produce a variety of intermediates, which also vary in the presence of different β-lactamase variant enzymes [98]. Inhibitor-resistant strains have been observed to arise amongst Class A β-lactamases as a result of one or more amino acid substitutions in the

composition of the enzyme [99]. Occurrences of a single amino acid substitution resulting in a clavulanic acid resistant phenotype have been observed in *E. coli* and *Klebsiella pneumoniae* [100-102]. With only a small number of mutations required to produce an inhibitor-resistant enzyme and under selective pressure, it would seem likely that resistance to inhibitors would spread rapidly.

Although generally considered tolerable at therapeutic doses, there have been observations of side effects following the use of amoxicillin-clavulanic acid combinations [103, 104]. The piperacillin-tazobactam combination was linked to an increased risk of acute renal failure in adults receiving the drug during two 3 month periods in 2009 and 2010 [105].

Alternative approaches to the ever-growing problem of β-lactamase-mediated resistance, such as the inhibition of the expression of β-lactamase, would be desirable.

## 1.4. Inhibition of enzyme expression by synthetic antisense/antigene oligonucleotide analogues

### 1.4.1. Development of synthetic oligonucleotide analogues as gene expression inhibition agents

Early studies, dating back from the late 1970s in a variety of both prokaryotic and eukaryotic organisms, demonstrated the ability of short lengths of DNA/RNA and their analogues to affect gene regulation and expression [106-109].

In bacteria, natural antisense/antigene mechanisms are well known to perform a wide range of functions, most notably to regulate gene expression [110, 111]. Coleman *et al.* (1984) demonstrated that an inducible plasmid could be designed to express a sequence

of complementary RNA to inhibit expression of lipoproteins in *E. coli*, and also observed that the most effective mRNA target region was the Shine-Dalgarno sequence [112]. Due to the inherent instability and delivery problems with RNA/DNA and whole plasmids respectively, the potential of developing therapeutic applications using this method of gene inhibition seemed limited. However, the development of synthetic oligonucleotide analogues as antisense agents in the 1990s [113] created the possibility of targeted protein inhibition by ribosomal hindrance as a viable therapeutic option [114]. A range of synthetic oligonucleotide analogues have now been developed, with varying backbone chemical structural modifications. The synthetic antisense oligonucleotide analogues, hereafter referred to as antisense oligomers, most widely studied in bacteria are peptide nucleic acids (PNA) and phosphorodiamidate morpholino oligomers (PMO).

### 1.4.2. Polyamide (peptide) nucleic acids

Described and developed in 1991 by Peter Nielsen *et al.*[115], a synthetic DNA mimic was created by replacing the sugar-phosphate backbone of DNA with a polyamide backbone (Figure 1-2). These peptide nucleic acids (PNAs) were demonstrated to be able to hybridise and interact with DNA or RNA by Watson-Crick base pairing [116], showed a high level of stability and were not degraded by endonucleases [115]. PNAs with a net neutral charge in the polyamide backbone, do not suffer from electrostatic repulsion associated with natural DNA-RNA (or combinations thereof) interactions [117], which contribute to their overall high binding affinity. The flexibility of the polyamide backbone is also believed to contribute to the strong affinity for its target molecule and the stability of the hybrid complex [115].

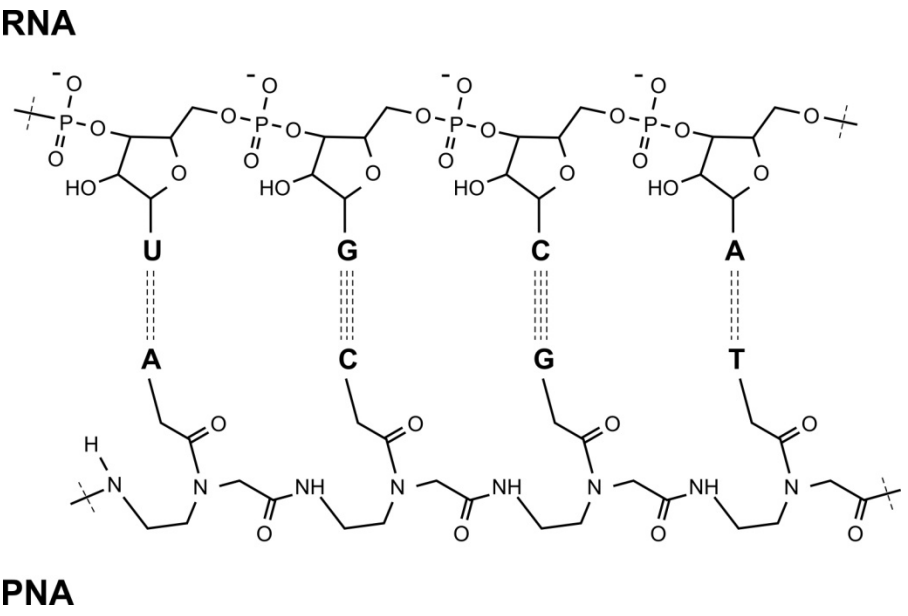


Figure 1-2. Comparison of backbone structures of RNA and PNA (adapted from Armitage [117]), shown hybridising for illustrative purposes.

PNAs were developed with the intent to bind to DNA duplexes in the major groove of the double helix, via Hoogsteen pairing, in a similar manner to triplex-forming oligonucleotides (TFOs) [117]. Experimentation revealed, however, that one strand of a poly-thymine:poly-adenosine DNA duplex was displaced by a 10-mer poly-thymine PNA. A second PNA strand was also found to hybridise to this complex, also by Hoogsteen pairing, resulting in a stable $PNA_2$:DNA complex.

Antisense oligomers have been shown to inhibit protein expression at the translation level. Lecosnier *et al.* described the effects of anti-insulin-like growth factor 1 receptor (IGF-1R) PNA, PMO and another synthetic antisense agent, locked nucleic acid (LNA). A 17-mer PNA was found to inhibit expression of IGF-1R by 70-80%, without any decrease in mRNA levels, as determined by quantitative RT-PCR [118].They also showed that a 17-mer PNA did not induce mRNA degradation, in contrast with an equivalent siRNA and also noted the unique ability among the three synthetic antisense

agents they tested (PMO, PNA and LNA) of PNA to form a $PNA_2$:mRNA triplex structure.

PNAs have been successfully employed to inhibit the expression of a wide range of bacterial genes at the translational level; a representative sample selection of previous studies is shown in Table 1-1. Although PNAs have been shown to have strong inhibitory effects when used in cell free studies and in bacterial strains with atypically permeable cell walls, strains with intact cell walls however were not susceptible to PNA translational inhibition. This indicates a requirement for a PNA delivery strategy to penetrate this barrier [119]. A common strategy to facilitate the translocation of a PNA across the bacterial cell wall is by the covalent attachment to a cell-penetrating carrier peptide, which is discussed in section 1.4.6.1.

Table 1-1. Previous PNA gene expression inhibition studies in bacteria

| Organism | Target | Length / conc | Significant Finding | CPP | Ref |
|---|---|---|---|---|---|
| *Pseudomonas aeruginosa* | *ftsZ* | 10-mer / 3 μM | Inhibited growth | $(R\text{-}Ahx)_6$-βala | [120] |
| *Pseudomonas aeruginosa* | *acpP* | 11-mer / 2 μM | Inhibited growth | $(R\text{-}Ahx\text{-}R)_4$-Ahx-βala | [120] |
| *Escherichia coli* | *acpP* | 9-12-mer / 2 μM | Cured infected HeLa cells | $(KFF)_3K$ | [121] |
| *Escherichia coli AS19* | *rRNA* | | Inhibited translation | None | [122] |
| *Klebsiella pneumoniae* | *gyrA* | 15-mer / 20 μM | Inhibited growth, cured IMR90 cell cultures | $(KFF)_3K$ | [123] |
| *Klebsiella pneumoniae* | *ompA* | 16-mer / 40 μM | Inhibited growth, cured IMR90 cell cultures | $(KFF)_3K$ | [123] |
| *Staphylococcus aureus* | *fmhB* | 10-mer / 10 μM | Inhibited growth | $(KFF)_3K$ | [124] |
| *Salmonella enterica* | *rpoD*, *rpoA* | 11-mer / 20 μM | Reduction in viable cells | $(KFF)_3K$ | [125] |

### 1.4.3. Phosphorodiamidate morpholino oligomers

Phosphorodiamidate morpholino oligomers (PMOs), incorporate natural DNA bases with a morpholine-phosphorodiamidate backbone (Figure 1-3) [126]. Like PNAs, they are able to bind to their DNA/RNA sequence-specific target through Watson-Crick base pairing. A PMO is structurally stable, electrically neutral and resistant to degradation by nucleases [126].

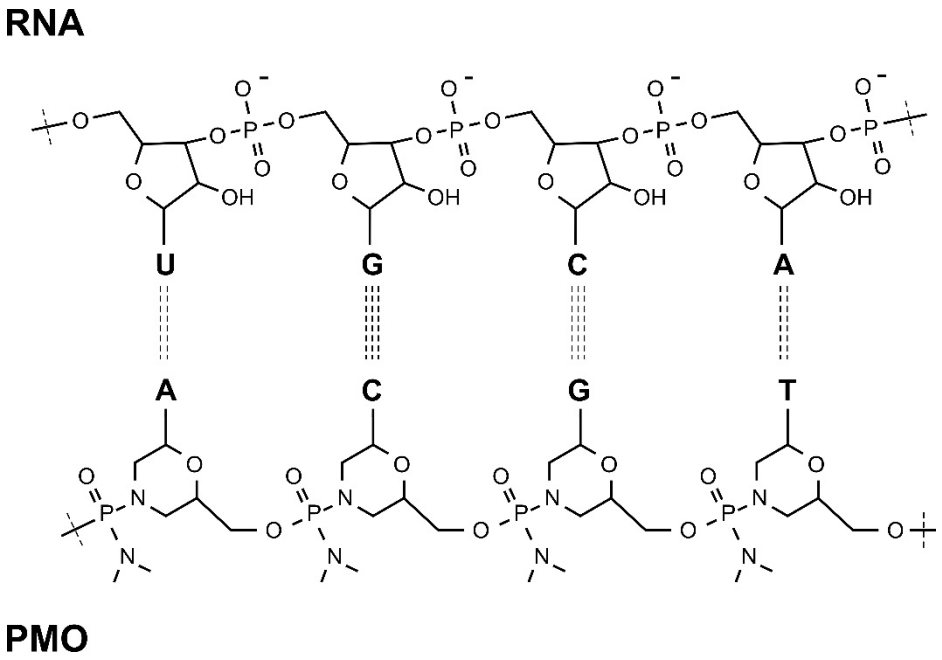


Figure 1-3. Comparison of backbone structures of PMO and RNA (adapted from Geller *et al.* [126]) shown hybridising for illustrative purposes.

In bacteria, PMOs have been shown to inhibit targeted gene expression in a sequence specific manner. For example, Geller *et al.* (2005) demonstrated an 11 base PMO targeted to an essential gene responsible for the biosynthesis of phospholipid (*acpP),* was able to significantly slow the growth of *E. coli* in culture, and reduced the amount of viable colony forming units in infected mice [127].

Table 1-2 shows some representative examples of previous studies using PMOs as targeted gene expression inhibitory agents.

Table 1-2. Previous PMO gene expression inhibition studies in bacteria

| Organism | Gene Target | Length/ concentration | Significant Finding | CPP* | Ref |
|---|---|---|---|---|---|
| *Salmonella enterica* | *acpP* | 11-mer / 1.25 µM | Inhibited growth | $(RXR)_4XB$ | [128] |
| *Bacillus anthracis* | *acpP*, *gyrA* | 11-mer / 1.25 µM | Inhibited growth *in vitro*, protected mice *in vivo* | $(RFF)_3R$ | [129] |
| *Acinetobacter lwoffii* and *Acinetobacter baumannii* | *acpP* | 11-mer / 0.1 – 64 µM | Strain/PMO dependant inhibition of growth *in vitro*, increased infected mice survival | $(RXR)_4$ | [130] |
| *E. coli* | *acpP* | 11-mer / 20 µM | Reduced viable cells by 61% (pure culture), significantly reduced peritoneal cfu | None | [127] |
| *Burkholderia multivorans* | *acpP* | 10-mer / 2.5 µM | Inhibited growth in pure culture | $(RFF)_3RXB$ | [131] |

*(R, X, and B indicate arginine, 6-aminohexanoic acid, and beta-alanine, respectively)

### 1.4.4. Antisense oligomer sequence design

Synthetic antisense oligomer design is, in part, a balance of specificity and efficacy – a shorter PMO/PNA, being a smaller molecule, is able to enter a bacterial cell more efficiently, however, a longer antisense oligomer can be designed to achieve a higher degree of specificity with a reduced chance of unwanted off-target homology. The length of an antisense oligomer also affects the translational inhibitory efficiency.

For maximal engagement with the target sequence by an antisense oligomer, it is advantageous to target an exposed, accessible and recognisable region of mRNA. The lack of a complementary strand in single-stranded RNA (ssRNA) allows for the formation of complex 3D secondary structures such as helices and hairpin loops. This presents a challenge to any antisense agent design – the target region must be accessible to the antisense agent for hybridisation, or the agent must be able to invade a base-paired strand. One such candidate region is the sequence at the 5' end of the mRNA around the start codon position, and the non-translated region immediately (5 to 20 bases) upstream of that. In prokaryotic organisms, the Shine-Dalgarno (SD) region is a short purine-rich sequence of between 2 and 9 bases complementary to a region on the 3' tail of the 16s ribosomal RNA subunit, and has been linked with the rate of protein synthesis [132]. The SD region and the translational initiation start codon have been previously shown to be the most effective areas to target by RNA and synthetic antisense agents for maximum translational inhibition, with the hindrance of translation initiation a likely mechanism for this inhibition [112, 133]. Coleman and colleagues noted that in their RNA experiments it was effective to target an area encompassing the Shine-Dalgarno region and the start codon of the mRNA of interest [112]. Dryselius *et al.* (2003) designed a series of 10-mer PNAs spanning the length of β-lactamase and *acpP* mRNA, providing an unbiased head-to-tail coverage and concluded the area most

susceptible for translational inhibition was the start codon region [133]. Panchal *et al.* (2012) targeted essential genes *acpP* and *gyrA* in the gram-positive bacterium *Bacillus anthracis* using 11-mer PMO antisense agents, and found that the most effective region was mRNA location -17 to -7, upstream from translation initiation [129]. Deere *et al.* (2005) identified the start codon and ribosome binding regions as effective for *E. coli* translational inhibition in a cell-free system, and also noted that 3' regions, or 5' non-translated regions, other than the SD region, were ineffective target sites [134].

Experimental evidence presented to date appears to indicate that a PNA oligomer of 9 - 15 bases is a suitable length for effective protein expression inhibition in bacteria whilst maintaining specificity. Deere *et al.* (2005) tested PMOs of various lengths between 7 and 20 bases for inhibition efficiency against a luciferase reporter and concluded that in a cell-free system longer PMOs exhibited greater inhibitory effects than shorter PMOs. In whole cells however, shorter PMOs exhibited greater inhibitory effect than longer PMOs [134].

### 1.4.5. Use of antisense to inhibit antimicrobial resistance and restore the activity of antibiotics

The ability of targeted synthetic antisense oligomers to specifically inhibit the translation of particular bacterial genes has been successfully demonstrated against a variety of targets. The strategy of combating antibiotic resistant bacteria by inhibiting the activity of β-lactamase has been shown to be effective with inhibitors such as clavulanic acid, sulbactam and tazobactam [91]. Restoration of antibiotic sensitivity in bacteria through translational inhibition of β-lactamase activity therefore potentially represents a viable and effective therapeutic solution [135].

Previous studies have demonstrated the principle of inhibiting the expression of resistance genes in bacteria, some example studies include the following: Good and Nielsen (1998) re-sensitised an atypically permeable *E. coli* strain (AS19) harbouring a plasmid (pBR322) carrying an ampicillin resistance gene, by inhibition of the β-lactamase transcript with a targeted PNA [136]. Jeon and Zhang (2009) employed a targeted PNA to inhibit the expression of the CmeABC multidrug efflux transporter in *Campylobacter jejuni,* which reduced the MICs of the antibiotics erythromycin and ciprofloxacin by 4 and 8 fold [137]. Wang *et al.* (2010) increased the susceptibility of multi-drug resistant *Pseudomonas aeruginosa* to five antibiotics by inhibition of the expression of the efflux pump OprM, with a transcript targeted phosphorothioate oligodeoxynucleotide [138]. Goh *et al.* demonstrated the ability of an anti-*mecA* PNA to significantly increase the susceptibility of methicillin-resistant Staphylococcus aureus (MRSA) to the β-lactam antibiotic oxacillin [139].

### 1.4.6. Cell penetration

Bacteria have many strategies to regulate and combat the intake of foreign material such as the impermeability of the lipopolysaccharide outer membrane, efflux pumps and selective membrane porins. Field and clinical isolates, with intact non-permeable membranes, are not susceptible to PNA/PMO translational inhibition, and it was surmised that the LPS membrane represents a significant obstacle to be overcome [119, 136]. Good and Nielsen (1998) found PNAs were able to inhibit β-lactamase expression in *E. coli* sufficiently to restore ampicillin sensitivity in a strain with an atypically permeable cell wall, but much less so in a strain with a typically permeable phenotype [136]. Peptides taken up by gram-negative bacteria typically are a maximum size of up to 650 Da, around 5 – 6 amino acid residues [140]. At around 2-3kDa [48], a 10-mer

oligomer is too large to efficiently enter a bacterial cell by porin-mediated passive transport, requiring an alternative delivery mechanism.

#### 1.4.6.1. Cell-penetrating peptides

Cell-penetrating peptides (CPPs) are short chains of amino acids, usually less than 30 residues in length, and usually consisting of a repeating pattern of positively charged and hydrophobic neutral residues which are able to traverse a bacterial cell wall. A cargo molecule attached, usually by a direct covalent bond, to a CPP is then translocated across the cell membrane into the cytoplasm. This approach has been shown to be effective in delivering synthetic antisense cargo molecules in eukaryotic cell lines [141] and bacterial strains [120].

Many different CPPs are known to be effective, naturally derived or artificially synthesised, often sharing common features. They typically are comprised of a series of repeating, alternating polar and hydrophobic residues with a net overall positive charge, required for affinity, and interaction with the bacterial cell wall [142]. Table 1-1 and Table 1-2 present a sample selection of PNA and PMO oligomers conjugated to cell-penetrating peptides in bacterial gene expression inhibition studies. Figure 1-4 shows commonly used cell-penetrating peptides and their motifs of alternating amino acid residues.

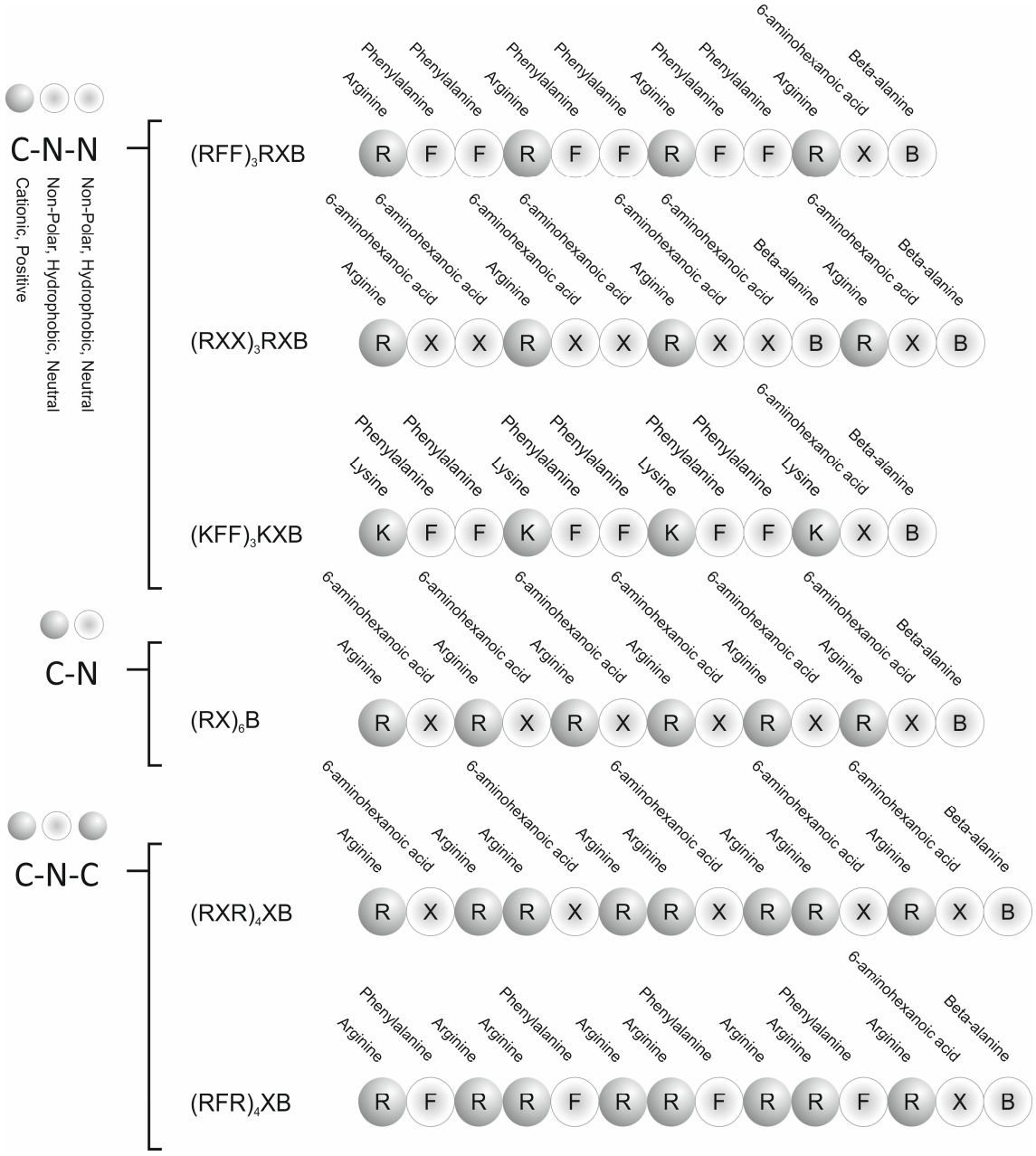


Figure 1-4. Common motifs and sequences of cell-penetrating peptides (adapted from Puckett *et al.* [143]).

The mechanism by which CPPs are able to traverse bacterial cell membranes has yet to be fully elucidated, with some disagreement and conflicting evidence relating to the proposed energy-dependent or energy independent mechanism of cell penetration [144]. Most cell-penetrating peptides do not show any cell specificity [145], which may

suggest that the translocation pathway is not dependent on any specific cell receptor [144, 146].

The lipopolysaccharide (LPS) component of the outer membrane layer of gram-negative bacteria such as *E. coli* is polyanionic, stabilised with cationic bridges [147]. Polycationic molecules, such members of the polymixin group, are able to form a complex with the LPS and disorganise and disrupt the outer membrane [148]. It would appear, however, due to a range of permeabilisation activity of similar polycationic agents, that cationicity alone is an insufficient explanation for the outer membrane permeabilisation effects. It is likely that the structure and position of the positive charges within the molecule contribute to this permeabilisation effect [148].
Cell-penetrating peptides bear a resemblance to antimicrobial peptides, both in terms of charge/structure and in their ability to translocate across a biological membrane [149]. Antimicrobial peptides (AMPs) are a group of short, variable length peptide chains, typically less than 10 kDa, have an overall net positive charge, are heat stable and have an affinity for prokaryotic membranes[150, 151]. AMPs often act against their target by their strong affinity for a bacterial membrane, and the formation of large transient pores [152] resulting in a compromised, permeabilised membrane [153]. This channel-forming, membrane perturbation effect has been proposed as a possible mechanism of energy-independent translocation of CPPs in bacteria [144].

Inner membrane transport protein SbmA has been implicated in the translocation and importation of peptides including cell-penetrating peptides [143], certain peptide antibiotics [154], and proline-rich antimicrobial peptides [155, 156]. Puckett *et al.* reported some bacteria developing resistance to PMOs conjugated to cell-penetrating peptides (P-PMOs) [143]. It was proposed that the spontaneous development of

resistance to P-PMOs was a result of an observed mutation in *sbm*A, and that this mutation prevented the translocation of the CPP, and as a consequence, the entire conjugate. In their study, s*bmA* mutants were challenged with a PMO targeting the essential gene *acpP*, conjugated to 6 different CPPs. Four CPP variants were found to be ineffective whilst two retained their activity compared with a non-*sbmA* mutant. The four CPPs found to be ineffective against the *sbmA* mutant varied in amino acid composition, and all motifs were either C-N-N or C-N-C (C-cationic, N-non-polar). Two cell-penetrating peptides were shown to be unaffected by the *sbm*A mutation with motifs C-N and C-N-C. It was suggested that the active transporter SbmA was at least partially responsible for the translocation of the four P-PMOs sensitive to the *sbmA* mutation, and that amino acid composition as well as residue properties of the CPP were an important factor in the function of cell-penetrating peptides [143]. The observation of two CPP-PMO conjugates which retained their activity in *sbm*A mutants may suggest at least one alternate/additional inner-membrane translocation pathway, and more studies are required to elucidate this further. Whilst Puckett *et al.* demonstrated that an *sbmA* mutant strain was less susceptible to a PMO targeting an essential gene when conjugated to certain CPPs, other studies have provided evidence that transportation of CPP-antisense oligomer conjugates based on specificity to the cell-penetrating peptide portion of the conjugate by SbmA is not necessarily a complete explanation. Observations to date, as partly discussed above, indicate that SbmA is flexible in its substrate specificity. Ghosal *et al.* conducted a series of studies to determine if a PNA, the CPP or the entire conjugate was a suitable SbmA substrate [157]. Their findings strongly suggested that SbmA was the transporter for an unmodified PNA across the inner membrane - an unmodified PNA showed specific activity against its target in *E. coli* mutant strains with a compromised outer membrane, and this activity was

significantly lower in *sbmA* deletion mutants. Further studies suggested the degradation of the PNA's peptide carrier within the periplasmic space by proteases when strains with a typical cell wall were challenged with a PNA conjugated to a biodegradable cell-penetrating peptide. In the case of a PNA conjugated to a stable peptide carrier, less susceptible to degradation by proteases, a proposed alternate penetration pathway of direct outer and inner membrane perturbation may be likely.

It is not known if an unmodified PMO is a suitable substrate for SbmA, and as Ghosal *et al.* studied the relationship between SbmA and a shorter antisense agent of a differing chemistry (an 11-mer PNA), the study conducted by Puckett *et al*. is not directly comparable. It would appear to be likely that there are multiple pathways of cell penetration by peptide-conjugated antisense agents, including the SbmA pathway, other possible active transporters and the direct penetration of the inner membrane by the same mechanism by which they penetrate the outer membrane. A quantifiable assay to determine the uptake of unmodified antisense oligomers, CPPs, and peptide conjugated antisense oligomers would be highly desirable to resolve this uncertainty surrounding the mechanism of cellular uptake of CPP conjugated antisense oligomers.

#### 1.4.6.2. Experimental evidence of the efficacy of cell-penetrating peptides in *E. coli*

Good *et al.* increased the potency of 9 - 12-mer PNAs targeting the essential gene *acpP* and ribosomal RNA (rRNA) by two orders of magnitude by the conjugation of the PNAs to the cell-penetrating peptide $(KFF)_3K$ [121]. Eriksson *et al.* showed that when challenged with a CPP-PNA conjugate, the membrane of the cell was permeabilised [158], indicating a level of disruption of the lipid membranes, as well as the efficacy of cell-penetrating peptides as carriers for PNAs. Kurupati *et al.* designed antisense PNAs

to target two essential genes, *gyrA* and *ompA,* in *Klebsiella pneumonia.* Unmodified PNAs were found to be ineffective, whereas the CPP-PNA conjugate was able to inhibit the target genes in a dose-dependent manner [123].

The cell penetrating peptide $(KFF)_3K$ was shown to act synergistically with certain antibiotics in enteric gram-negative bacteria, for example in *E. coli* the MIC for the antibiotic rifampin was reduced 300-fold, with outer membrane disruption and a resultant increase in cell permeability the suggested cause [147]. Eriksson *et al.* studied membrane permeabilisation and peptide-PNA uptake in *E. coli* and demonstrated the efficacy of $(KFF)_3K$. They also described an unexpected synergistic effect of the PNA component of the conjugate over the free peptide [158].

These studies demonstrated the ability of cell-penetrating peptides to penetrate a bacterial cell wall and deliver its covalently bound cargo to the cytoplasm. This suggests that cell-penetrating peptides could be a suitable carrier for anti-$bla_{\text{CTX-M-15}}$ agents for the inhibition of β-lactamase expression in field isolates in the current study. However, previous studies noting either a cell-permeabilisation effect or a synergistic effect of the cell-penetrating peptide with certain antibiotics may suggest membrane perturbation as the most likely mechanism of cell penetration, potentially contributing to bacterial culture growth inhibition.

## 1.5. Thesis Hypothesis

Resistance in *E. coli* to the 3rd generation cephalosporin cefotaxime is typically achieved through the expression of *bla*$_{CTX-M}$ [41, 159]. The hypothesis of the current project was that a targeted anti-*bla*$_{CTX-M}$ synthetic oligomer would inhibit expression of this enzyme, and the sensitive phenotype of the host bacterium would be restored. To achieve translational inhibition, PNA and PMO chemistries were chosen to be evaluated for efficacy.

### 1.5.1. Project Aims

The specific aims of this project were:

1. **Development of assays for the quantification of β-lactamase activity (Chapter 3).**

A sensitive, quantifiable and specific β-lactamase activity assay was required to evaluate the level of β-lactamase expression, and the efficacy of translational inhibition. Assays developed for β-lactamase quantification were a colourimetric nitrocefin based assay and high-pressure liquid chromatography (HPLC). Nitrocefin is a chromogenic β-lactamase substrate which undergoes a colour change from yellow ($\lambda_{max}$ = 390 nm) - intact nitrocefin, to red ($\lambda_{max}$ = 480 nm) - degraded. It is routinely used to detect the presence of β-lactamase and is rapid, inexpensive and quantifiable [160]. It is not specific, however, to any one type of β-lactamase. An HPLC assay for CTX degradation was adapted from a method developed to separate seven cephalosporins [161]. The assay developed by the current study was CTX specific, sensitive and reproducible and suitable for the quantification of cefotaximase activity.

**2. Design and construction of plasmids carrying *bla*$_{\text{CTX-M-15}}$ as a suitable test subject for inhibition studies in a cell-free system, and the inhibition of β-lactamase expression by synthetic antigene oligomers in a cell-free translation-transcription coupled system (Chapter 4).**

A plasmid harbouring β-lactamase from CTX-M group 1 was required for initial translational inhibition experiments. *E. coli* field isolates with a reduced-susceptibility (to CTX) phenotype often carry many different resistant genes on large plasmids, including different classes of β-lactamase. To avoid these potential confounding factors, two plasmids were constructed, each carrying a single copy of *bla*$_{\text{CTX-M-15}}$ cloned from field isolates. The expression vector chosen to carry these genes, pET-9a (Novagen) featured a T7 promoter and terminator region flanking the multi-cloning site, enabling cell-free protein expression in translation/transcription coupled systems utilising viral T7 polymerases.

Cell-free translational inhibition experiments were carried out in a cell-free translation/transcription coupled system. These commercially available systems typically employ T7 viral polymerases combined with *E. coli* whole cell extracts, and enable expression of proteins from linear or circular DNA without the need for living cells. Initial proof-of-concept studies were conducted with a range of three PNAs and one PMO of different sizes with different target regions. These were found to exhibit *bla*$_{\text{CTX-M-15}}$ activity inhibition under these conditions.

**3. Inhibition of β-lactamase CTX-M activity in whole cells (Chapter 5).**

Lipopolysaccharide layer defective mutant strain *E. coli* AS19 was transformed with the expression vector constructed to carry *bla*$_{\text{CTX-M-15}}$. This strain has previously been shown to have a permeable membrane, and take up unmodified antisense/antigene agents without any additional cell penetration strategies. It has been successfully used as a test subject in previous gene expression inhibition experiments in whole cells. The translational inhibition effects of the PMO and PNA shown to be effective in a cell-free system were investigated in this transformed AS19 strain.

With enzyme expression inhibition demonstrated in AS19, the translational inhibition effects of the PMO and PNA were investigated in a panel of CTX resistant field isolates. In order to achieve sufficient delivery of the antisense agents into the cytoplasm, these agents were each attached to a cell-penetrating peptide. Cell-penetrating peptides have been demonstrated in previous studies to be able to carry a cargo molecule across the bacterial cell wall without impeding their inhibition properties. Inhibition of β-lactamase expression was inferred by the increased sensitivity of the isolates to cefotaxime, established by growth curve assays. Minimum inhibitory concentrations were established by a spectrophotometric measurement of growth over an 18-24 hour period.

4. **Exposure to β-lactam antibiotics stimulates an increase of β-lactamase activity in strains harbouring *bla*$_{\text{CTX-M-3}}$ and *bla*$_{\text{CTX-M-15}}$ (Chapter 6).**

Suspected differential expression levels of *bla*$_{\text{CTX-M}}$ were investigated:

i) by exposing both field isolates and AS19 transformed with the *bla*$_{\text{CTX-M-15}}$ plasmid vector to varying concentrations of a 3$^{rd}$ generation cephalosporin (ceftriaxone) followed by supernatant incubation with cefotaxime. Resultant β-lactamase activity was quantified by HPLC.

ii) by the quantification of the rate of cefotaxime degradation in *E. coli* cultures. Whole cells were exposed to varying concentrations of cefotaxime and rates of degradation established by HPLC.

5. **Development of a bacterial intracellular delivery vector for targeted synthetic antisense/antigene oligomers (Chapter 7).**

A tetrahedral nucleic acid 3D structure was designed and developed as a carrier and delivery vehicle for PMO and PNA antisense oligomers. Its efficacy as a vector was evaluated by an evaluation of the re-sensitisation of field isolates to cefotaxime, and in comparison with cell penetrating peptide conjugates.

# Chapter 2.

# Materials and Methods

## 2.1. *E. coli* strains used in the current study

Strains used in this study are shown in Table 2-1. *E. coli* strains of human origin were obtained from Public Health England (Salisbury, UK), AS19 was donated by Liam Good (RVC, London), BZ693/P, B3804 and LREC525 were from the collection of strains at the Animal and Plant Health Agency (Addlestone, UK). LREC90, used for control studies, carried a plasmid harbouring *bla*$_{\text{CTX-M-14}}$, which encoded β-lactamase from CTX-M-group 9. All other CTX resistant strains used in this study harboured variants of CTX-M-group 1.

Table 2-1. *E. coli* strains used in study.

| **Designation** | **Plasmid** | ***bla* Resistance** | **Source and Notes** | **Ref** |
|---|---|---|---|---|
| NEB DH5α™ | None | None | Chemically competent lab strain | [162] |
| NEB Turbo | None | None | Chemically competent, rapid growth | |
| DH5α™-T1® | None | None | Chemically competent, enhanced uptake efficiency | |
| AS19 | None | None | Atypically permeable strain | [163] |
| NCTC10418 | None | None | Reference sensitive strain | |
| NCTC13351 | Not known | TEM-3 | ESBL ref strain | |
| LREC115 | Not known | Amp | AmpC hyper producer | |
| LREC460 | pEK516 | CTX-M-15 | Human | [74] |
| LREC461 | pEK204 | CTX-M-3 | Human | [74] |
| LREC454 | pEK499 | CTX-M-15 | Human pandemic strain | [74] |
| LREC525 | Not known | CTX-M-15 | Turkey | [164] |
| LREC90 | Not known | CTX-M-14 | Cattle | |
| BZ693/P | Not known | CTX-M-3 | Chicken | |
| B3804 | pIFM3804 | CTX-M-1 | Pig | [165] |
| 21/C0188/02/13 | Not known | Oxa1 | Bull Calf | |
| 12/B0118/10/11 | Not known | CTX-M-1 | Chicken | |
| 2013-6404 | Not known | TEM-1 | Not known | |

## 2.2. Plasmids used during study

Table 2-2. Plasmid vectors used during the study

| Plasmid | Features | Resistance | Source |
|---|---|---|---|
| pCR2.1 | TA Cloning vector | Ampicillin, Kanamycin | Invitrogen |
| pET-9A | Expression vector | Kanamycin | Novagen |

## 2.3. Synthetic antisense oligomer sequence design and synthesis

PNA and PMO antisense oligomers (Table 2-3) were designed to target and span the start and/or Shine-Dalgarno (SD) region of *bla*$_{\text{CTX-M-group 1}}$ mRNA. PNA1 and PNA3 were synthesised by, and purchased from Cambridge Research Biochemicals (Cleveland, UK, purity = 99.9%), and PMO1 was purchased from Genetools, LLC (Philomath, USA, estimated purity > 92%). PNA4 was synthesised by Cellmano Biotech (Hefei, China, purity = 95.51%). Peptide conjugated antisense oligomers (Table 2-4) were synthesised by Cambridge Research Biochemicals. Alignments of the group 1 CTX-M β-lactamases targeted in this study are shown in Figure 2-1. Figure 2-1 also shows the sequence and regions of complementarity with *bla*$_{\text{CTX-M-group 1}}$ of the antisense oligomers used in this study.

Table 2-3. Antisense oligomer sequences.

The PNAs are written from their N- (amino) to C- (carboxy) termini, with the N-terminus corresponding to the 5' end of a conventional oligonucleotide [123]. PMOs are commonly described as having 5’ and 3’ ends, corresponding to those of DNA/RNA. * - estimated.

| **Designation** | **Sequence (5’ – 3’)** | **Purity** |
|---|---|---|
| PNA1 | attccttattctg | 99.9% |
| PNA3 | catgggattcctt | 99.9% |
| PNA4 | ttccttattctgg | 95.51% |
| PMO1 | gcgcagtgatttttaaccatggga | > 92%* |


Figure 2-1. Alignments of *bla*CTX-M-15/1/3/33 mRNA with PMO1, PNA1, PNA3 and PNA4.

Asterisks (*) represent base homology between the *bla*CTX-M variants.

Table 2-4. Peptide conjugated antisense oligomer sequences.

| **Name** | **Sequence** | **Purity** |
|---|---|---|
| P-PNA4 | KFFKFFKFFK-ethylenediamine-[5’-ttccttattctgg-3’-[Cys]-maleimido-β-Ala] | >90% |
| P-PMO1 | KFFKFFKFFK-ethylenediamine-[5’-gcgcagtgatttttaaccatggga-3’-maleimido-β-Ala] | >90% |

## 2.4. DNA Oligonucleotides

### 2.4.1. PCR Primers

Oligonucleotide primer pairs (Table 2-5) designed for the amplification of DNA from genomic or plasmid DNA were supplied and synthesised by Sigma Custom Products (Suffolk, UK). Primers were suspended in sterile nuclease-free water (Qiagen, Manchester, UK) to a final concentration of 100 µM. Bold lower case text denotes restriction enzyme recognition sites incorporated into the primer.

Table 2-5. PCR primer pairs for the amplification of *bla*$_{\text{CTX-M-15}}$ and associated upstream region.
Bold text represents restriction enzyme recognition sites.

| **Reference** | | **DNA Sequence (5' to 3')** | **Amplicon** | **Amplicon Size (bp)** |
|---|---|---|---|---|
| CTX-M-pEK516 | Forward | actca**agatct**gaaattcagctttcacccattg | CTX-M-15 and IS26 from pEK516, | 2552 |
| | Reverse | ccatgt**cctagg**ccgtttccgctattacaaac | | |
| CTX-M-pEK499 | Forward | tactgg**catatg**cgcttgtgattcgccgccgtcaggttga | CTX-M-15 and IS*Ecp*1 from pEK499 | 2119 |
| | Reverse | gagcgt**ggatcc**ccgtttccgctattacaaac | | |

### 2.4.1.1. Sequencing/screening primers

Table 2-6. Primers for PCR screening, and sequencing.

| **Reference** | | **DNA Sequence (5' to 3')** | **Region Target** |
|---|---|---|---|
| M13 | Forward | cgccagggttttcccagtcacgac | M13 |
| | Reverse | tcacacaggaaacagctatgac | |
| CTX-M-SEQ | Forward01 | ccttcgaccagaacccgg | Cloned region sequencing/ screening primers |
| | Forward02 | gcacggcccggtacagatac | |
| | Reverse03 | cggcatcagttaccgtgagc | |
| | Reverse04 | cgggcgaacgcggtgacg | |
| T7 | Forward | taatacgactcactataggg | Region between T7 promoter and terminator |
| | Reverse | gctagttattgctcagcgg | |

### 2.4.1.2. Primers for site-directed mutagenesis

Table 2-7. Primers for site-directed mutagenesis and for SDM screening.

| **Reference** | | **DNA Sequence (5' to 3')** | **Description** |
|---|---|---|---|
| SDM | Forward | atacatcgcgacggc**t**ttctgccttaggttg | SDM primers for the area surrounding the single base mutation. Primers incorporate mutation correction (bold). |
| | Reverse | caacctaaggcagaa**a**gccgtcgcgatgtat | |
| SDM-SCREEN | Forward | cttcctttcgggctttgtta | PCR primers for the amplification of 164bp region surrounding mutation for RE digestion and screening |
| | Reverse | tggccaaaagatcgtgcgcc | |

#### 2.4.1.3. DNA sequences for tetrahedron construction

The sequence of single-stranded DNA (ssDNA) forming the structural frame of each 3D tetrahedral vector was designed with areas on each strand to be complementary to regions on the other structural strands (Table 2-8). These regions of complementarity facilitated the formation of the rigid 3D double-stranded DNA (dsDNA) tetrahedron structure. ssDNA strands were checked for unwanted hetero and homo dimerisation using Multiple Primer Analyzer (ThermoFisher Scientific) [166].

Table 2-8. DNA sequences used to form a 3D tetrahedron structural framework to carry antisense oligomers.

| Tetrahedron Designation | Description | Reference | DNA Sequence (5' to 3') |
|---|---|---|---|
| JBRPMOP | Prototype design – single 25-mer PMO forming one tetrahedron face. Each edge = 9 bp. | JBRPMOP-F1 | ggtaccctgtcactaagtaggattg |
| | | JBRPMOP-F2 | agcgtccccttagtgaccgcgtcac |
| | | JBRPMOP-F3 | gggacgcttaaaaaattcaatccta |
| JBRCPMOP1 | 25-mer PMO-carrying tetrahedron, 18 bp edges. Total size = 108 bp | JBRCPMOP1-A | gcggtgagttgtatccaccacggtgtgcc |
| | | JBRCPMOP1-B | cgattagcctaagatcgggttctcaccgccttgccaaccgctcccatggttaaa |
| | | JBRCPMOP1-C | ccgtggtggatacaactctggcaaggcggtgagaactgtcctacgaagagtgta |
| | | JBRCPMOP1-D | ccgatcttaggctaatcgaaatcactgcgcggcacatacactcttcgtaggaca |
| | | JBRCPMOP1-PMO | gcgcagtgatttttttaaccatggga |
| JBRSPNAP2 | 13-mer PNA-carrying tetrahedron, 18 bp edges. Total size = 108 bp | JBRSPNAP2-A | actccagacccgttcactccctccgttgtcctaacgctaag |
| | | JBRSPNAP2-B | cgcgacttaggtccataatcaaggggccggtgagatgggagtgaacgggtctgg |
| | | JBRSPNAP2-C | tagcgttaggacaacggaatctcaccggccccttgatacgtgcgggtctgataa |
| | | JBRSPNAP2-D | ttatggacctaagtcgcgagtccagaataaggaactttatcagacccgcacgta |
| | | JBRSPNAP2-PNA | ttccttattctgg |

## 2.5. Chemicals and antimicrobials

All reagents, chemicals and antimicrobial agents were obtained from Sigma-Aldrich (Dorset, UK) unless otherwise stated.

## 2.6. Bacterial Methodology

### 2.6.1. Storage of *E. coli* strains

All bacterial strains were stored at -80° C using the Protect Microorganism Preservation System (Technical Service Consultants, Lancs, UK). A single colony from an overnight culture grown on LB agar media was selected and typically suspended in 5 ml LB at 37° C with shaking at 200 rpm. When the culture had reached approximately O.D. $_{600\ nm}$ 0.3, 200 µl of liquid from a single Protect Microorganism Preservation System vial was replaced with 200 µl bacterial suspension and stored at -80° C.

### 2.6.2. Bacterial culture

Unless otherwise stated, *E. coli* strains were cultured in lysogeny broth (LB) or on LB solid agar with antibiotic supplements where required. Cultures were grown at 37° C, and liquid cultures with the addition of shaking at 200 rpm. Typical final antibiotic selection concentrations were: cefotaxime – 2 µg/ml, ampicillin – 100 µg/ml, kanamycin – 40 µg/ml.

### 2.6.3. Estimation of DNA concentration

Concentration of circular and linear DNA preparations and purifications were estimated by spectrophotometric analysis using a Thermo Scientific NanoDrop™ 1000 Spectrophotometer (Thermo Fisher Scientific, MA, USA).

### 2.6.4. Plasmid preparation and purification

Plasmids were extracted and purified from *E. coli* cultures using the peqGOLD Plasmid Miniprep Kit (Peqlab Ltd, Southampton), and the manufacturer's protocol followed. Plasmid DNA was typically prepared from a 2 - 4 ml overnight culture. A manufacturer's estimation of 80 - 95% of plasmid DNA was obtained with two dd$H_2O$ elutions of 25 - 50 µl each. Plasmid purity and concentration was verified and estimated by agarose gel analysis, and by spectrophotometric analysis using a Thermo Scientific NanoDrop™ 1000 Spectrophotometer (Thermo Fisher Scientific).

### 2.6.5. Establishment of minimum inhibitory concentration (MIC) values for *E. coli* strains

*E. coli* strains were cultured in 96-well microtiter plates (Falcon) and incubated at 37°C in a Fluostar Optima (BMG Labtech, Aylesbury, UK) spectrophotometer, with a constant temperature of 37° C. Growth was monitored at O.D. $_{600\ nm}$ for 18 – 24 hours. MIC values were reported as the minimum concentration of an agent or agents required to inhibit growth (O.D. $_{600\ nm} < 0.1$) in a minimum of 50% of replicates after 18 hours incubation at 37° C.

### 2.6.6. Restriction endonuclease digestion of DNA

All restriction enzymes were supplied by NEB (New England BioLabs, Herts, UK) or Promega (Southampton, UK) unless otherwise stated. Typically, 1 µg DNA was incubated with 10% (v/v) manufacturer's supplied reaction buffer and the manufacturer's recommendation of 1 µl enzyme in a 50 µl reaction at 37° C for between 15 and 60 minutes.

### 2.6.7. Separation of DNA fragments by agarose gel electrophoresis

Agarose gels were typically prepared with approximately 1.5% (w/v) agarose in TAE buffer (40 mM Tris-acetate, 2 mM EDTA) and stained with ethidium bromide or SYBR® Safe DNA gel stain (Invitrogen, Paisley, UK) at a concentration of 1:10,000. Unless otherwise stated, TAE was used for the running buffer and samples were typically run at 80V. DNA fragments were visualised and photographed using a Syngene GeneGenius UV Transilluminator (Syngene, Cambridge, UK). A 100 bp or 1 kb DNA marker ladder (Promega) was used to estimate fragment sizes and DNA quantity.

### 2.6.8. Polymerase Chain Reaction (PCR)

Typically 10 - 100 ng DNA template was used in a 50 µl reaction consisting of 0.5 µl of 50 mM dNTPs, 1 µl of each primer (10µM), 1 µl of polymerase (1 unit/µl), concentrated reaction buffer to a final concentration of 1x, and water to a final volume of 50 µl. The PCR reaction was completed using a GeneAmp® PCR System 9700 (PE Applied Biosystems) PCR thermocycler under the cycle conditions shown in Table 2-9.

Table 2-9. Typical PCR cycle conditions.

| **Iterations** | **Temperature** | **Time** | **Purpose** |
|---|---|---|---|
| **Throughout** | Heat Lid 100° C | - | Condensation prevention |
| **Once** | 94° C | 5 minutes | Initial cell breakage and DNA denaturation |
| **Loop (32-35x)** | 92° C | 30 seconds | Denaturation |
| | X° C | 40 seconds | Annealing |
| **End Loop** | 72° C | 60-150 seconds | Extension (~ 1kb/min for *Taq*) |
| **Once** | 72° C | 5 minutes | Final Extension |
| **Forever** | 4° C | ∞ | Storage/end |

### 2.6.9. Colony PCR

Typically, colony PCR was performed in a 50µl reaction using a GeneAmp® PCR System 9700 (PE Applied Biosystems) PCR thermocycler, using typical PCR cycle conditions (Table 2-9). A colony was selected, re-streaked and dipped into a typical PCR reaction mixture.

### 2.6.10. Culture of transformants

Individual colonies were selected from incubated plates and a sterile loop was used to transfer the selected colonies into a 50 ml culture tube containing 10 ml LB medium with appropriate selective antibiotics. They were then incubated overnight at 37° C with continuous shaking at 200 rpm.

### 2.6.11. Vector/Insert Ligation

Molar ratios of vector:insert typically ranged between 1:1 and 1:3. Molar ratio calculations were verified and assisted with the NEBioCalculator™ v1.3.9 [167].

Ligations were typically performed in a 30 µl reaction in the presence of 10x T4 buffer (Promega; 3 µl) and T4 DNA ligase (3 µl), the volume adjusted with nuclease-free water. The ligation reaction was incubated at 4° C for 14 - 16 hours.

### 2.6.12. Construction of expression plasmid vector carrying cloned *bla*$_{\text{CTX-M-15}}$ and associated upstream regions

#### 2.6.12.1. PCR amplification of *bla*$_{\text{CTX-M-15}}$ from pEK499 and pEK516

Two suitable, fully sequenced resistance plasmids were selected as donor plasmids for the cloning of *bla*$_{\text{CTX-M-15}}$, LREC454 field isolate harboured the resistance plasmid pEK499 [74] and isolate LREC460 harboured the resistance plasmid pEK516 [74]. The

open reading frames for *bla*$_{\text{CTX-M-15}}$ shared 100% sequence identity, but differed in the upstream genetic environment, including promoter loci and composition. Primers were designed to amplify the entire gene and the upstream insertional elements associated with *bla*$_{\text{CTX-M-15.}}$ To facilitate the incorporation of the resultant amplicon into the expression vector pET-9a, restriction enzyme recognition sites were incorporated into the primer design (Table 2-5). Primers designed for the amplification of *bla*$_{\text{CTX-M-15}}$ from pEK499 incorporated the restriction enzyme site recognised by *Nde*I in the forward primer, and *Bam*HI in the reverse primer. Primers designed to amplify *bla*$_{\text{CTX-M-15}}$ from pEK516 incorporated *Xba*I in the forward primer and *Bam*HI in the reverse. The PCR reactions took place under typical conditions. The use of two different restriction recognition sites in each of the PCR primer pairs used to amplify the target region facilitated the directional insertion of *bla*$_{\text{CTX-M-15}}$ in the correct, functional orientation in the expression plasmid pET-9a.

#### 2.6.12.2. Non-directional incorporation of PCR products into pCR™2.1-TOPO® cloning vector

The ligation of PCR products with the linear cloning vector, pCR™2.1-TOPO (Invitrogen) was carried out using the Quick Ligation™ Kit (NEB) under the following conditions: approximately 50 ng amplified and purified DNA PCR product was incubated with between 25 and 100 ng of the linear vector backbone pCR™2.1-TOPO, $dH_2O$ to 10 µl, 2x Quick Ligation Buffer (2 µl), Quick T4 DNA Ligase (1 µl). This reaction mixture was incubated at 25° C for 5 minutes, and then chilled on ice. This was then used to transform One Shot® MAX Efficiency™ DH5α-T1® *E. coli* (Invitrogen).

#### 2.6.12.3. Blue-white screening of recombinant bacteria

LB agar plates were prepared, supplemented with CTX (2 µg/ml) and KAN (40 µg/ml), and allowed to dry. X-Gal (100 µl; 20 mg/ml) was spread onto the surface and allowed to dry. IPTG was not required for the chromogenic reaction when using *E. coli* strain DH5α™-T1®. Transformation reactions were spread onto the plate and cultured overnight at 37° C. The next morning the plates were incubated at 4° C for 1 hour to enhance the development of the blue colour. Successful transformants appeared white and were selected, cultured and stored at -80° C.

#### 2.6.12.4. Screening of recombinant plasmid for successful insertion of cloned region

Plasmids were extracted and purified using the peqGOLD Plasmid Miniprep Kit (Peqlab), and used as the DNA template in a typical PCR reaction. M13 forward and reverse primers (Table 2-6) were used to amplify the entire section of DNA ligated into pCR™2.1-TOPO. The PCR products were analysed by gel electrophoresis with a 1kb reference DNA ladder (Promega). Plasmids containing inserts of the correct size (2552 bp for the section cloned from pEK516, and 2119 bp for the section cloned from pEK499) were selected and sequenced for verification of successful incorporation of the cloned region. These plasmids were designated pCR2.1-CTX-M499 and pCR2.1-CTX-M516 respectively.

#### 2.6.12.5. Restriction enzyme digestion of recombinant plasmids pCR2.1-CTX-M499 and pCR2.1-CTX-M516

Recombinant plasmids pCR2.1-CTX-M499 and pCR2.1-CTX-M516 were extracted and purified using peqGOLD Plasmid Miniprep Kit. pCR2.1-CTX-M499 was digested with *Bam*HI and *Nde*I, to release the cloned sections, under the following conditions:

approximately 1 µg of plasmid DNA was incubated with 5 µl buffer 3.1 (NEB), 0.5 µl BSA, 1 µl *Bam*HI-HF® (NEB), 1 µl *Nde*I (NEB) and dd$H_2O$ to a final reaction volume of 50 µl, at 37° C for 60 minutes. The DNA was purified with the peqGOLD MicroSpin Cycle Pure Kit (Peqlab) with one elution of 20 µl in dd$H_2O$. pCR2.1-CTX-M516 was digested with *Bam*HI and *Xba*I, to release the cloned sections, under the following conditions: approximately 1 µg of plasmid DNA was incubated with 2 µl restriction enzyme reaction buffer (Promega), 0.2 µl BSA, 0.5 µl *Xba*I (Promega) at 37° C for 60 minutes. This reaction was purified with the peqGOLD MicroSpin Cycle Pure Kit (Peqlab) with one dd$H_2O$ elution (46 µl). The purified DNA was then incubated with 10x NEB restriction enzyme buffer 3 (5 µl) and *Bam*HI-HF (NEB; 1 µl) at 37° C for 10 minutes. The DNA was purified with the peqGOLD MicroSpin Cycle Pure Kit (Peqlab) with one dd$H_2O$ elution (25 µl).

#### 2.6.12.6. Separation and purification of cloned DNA sequences by agarose gel excision

The products of the restriction enzyme digestion reactions were loaded onto a 1.5% (w/v) agarose in TAE buffer and stained with SYBR® Safe DNA gel stain (Invitrogen) at a concentration of 1:10,000 and run at 80V until the marker dye had travelled approximately two thirds of the total length of the gel. They were visualised for less than 10 seconds under UV illumination and the bands corresponding to the sizes of the released insert was excised with a sterile scalpel blade. The peqGOLD Gel Extraction Kit (Peqlab) was used to release the DNA fragments from the agarose gel, following the manufacturer's protocol, with one dd$H_2O$ elution (30 µl).

### 2.6.12.7. Linearisation of pET-9a by restriction enzyme digestion

Expression plasmid vector pET-9a was digested with restriction enzymes, leaving compatible staggered cuts with the overhangs generated in the insert released from the recombinant plasmids pCR2.1-CTX-M499 and pCR2.1-CTX-M516. To generate a suitable linearised vector for the ligation of *bla*$_{\text{CTX-M-15}}$ cloned from pEK499, pET-9a was digested under the following conditions: approximately 1 µg of plasmid DNA was incubated with buffer 3.1 (5 µl) (NEB), BSA (0.5 µl), *Bam*HI-HF® (1 µl) (NEB), *Nde*I (1 µl) (NEB) and dd$H_2O$ to a final reaction volume of 50 µl, at 37° C for 60 minutes. The DNA was purified with the peqGOLD MicroSpin Cycle Pure Kit (Peqlab) with one dd$H_2O$ elution (20 µl).

To provide a compatible backbone for the region amplified from pEK516, pET-9a was digested under the following conditions: plasmid DNA (approximately 1 µg) was incubated with restriction enzyme reaction buffer (2 µl) (Promega), BSA (0.2 µl), *Xba*I (Promega; 0.5 µl) at 37° C for 60 minutes. This reaction was purified with the peqGOLD MicroSpin Cycle Pure Kit (Peqlab) with one dd$H_2O$ elution (46 µl). The purified DNA was then incubated with 10x NEB restriction enzyme buffer 3 (5 µl) and *Bam*HI-HF (1 µl; NEB) at 37° C for 10 minutes. The DNA was purified with the peqGOLD MicroSpin Cycle Pure Kit (Peqlab) with one dd$H_2O$ elution (25 µl).

The digested plasmids were verified for size and purity by agarose gel electrophoresis, and concentration determined by spectrophotometry using a NanoDrop™ 1000 Spectrophotometer (Thermo Fisher Scientific).

#### 2.6.12.8. Ligation of *bla*$_{CTX-M-15}$ and upstream insertional elements with linearised pET-9a expression vector

Gel purified inserts and the linearised vector backbone pET-9a were ligated using the Quick Ligation™ Kit (NEB) under the following conditions: gel purified insert DNA (approximately 50 ng) was incubated with linearised vector backbone pET-9a (between 25 and 100 ng), $dH_2O$ to 10 µl, 2x Quick Ligation Buffer (2 µl), Quick T4 DNA Ligase (1 µl). This reaction mixture was incubated at 25° C for 5 minutes and then chilled on ice. The recombinant plasmids were designated pJBRCTX499 and pJBRCTX516.

#### 2.6.12.9. Screening of recombinant plasmid for successful insertion of cloned region

*E. coli* strains harbouring pJBRCTX499 and pJBRCTX516 were cultured overnight on LB agar supplemented with CTX (final concentration: 2 µg/ml) and KAN (40 µg/ml) at 37° C. Multiple single colonies of each transformant were selected and cultured separately in LB (10 ml) with CTX (1 µg/ml) at 37° C with shaking at 200 rpm until culture growth, measured by spectrophotometry at a wavelength of 600 nm, reached an optical density of 0.6. Plasmids were extracted and purified using the peqGOLD Plasmid Miniprep Kit (Peqlab). They were screened for successful incorporation of the inserted sequence by 3 methods:

1. pJBRCTX516 was digested with the restriction enzymes *Bam*HI and *Xba*I under typical conditions, and analysed for size by agarose gel electrophoresis. pJBRCTX499 was digested with the restriction enzymes *Bam*HI and *Nde*I under typical conditions, and analysed by agarose gel electrophoresis.
2. Plasmids were screened by PCR under typical conditions, using T7-forward and T7-reverse primers (Table 2-6) to amplify the plasmid region between the T7

promoter and T7 terminator, corresponding to the DNA ligated into the vector. The amplicons were analysed for size by agarose gel electrophoresis.

3. The plasmids were sequenced (APHA sequencing dept) using the dideoxy chain termination / cycle sequencing method using CTX-M-SEQ primers (Table 2-6).

#### 2.6.12.10. Site-directed mutagenesis

To correct a point mutation discovered in pJBRCTX499 the GENEART® Site-Directed Mutagenesis System (Invitrogen) was used. Primers were designed containing the corrected mutation in a central position, 100% complementary with no overhangs (Table 2-7). Both primers were 31 nucleotides in length. The reaction mixture was prepared as follows: 10x AccuPrime™ *Pfx* reaction mix (5 µl), 10x enhancer (5 µl), 10 µM forward primer (1.5 µl), 10 µM reverse primer (1.5 µl), DNA methylase (4 U/µl, 1 µl), 25x SAM (2 µl), AccuPrime™ Pfx (2.5 U/µl, 0.4 µl), plasmid DNA (approximately 20 ng), dd$H_2O$ to a final volume of 50 µl. The PCR methylation and mutagenesis reaction took place under the PCR conditions shown in Table 2-10.

Table 2-10. SDM mutagenesis PCR conditions.

| **Iterations** | **Temperature** | **Time** |
|---|---|---|
| **Throughout** | Heat Lid 100° C | - |
| **Once** | 37° C | 15 minutes |
| **Once** | 94° C | 2 minutes |
| **Loop (15x)** | 94° C | 20 seconds |
| | 57° C | 30 seconds |
| **End Loop** | 68° C | 20 minutes |
| **Once** | 68° C | 5 minutes |
| **Forever** | 4° C | ∞ |

The recombination reaction mixture was prepared as follows: 5x reaction buffer (4 µl), ddH2O (10 µl), PCR reaction (4 µl), 10x enzyme mix (2 µl). This reaction was incubated at 20° C for 10 minutes, and then placed on ice. The reaction was used to transform DH5α™-T1® using typical heat shock transformation conditions.

### 2.6.12.11. Screening for successful site-directed mutagenesis

Colonies from an overnight culture were selected and plasmids extracted using the peqGOLD Plasmid Miniprep Kit. A 164 bp section surrounding the mutation site was amplified by PCR under typical conditions using primers SDM-SCREEN-Forward and SDM-SCREEN-Reverse (Table 2-7). The amplified section was digested with the restriction enzyme *Cvi*KI-1 (NEB): approximately 1 µg DNA, 10x CutSmart buffer (5 µl), restriction enzyme (2 µl) and dd$H_2O$ to a final volume of 50 µl. The digestion reaction was incubated at 37° C for 60 minutes and loaded onto an agarose gel prepared with approximately 2.0% (w/v) agarose in TBE buffer (Tris-borate-EDTA) and stained with ethidium bromide at a concentration of 1:10,000. The samples were run at 80V until the dye marker had travelled a distance to indicate sufficient separation. DNA fragments were visualised using a Syngene GeneGenius UV Transilluminator (Syngene). A 100 bp (Promega) DNA marker ladder was used to estimate fragment sizes.

### 2.6.13. Transformation of *E. coli* with plasmid DNA by heat shock

Chemically competent *E. coli* strain, NEB DH5α™ (NEB), was typically used for transformations, although other similar commercially obtained chemically competent strains, such as DH5α™-T1® (NEB) or One Shot® INVαF' (Invitrogen) were often substituted. The manufacturer's (NEB) high efficiency transformation protocol was followed. Cells were stored at -80° C until required and thawed on ice for 10 minutes.

Approximately 10 - 50 ng purified plasmid DNA (estimated from agarose gel band intensity or spectrophotometry) was mixed with 50 µl of chemically competent cells and incubated on ice for 30 minutes. They were then heat-shocked at 42° C for exactly 30 seconds and returned to ice for 5 minutes. 950 µl room temperature super optimal broth with catabolite repression (SOC) medium was added and incubated at 37° C for 1 hour with rotation at 200 rpm. In a deviation from the protocol, the cells were then concentrated by centrifugation and resuspended in 100 µl LB medium and plated onto room temperature LB agar supplemented with selective antibiotics, and incubated at 37° C overnight until colonies were evident.

### 2.6.14. Preparation of electrocompetent AS19

Typically, AS19 was cultured in LB until mid-log phase (O.D. $_{600\ nm}$ = 0.3 - 0.6). All tubes, cuvettes and solutions were pre-chilled on ice. Aliquots (1 ml) were chilled on ice for 10 - 15 minutes. The aliquots were centrifuged for 2 minutes at 13,000 rpm in a bench top micro-centrifuge and each aliquot resuspended in 1 ml 10% glycerol solution. The centrifugation step was repeated and the cells were resuspended in 500 µl 10% glycerol. The centrifugation step was repeated and the cells were resuspended in 100 µl 10% glycerol.

### 2.6.15. Transformation of AS19 with plasmid DNA by electroporation

Aliquots (100 µl) of electrocompetent AS19 were mixed with 50 - 200 ng pre-chilled plasmid DNA, and transferred to Gene Pulser® 0.1 cm electrode cuvettes (Bio-Rad, Herts, UK). Mixtures were pulsed at 1.8kV, 25 µF, 200 ohms in a Bio-Rad Gene Pulser (Bio-Rad). Pre-warmed SOC (900 µl; 37° C) was added to the mixture and incubated for 30 minutes. They were then diluted and recovered onto LB agar supplemented with appropriate antibiotics for selection of successful transformants. They were incubated

overnight at 37° C and single colonies selected and screened for successful transformation by plasmid extraction followed by PCR characterisation of the plasmid, restriction enzyme digestion and sequencing.

### 2.6.16. Assay for the quantification of protein expression in *E. coli*

To determine the protein concentration of microbial supernatant extracts, the following assay was used. Working standards of BSA of 1, 0.5, 0.25, 0.1, 0.05 and 0 mg/ml BSA were prepared. In duplicate, 250 µl of each standard and each test sample was incubated with Bradford reagent (1 ml) for not more than 30 minutes. The optical densities of the reactions were then measured at 600 nm and the protein concentration of the test samples established by reference to the standard curve, interpolated by Prism® 6 software (GraphPad).

### 2.6.17. Nitrocefin based colourimetric assay for β-lactamase activity quantification

*E. coli* strains were typically cultured from frozen glycerol stocks until early log phase (O.D. $_{600\ nm}$ = 0.1 – 0.2) was reached. Cultures were split into equal aliquots and supplements or growth media added where required. The aliquots were cultured for pre-determined times and cells were disrupted by bead milling. Supernatants were separated by centrifugation and samples added to wells in a 96-well microtiter plate pre-prepared with nitrocefin solution. Optical density measurements were taken at a light wavelength of 492 nm approximately every 30 seconds over 30 – 60 minutes. Rates of nitrocefin hydrolysis were calibrated using a standard curve constructed from dilutions of the commercial purified β-lactamase M02075 (Fluorochem, Derb, UK).

### 2.6.18. Reverse-phase HPLC assay for the quantification of cefotaxime in solution

The reverse-phase HPLC (RP-HPLC) method was adapted from Nemutlu *et al.* for the detection of cefotaxime and other cephalosporins [161]. RP-HPLC was performed using an Xterra C18 (250 mm x 4.6 mm, 5 µm i.d.) column using Agilent Technologies 1100 series liquid chromatography system comprising of automated solvent delivery, sampler and array detector system. Analysis and quantification of cefotaxime was performed with ChemStation software (Agilent Technologies). Standard calibration curves were constructed using cefotaxime dilutions (typically 1 – 400 µg/ml). Cefotaxime dilutions were prepared using MHB, dd$H_2O$ or LB. Analysis was performed with ChemStation software (Agilent Technologies) which generated a graphical visualisation of a single peak representing cefotaxime quantity. Standards were prepared and quantified for each study from the same cefotaxime stock used, and diluted in the carrier medium used in the study. Cefotaxime amounts in test samples were quantified with reference to reported size of the area under the resolved curve calibrated against the standard curve.

Chromatographic conditions were as follows: phosphate buffer (sodium dihydrogen orthophosphate dihydrate 40 mM; pH 3.2) was mixed with MeOH during automated analysis with a gradient pump to the following amounts (MeOH: Phosphate buffer) ; t=0 mins 18:82%, t=5 mins 18:82%; t= 15 mins 45:55%; t=16 mins 55:45%; t= 21 mins 55:45 %; t=22 mins 18: 82%; t = 30 next injection at a flow rate of 0.85 ml/min, with an injection volume of 25 µl per sample. Cefotaxime was detected at a light wavelength of 254 nm.

### 2.6.19. Cell-free *bla*$_{CTX-M}$ inhibition studies by antisense agents in a translation/transcription coupled system

The Expressway™ Mini Cell-Free Expression System (Invitrogen) was used for all cell free inhibition studies. This system utilised a translation/transcription coupled reaction to produce active proteins from naked linear or circular DNA. The system contained *E. coli* extract and amino acids to provide the translation machinery to express proteins, and T7 RNA polymerase. The use of viral polymerase required the incorporation of a T7 promoter in the template DNA. A T7 terminator is also desirable downstream of the gene to be expressed to facilitate the release of the T7 polymerase.

The manufacturer's supplied protocol was followed; briefly, a reaction master mix was made up in a 1.5 ml reaction tube consisting of the manufacturer's supplied reagents: *E. coli* SlyD- extract (20 µl), 2.5x IVPS *E. coli* buffer without amino acids (20 µl), 50mM amino acids minus methionine (1.25 µl), 70mM methionine (1 µl), T7 enzyme mix (1 µl) and plasmid DNA (500-1000 ng). The reaction was incubated at 30° C with rotation at 300rpm for 30 minutes. After 30 minutes, a feed buffer was added comprising of: 2x IVPS feed buffer (25 µl), 50 mM amino acids minus methionine (1.25 µl), 70 mM methionine (1 µl), and nuclease free water to a final volume of 100 µl. This reaction was continued at 30° C with 300 rpm rotation for 3 - 5 hours and then rapidly chilled on ice.

### 2.6.20. Evaluation of the effects of β-lactamase activity inhibition by antisense agents in AS19 *E. coli* transformants by growth curves produced by spectrophotometry

AS19 transformed with recombinant plasmid carrying *bla*$_{CTX-M-15}$ was cultured overnight at 37° C in a shaking incubator from frozen glycerol/bead stocks in MHB

(Mueller-Hinton Broth) supplemented with CTX (2 µg/ml). The next morning, the culture was used to inoculate fresh MHB (10 ml) supplemented with CTX (final concentration 2 µg/ml) and cultured until early to mid-log phase was observed (O.D. $_{600\ nm}$ = 0.1 - 0.3). Cells were separated from their growth medium by centrifugation at 13,000 rpm in a Heraeus™ Biofuge™ centrifuge (Thermo Fisher Scientific) and resuspended in fresh MHB media. The cell suspension was diluted to achieve a concentration of 100,000 CFU/ml. The cell culture was diluted 1:10 in MHB and 10 – 30 µl were cultured overnight on LB agar at 37° C to verify CFU/ml. Aliquots (50 µl) were added to wells of a 96-well microtiter plate (Falcon) in duplicate. Growth medium (50 µl) was transferred to each well, comprising of MHB supplemented with CTX and antisense inhibitory agents where appropriate. The plate was transferred to a Fluostar Optima (BMG Labtech) automated spectrophotometer, controlled at 37° C, and optical density readings taken over 18-24 hours. The culture turbidity, measured at O.D. $_{600\ nm,}$ was recorded over 250 cycles, with 15 flashes per well per cycle approximately every 5 minutes, the plate was rotated at 220 rpm for 6 seconds every cycle. Growth curves and statistical analyses were produced using Prism® 6 software (GraphPad).

### 2.6.21. Evaluation of the effects of β-lactamase expression inhibition by antisense agents in field and clinical isolates by growth curves produced by spectrophotometry

Typically, strains were cultured from either a single colony from an overnight culture grown on LB agar supplemented with CTX (final concentration 2 µg/ml) at 37° C, or from glycerol bead stocks, in 10 ml MHB supplemented with CTX at 37° C with shaking at 200 rpm until optical density measured at a light wavelength of 600 nm reached 0.1 - 0.3. Calibration curves had previously been constructed for each strain to

establish a linear correlation between culture turbidity measured at O.D. $_{600\ nm}$, and colony forming units in this range. The culture was diluted in fresh MHB to yield approximately 100,000 CFU/ml. The cell culture was diluted 1:10 in MHB and 10 – 30 µl were cultured overnight on LB agar at 37° C to verify CFU/ml. Aliquots (50 µl) were added to wells of a 96-well plate (Falcon) in duplicate. Growth medium (50 µl) was transferred to each well, comprising of MHB supplemented with CTX and antisense agents where appropriate. The plate was transferred to a Fluostar Optima (BMG Labtech) automated spectrophotometer, controlled at 37° C, and optical density readings taken over 18 - 24 hours. Culture turbidity was measured at O.D. $_{600\ nm}$ over 250 cycles, with 15 flashes per well per cycle followed by shaking (6 seconds; 220rpm) approximately every 5 minutes. Growth curves and statistical analyses were produced using Prism® 6 software (GraphPad).

### 2.6.22. Controls used in the evaluation of inhibition of β-lactamase activity inhibition by unmodified and peptide-conjugated PNA4/PMO1

Specificity and any inherent toxicity of peptide-conjugated and unmodified PNA4 and PMO1 were demonstrated in the following studies. A scrambled non-specific 25-mer PMO was incubated in the presence of pJBRCTX516 in a cell-free translation/transcription coupled system followed by the quantification of cefotaximase activity. AS19/pJBRCTX516 was cultured in the presence of the scrambled PMO in the presence and absence of CTX and growth measured by spectrophotometry over 18 – 24 hours. Field isolates harbouring *bla*$_{\text{CTX-M-group 1}}$ were cultured in the presence of P-PMO1 or P-PNA4 in the absence of CTX and growth measured by spectrophotometry over 18 – 24 hours. Field isolate LREC90 harbouring *bla*$_{\text{CTX-M-14}}$ (non-complementary with anti-*bla*$_{\text{CTX-M-15}}$ PNA4 and PMO1) was cultured in the presence and absence of P-PNA4, P-PMO1 and CTX, and growth measured by spectrophotometry over

18 - 24 hours. Minimum inhibitory concentrations (CTX) were established for LREC90 in the presence and absence of P-PNA4.

### 2.6.23. Evaluation of bactericidal effects of P-PNA4 on *E. coli* field isolate LREC525 cultures

Field isolate LREC525 harbouring *bla*$_{\text{CTX-M-15}}$ was cultured from glycerol stocks in MHB (5 ml) supplemented with cefotaxime (final concentration 2 µg/ml), until early-mid log phase (O.D. $_{600\ nm}$ = 0.2 - 0.3). Four aliquots of 92 µl cell suspension were taken and made up to 100 µl with supplements or carrier medium to yield the following combinations: a) no P-PNA4 or CTX; b) CTX (48 µg/ml); c) P-PNA4 (3.2 µM); and d) P-PNA4 (3.2 µM) and CTX (48 µg/ml). The aliquots were incubated at 37° C with shaking (200 rpm) and 10 µl samples removed approximately every 10 minutes. The samples were diluted between 10,000 and 100,000 fold and 10 µl was spread onto LB agar plates and cultured overnight at 37° C. The next day, visible colonies were counted.

### 2.6.24. Quantification of CTX induced β-lactamase expression upregulation by colourimetric nitrocefin based assay

AS19/pJBRCTX516 was cultured overnight at 37° C with shaking at 200 rpm from frozen glycerol/bead stocks in MHB supplemented with CTX (2 µg/ml) and KAN (40 µg/ml) until early log phase (O.D. $_{600\ nm}$ = 0.1) was reached. The culture was diluted 1:500 and split into 5 equal (7.5 ml) aliquots. Each aliquot was cultured in the presence of CTX (final concentrations = 0, 2, 16, 32 and 64 µg/ml) and cultured at 37° C. Aliquots (2 ml) were removed at 60 minute intervals and the optical density at a wavelength of 600 nm was recorded. Bacterial cells were collected by centrifugation at 13,000 rpm in a Heraeus™ Biofuge™ centrifuge (Thermo Fisher Scientific) and the

supernatant retained. In a 96-well microtiter plate (Falcon), aliquots of each supernatant (20 µl) were added to dd$H_2O$ and nitrocefin solution (20 µl x 1 mM) to yield a final volume of 100 µl and nitrocefin final concentration of 200 µM. Each culture was prepared in duplicate. The 96-well plate was transferred to a Fluostar Optima (BMG Labtech) automated spectrophotometer, controlled at 37° C, and optical density readings taken over 60 minutes at O.D. $_{492\ nm}$, with 15 flashes per well per cycle (250 cycles in total), and rapid rotation (220 rpm) for 5 seconds every cycle, approximately every 30 seconds.

### 2.6.25. Quantification of cefotaxime induced β-lactamase activity upregulation in AS19/pJBRCTX516 by RP-HPLC

*E. coli* strain AS19/pJBRCTX516 was cultured in MHB (100 ml) from frozen glycerol/bead stocks until early log phase (O.D. $_{600\ nm}$ = 0.1 - 0.2) was reached. The culture was diluted 1:500 in fresh MHB and split into 5 equal (20 ml) aliquots. Each aliquot was supplemented with CTX, or carrier medium, to achieve the following final concentrations: 0, 2, 16, 32 and 64 µg/ml and incubated at 37° C. At approximately 1 hour intervals, culture growth was measured by spectrophotometry and aliquots (1 ml) were removed. The acidity of each aliquot was increased to pH 2.2 by the addition of 1M HCl (85 µl) to halt enzymatic activity. The cells were then centrifuged at 10,000 g for 2 minutes and the supernatant collected. Supernatant (700 µl) was then incubated at 37$^o$ C with 700 µl cefotaxime (800 µg/ml) with shaking at 200 rpm. Aliquots (125 µl) were removed at 10 - 20 minute time intervals and added to pre-prepared HPLC vials containing 125 µl phosphate buffer/ HCl, pH 2.2. The cefotaxime degradation, correlating with β-lactamase expression levels, was quantified by RP-HPLC.

### 2.6.26. Quantification of ceftriaxone induced β-lactamase activity upregulation by RP-HPLC

*E. coli* strains were cultured overnight in MHB (50 ml) from frozen glycerol/bead stocks until early log phase (O.D. $_{600\,nm}$ = 0.1 - 0.2) was reached. Aliquots (2 ml) were removed from the culture and incubated with increasing final concentrations of ceftriaxone (0 – 384 µg/ml) for 30 minutes at 37° C with shaking at 200 rpm. Cells were disrupted by bead milling in a Retsch Mixer MM301 shaking homogeniser (F. Kurt Retsch GmbH, Haan, Germany) at full speed for 5 minutes with 0.2 - 0.4 mm glass beads. The cells were then centrifuged at 10,000 g for 2 minutes and the supernatant collected. 700 µl supernatant was then incubated at 37º C with 700 µl cefotaxime (800 µg/ml) with shaking at 200 rpm. 125 µl aliquots were removed at 10 - 20 minute time intervals and added to pre-prepared HPLC vials containing 125 µl phosphate buffer/ HCl, pH2.2. The cefotaxime degradation, and hence β-lactamase activity, was quantified by HPLC.

### 2.6.27. Assembly of 3D DNA tetrahedron

In a method adapted from Pei *et al.*[168], single stranded DNA oligonucleotides were mixed with either a 13-mer PNA or a 25-mer PMO antisense oligomer in equimolar amounts in a 20 mM Tris, 50 mM $MgCl_2$, annealing buffer (pH 8.0). The mixture was heated to 95° C for 4 minutes and immediately transferred to ice for 30 minutes. Assembly of the tetrahedron was verified by gel electrophoresis.

### 2.6.28. Verification of assembly of DNA tetrahedral antisense oligomer delivery vehicle by gel electrophoresis

Assembly of the tetrahedron was verified on a 2% w/v TBE gel, and 100V applied until sufficient separation was observed. Individual DNA strands, and combinations of

strands: strand A + B, strand A + B + C, strand A + B + C + D and strand A + B + C + D + PMO/PNA4, were visualised on a gel, and single discreet bands of increasing size were regarded as evidence of successful annealing and complete tetrahedron formation.

### 2.6.29. Statistical analysis

All results are presented as standard deviations of the mean. Comparisons between treatment group growth means were performed using an unpaired two-tailed t-test by GraphPad Prism software version 6.01 (GraphPad Software, Inc.), not assuming equal standard deviations and using Welch's correction, as used by Geller *et al.* [127]. All other statistical comparisons were made using a Wilcoxon signed-rank non-parametric test (GraphPad Software, Inc.). A p-value of less than 0.05 was taken to represent statistical significance.

### 2.6.30. Determination of synergistic relationship between inhibitory agents

The fractional inhibitory concentration index (FICI) is commonly used to determine a synergistic, antagonistic or neutral interaction between inhibitory compounds. In the current study it was defined as: MIC of the combination of CTX and antisense oligomer/MIC of CTX alone + MIC of the combination of CTX and antisense oligomer/MIC of antisense oligomer alone:

$$\text{FICI} = \frac{\text{MIC of CTX/antisense oligonucleotide combination}}{\text{MIC of CTX alone}} + \frac{\text{MIC of CTX/antisense oligonucleotide combination}}{\text{MIC of antisense oligonucleotide alone}}$$

The FICI was interpreted as: less than or equal to 0.5: synergistic, between 0.5 and 1: no synergy (additive), greater than 1: antagonistic [169].

# Chapter 3.

# Development of assays for the quantification of β-lactamase CTX-M activity

## 3.1. Introduction

Methods for quantifying β-lactamase were required to assess the effect of antisense/antigene agents on β-lactamase activity in *E. coli* strains. The current study established two assays for this purpose: a colourimetric nitrocefin based assay, and an HPLC assay to quantify the degradation of cefotaxime. These assays both indirectly measured β-lactamase expression levels by determining enzyme activity based on the quantification of a β-lactamase substrate. Assays were validated to ensure the reaction was linear with time and enzyme concentration under saturating substrate concentrations. The substrates, nitrocefin and cefotaxime, used in the colourimetric and HPLC assays respectively, were both shown to have a practical relationship with β-lactamase levels and, as such, were suitable for its quantification. These assays enabled an evaluation of the efficacy of downstream β-lactamase inhibition studies.

### 3.1.1. Nitrocefin based colourimetric assay for β-lactamase activity quantification

The chromogenic cephalosporin nitrocefin is a commonly and routinely used reporter substrate for β-lactamase activity. Nitrocefin undergoes a colour change reaction from yellow ($\lambda_{max}$ = 390 nm), to red ($\lambda_{max}$ = 480 nm) when hydrolysed by β-lactamase in a rapid reaction [170]. It is inexpensive and quantifiable, however it is hydrolysed by all four Ambler classes of β-lactamases and as such, not specific to any one β-lactamase – multiple β-lactamase enzyme variants affect the colour change reaction. For inhibition studies of β-lactamase produced by artificially constructed plasmids harbouring a single *bla*$_{\text{CTX-M-15}}$ with no other β-lactamase-producing genes present, this was a suitable

substrate. Field isolates however, frequently harbour multiple β-lactamase variants, requiring an alternative β-lactamase detection assay specific for the enzyme in these situations.

Typically, a 96-well plate format was used for the quantification of nitrocefin degradation measured by spectrophotometry at a wavelength of 492 nm, the endpoint of the colour-change reaction. In the first instance, the operational range of the colourimetric assay and the proportional relationship between β-lactamase quantity and nitrocefin reaction was ascertained using commercially available and purified β-lactamase, M02075 (Fluorochem, Derb, UK). M02075 was isolated and purified from *Bacillus cereus*.

To establish the operational range of the assay, the minimum detection levels, saturating concentrations and reaction times, a range of concentrations of nitrocefin and a range of β-lactamase concentrations were incubated in the presence of nitrocefin and the reaction monitored by optical density measurement in an automated spectrophotometer at a wavelength of 492 nm. M02075 and supernatant extracts obtained from a panel of β-lactamase producing strains of *E .coli* were used to establish typical reaction rates and assay ranges.

*E. coli* strains were typically cultured from frozen glycerol stocks until early log phase (O.D. $_{600\ nm}$ = 0.1 – 0.2) was reached. Cultures were split into equal aliquots and supplements or growth media added where required. The aliquots were cultured for pre-determined times and cells were disrupted by bead milling. Supernatants were separated by centrifugation and samples added to wells in a 96-well plate pre-prepared with nitrocefin solution. Optical density measurements were taken at 492 nm approximately every 30 seconds over 30 – 60 minutes.

### 3.1.2. Quantification of cefotaxime as a marker for β-lactamase activity by RP-HPLC

Reverse-phase high-pressure liquid chromatography (RP-HPLC) was used to separate and detect cefotaxime from degradation products. These fractions were identified by their retention time, and quantified as they exited the column by UV-vis spectrophotometry. An assay was established for the specific quantification of cefotaxime, adapted from Nemutlu *et al.* [161], as the reporter substrate for *bla*$_{\text{CTX-M}}$ activity. This was found to be highly sensitive with CTX detection limits ranging from around 1 µg/ml to greater than 800 µg/ml, making this a suitable assay for the specific quantification of *bla*$_{\text{CTX-M}}$ activity. Typically strains were cultured from glycerol stocks until early log phase (O.D. $_{600\ \text{nm}}$ = 0.1- 0.2) was reached. The culture was diluted and supplements, or an equivalent volume of supplement carrier solvent for experimental control, added where required. The cultures were incubated for pre-determined amounts of time and aliquots were transferred to solid agar and cultured overnight to establish the number of colony-forming units present in each sample. Cells were disrupted by bead milling and cell debris separated by centrifugation. Supernatants were removed and aliquots were transferred to a cefotaxime solution (typically yielding a final concentration of 400 µg/ml) and incubated at 37 °C. Samples were removed at regular time intervals and transferred to HPLC vials containing phosphate buffer (pH 2.2). Cefotaxime in solution was quantified by RP-HPLC. A standard calibration curve was constructed using cefotaxime dilutions (typically 1 – 400 µg/ml) for each study. Analysis was performed with ChemStation software (Agilent Technologies) which generated a graphical visualisation of a single peak representing cefotaxime quantity (Figure 3-1). Cefotaxime was quantified by the reported size of the area under the resolved curve, and calibrated with reference to a standard curve.

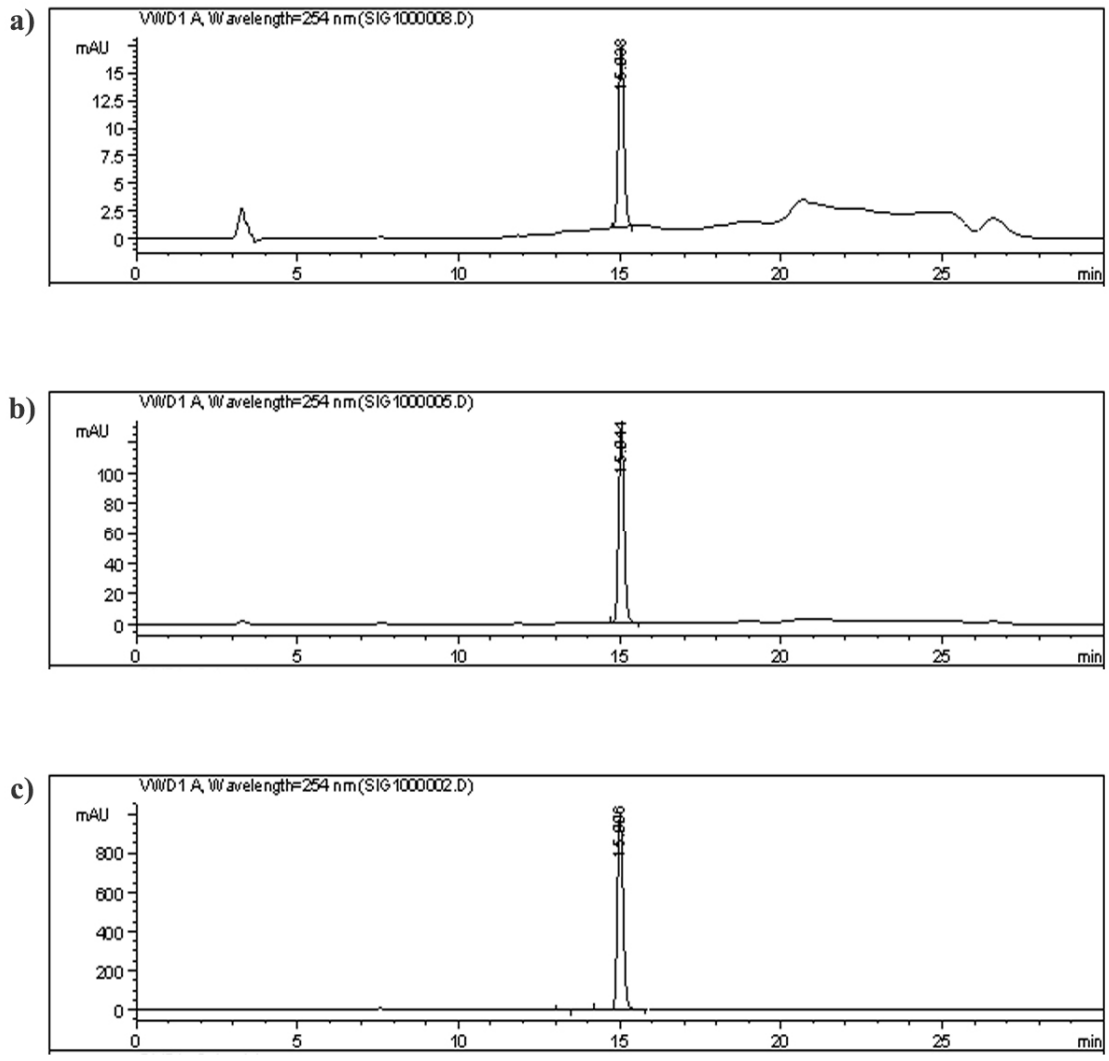


Figure 3-1. Sample chromatograms each showing a single resolved peak representing cefotaxime with a retention time of approximately 15 minutes.
**a)** Cefotaxime concentration = 3.125 µg/ml, **b)** cefotaxime concentration = 25 µg/ml, **c)** cefotaxime concentration = 200 µg/ml.

The optimum pH for β-lactamase activity has been shown to be in the range of pH 7.0 - 7.2 (Figure 3-2). Experimentation with methods of inactivating β-lactamase activity was undertaken in the current study including heat inactivation and the adjustment of the acidity/alkalinity of the incubation solution. The activity of

β-lactamase was completely inhibited in conditions of low pH (< 3) and high pH (> 10). To halt enzymatic reactions at specific time points for a determination of β-lactamase activity, solutions were treated with HCl (1 M) sufficient to yield an increase in acidity to pH 2.2.

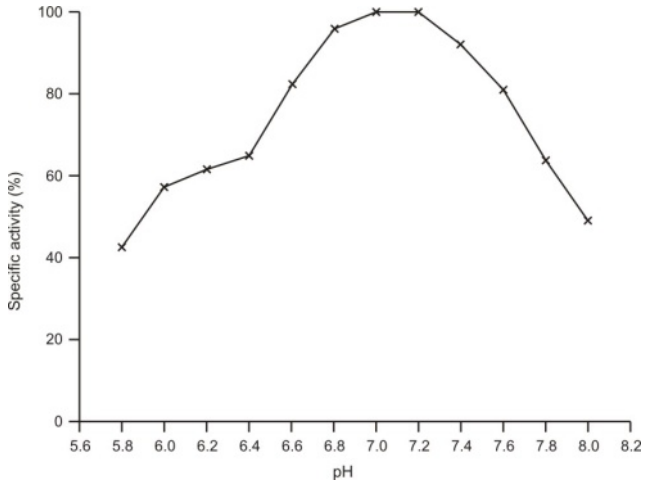


Figure 3-2. Operational pH range of β-lactamase [171].

## 3.2. Results

### 3.2.1. Nitrocefin based colourimetric assay validation for β-lactamase quantification

The nitrocefin 96-well plate assay was validated and the operational detection ranges established by two methods. Supernatant extracts were prepared as previously described and diluted 1 to 256-fold. Commercial β-lactamase M02075 (concentration: 5 units/ml) was also diluted 1 – 256-fold. 50 µl of each supernatant / M02075 dilution was added to 200 µl nitrocefin solution (final concentration 190 µM) and the reaction monitored at O.D. $_{492\ nm}$ (Figure 3-3). Results showed a dose dependant response to enzyme concentration.

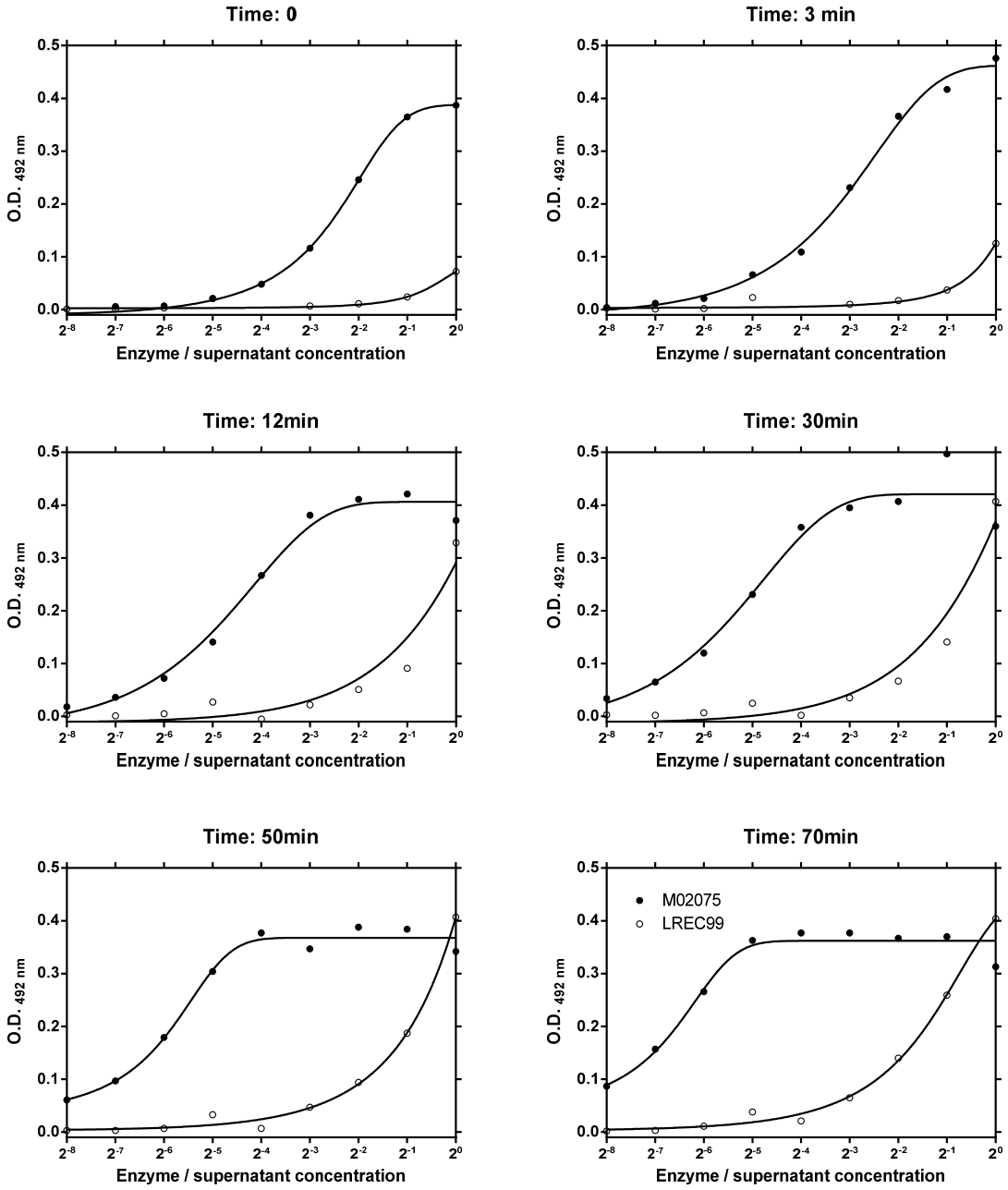


Figure 3-3. Nitrocefin reaction (final concentration 190 μM) with commercial β-lactamase M02075 and supernatant extract dilutions originating from *E. coli* strain LREC99 harbouring *bla*$_{\text{CTX-M-15}}$.

Filled circles (●) denote M02075, concentration: $2^0$ = 5 units/ml, hollow circles (○) denote LREC99, concentration: $2^0$ = supernatant used neat.

Supernatant dilutions were prepared, as previously described, from a panel of five *E .coli* strains (AS19/pJBRCTX499, 21/C0188/02/13, 12/B0118/10/11, NCTC10418 and LREC99). Supernatant dilutions and commercial β-lactamase M02075 dilutions (100 µl) were each added to nitrocefin solution (final concentration 200 µM) in separate incubations (final volumes of 250 µl), and the reaction monitored by spectrophotometry over 2 hours at a wavelength of 492 nm (Figure 3-4; Figure 3-5; Figure 3-6). Results showed a dose dependant response to enzyme concentration.

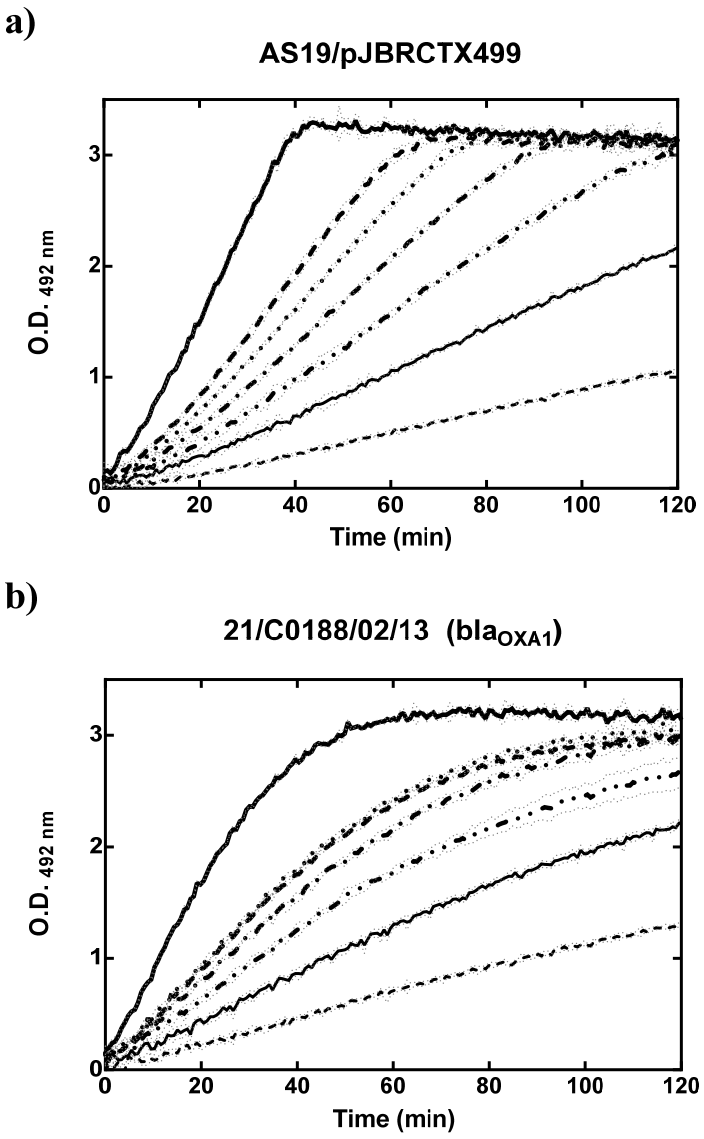


Figure 3-4. Nitrocefin reaction with *E. coli* strains AS19/pJBRCTX499 and 21/C0188/02/13 supernatant extract dilutions.

Dilutions: Thick solid line: neat supernatant, thick dashed line: 1.33-fold dilution, thick dotted line: 1.6-fold dilution, thick dash-dot line: 2-fold dilution, thick dash-dot-dot line: 2.66-fold dilution, thin solid line: 4-fold dilution, thin dashed line: 8-fold dilution. **a)** Supernatant preparation dilutions originating from *E. coli* strain AS19/pJBRCTX499 harbouring *bla*$_{CTX\text{-}M\text{-}15}$, **b)** Supernatant preparation dilutions originating from *E. coli* strain 21/C0188/02/13 harbouring *bla*$_{OXA\text{-}1}$. Error bars indicate ± 1 standard deviation (n=3).

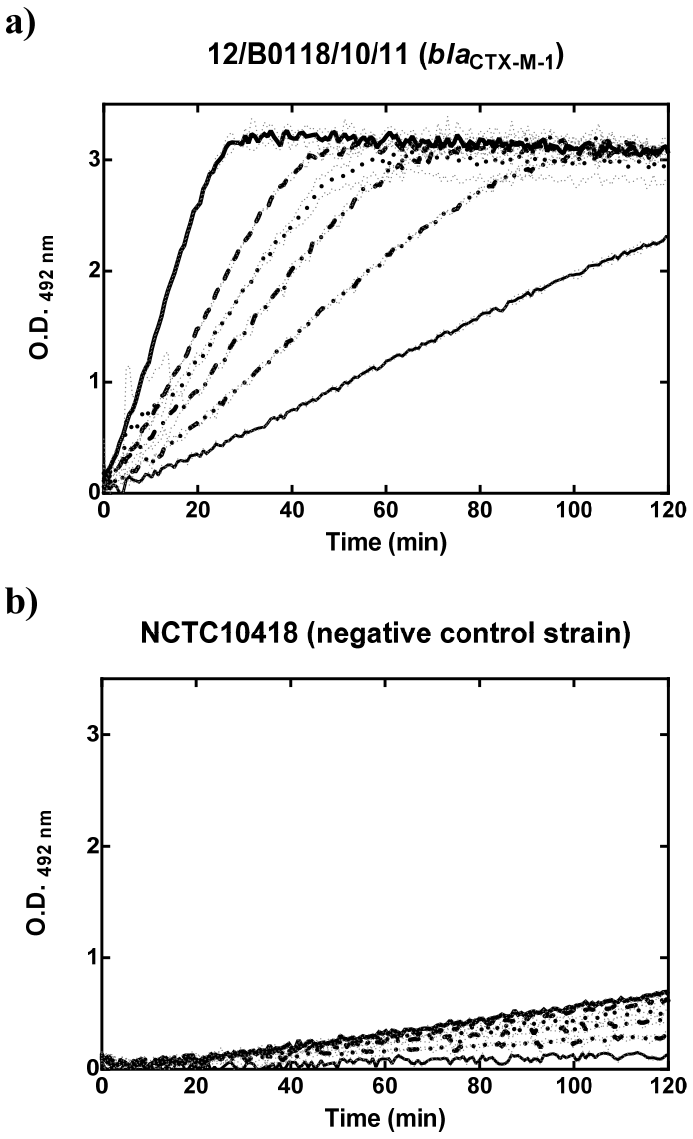


Figure 3-5. Nitrocefin reaction with *E. coli* strains 12/B0118/10/11 and NCTC10418 supernatant extract dilutions.

Dilutions: thick solid line: neat supernatant, thick dashed line: 1.6-fold dilution, thick dotted line: 2-fold dilution, thick dash-dot line: 2.66-fold dilution, thick dash-dot-dot line: 4-fold dilution, thin solid line: 4-fold dilution. **a)** Supernatant preparation dilutions originating from *E. coli* strain 12/B0118/10/11 harbouring $bla_{\text{CTX-M-1}}$, **b)** Supernatant preparation dilutions originating from *E. coli* strain NCTC10418 (negative control strain). Error bars indicate ± 1 standard deviation (n=2).

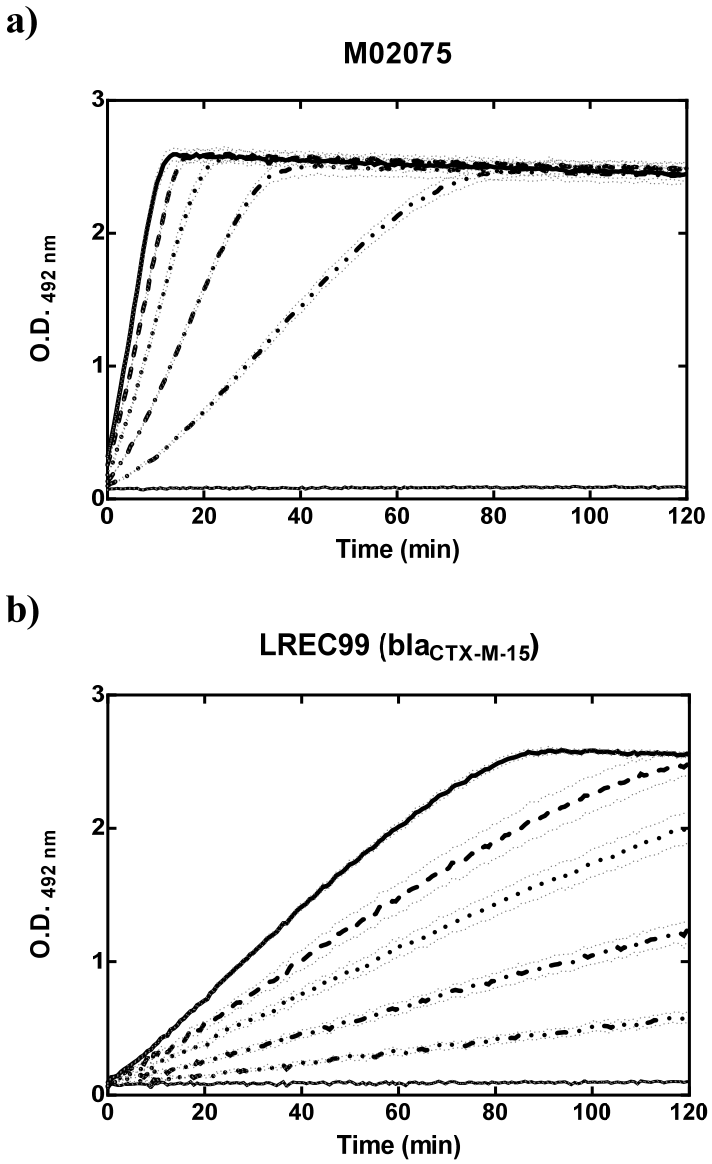


Figure 3-6. Nitrocefin reaction with *E. coli* strain LREC99 supernatant extract dilutions and commercial β-lactamase dilutions.

Dilutions: thick solid line: neat supernatant / commercial β-lactamase preparation, thick dashed line: 1.33-fold dilution, thick dotted line: 2-fold dilution, thick dash-dot line: 4-fold dilution, thick dash-dot-dot line: 10-fold dilution, thin solid line: negative control (growth media only). **a)** Commercial β-lactamase M02075 (5 units/ml), **b)** Supernatant preparation dilutions originating from *E. coli* strain LREC99 harbouring *bla*$_{\text{CTX-M-15}}$. Error bars indicate ± 1 standard deviation (n=2).

## 3.3. High-Pressure Liquid Chromatography

### 3.3.1. Validation of HPLC assay for cefotaxime quantification as a marker for β-lactamase activity

The HPLC assay was validated by quantification of cefotaxime at concentrations ranging from 0.78 µg/ml to 2000 µg/ml (Figure 3-7). The cefotaxime standard curve data presented in Figure 3-7 were accumulated from separate experiments with each experiment consisting of two biological and two procedural replicates for each sample.

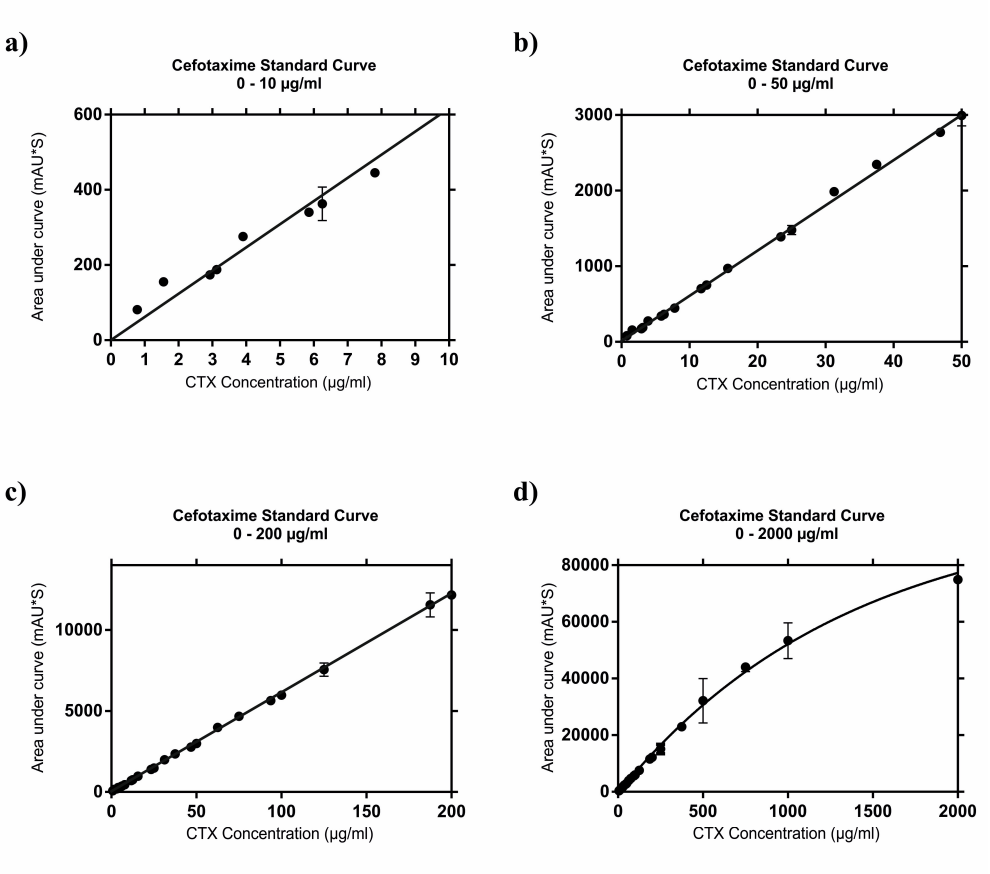


Figure 3-7. Cefotaxime standard curves, quantified by HPLC.
Standard curves were produced by the preparation of CTX dilutions (0.78 - 2000 µg/ml) and HPLC quantification. CTX quantity was determined by the area reported under the resolved peak, generated with ChemStation (Agilent Technologies) software. **a)** CTX 0 – 10 µg/ml, **b)** CTX 0 – 50 µg/ml, **c)** CTX 0 – 200 µg/ml, **d)** CTX 0 – 2000 µg/ml. Error bars indicate ± 1 standard deviation (n=8).

### 3.3.2. Validation of HPLC assay for specific cefotaximase activity

To verify and validate the ability of the HPLC assay to discriminate cefotaximase activity from other β-lactamase activity, supernatant extracts (1.5 ml), prepared from five *E. coli* strains harbouring different β-lactamase variants, were incubated with CTX solution (1.5 ml; 800 µg/ml) and 120 µl aliquots removed at regular intervals between 0 and 65 minutes. Total protein content was quantified (section 2.6.16.) to normalise the results. Results showed supernatant preparations from the two strains harbouring *bla*$_{\text{CTX-M}}$ variants degraded CTX. No significant degradation of CTX was observed in supernatant preparations from strains harbouring *bla*$_{\text{OXA-1,}}$ and *bla*$_{\text{TEM-1.}}$ Supernatant preparations from strain LREC115 harbouring *bla*$_{\text{AMP}}$ demonstrated a small but significant ($P < 0.05$) amount of CTX degradation (Figure 3-8). This was not unexpected as hyper AmpC β-lactamase producers can be confused for extended-spectrum β-lactamases due to over-expression conferring some reduced susceptibility to 3$^{rd}$ generation cephalosporins [66].

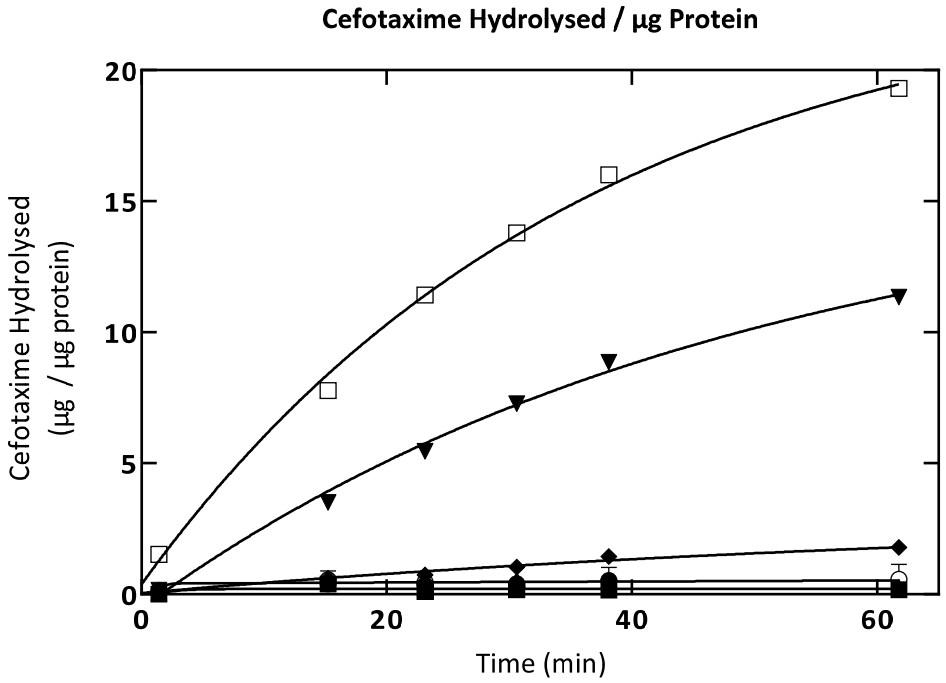


Figure 3-8. Cefotaxime degradation by *E. coli* supernatants from five *E. coli* strains, and commercial β-lactamase M02075.

Filled circles (●) – Blank (HPLC control – growth media only), filled squares (■) – negative control (NCTC10418), triangles (▲) – 21/C0188/02/13 (*bla*$_{\text{OXA-1}}$), down-pointing triangles (▼) – 12/B0118/10/11 (*bla*$_{\text{CTX-M-1}}$), diamonds (♦) – LREC115 (*bla*$_{\text{AMP}}$), hollow circles (○) - 2013-6404 (*bla*$_{\text{TEM-1}}$), hollow squares (□) – AS19/pJBRCTX499(*bla*$_{\text{CTX-M-15}}$). Error bars indicate ± 1 standard deviation (n=2).

### 3.4. Discussion

Both the HPLC and the nitrocefin based assays developed were suitable for the detection and quantification of β-lactamase. Both assays quantified reporter substrates as markers for β-lactamase activity, nitrocefin and CTX, both were sensitive and reproducible. β-Lactamase activity was shown by experiments with the commercial purified β-lactamase M02075 to have a direct proportional relationship with β-lactamase quantity, validating the use of a reporter substrate to determine β-lactamase quantity present.

The nitrocefin based assay was rapid and inexpensive, but the lack of ability to differentiate between β-lactamase variants made it useful only in a single gene environment. The HPLC assay was sensitive to the detection of cefotaxime from less than 1 µg/ml to greater than 800 µg/ml and was highly reproducible. The optimum range for accurate reproducible CTX quantification was observed to be 30 – 500 µg/ml, and the data show a consistently reproducible linear relationship between cefotaxime concentration and peak height / area under the curve in this range. Subsequent studies utilised concentrations within this range. The HPLC assay, quantifying the *bla*$_{\text{CTX-M}}$ substrate (CTX) was a specific and suitable assay for downstream studies evaluating the inhibitory ability of anti-*bla*$_{\text{CTX-M}}$ agents. Standards and quality assurance samples were run with every subsequent study.

# Chapter 4. Design and construction of expression plasmids carrying *bla*$_{\text{CTX-M-15}}$ and the inhibition of β-lactamase expression by PNA/PMO oligomers in a cell free translation-transcription coupled system

## 4.1. Introduction

### 4.1.1. Design and construction of expression plasmids carrying *bla*$_{\text{CTX-M-15}}$ as a suitable test subject for translational inhibition experiments in cell-free translation/transcription coupled systems and in whole cells

β-lactamase resistance genes are most often carried on large (>100 kb) plasmids which commonly harbour multiple copies and different resistance genes, including different β-lactamase classes [74]. Initial proof-of-concept of the efficacy of PNAs and PMOs to inhibit the expression of β-lactamase was required without the inherent confounding factors associated with field and clinical isolates such as, for example cell impermeability, multiple β-lactamase genes, and the presence of functional efflux pumps. This necessitated the construction of a plasmid harbouring *bla*$_{\text{CTX-M-15}}$ which could be used in a cell-free translation/transcription coupled system, and also subsequently used to transform a range of sensitive *E. coli* strains to yield a resistant phenotype with a controlled genotype.

To construct a suitable plasmid, two representative field isolates harbouring *bla*$_{\text{CTX-M-15}}$ were selected, and PCR primers were designed to amplify *bla*$_{\text{CTX-M-15}}$ and associated upstream regions, incorporating restriction enzyme recognition sites to facilitate directional cloning. IS*Ecp*1 harbours at least one *bla*$_{\text{CTX-M-15}}$ promoter [76, 81, 82]. To ensure all native regulatory elements were included in the recombinant plasmid and to ensure that a valid genetic environment was replicated for an evaluation of the

inhibitory potential of the antisense oligomers, *bla*$_{\text{CTX-M-15}}$ and the associated upstream insertional element IS*Ecp*1 was amplified by PCR.

The amplified region, incorporating *bla*$_{\text{CTX-M-15}}$ and upstream regions, were TA cloned into a commercial cloning vector. This was used to transform a chemically competent lab strain which was cultured and the recombinant plasmids extracted. The plasmids were digested with the restriction enzymes recognising the sites incorporated into the PCR primers. DNA fragments were separated and purified by agarose gel excision. A commercially available expression vector, pET-9a, was digested with the restriction enzymes used to release the *bla*$_{\text{CTX-M-15}}$ fragment from the cloning vector, leaving compatible overhanging DNA ends, and ligated with the *bla*$_{\text{CTX-M-15}}$ fragment.

#### 4.1.1.1. β-lactamase expression and inhibition in a cell-free translation/transcription coupled system

Commercially available translation/transcription coupled systems such as the Expressway™ Cell-Free *E. coli* Expression System (Invitrogen), containing all the *E. coli* cellular machinery required to express proteins in a single reaction, and utilise a T7 bacteriophage RNA polymerase. This system utilises an optimised *E. coli* extract [172], an optimised reaction buffer composing of an ATP regenerating system [173, 174], amino acids, and viral T7 RNA polymerase [175]. Using this system, proteins can be expressed from linear or circular DNA. T7 RNA polymerase exhibits a high specificity and affinity for its own promoter sequences, which do not occur naturally in other *E. coli* genes [175]. Therefore, in these cell-free systems, a T7 promoter sequence is required to drive this specific gene/protein expression. Additionally, it is desirable to position a T7 terminator sequence downstream of the DNA sequence to be transcribed, resulting in only the gene(s) of interest being transcribed.

#### 4.1.1.2. Selection of a plasmid for the expression of *bla*$_{CTX-M-15}$ in cell-free T7 based systems and for the transformation of CTX sensitive *E. coli* strains

The commercially available expression plasmid, pET-9a (Novagen) was selected as a suitable vector for the expression of *bla*$_{CTX-M-15}$ in a cell-free system, and also for transformation of CTX sensitive strains for downstream experimentation using whole cells. pET-9a is a 4341bp plasmid harbouring the required T7 promoter and terminator sequences for T7 based cell-free systems flanking its multi-cloning site (Figure 4-1). For selection purposes, it also harbours a single kanamycin resistance gene, in the reverse orientation to the T7 promoter/terminator sequences to prevent unintended transcription.

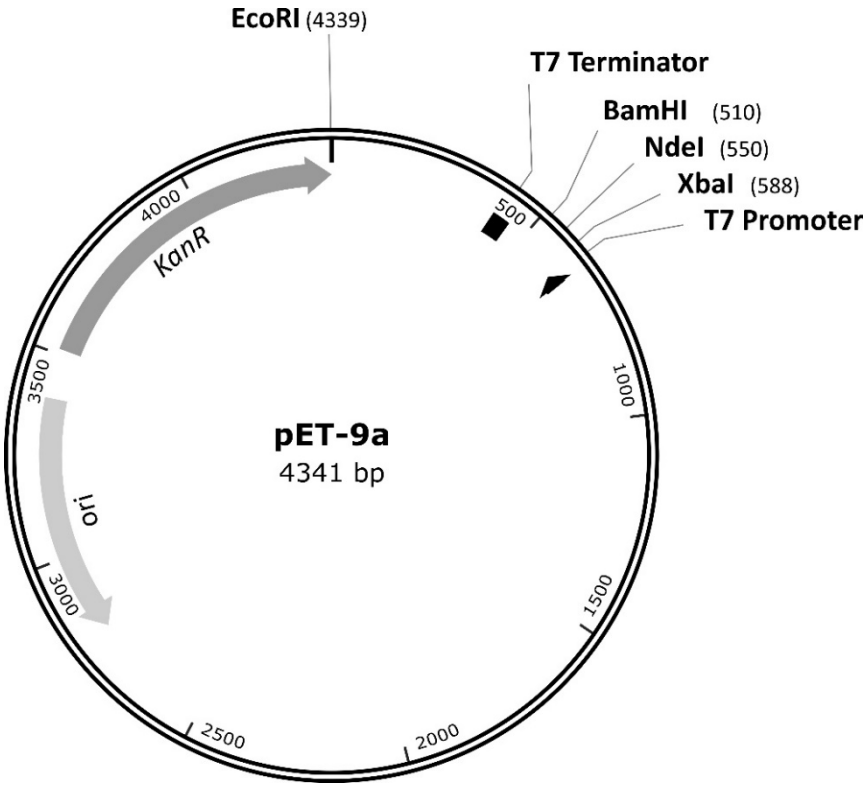


Figure 4-1. Expression Plasmid pET-9a.
The kanamycin resistance gene is in the reverse orientation to the T7 system to minimise any unintended expression.

#### 4.1.1.3. Selection of *bla*$_{\text{CTX-M-15}}$ genes for cloning

It has been observed that *bla*$_{\text{CTX-M-15}}$ is differentially expressed depending upon its genetic environment. Dhanji *et al.* (2011) ascribed these differential expression levels to differences in the number and positions of promoter sequences, and also the distance from the promoter sequence to the translational start region, affecting the amount of transcript available for translation [81]. Two donor plasmids from field isolates were selected on the basis of availability and previously published complete sequences as suitable examples of *bla*$_{\text{CTX-M-15}}$ and its genetic environment: pEK499 is a large plasmid of 117,536 bp and harbours ten antibiotic resistance genes, including three β-lactamases – CTX-M-15, OXA-1 and TEM-1, pEK516 is a plasmid of 64,471bp, and harbours seven antibiotic resistance genes, including the β-lactamases CTX-M-15, OXA-1 and TEM-1 [74].

### 4.1.2. Inhibition of β-lactamase expression by antisense oligomers in a cell free translation-transcription coupled system

For initial proof-of-concept studies, demonstrating the ability of synthetic antisense agents to inhibit the expression of *bla*$_{\text{CTX-M-15}}$ with a minimum amount of potential confounding factors (such as cell wall penetration, efflux removal of antisense agents, and biological activity within a live cell), in the first instance antisense oligomers were evaluated in a cell-free translation / transcription coupled system. The Expressway™ Mini Cell-Free Expression System (Invitrogen) was used for all cell free inhibition experiments. This system contains all of the bacterial cellular machinery required to express functional proteins without any requirement for living cells. Circular or linear DNA can be used to express proteins in this system. For these initial experiments, the two previously constructed plasmids; pJBRCTX516 and pJBRCTX499 (Chapter 4) were used to express *bla*$_{\text{CTX-M-15}}$, and to evaluate the protein expression inhibition

properties of anti-*bla*$_{\text{CTX-M}}$ PMO and PNA antisense agents. Both of these plasmids harboured identical *bla*$_{\text{CTX-M-15}}$ genes, but differed in their surrounding genetic environment. pJBRCTX499 harboured the cloned region from pEK499 complete with the upstream insertional sequence IS26 and a truncated IS*Ecp*1. Due to promoter positions, and reports from previous studies [76, 81], this genetic environment was expected to result in a higher level of β-lactamase expression than pJBRCTX516. pJBRCTX516 harboured the *bla*$_{\text{CTX-M-15}}$ gene cloned from the resistance plasmid pEK516.

#### 4.1.2.1. Design of antisense PMO and PNA oligomers targeting the translation initiation region of *bla*$_{\text{CTX-M-15}}$ mRNA

The length of antisense oligomers are hereafter defined by the number of their constituent nucleotide-like units – for example, a PMO comprising of 25 nucleotides is referred to as a 25-mer PMO.

A 25-mer PMO (PMO1) was designed to target the translational start codon region and a series of three 13-mer PNAs were designed to target the Shine-Dalgarno (SD) ribosome binding site, with one PNA (PNA3) spanning both the SD and the start codon region (Figure 4-2.). Previous antisense/antigene studies have revealed these target areas to be optimal for translational inhibition efficacy [133].

Initial PMO sequence designs for *bla*$_{\text{CTX-M}}$ covering both of these regions were revised under the advice of the manufacturer (Gene Tools LLC) due to a high probability of self-dimerisation and hairpin loop formation. The final PMO design had a low probability of these issues and BLAST searching revealed negligible homology with any other *E. coli* genes. As a result of the short length of PNA1, PNA3 and PNA4 (13 bases each), combined with their extra-genic target regions, each PNA shared partial

sequence similarity (12/13 bases) with four off-target bacterial gene transcripts, and multiple mammalian transcripts.

PNA4 was designed and synthesised after the initial testing of PMO1, PNA1 and PNA3 had been completed in a cell-free environment. It was expected that PNA4, targeting a region shifted 1 base upstream and encompassing the SD region (Figure 4-2), would not have significantly greater or lesser inhibitory properties than PNA1. The slightly altered design of PNA1 to create PNA4 allowed for potential downstream inhibition studies combining PMO1 with PNA4 with no overlapping areas, and allowed for a greater target region (38 bases) to be covered by antisense agents if desired. This design could also potentially reveal any unknown synergistic effects of utilising PMO and PNA chemistries combined.

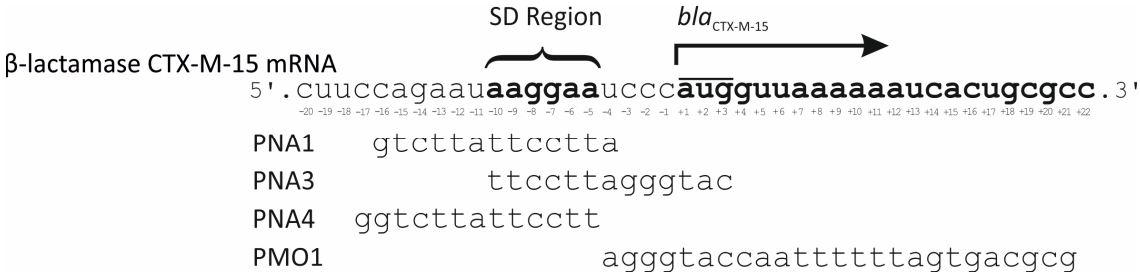


Figure 4-2. PMO and PNA antisense oligomer design.
Three 13-mer PNA and one 25-mer PMO were designed to base-pair and bind to the region of *bla*CTX-M messenger RNA and prevent translation by steric hindrance of the ribosome. All antisense agents targeted the Shine-Dalgarno (SD) region, the start codon, or both.

## 4.2. Results

### 4.2.1. Design and construction of expression plasmids carrying *bla*$_{\text{CTX-M-15}}$ as a suitable test subject for translational inhibition experiments in cell-free translation/transcription coupled systems and in whole cells

#### 4.2.1.1. Amplification of *bla*$_{\text{CTX-M-15}}$ from field isolates

Primers were designed to amplify *bla*$_{\text{CTX-M-15}}$ and the upstream region incorporating promoters, insertional elements IS26 and IS*Ecp*1 [74], and incorporating restriction enzyme recognition sites to facilitate directional cloning into expression vector pET-9a. *bla*$_{\text{CTX-M-15}}$ and associated upstream regions were amplified by colony PCR under typical conditions (section 2.6.9.) from two field isolates, LREC454 and LREC460, harbouring respectively pEK499 and pEK516, using CTX-M-pEK499-forward and -reverse primers for LREC454 and CTX-M-pEK516-forward and -reverse primers for LREC460 (Figure 4-3; Table 2-5). PCR products were visualised by gel electrophoresis for an estimation of size and DNA concentration (Figure 4-4).

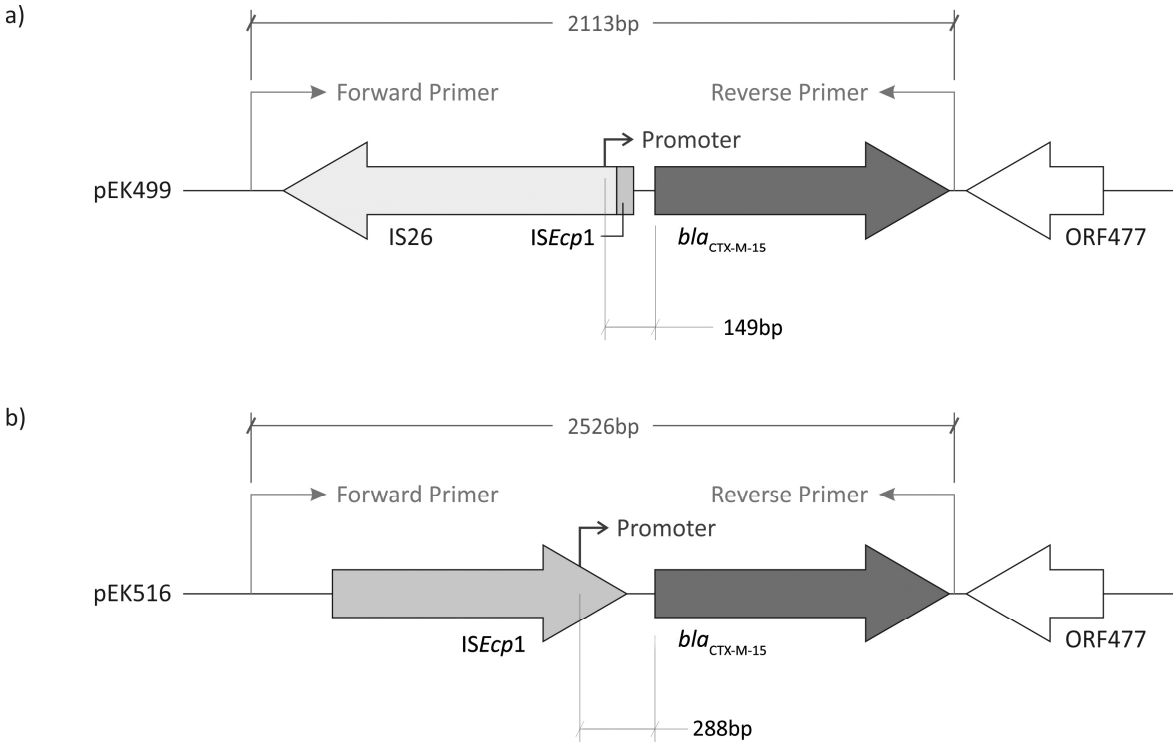


Figure 4-3. Diagram showing the genetic environment surrounding *bla*CTX-M-15 in two donor plasmids, pEK499 and pEK516 [81].

Relative PCR primer positions for the amplification of each region are shown in the indicated positions.

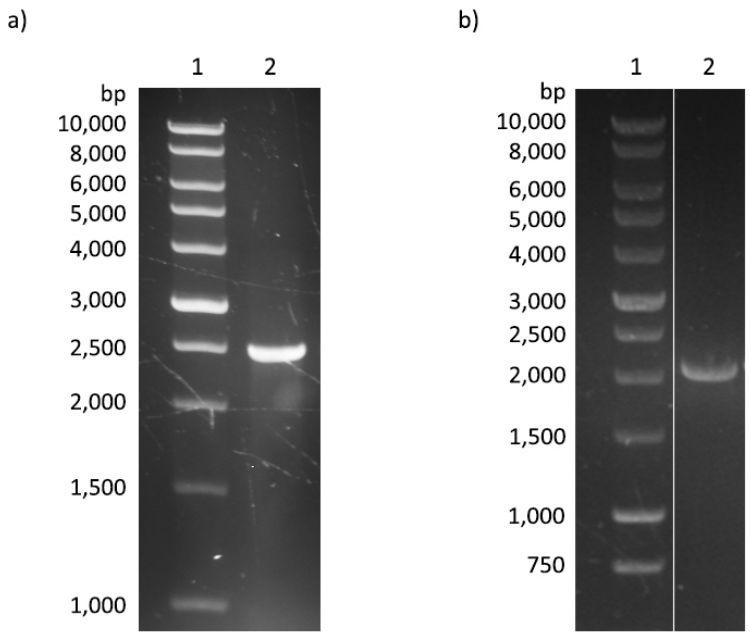


Figure 4-4. Amplification of *bla*$_{\text{CTX-M-15}}$ region by colony PCR from field isolates, visualised by agarose gel electrophoresis and ethidium bromide or SYBR® Safe (Invitrogen) staining.

a) 1; Promega 1 kb DNA Ladder. 2; 2526 bp PCR product amplified from pEK516 in *E. coli* strain LREC460. b) 1; Promega 1 kb DNA Ladder. 2; 2113 bp PCR product amplified from from pEK499 in *E. coli* strain LREC454.

#### 4.2.1.2. Non-directional TA cloning of PCR products into pCR™2.1-TOPO® cloning vector

*Taq* polymerase, used in the PCR to amplify *bla*$_{\text{CTX-M-15,}}$ adds a single deoxyadenosine to both the 3' ends of the PCR products. This allows quick and efficient incorporation of PCR products into commercially available cloning vectors. Amplicons were ligated with the linearised plasmid pCR™2.1-TOPO® (Invitrogen; Figure 4-5; section 2.6.12.2.) using the Quick Ligation™ Kit (NEB) under the manufacturers recommended conditions.

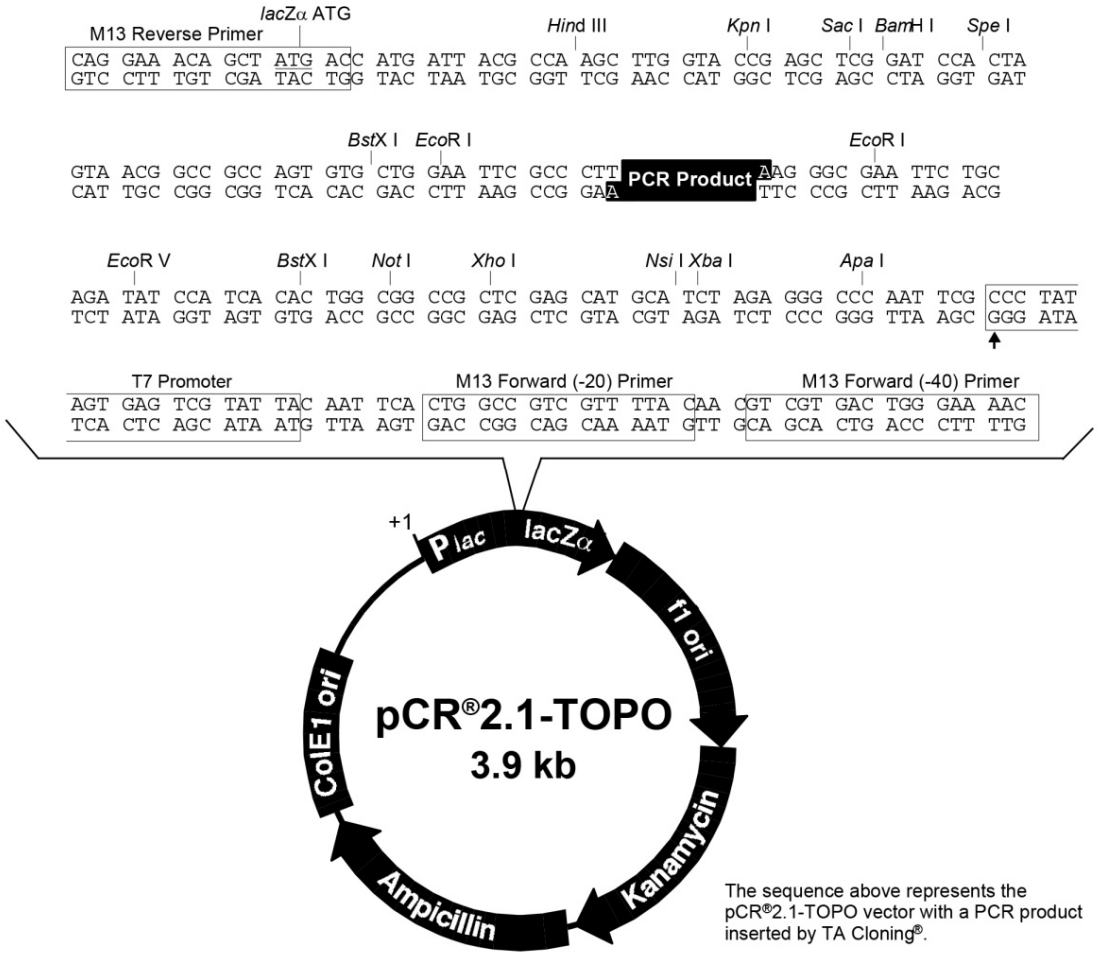


Figure 4-5. pCR™2.1-TOPO® (Invitrogen) cloning vector [176].
Commercially available cloning vector, supplied pre-linearised with single overhanging thymine to each 5' end for TA cloning.

The ligation reaction was used to transform chemically competent *E. coli* One Shot® INVαF' (Invitrogen) following the One Shot™ transformation protocol (Invitrogen). The transformation reaction was cultured overnight at 17° C on solid LB supplemented for selection of successful transformants with kanamycin (40 µg/ml) and with X-Gal for blue-white screening (section 2.6.12.3.). White colonies were selected and cultured in liquid LB. Plasmids were extracted and purified from *E. coli* strains using the peqGOLD Plasmid Miniprep Kit (Peqlab, section 2.6.4.).The plasmids were screened for successful PCR amplicon incorporation by a PCR reaction using M13 forward and

reverse primers (Table 2-6), and by a PCR reaction using M13 forward primers and the reverse primer to used amplify *bla*$_{\text{CTX-M-15}}$ from field isolates (Table 2-5; Table 2-6). M13 sequences in pCR™2.1-TOPO® (Invitrogen; Figure 4-5) flank the insertion site of the vector, and thus a PCR reaction utilising primers complementary to these sequences amplify any sequence between these regions. A PCR reaction using one primer complementary to a sequence on the plasmid backbone and one complementary to a sequence on the insert will yield a product if the insert is present and none if it is absent. Figure 4-6 shows the result of PCR reaction to verify the incorporation of DNA fragment amplified from pEK499, fragments separated and visualised by agarose gel electrophoresis.

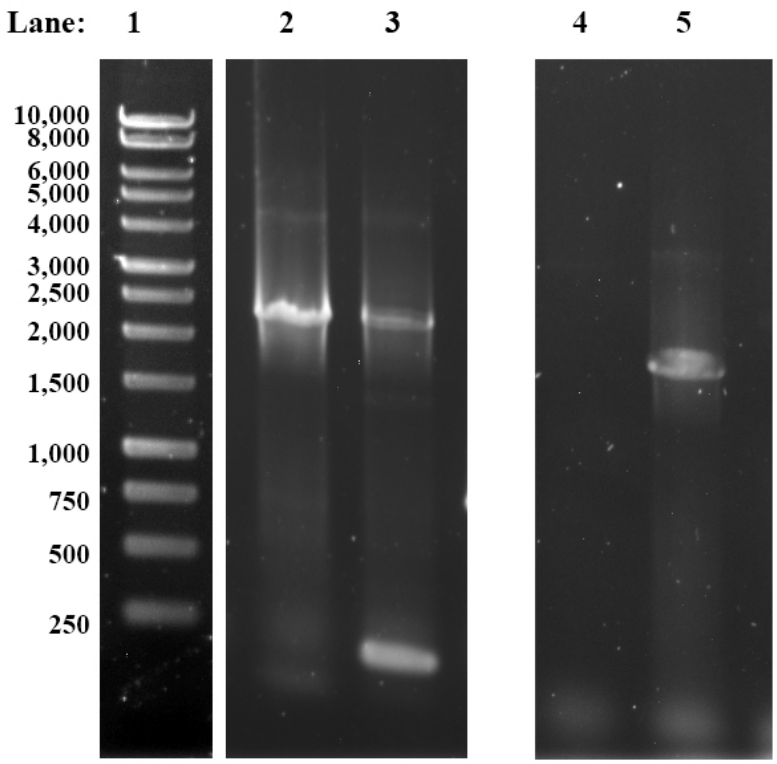


Figure 4-6. Agarose gel showing the results of PCR reactions to screen for the presence and size of DNA fragments amplified from pEK499 incorporated into pCR™2.1-TOPO® (Invitrogen).

All lanes were taken from the same gel, for clarity only the relevant lanes are shown. Lane 1: Promega 1 kb DNA Ladder, sizes of fragments shown adjacent (bp). Lane 2: PCR products amplified from plasmid preparation 1 with M13-forward and –reverse primers (Table 2-6). Lane 3: PCR products amplified from plasmid preparation 2 with M13-forward and –reverse primers. Lane 4: PCR products amplified from plasmid preparation 1 with M13-forward primer and CTX-M-pEK499-reverse (Table 2-5; Table 2-6). Lane 5: PCR products amplified from plasmid preparation 2 with M13-forward primer and CTX-M-pEK499-reverse.

Purified recombinant pCR™2.1-TOPO®/*bla*$_{CTX-M-15}$ plasmids were digested with restriction endonucleases *Bam*HI and *Nde*I for the recombinant plasmid harbouring the amplified region from LREC454, and *Bam*HI and *Xba*I for the recombinant plasmid harbouring the amplified region from LREC460 (section 2.6.12.5.2.6.12.5. ). The digested fragments were separated by gel electrophoresis, and the *bla*$_{CTX-M-15}$ fragment was excised and purified with the peqGOLD Gel Extraction Kit (Peqlab, section 2.6.12.6.).

Plasmid pET-9a was digested with *Bam*HI and *Nde*I to leave compatible overhanging ends with the fragment originating in LREC454, and *Bam*HI and *Xba*I to leave compatible overhanging ends with the fragment originating in LREC460. *bla*$_{CTX-M-15}$ fragments were ligated with pET-9a under typical conditions (section 2.6.12.8.), which was then used to transform chemically competent *E. coli* DH5α-T1® (Invitrogen). The transformants were recovered onto LB agar supplemented with cefotaxime (1 µg/ml) and kanamycin (40 µg/ml) overnight at 37° C. Colonies observed on cefotaxime (1 µg/ml) and kanamycin (40 µg/ml) selection plates (Figure 4-7) were sampled, cultured, and recombinant plasmids extracted.

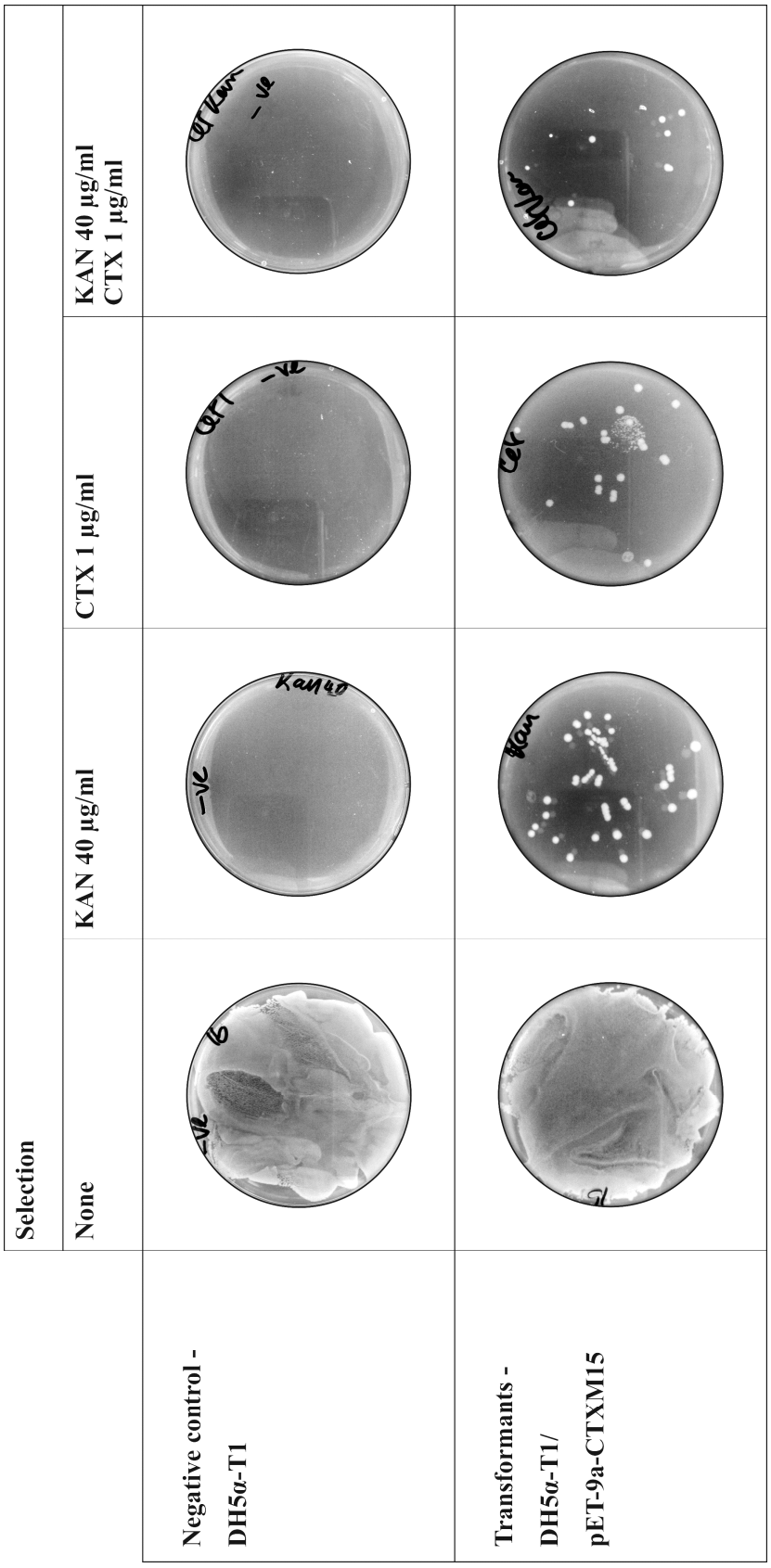


Figure 4-7. Resultant colonies from transformation of DH5α with pET-9A/CTX-M-15

The purified plasmids were screened for successful incorporation of the desired insert by restriction enzyme digestion and visualisation of fragment sizes by gel electrophoresis (Figure 4-8; Figure 4-9); and by sequencing (APHA sequencing dept) using the dideoxy chain termination/cycle sequencing method using CTX-M-SEQ primers (Table 2-6).

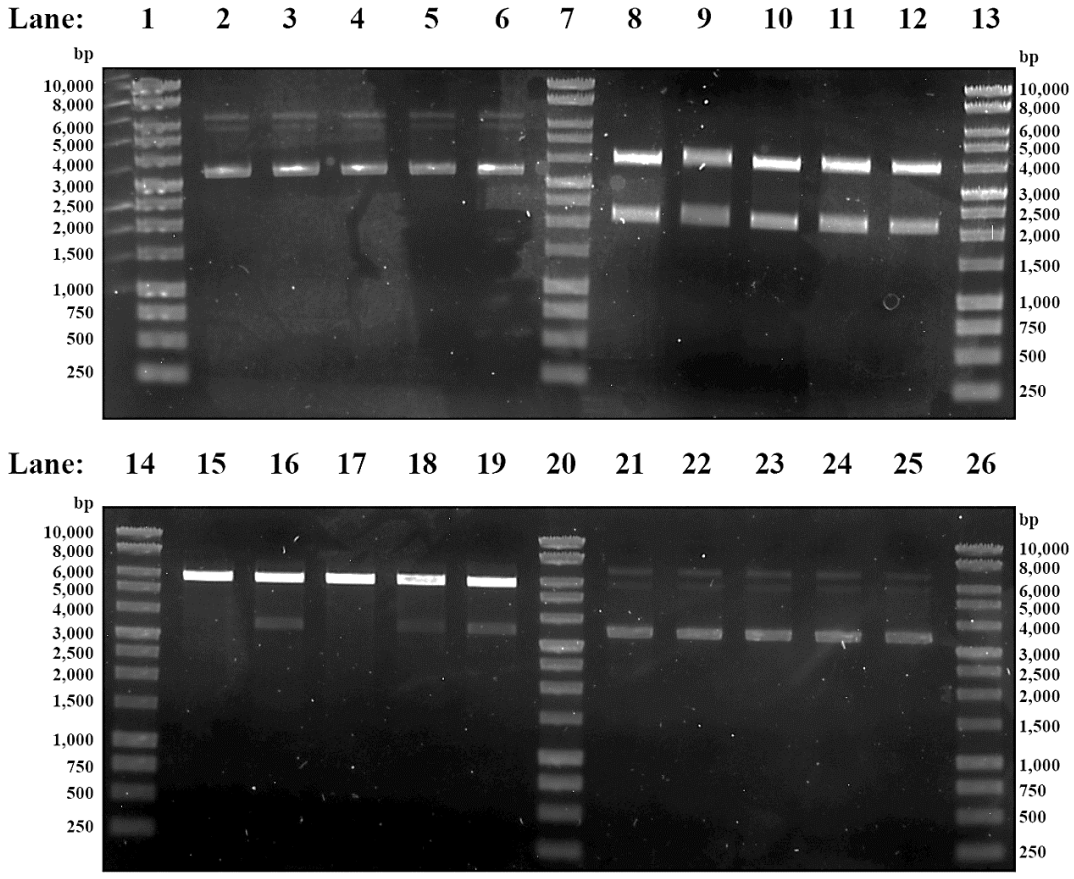


Figure 4-8. Gel showing screening restriction enzyme digestion of pET-9A/CTX-M15-499.

i): Lane 1: Promega 1 kb DNA Ladder, sizes of fragments shown adjacent. Lanes 2-6: plasmid miniprep. Lane 7): Promega 1 kb DNA Ladder. Lanes 8-12: Plasmid miniprep digested with *Bam*HI and *Xba*I.

ii): Lane 14): Promega 1 kb DNA Ladder, sizes of fragments shown adjacent (bp). Lanes 15-19: Plasmid miniprep digested with *Xba*I. Lane20: Promega 1 kb DNA Ladder. Lanes 21-25: Plasmid miniprep.

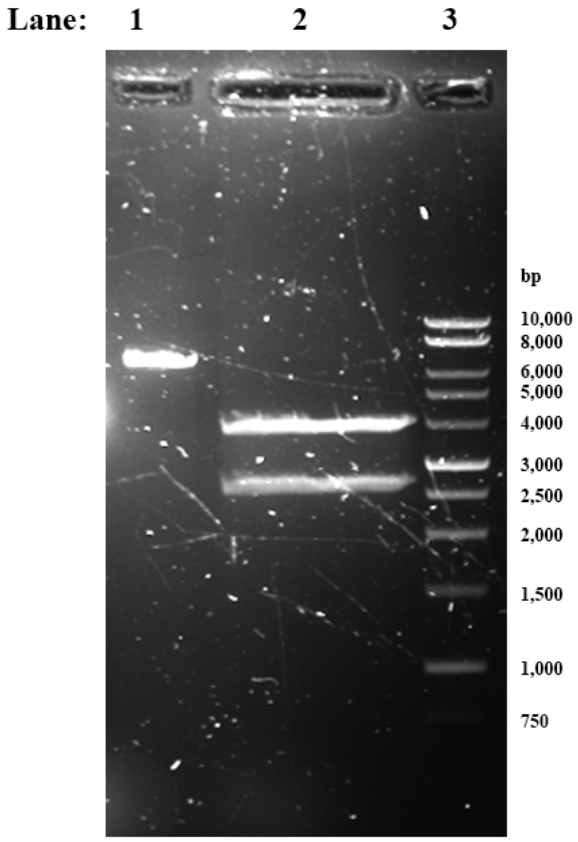


Figure 4-9. Gel showing screening restriction enzyme digestion of pET-9A/CTX-M15-516.
Restriction enzyme digestion screen for successful incorporation of *bla*$_{\text{CTX-M-15}}$ region into expression vector pET-9a. Lane 1: plasmid linearised with single *Xba*I disgestion. Lane 2: plasmid digested with *Xba*I and *Bam*HI, cleaving either side of insert to release 2 fragments. Lane 3: Promega 1 kb DNA Ladder, sizes of fragments shown adjacent (bp).

The insert originating from *E. coli* strain LREC460, harbouring pEK516, was found to have been ligated with pET-9a in the correct orientation and position. Sequencing revealed no unexpected mutations. This recombinant plasmid was designated pJBRCTX516. The insert originating from *E. coli* strain LREC454, harbouring pEK499, was found to have been ligated with pET-9a in the correct orientation and position. However, sequencing revealed 2 point mutations, possibly due to the use of

non-proof-reading *Taq* DNA polymerase, which has a higher mis-incorporation rate compared with other polymerases [177]. The two mutations were both single base substitutions: one in an extragenic non-coding region 138 bp downstream of the insertional element IS26; and one intragenic mutation at $bla_{\text{CTX-M-15}}$ locus +822. The intragenic mutation was an adenine to guanine substitution and would result in a translated amino acid change of serine to glycine in the expressed enzyme. This mutation could have potentially altered the conformation and function of the enzyme and so it was deemed necessary to restore this to its original sequence. This was corrected with site-directed mutagenesis.

#### 4.2.1.3. Site-Directed Mutagenesis

Site-directed mutagenesis (SDM) is PCR based technique by which mutations can be introduced or corrected in plasmids. The commercially available GENEART® Site-Directed Mutagenesis System (Invitrogen) was used to correct the intragenic point mutation. Two overlapping primers, SDM-forward and –reverse (Table 2-7; Figure 4-10) were designed which were, in accordance with the manufacturer's (Invitrogen) recommendations, 31 nucleotides in length with the corrected mutation located centrally, 100% complementary with no overhangs and with the desired mutation located centrally (Figure 4-10). The SDM reaction proceeded under manufacturer's (Invitrogen) recommended conditions (section 2.6.12.10.).

#### 4.2.1.4. SDM Primer Design

pJBRCTX499 5' ...atacatcgcgacggc**g**ttctgccttaggttg... 3'

Primer-R 3' tatgtagcgctgccg**A**aagacggaatccaac 5'

Primer-F 5' atacatcgcgacggc**T**ttctgccttaggttg 3'

pJBRCTX499 3' ...tatgtagcgctgccg**c**aagacggaatccaac... 5'

Figure 4-10. SDM Primer Design.
Point mutation in the recombinant plasmid shown in bold lowercase, corrected in the mutagenic primers shown in bold uppercase.

#### 4.2.1.5. Screening for successful mutation

Screening for the correction of a single point mutation by restriction enzyme digestion relies on the point mutation being located with a recognition site. Restriction enzyme digestion and visualisation by gel electrophoresis is then able to reveal the presence or absence of a corrected mutation. One restriction enzyme, *Cvi*KI-1 (NEB), was found to cleave the DNA if a successful mutation correction had occurred, and not recognise, and therefore not cleave, if the original mutation had not been corrected. *Cvi*KI-1 recognises a 4 base-pair sequence, RGCY (R=A or G, Y=C or T) and cuts between G and C. This enzyme, being a frequent (4-base recognition site) cutter, recognised many sites in the surrounding area - the longest section between recognition sites flanking the mutation site was 164 bp. Plasmids were extracted, purified and the 164 bp area surrounding the site at the point mutation was amplified by PCR using primers SDM-SCREEN-forward and -reverse (Table 2-7). This amplicon was digested with *Cvi*KI-1 under manufacturer's recommended condition (NEB). A successful mutation, when visualised with gel electrophoresis, would yield two bands of 65 bp and 99 bp, whereas an unsuccessful mutation would generate a single band of 164 bp. To visualise bands of such diminutive size, samples were run on 3% high resolution agarose in TBE. Under

these conditions, however, it was not possible to resolve such small fragments, and so colonies were selected at random and sequenced. Sequencing data revealed approximately 50% of the colonies selected carried a plasmid with a successfully corrected mutation. *E. coli* strain DH5α-T1® (Invitrogen) harbouring this corrected plasmid, designated pJBRCTX499, were cultured and stored for use in subsequent studies.

### 4.2.2. Inhibition of β-lactamase expression by PNA and PMO antisense agents in a cell free translation-transcription coupled system

Initial experiments were undertaken to evaluate the relative expression levels of the previously constructed plasmids, pJBRCTX499 and pJBRCTX516 in the Expressway™ Mini Cell-Free Expression System (Invitrogen), and the inhibitory properties of PNA1, PNA3, PNA4 and PMO1. The four antisense agents were evaluated for inhibition efficacy using each of the constructed plasmids pJBRCTX516 and pJBRCTX499 as the DNA template in a cell-free translation/transcription coupled system. Plasmids pJBRCTX499 and pJBRCTX516 were incubated in the cell-free system in the presence and absence of a range of antisense agent concentrations (50 – 1000 nM), and the reaction proceeded for the manufacturer's recommended amount of time (3 – 4 hours). After the allotted incubation period, β-lactamase activity was quantified by HPLC - each reaction was incubated in the presence of cefotaxime (400 - 800 μg/ml final concentration) and aliquots removed at regular time intervals. The CTX concentration was quantified by HPLC and the β-lactamase quantity and, thus, inhibition efficacy was determined by the amount of observed cefotaxime hydrolysis.

#### 4.2.2.1. Evaluation of the reduction of *bla*$_{CTX-M-15}$ expression by PNA1 and PMO1 in a cell-free system using pJBRCTX499 as DNA template

Plasmid pJBRCTX499 (271 ng, as determined by spectrophotometry) was incubated in the cell-free expression system in the presence of PMO1 (500 nM), PNA1 (500 nM) or an equivalent volume of dd$H_2O$ (control) and the reaction allowed to proceed for 3 hours. An aliquot of each reaction (70 µl) was taken from each reaction and added to cefotaxime solution (1.5 ml; 800 µg/ml) and incubated at 37° C. At regular time intervals, aliquots (120 µl) were removed and added to pre-prepared HPLC vials containing phosphate buffer (120 µl; pH 2.2). CTX hydrolysis that had occurred at each time point was quantified by HPLC (Figure 4-11). Cell-free reactions in the presence of PMO1 and PNA1 both resulted in a lower rate of CTX degradation than the reaction that occurred in the absence of antisense agents. There was no significant difference ($p = 0.803$) in the rate of CTX degradation observed in the reactions occurring in the presence of PMO1 and PNA1. In relation to the cell-free reaction in the absence of antisense agents, the presence of PMO1 (500 nM) was observed to have inhibited CTX degradation by 82% and PNA1 (500 nM) by 81%.

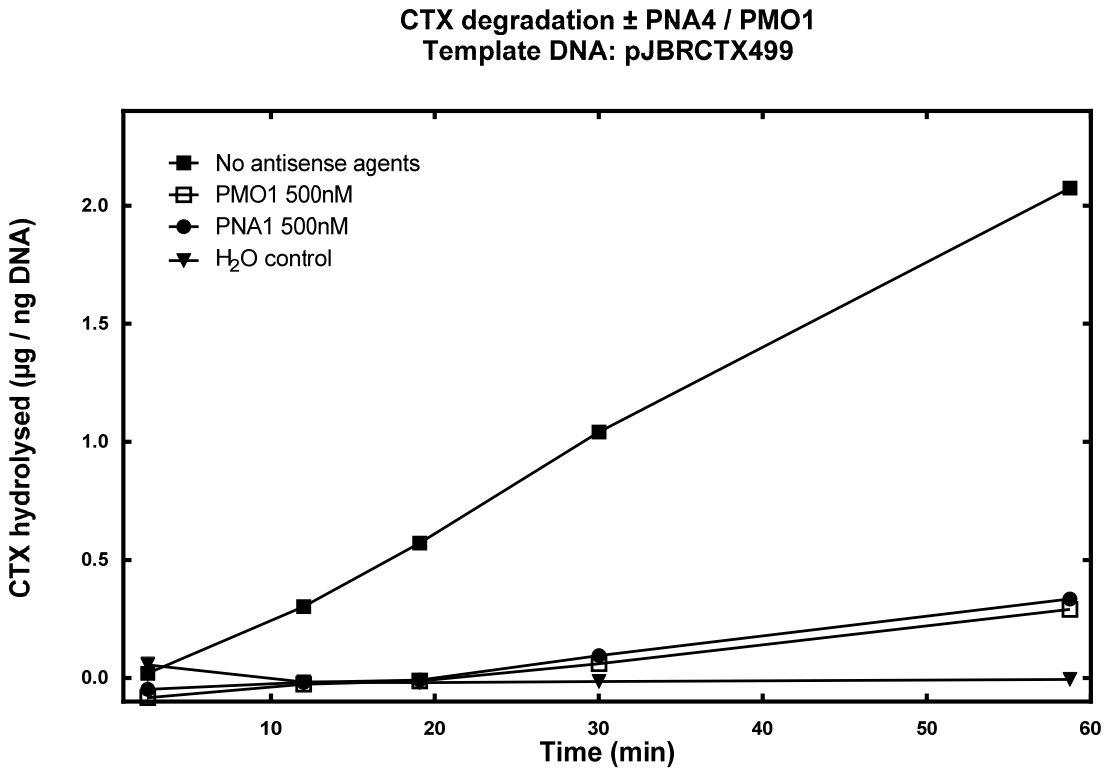


Figure 4-11. β-Lactamase activity after expression in a cell-free system using pJBRCTX499 as DNA template in the presence of PNA1 (500 nM) and PMO1 (500 nM).

271 ng plasmid (pJBRCTX499) was used in each 3 hour reaction. Filled squares (■): control reaction (no antisense agent), hollow squares (□): reaction in the presence of PMO1 (500 nM), filled circles (●): reaction in the presence of PNA1 (500 nM), inverted filled triangles (▼): HPLC control (CTX solution and the equivalent volume of cell-free reaction growth media in the absence of plasmid DNA template). Error bars indicate +/- 1 standard deviation (n=2).

#### 4.2.2.2. Reduction of β-lactamase activity by inhibition of *bla*$_{CTX-M-15}$ expression by PNA1, PNA3 and PMO1 in a cell-free system using pJBRCTX516 as DNA template

Plasmid pJBRCTX516 (285 ng, as determined by spectrophotometry) was incubated in the cell-free expression system in the presence of PMO1 (500 – 1000 nM), PNA1 (500 – 1000 nM), PNA3 (500 – 1000 nM) or an equivalent volume of $ddH_2O$ (control) and the reaction and subsequent HPLC quantification of remaining cefotaxime proceeded as previously described (section 4.2.2.1.).

Cell-free reactions in the presence of PMO1, PNA1 and PNA3 resulted in a lower rate of CTX degradation than the reaction that occurred in the absence of antisense agents and a dose-dependent effect was observed. There was no significant difference ($p > 0.05$) in the rate of CTX degradation observed in the reactions occurring in the presence of PMO1 and PNA1 at concentrations of either 500 nM or 1000 nM. A dose dependent response was observed in the rate of CTX degradation in the cell-free reaction inhibited by PNA3. However, the rate of β-lactamase activity inhibition was consistently lower than that observed in reactions incubated in the presence of either PMO1 or PNA1 (Figure 4-12), although not significantly different ($p > 0.05$) when compared with both PNA1 and PMO1 at concentrations of 500 nM and 1000 nM).

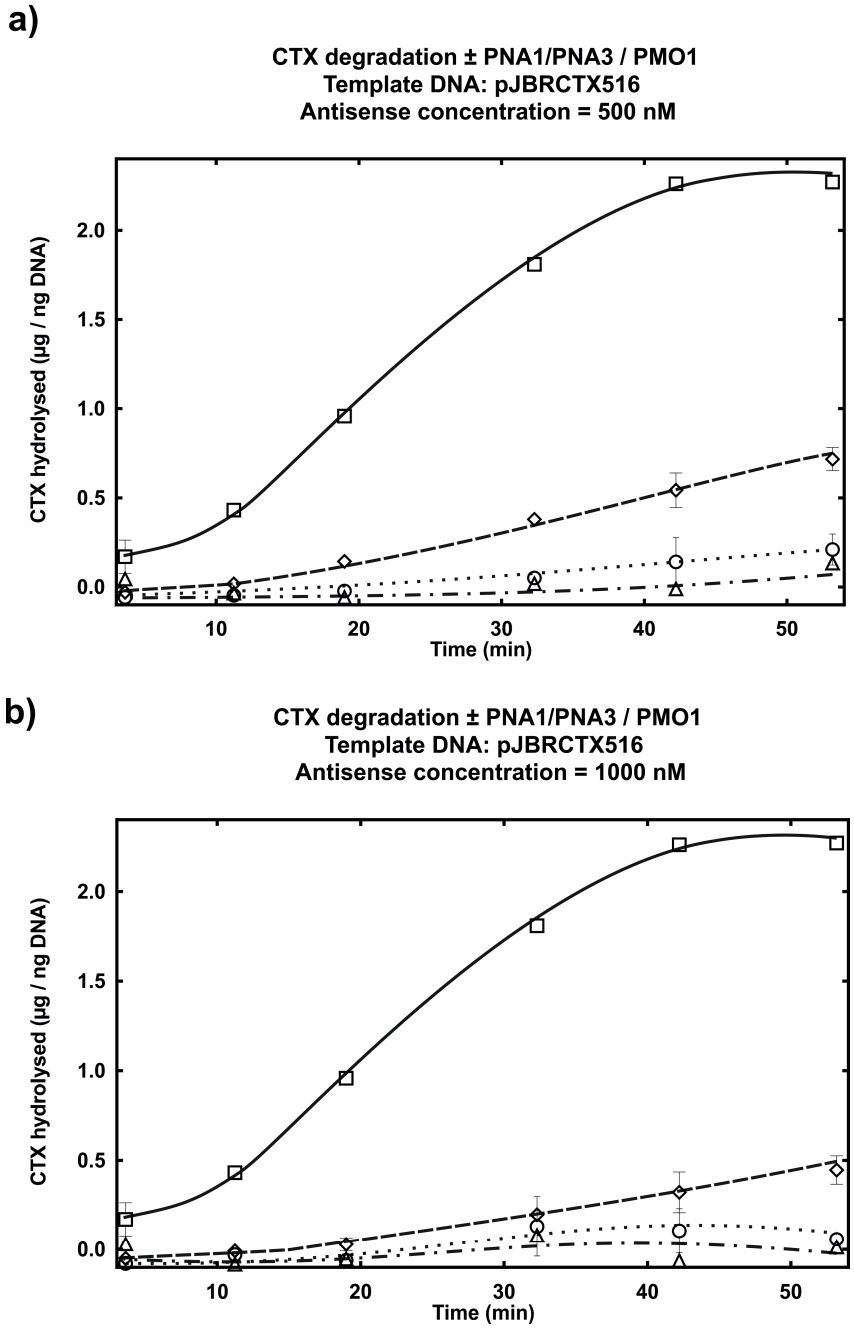


Figure 4-12. β-Lactamase activity after expression in a cell-free system using pJBRCTX516 as DNA template in the presence of PMO1, PNA1 and PNA3. 285 ng plasmid (pJBRCTX499) was used in each 3 hour reaction. **a) S**quares (□): control reaction (antisense agent absent), dash-dot line, triangle (△):PMO1 (500 nM), dotted line, circles (○): PNA1 (500 nM), dashed line, diamonds (◇): PNA3 (500 nM). **b)** : squares (□): control reaction (no antisense agent), dash-dot line, triangle (△): PMO1 (1000 nM), dotted line, circles (○): PNA1 (1000 nM), dashed line, diamonds (◇): PNA3 (1000 nM). Error bars indicate +/- 1 standard deviation (n=2).

The amount of β-lactamase expression inhibition, quantified by cefotaxime degradation, relative to the reaction incubated in the absence of any antisense agent (uninhibited reaction = 100%), is presented in Figure 4-13.

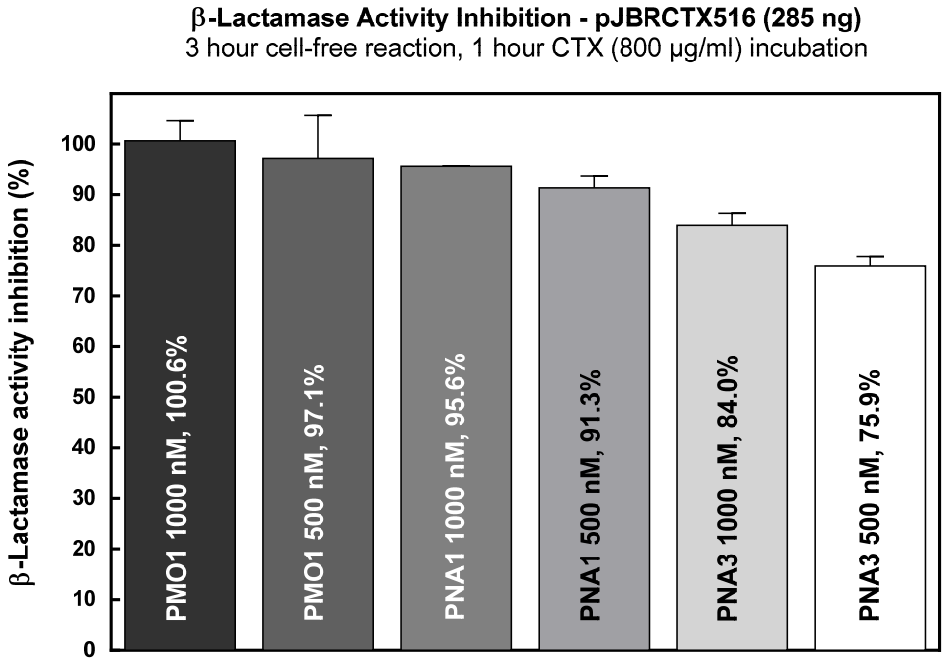


Figure 4-13. Observed inhibition of β-lactamase activity in a cell-free translation/transcription coupled system with PMO1, PNA1 and PNA3.
Rates of CTX hydrolysis were derived from the linear section of each curve (Figure 4-12) and inhibition amount calculated in comparison with the rate of hydrolysis of the uninhibited reaction (in the absence of antisense agents).

#### 4.2.2.3. Reduction of β-lactamase activity by inhibition of *bla*$_{\text{CTX-M-15}}$ expression by PNA4 and PMO1 in a cell-free system using pJBRCTX516 as DNA template.

PMO1 and PNA4 were evaluated using pJBRCTX516 as the DNA template, for anti-*bla*$_{\text{CTX-M-15}}$ activity in a cell-free translation/transcription coupled system. A range of concentrations of each antisense agent (50 – 1000 nM) was added to each reaction (with final reaction volumes normalised with carrier medium). Each reaction consisted of an equal quantity of purified plasmid pJBRCTX516 (485 ng total quantity, quantified by

spectrophotometry), and was incubated at 30° C for 4 hours. After the protein expression reaction incubation had proceeded for 4 hours, 70 µl aliquots were taken and added to 1.2 ml cefotaxime solutions (800 µg/ml) and incubated at 37° C. At regular time intervals, aliquots (120 µl) were removed and added to prepared HPLC vials containing phosphate buffer (pH 2.2). The CTX remaining in solution was then quantified by HPLC and the β-lactamase activity in each incubation determined by the amount of observed CTX degradation.

The amount of activity, quantified by HPLC analysis of cefotaxime degradation, is presented in Figure 4-14a (in the presence and absence of PMO1) and Figure 4-15a (in the presence and absence of PNA4). Figure 4-14b (PMO1) and Figure 4-15b (PNA4) represent β-lactamase activity inhibition in relation to uninhibited reactions.

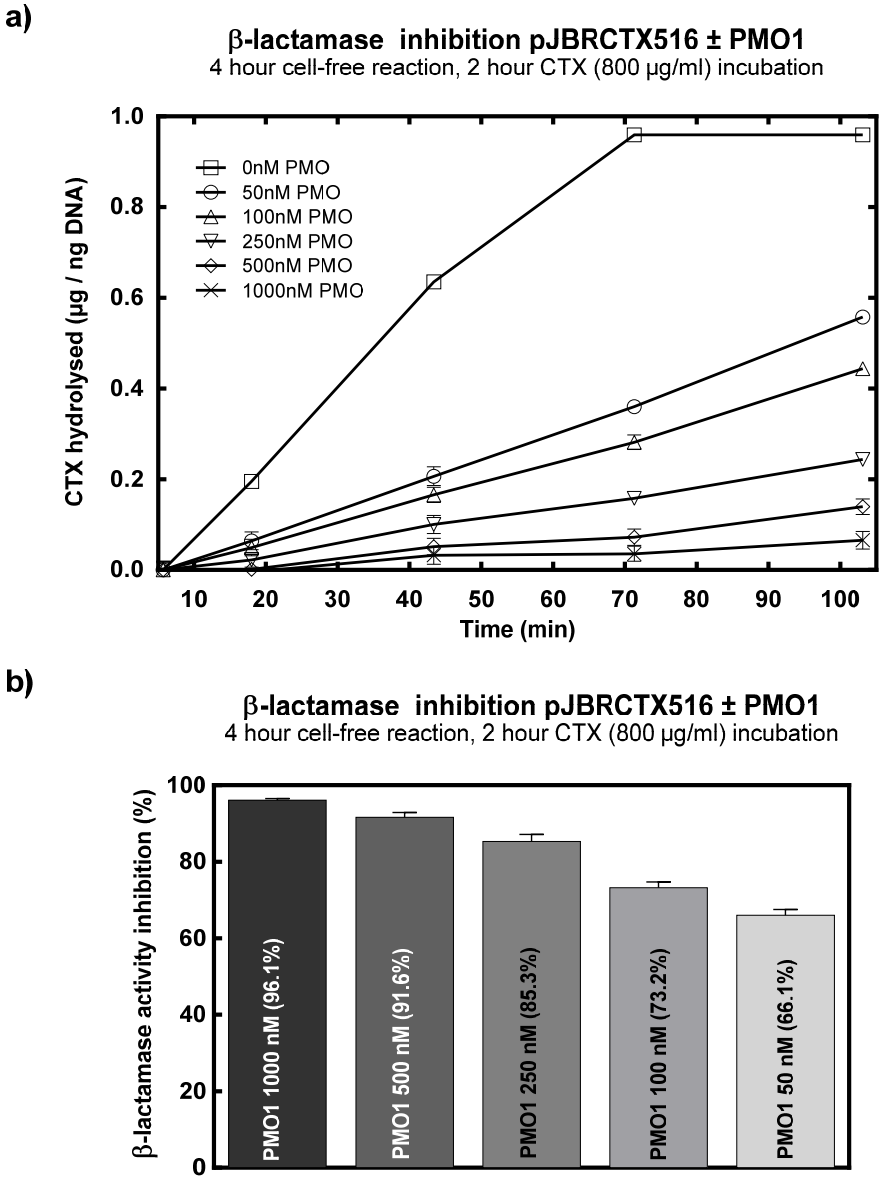


Figure 4-14. Observed β-lactamase activity resulting from expression in a cell-free translation/transcription coupled system in the presence of PMO1 using pJBRCTX516 as template DNA.

485 ng plasmid (pJBRCTX516) was used in each 4 hour reaction. **a)** Squares (□): control reaction (no antisense agent), circles (○): PMO1 (50 nM), triangles (△): PMO1 (100 nM), inverted triangles (▽): PMO1 (250 nM), diamonds (◇): PMO1 (500 nM), crosses (×): PMO1 (1000 nM). Error bars indicate +/- 1 standard deviation (n=4). **b)** Representation of data as percentage inhibition calculated as a comparison with maximum rate of uninhibited reaction (no antisense agent).

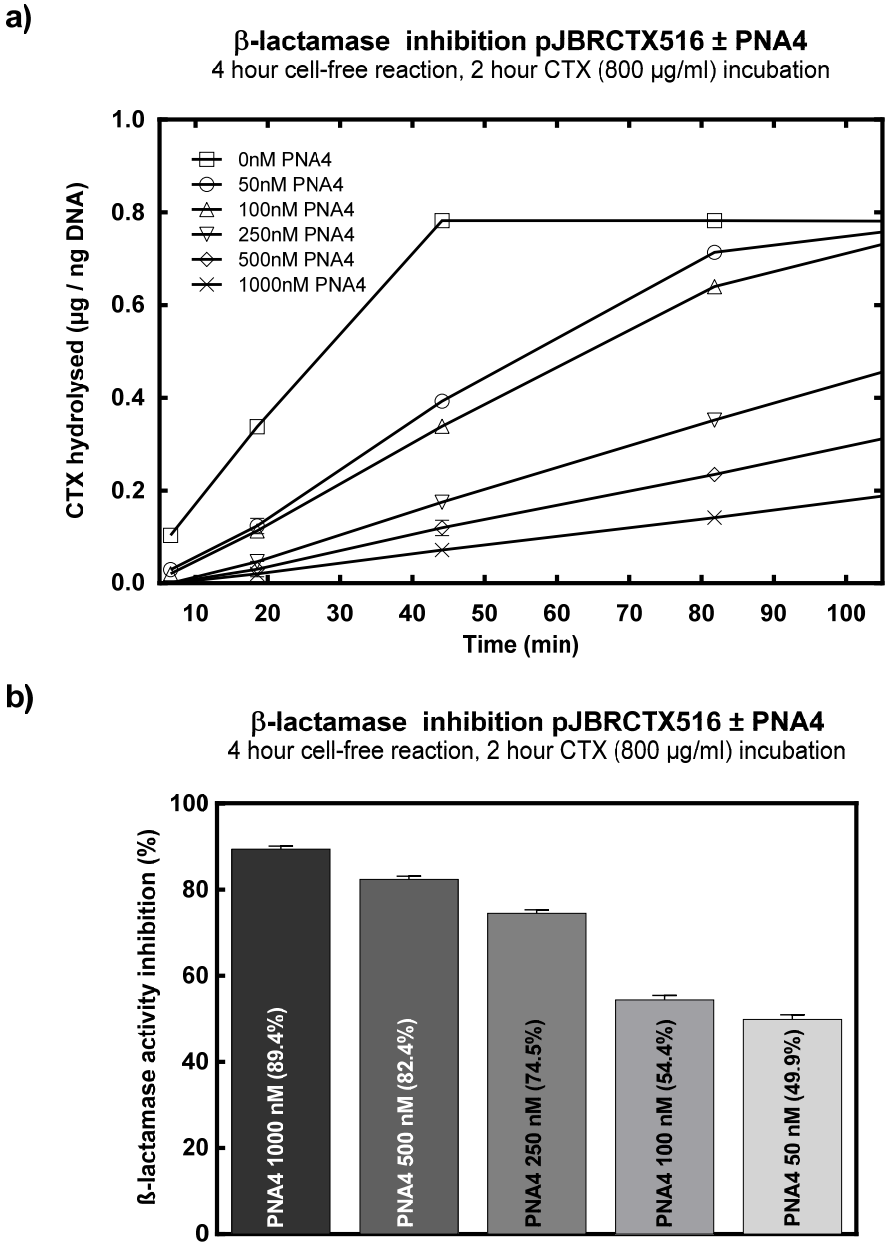


Figure 4-15. Observed β-lactamase activity resulting from expression in a cell-free translation/transcription coupled system in the presence of PNA4 using pJBRCTX516 as template DNA.

485 ng plasmid (pJBRCTX516) was used in each 4 hour reaction. **a)** Squares (□): control reaction (no antisense agent), circles (○): PNA4 (50 nM), triangles (△): PNA4 (100 nM), inverted triangles (▽): PNA4 (250 nM), diamonds (◇): PNA4 (500 nM), crosses (×): PNA4 (1000 nM). Error bars indicate +/- 1 standard deviation (n=4). **b)** Representation of data as percentage inhibition calculated as a comparison with maximum rate of uninhibited reaction (no antisense agent).

## 4.3. Discussion

### 4.3.1. Design and construction of expression plasmids carrying *bla*$_{\text{CTX-M-15}}$

Two plasmids were constructed, pJBRCTX499 (Figure 4-16), and pJBRCTX516 (Figure 4-17). The plasmids both harboured a single *bla*$_{\text{CTX-M-15}}$ sequence, cloned from two different field isolates, LREC454 and LREC460 respectively. They differed only in the upstream regions which contain associated insertional elements and *bla*$_{\text{CTX-M-15}}$ promoters. These plasmid were both suitable for *bla*$_{\text{CTX-M-15}}$ expression in a cell-free translation/transcription coupled system as the cloned region was flanked by T7 promoter and terminator sequences, and also for *bla*$_{\text{CTX-M-15}}$ expression in transformed strains as they included the naturally occurring promoter and putative regulatory sequences from their original host strains.

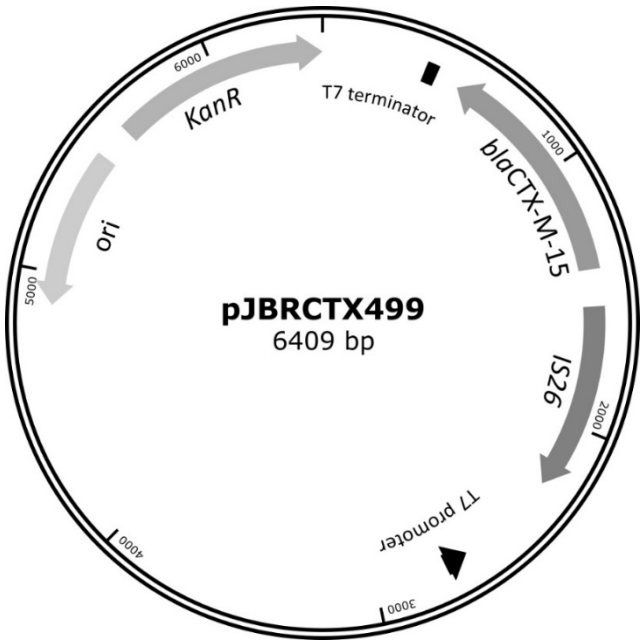


Figure 4-16. Recombinant plasmid pJBRCTX499.
Showing the incorporation of amplified section from resistance plasmid pEK499 into expression vector pET-9a.

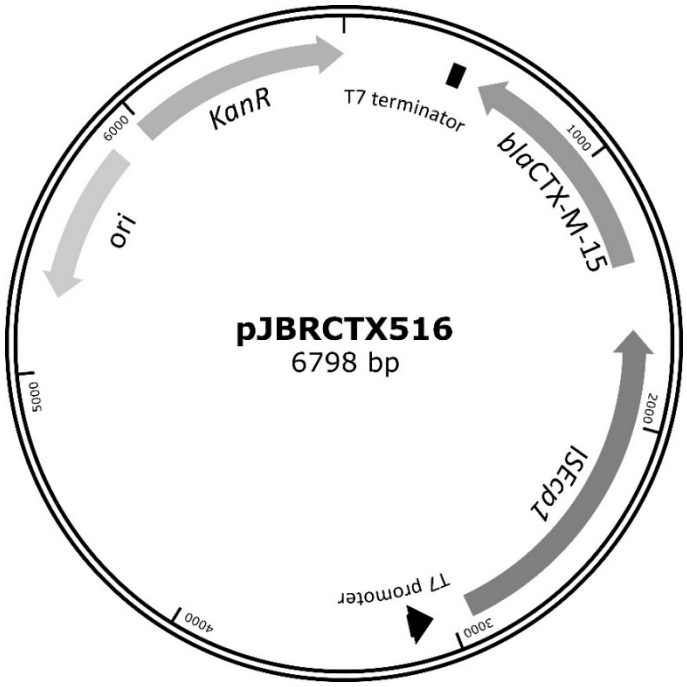


Figure 4-17. Recombinant plasmid pJBRCTX516.
Showing the incorporation of amplified section from resistance plasmid pEK516 into expression vector pET-9a.

### 4.3.2. Inhibition of β-lactamase expression by antisense oligomers in a cell free translation-transcription coupled system

The results demonstrated the ability of PMO and PNA antisense agents to inhibit the expression of β-lactamase in a cell-free environment. A high level of inhibition was observed with PMO1 (observed inhibition of 100% at 1000 nM using pJBRCTX516 as the DNA template), PNA1 (96% at 1000nM using pJBRCTX516 as the DNA template) and PNA4 (89% at 1000 nM using pJBRCTX516 as the DNA template). PNA3, which was designed to be complementary to the region spanning both the Shine-Dalgarno region and the translational start region, was unexpectedly the least effective inhibition agent. As both of these regions had previously shown to be the most effective areas to target for antisense inhibition, a PNA that spanned both of these regions had been hypothesised to be the most likely to yield the greatest effect.

Another notable observation from cell-free inhibition studies was the amount of difference in inhibition efficacy that a relatively minor change in the target region made. The maximum observed inhibition of PNA3, the same length as PNA1, shifted six bases upstream was 84% at a concentration of 1000 nM, PNA1 achieved 96% in directly comparable experiments conducted under the same conditions with the same protein expression reagents, at the same time. This would suggest that there would be scope to increase inhibition effectiveness by target region and antisense oligomer size optimisation. Time and financial constraints, however, did not allow for a larger range of PNA/PMO sizes and target regions to be evaluated.

Table 4-1 summarises the observed inhibition efficiencies in anti-*bla*$_{\text{CTX-M-15}}$ antisense agents (500 nM) used in cell-free studies in plasmids pJBRCTX499 and pJBRCTX516.

Table 4-1. Summary of observed reduction of β-lactamase activity by inhibition of *bla*$_{\text{CTX-M-15}}$ by all antisense agents (500 nM) in a cell-free translation/transcription coupled system.

| | **Maximum observed β-lactamase inhibition (%)** | |
|---|---|---|
| **Antisense Agent (500 nM)** | **pJBRCTX499** | **pJBRCTX516** |
| PMO1 | 81.85 | 97.1 |
| PNA1 | 81.39 | 91.3 |
| PNA3 | Not tested | 75.9 |
| PNA4 | Not tested | 82.4 |

PNA4 was a slight variation on PNA1, differing in only 1 base of the target region, and designed with the potential for complementary studies with PMO1 - the combination of PNA4 and PMO1 with no overlapping areas would span a 38 base target region, and would also provide the option for PMO/PNA synergy studies.

For subsequent studies in whole cells, a PMO and a PNA were selected as representatives of the two different chemistries. PMO1 and PNA4 were selected as the antisense agents of interest for the greatest potential of inhibitory activity in whole cells - PMO1 had demonstrated the greatest amount of β-lactamase activity inhibition in a cell-free system, and PNA4, with a difference of a single base shift in target region from PNA1, had the potential to be used alone or in combination with PMO1 to span a 38-nt target region.

# Chapter 5.

# Effects of antisense oligomers on sensitivity to cefotaxime in *E. coli* strains with reduced susceptibility to CTX

## 5.1. Introduction

Anti-*bla*$_{\text{CTX-M}}$ synthetic antisense PNA/PMOs were previously found in the current study to be effective in reducing CTX degradation after expressing *bla*$_{\text{CTX-M-15}}$ in the presence and absence of antisense oligomers in a cell-free translation/transcription coupled system. This effectively demonstrated inhibition of *bla*$_{\text{CTX-M}}$ activity, and hence a reduction in the expression levels of β-lactamase by the presence of antisense agents. The template DNA used in the initial cell-free studies was the plasmid constructed in this study, pJBRCTX516, which carried a single copy of *bla*$_{\text{CTX-M-15}}$ cloned from field isolate LREC460.

To evaluate efficacy of inhibition of protein expression by synthetic antisense agents in live *E. coli* cultures, a growth assay was established. Increases in biomass, and hence culture growth, was quantified by optical density measurement by spectrophotometry at a light wavelength of 600 nm. The assay revealed that, in all strains, the presence of CTX at sub-inhibitory concentrations caused a lengthening of the time taken to achieve logarithmic growth phase of the culture's growth cycle. The length of the increase time taken to reach log phase was related to the concentration of CTX (Figure 5-4), and was strain-variable. Under these conditions the terminal biomass level when stationery phase was reached, on occasion showed a decrease when inoculated with increasing concentrations of CTX and/or antisense agents. The observation of differences in terminal culture turbidity, measured at O.D. $_{600\ \text{nm}}$, was not reliably reproducible and typically did not correlate well with media supplement dose. The diagnostic criteria for

establishing the growth inhibitory effects of CTX exposure on *E. coli* growth, observed in all experiments, was therefore determined to be the extension of the time taken to achieve logarithmic growth phase of the culture.

As previously discussed, the bacterial cell wall has been well established to be a significant obstacle to gene expression inhibition by synthetic antisense agents [119]. To enable a preliminary evaluation of the efficacy of PNA/PMOs in live cultures, atypically permeable *E. coli* strain AS19 transformed with pJBRCTX516 cultures were treated with combinations of CTX and PNA4/PMO1, and CTX sensitivity due to the presence of antisense agents was evaluated by growth curve assays. A range of field and clinical isolates known to express *bla*$_{\text{CTX-M-}}$ group 1 were selected and the efficacy of PNA4 and PMO1 were evaluated by co-administering with CTX/PNA/PMO combinations. To achieve efficient cell penetration, cell-penetrating peptide $(KFF)_3K$ was covalently bound to PNA4 and PMO1 to form peptide conjugated PMO1 (P-PMO1) and PNA4 (P-PNA4). The effects of P-PMO1 and P-PNA4 on field and clinical isolates were evaluated by the co-administration of peptide-conjugated antisense agents and CTX, and cell culture growth was measured by spectrophotometry.

Stein and Krieg highlighted several problems in demonstrating efficacy of antisense agents relating to non-specific effects of antisense agents, and suggested a minimum requirement of the use of two control oligomers in addition to the antisense oligomer, as well as noting the importance of demonstrating a decrease of the target protein [178]. The current study attempting the inhibition of the non-essential β-lactamase enzyme was able to investigate the effects of anti-*bla*$_{\text{CTX-M}}$ agents tested in the absence of CTX as a highly suitable control.

A range of field and clinical isolates expressing CTX-M-group 1 β-lactamases were selected for PNA/PMO inhibition studies (Table 5-1).

Table 5-1. CTX-M Group 1-expressing field and clinical isolates used in studies.

| **Designation** | **Plasmid** | ***bla* Resistance** | **Source Species** |
|---|---|---|---|
| LREC460 | pEK516 [74] | CTX-M-15 | Human |
| LREC461 | pEK204 [74] | CTX-M-3 | Human |
| LREC454 | pEK499 [74] | CTX-M-15 | Human pandemic strain |
| LREC525[164] | Not known | CTX-M-15 | Turkey |
| BZ693/P [164] | Not known | CTX-M-3/33 | Chicken |
| B3804 [165] | Not known | CTX-M-1 | Pig |
| LREC90 | Not known | CTX-M-14 | Cattle |

The region surrounding the Shine-Dalgarno and translational initiation region are highly conserved in group 1 CTX-M β-lactamases. PNA4 was designed to be 100% complementary with *bla*$_{\text{CTX-M-15}}$ , *bla*$_{\text{CTX-M-3/33}}$ and *bla*$_{\text{CTX-M-1}}$ transcripts, and PMO1 was designed to be 100% complementary with *bla*$_{\text{CTX-M-15}}$ and *bla*$_{\text{CTX-M-3/33}}$, and 96% (24 out of 25 bases) complementary with *bla*$_{\text{CTX-M-1}}$ transcript (Figure 5-1).


Figure 5-1. Alignment of *bla*CTX-M-15, *bla*CTX-M-3/33 and *bla*CTX-M-1 transcript sequences. Shine-Dalgarno (SD) region is shown in bold lowercase and translational start codon is shown in bold uppercase. Translated region of mRNA is shown in upper case. Asterisks indicate regions of shared homology between CTX-M types.

### 5.1.1. Experimental controls used for the evaluation of sequence specificity of antisense effects in field isolates

Specificity and any inherent toxicity of peptide-conjugated and unmodified PNA4 and PMO1 were demonstrated in whole cells in the following studies:

i. AS19/pJBRCTX516 was cultured in the presence of a scrambled non-specific PMO in the presence and absence of CTX and growth measured by spectrophotometry over 18 – 24 hours.
ii. Field isolates harbouring *bla*CTX-M-group 1 were cultured in the presence of P-PMO1 or P-PNA4 in the absence of CTX and growth measured by spectrophotometry over 18 - 24 hours. The targeting of non-essential *bla*CTX-M allowed the use of P-PMO1 and P-PNA4 in the absence of CTX as a highly suitable control for isolating the effects of the antisense agents and/or cell-penetrating peptide on growth. Additionally, studies typically included a set of control replicates of the antisense agent in the absence of CTX.

A field isolate, LREC90, was selected for control studies to isolate non-specific effects of P-PMO1 and P-PNA4. LREC90 carried a plasmid harbouring *bla*CTX-M-14, which

encoded β-lactamase from CTX-M-group 9. All other CTX resistant strains used in this study harboured variants from CTX-M-group 1. P-PMO1 and P-PNA4 were non-complementary to *bla*$_{\text{CTX-M-14}}$ mRNA - PNA4 shared 15.4% sequence complementarity (2 out of 13 bases) over the target region and PMO1 shared 56% (14 out of 25 bases) sequence complementarity over the target region (Figure 5-2) making this an equivalent control to a non-specific scrambled antisense oligomer with *bla*$_{\text{CTX-M-15}}$. This control option was considered preferable to a scrambled or mismatched antisense conjugate as the subject itself was assessed for potential non-specific effects in the control strain.

Field isolate LREC90 was cultured in the presence and absence of P-PNA4, P-PMO1 and CTX, and growth measured by spectrophotometry over 18 – 24 hours. Minimum inhibitory concentrations (CTX) were established for LREC90 in the presence and absence of P-PNA4.

```
CTX-M-14 mRNA 5'.gaccguauugggaguuugag AUG GUGACAAAGAGAGUGCAA.3'
pmo1                                agggtaccaatttttagtgacgcg
pna4                 ggtcttattcctt
                     *          *  *   ***** * ***   * ***
```

Figure 5-2. Region of maximum complementarity between PMO1, PNA4 and *bla*$_{\text{CTX-M-14}}$ mRNA.
Translational start region is shown in bold uppercase. Asterisks represent complementary bases. *bla*$_{\text{CTX-M-14}}$ is a mismatched control with anti-*bla*$_{\text{CTX-M-15}}$ PNA4 and PMO1. Best alignment of PMO1 = 56% complementarity. Best alignment of PNA4 = 15% complementarity. Asterisks represent complementary bases.

Table 5-2. Conversion tables of commonly used concentrations to facilitate antisense oligomer/CTX dose comparison.

| PMO1 | |
|---|---|
| **µM** | **µg/ml** |
| 10 | 85.1 |
| 20 | 170.3 |
| 30 | 255.4 |
| 40 | 340.6 |

| PNA4 | |
|---|---|
| **µM** | **µg/ml** |
| 10 | 36.2 |
| 20 | 72.4 |
| 30 | 108.6 |

| CTX | |
|---|---|
| **µg/ml** | **µM** |
| 2 | 4.2 |
| 8 | 16.8 |
| 10 | 20.9 |
| 12 | 25.1 |
| 16 | 33.5 |
| 24 | 50.3 |
| 32 | 67.0 |
| 48 | 100.5 |
| 64 | 134.0 |
| 96 | 201.1 |
| 128 | 268.1 |

| P-PMO1 | |
|---|---|
| **µM** | **µg/ml** |
| 10 | 102.2 |
| 20 | 204.4 |
| 30 | 306.6 |
| 40 | 408.8 |

| P-PNA4 | |
|---|---|
| **µM** | **µg/ml** |
| 1.6 | 8.3 |
| 3.2 | 16.6 |
| 5.0 | 26.0 |

## 5.2. Results

Minimum inhibitory concentrations (to CTX) were established by spectrophotometry for each *E. coli* strain, and was determined to be the minimum concentration of CTX required to inhibit growth ($O.D._{600\,nm} < 0.05$) in a minimum of 50% of replicates over 18 hours. A characteristic observation of increasing CTX concentrations in all strains was the lengthening in time taken to achieve logarithmic growth phase of the culture's growth cycle (Figure 5-4). Additionally, cultures incubated with an increasing, but sub-lethal, concentration of CTX were observed to display an increase in the numbers of replicates that were completely inhibited (Figure 5-3). The replicates able to grow under these conditions, although displaying an increased lag phase, often achieved a similar

terminal optical density to those at lower CTX concentrations. Minority surviving replicates were analysed for the presence of contaminants by recovery onto diagnostic media such as Brilliance™ UTI Clarity (ThermoScientific), and 5% sheep blood agar. Minority surviving replicates were also recovered into fresh media, split into equal aliquots, and each aliquot supplemented with an increasing amount of CTX to investigate the possibility of revertants or mutants with a reduced CTX susceptibility. In all cases, the aberrant cultures able to survive in conditions that inhibited the growth of the majority of the other replicates were found to have the same CTX susceptibility profile of the parent cultures, and no contaminants were observed. The explanation for the observed growth by some replicates and no growth in other replicates remains undefined but is likely to be due to biological variation more apparent at CTX levels approaching inhibitory concentrations – illustrated in Figure 5-3.

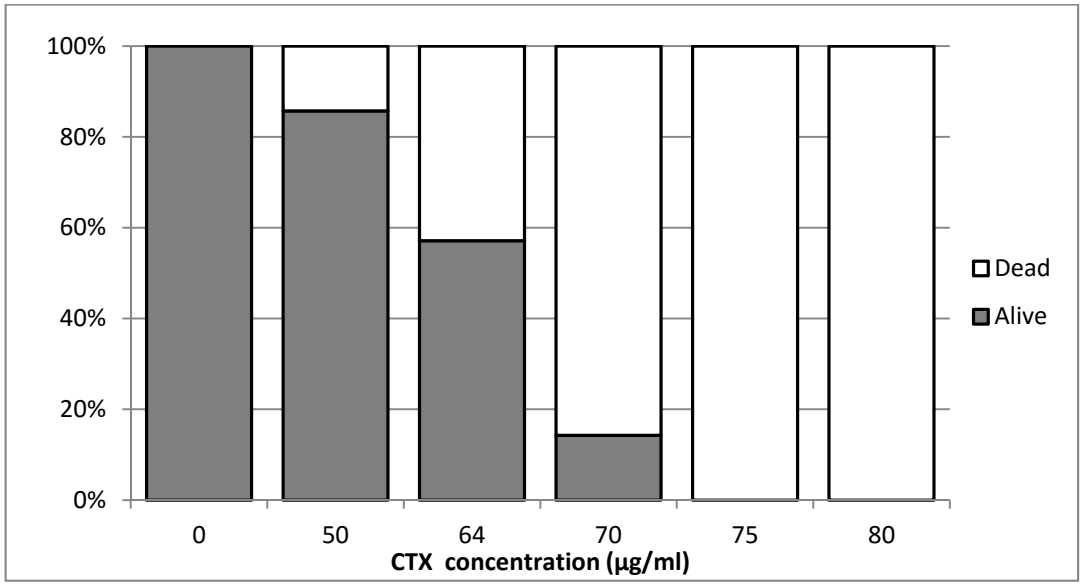


Figure 5-3. Survival graph showing survival of *E. coli* AS19/pJBRCTX516 replica cultures in increasing concentrations of cefotaxime.

Number of replicates for each CTX concentration = 7; dead = no growth (O.D. $_{600\ nm} < 0.05$) measured spectrophotometrically after 18 hours; alive = O.D. $_{600\ nm} > 0.5$ after 18 hours.

Atypically permeable cell-wall mutant *E. coli* strain AS19 allows the uptake of small molecules that would otherwise be unable to achieve cellular penetration in field isolates. It has previously been used extensively as a model organism for gene expression inhibition by synthetic antisense oligomers [122, 127, 135, 136, 179]. AS19 was transformed with recombinant plasmids pJBRCTX499 and pJBRCTX516 by electroporation. Growth curves determined by culture turbidity, measured by spectrophotometry, revealed the minimum inhibitory concentration (to CTX) of AS19/ pJBRCTX516 under these conditions to be greater than 64 µg/ml, and less than 128 µg/ml (Figure 5-4). After further refinements in this concentration range, the MIC (to CTX) was observed to be approximately 80 µg/ml.

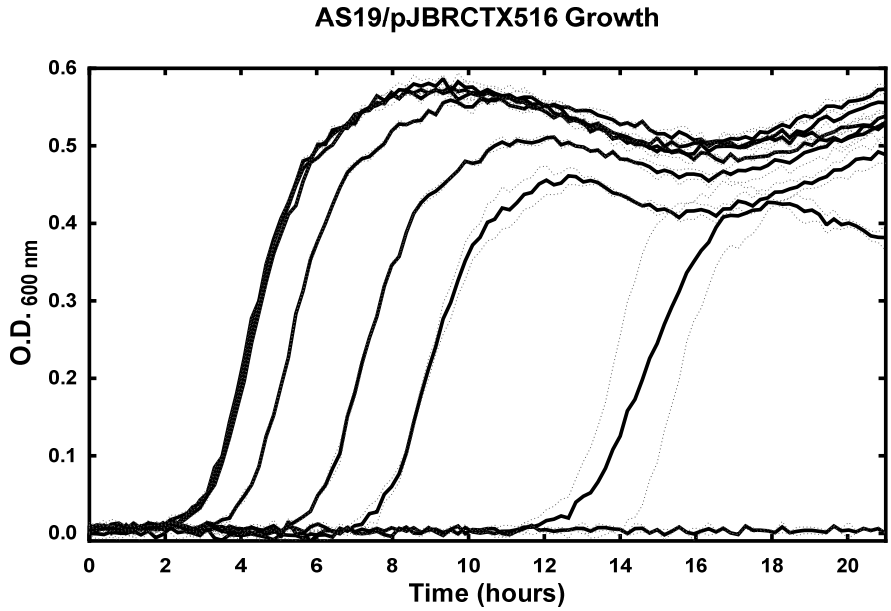


Figure 5-4. Growth curves showing the sensitivity of AS19/pJBRCTX516 to CTX (0 - 128 µg/ml).

Increasing CTX concentrations (2 – 128 µg/ml) result in an extension in time taken to achieve logarithmic growth phase in a dose dependant manner. Bacterial growth curves from left to right: CTX (0 µg/ml), CTX (2 µg/ml), CTX (4 µg/ml), CTX (8 µg/ml), CTX (16 µg/ml), CTX (32 µg/ml), CTX (64 µg/ml), CTX (128 µg/ml; no growth). Error bars indicate ± 1 standard deviation (n=3).

### 5.2.1. Levels of *bla*$_{CTX-M}$ activity in a laboratory cell-wall mutant strain of *E. coli* are reduced by antisense oligomer treatment

AS19/ pJBRCTX516 was challenged with PMO1 (0 – 40 μM) in combination with cefotaxime (4 μg/ml). The results showed an increasing sensitivity to cefotaxime in a PMO1 dose dependant manner (0 – 40 μM; Figure 5-5). Complete inhibition of growth was observed at a CTX concentration of 4 μg/ml when combined with PMO1 at a concentration of 40 μM. The cultures showing no growth were recovered onto LB agar to confirm the bactericidal effects. No colony growth was observed after an overnight incubation at 37° C. When incubated with PMO1 (5 – 30 μM) in the absence of CTX, no inhibitory effects were observed (Figure 5-6), indicating that the PMO alone had no inherent inhibitory properties.

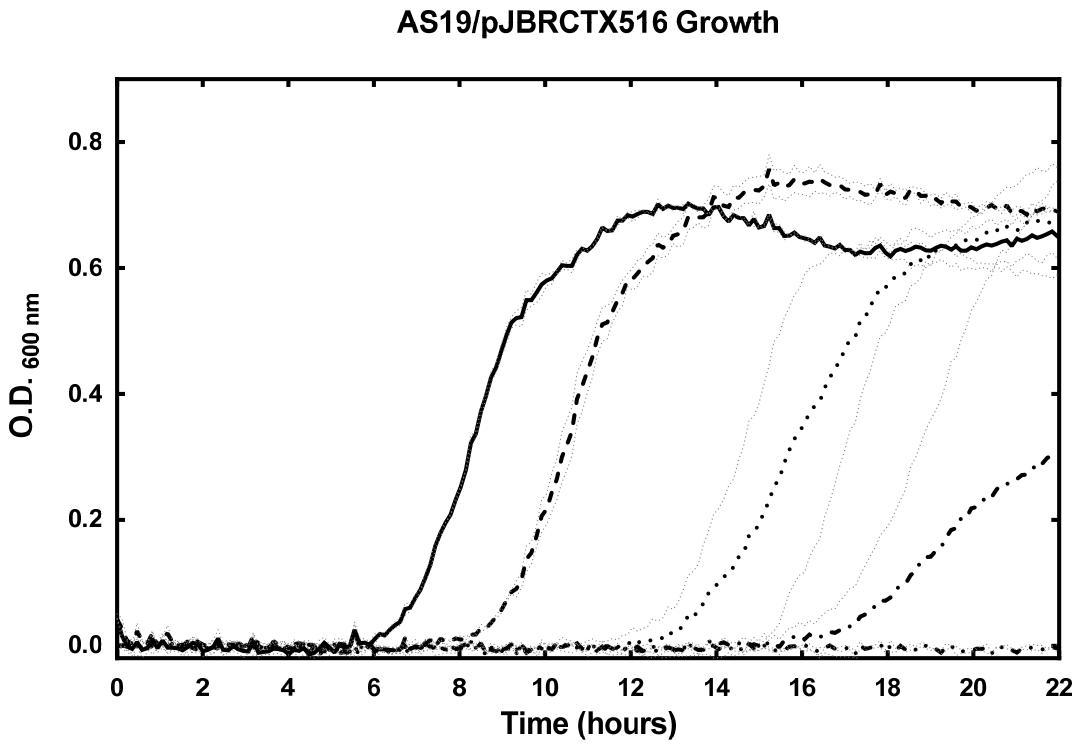


Figure 5-5. Growth curves showing the increasing sensitivity of AS19/pJBRCTX516 to CTX (4 µg/ml) in the presence PMO1 (0-40 µM).

All samples were treated with 4µg/ml CTX and increasing PMO concentrations (0-40 µM). At 40 µM PMO concentration, growth was completely inhibited. Solid line: CTX (4 µg/ml), dashed line: CTX (4 µg/ml) + PMO1 (10 µM), dotted line: CTX (4 µg/ml) + PMO1 (20 µM), dash-dot line: CTX (4 µg/ml) + PMO1 (30 µM), dash-dot-dot line: CTX (4 µg/ml) + PMO1 (40 µM). Error bars indicate ± 1 standard deviation (n=2).

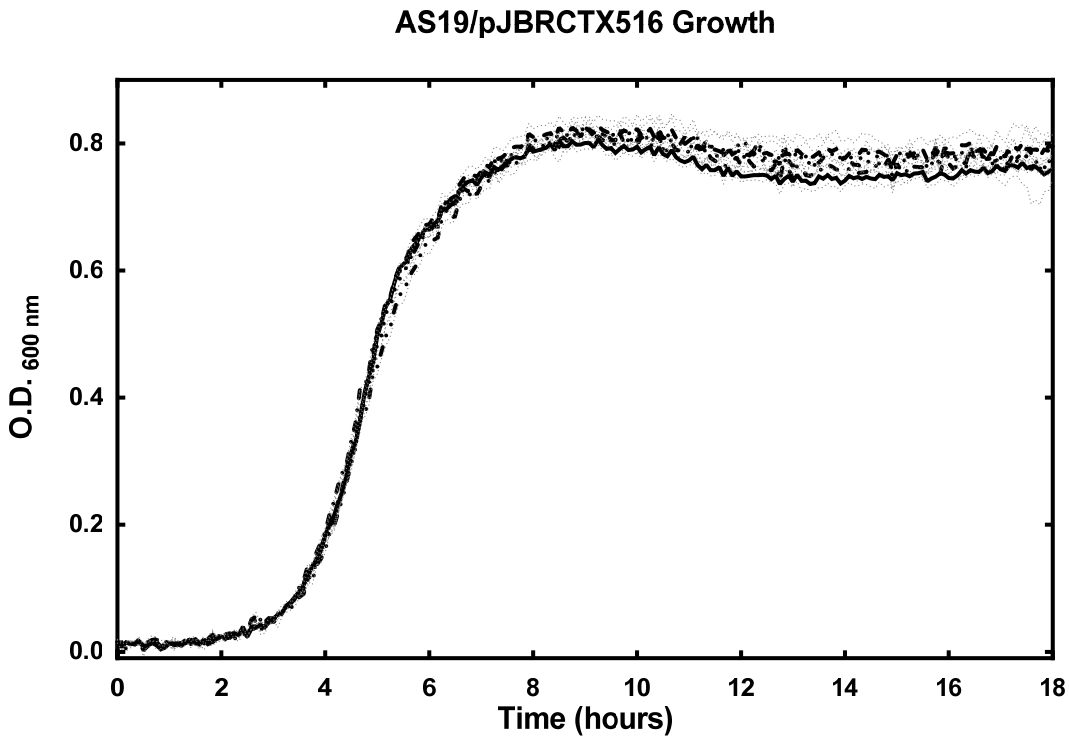


Figure 5-6. Growth curves showing the insensitivity of AS19/pJBRCTX516 to PMO1 alone (0 - 30 μM).
Graph showing no effect on growth when cultures were treated with PMO1 alone at any concentration (5 - 30 μM). Six curves shown (5, 10, 15, 20 and 30 μM) with no significant differences between any. Error bars indicate ± 1 standard deviation (n=2).

AS19/ pJBRCTX516 was challenged with the combination of cefotaxime (4 μg/ml) and PNA4 at concentrations of 0, 10 and 20 μM (Figure 5-7). In contrast with the higher inhibitory efficacy of PMO1 observed in a cell-free translation/transcription coupled system, PNA4 completely inhibited growth at 20 μM - half the concentration required of PMO1 to yield complete growth inhibition. Recovery was again attempted on non-selective media of the cultures observed to have shown no growth, and no colonies were observed, affirming the bactericidal effects of the combination of CTX and PNA4.

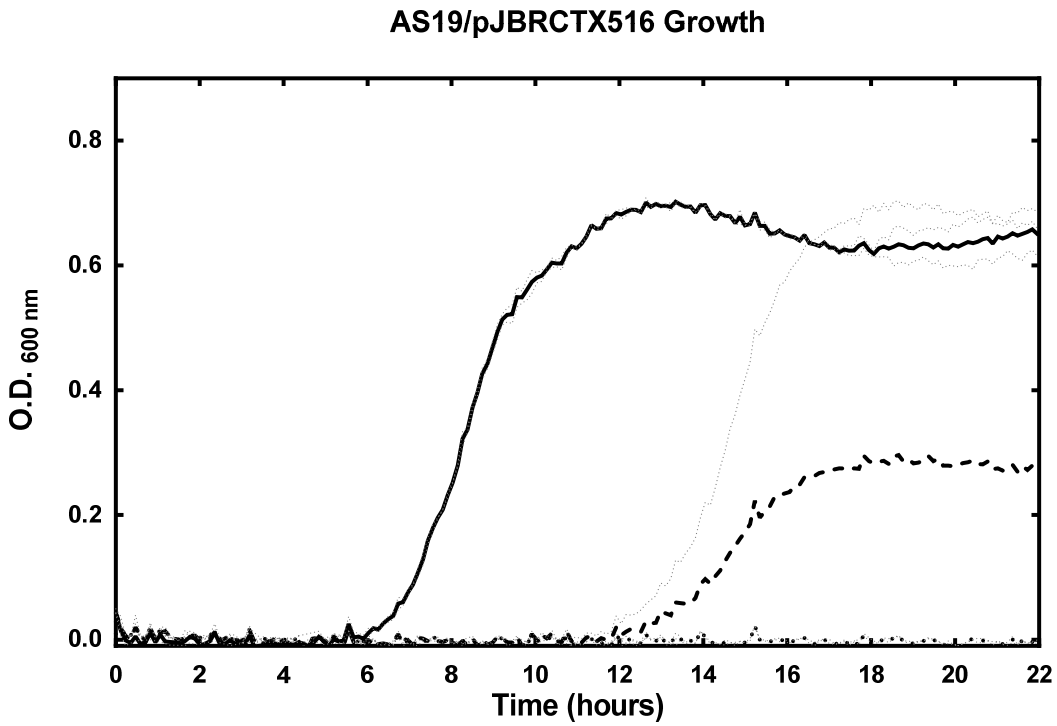


Figure 5-7. Growth curves showing the sensitivity of AS19/pJBRCTX516 to CTX (4 μg/ml) in the presence and absence of PNA4 (0-20 μM).
Increase in sensitivity to CTX by the addition of PNA4. 4 μg/ml and 20 μM PNA4 inhibited growth. Solid line: CTX (4 μg/ml), dashed line: CTX (4 μg/ml) + PNA4 (10 μM), dotted line: CTX (4 μg/ml) + PNA4 (20 μM). Error bars indicate ± 1 standard deviation (n=2).

When challenged with PNA4 alone, a significant inhibitory growth effect was observed in a dose dependent manner (Figure 5-8) suggesting an inherent bactericidal or inhibitory property of PNA4. A significant inhibitory effect on growth was noted at concentrations range greater than 5 μM.

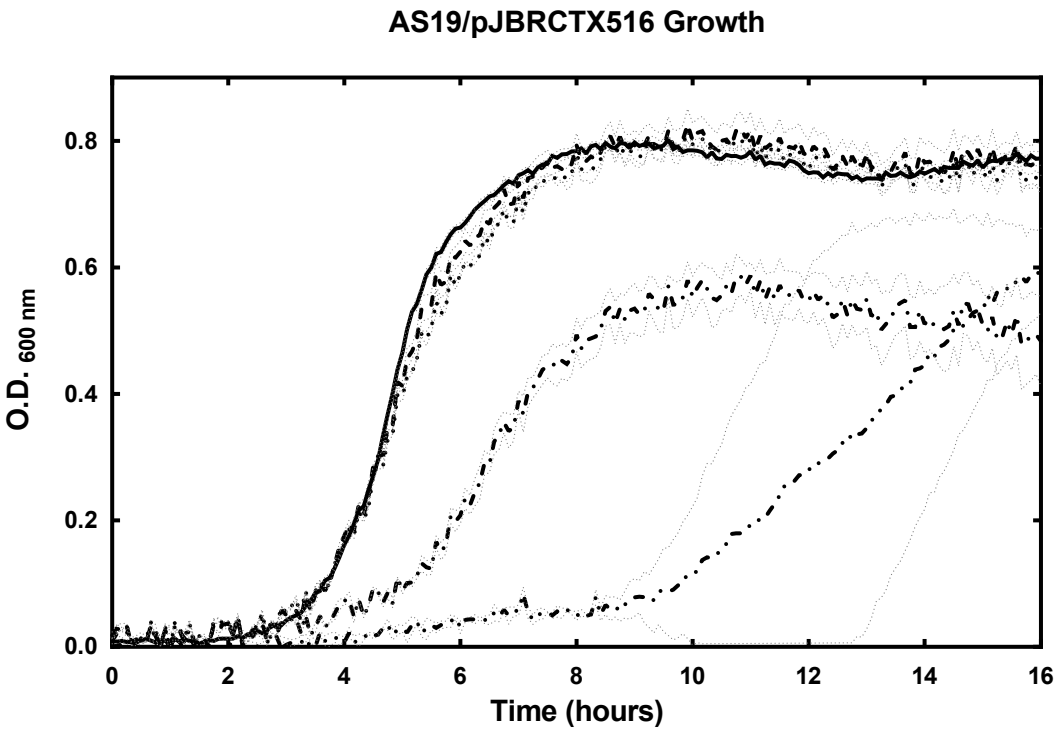


Figure 5-8. Growth curves showing the sensitivity of AS19/pJBRCTX516 to PNA4 (5 - 30 μM) in the absence of CTX.

Cultures treated with PNA4 (5 – 30 μM) alone showed a dose dependant increase in the time taken to achieve logarithmic growth phase, indicating inherent toxicity. Solid line: PNA4 (0 μM), dashed line: PNA4 (5 μM), dotted line: PNA4 (10 μM), dash-dot line: PNA4 (20 μM), dash-dot-dot line: PNA4 (30 μM). Error bars indicate ± 1 standard deviation (n=3).

### 5.2.2. Levels of *bla*$_{CTX-M}$ activity in field isolate strains of *E. coli* are effectively reduced by treatment with antisense oligomers conjugated to a cell-penetrating peptide

Field isolate LREC461 was evaluated in the presence of CTX and unmodified PNA4 and PMO1 for evidence of increased antibiotic susceptibility. Cultures were incubated with either PMO1 (5 - 20 μM) or PNA4 (5 - 40 μM) and CTX (16 μg/ml) at 37° C for 18 hours and optical density measured at a light wavelength of 600 nm at 5 minute intervals. No significant increased sensitivity to CTX, evidenced by a lack of any

increased duration in time taken to achieve logarithmic growth, was observed at any concentration of either PMO1 or PNA4 (Figure 5-9; Figure 5-10 respectively). This was consistent with the expectation that an unmodified PNA or PMO would be unable to efficiently penetrate a typical bacterial cell wall.

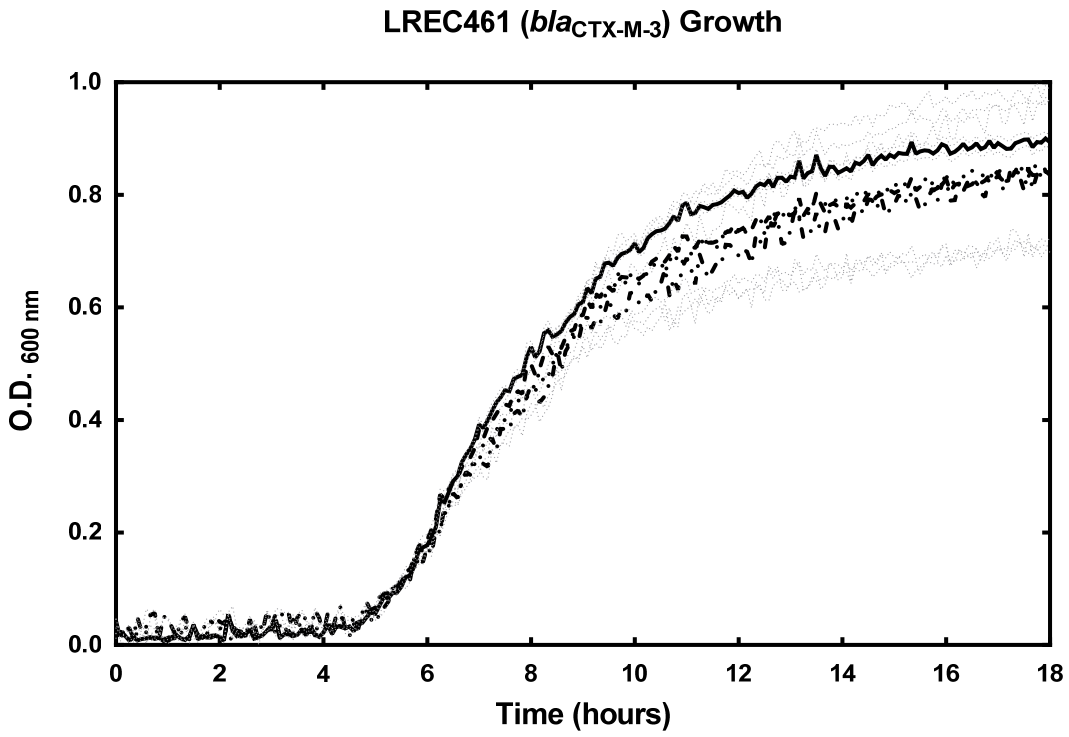


Figure 5-9. Growth curves showing effect of CTX (16 µg/ml) in the presence of PMO1 (5 – 20 µM) on field isolate LREC461 harbouring *bla*$_{\text{CTX-M-3}}$.
LREC461 incubated with CTX (16 µg/ml) and PMO1 (5, 10 and 20 µM). LREC461 incubated with CTX (16 µg/ml) and PMO1 (5, 10 and 20 µM). Solid line: CTX (16 µg/ml), dashed line: CTX (16 µg/ml) + PNA4 (5 µM), dotted line: CTX (16 µg/ml) + PMO1 (10 µM), dash-dot line: CTX (16 µg/ml) + PMO1 (20 µM). Error bars indicate ± 1 standard deviation (n=3).

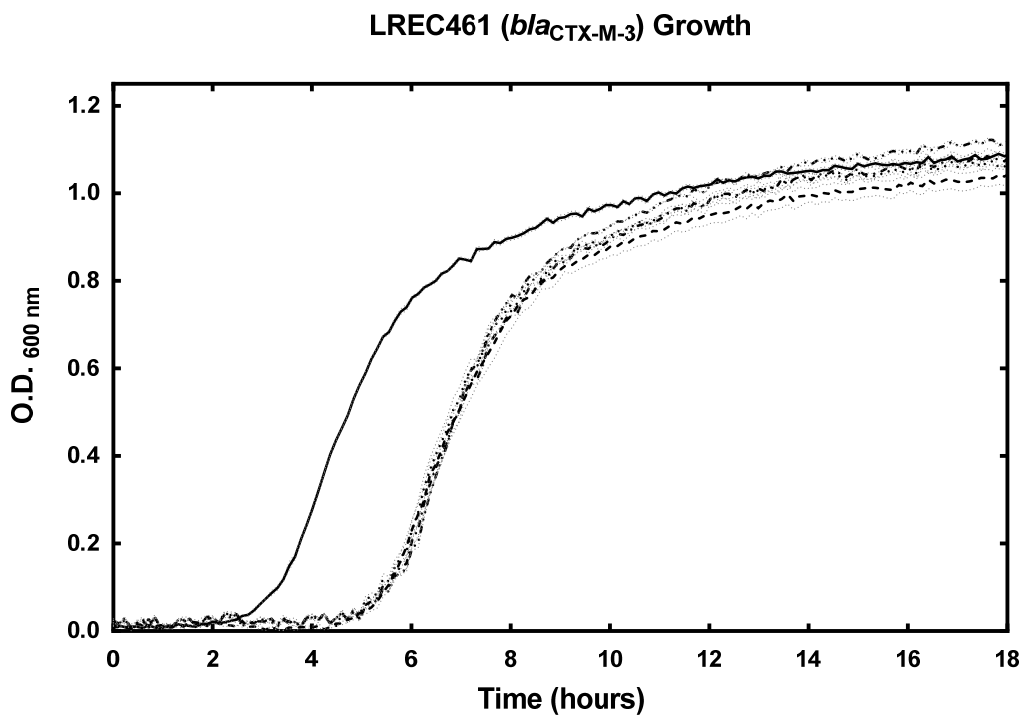


Figure 5-10. Growth curves showing effect of CTX (16 µg/ml) in the presence of PNA4 (10 – 30 µM) on field isolate LREC461 harbouring *bla*$_{CTX-M-3}$.
Growth curves showing effect on growth of field isolate LREC461 incubated with CTX and PNA4. Solid line: Control, dashed line: CTX (16 µg/ml), dotted line: CTX (16 µg/ml) + PNA4 (10 µM), dash-dot line: CTX (16 µg/ml) + PNA4 (20 µM), dash-dot-dot line: CTX (16 µg/ml) + PNA4 (30 µM). Error bars indicate +/- 1 standard deviation (n=2).

To facilitate the entry of PNA4 and PMO1, these antisense oligomers were covalently attached to the cell-penetrating peptide, $(KFF)_3K$. This cell-penetrating peptide has previously been shown by many studies to be an effective bacterial delivery vehicle for both PMO and PNA chemistries.

Peptide-conjugated PMO1 (P-PMO1) and peptide-conjugated PNA4 (P-PNA4) were evaluated in combination with CTX for growth inhibitory effects in a panel of field isolates (LREC460, LREC461, LREC454, B3804, LREC525, BZ693/P and LREC461; Table 5-1). *E. coli* strain LREC90, used for control studies, carried a plasmid

harbouring *bla*$_{\text{CTX-M-14}}$, which encoded β-lactamase from CTX-M-group 9. All other CTX resistant strains used in this study harboured variants of CTX-M-group 1. Cefotaxime concentrations were selected based on estimations of the concentrations required to create inhibitory conditions with the presence of P-PMO1 (10 – 30 μM), and P-PNA4 (2 – 5 μM). Cefotaxime concentrations observed to be favourable to optimum effect when combined with peptide-conjugated antisense oligomers were the concentrations required to delay the exponential growth phase of the culture by approximately 2 – 4 hours. If a larger or smaller than expected effect size was observed, CTX concentration, antisense oligomer concentration, or both, were adjusted accordingly. Peptide-conjugated antisense oligomer concentrations were initially selected based upon AS19/pJBRCTX516 studies at maximum levels used which were observed to have no significant effect on the growth of the cultures when the cultures were treated in the absence of CTX.

All isolates showed an increased sensitivity to CTX when treated with anti-*bla*$_{\text{CTX-M}}$ P-PMO1 (30 μM) ranging from a reduction in the MIC (to CTX) in *bla*$_{\text{CTX-M-3}}$-harbouring strain from 35 μg/ml to 16 μg/ml (2.19-fold increase in sensitivity), to a strain harbouring *bla*$_{\text{CTX-M-1}}$ from 48 μg/ml to 10 μg/ml (4.8-fold increase in sensitivity). The same isolates when treated with P-PNA4 (3.2 μM) had an observed increase in CTX sensitivity ranging from a reduction in MIC (to CTX) in *bla*$_{\text{CTX-M-3/33}}$-harbouring strain BZ693/P from 40 μg/ml to 12 μg/ml (3.3-fold) to a strain harbouring *bla*$_{\text{CTX-M-15}}$ (LREC454) from 110 μg/ml to 2 μg/ml (55-fold). Growth curves representing these findings are presented in Appendix A from Figure A-1 to Figure A-12. Wherever resources allowed, dose response data was experimentally obtained. All replicates were independent cultures. Table 5-3 summarises the reduction in MICs (to CTX) observed in these strains.

Table 5-3. Summary of findings of increased sensitivity of field and clinical *E. coli* isolates to CTX when treated with anti-*bla*$_{\text{CTX-M-15}}$ peptide-conjugated antisense agents. † P-PNA4 concentration = 5 µM, ‡ P-PMO1 concentration = 40 µM

| Strain Reference | Plasmid | *bla*$_{\text{CTX-M}}$ | Source Species | MIC – CTX (µg/ml) | MIC – CTX + P-PMO1 (30 µM) (µg/ml) | MIC – CTX + P-PNA4 (3.2 µM) (µg/ml) |
|---|---|---|---|---|---|---|
| LREC460 | pEK516 [74] | CTX-M-15 | Human | 100 | 32‡ | 24 |
| LREC454 | pEK499 [74] | CTX-M-15 | Human | 110 | 24 | 2 |
| BZ693/P [164] | Not known | CTX-M-3/33 | Chicken | 40 | 15 | 12 |
| B3804 [165] | pIFM3804 | CTX-M-1 | Pig | 48 | 10 | 2 |
| LREC525 [164] | Not known | CTX-M-15 | Turkey | 260 | 96 | 48 |
| LREC461 | pEK204 [74] | CTX-M-3 | Human | 35 | 16 | 8† |
| LREC90 | Not known | CTX-M-14 | Cattle | 20 | Not tested | 20 |

### 5.2.3. Evaluation of the sequence specificity of antisense effects on expression of CTX-M-15 activity in field isolates

A series of control studies were undertaken to establish and isolate any non-specific effects of peptide-conjugated antisense oligomers on the growth on *E. coli* strains with intact cell walls. It had been previously established in studies using AS19/pJBRCTX516 that PMO1 had no significant negative effects on growth when administered in the absence of cefotaxime (Figure 5-6). This would suggest that PMO1 alone had no non-specific inhibitory activity, and was non-toxic to the bacteria cultured in its presence.

*E. coli* field isolate, LREC454, harbouring plasmid pEK499, expressing *bla*$_{\text{CTX-M-15,}}$ was cultured in the presence of P-PMO1 (10 – 30 μM) in the absence of cefotaxime. Results showed a dose-dependent inhibitory effect (Figure 5-11).

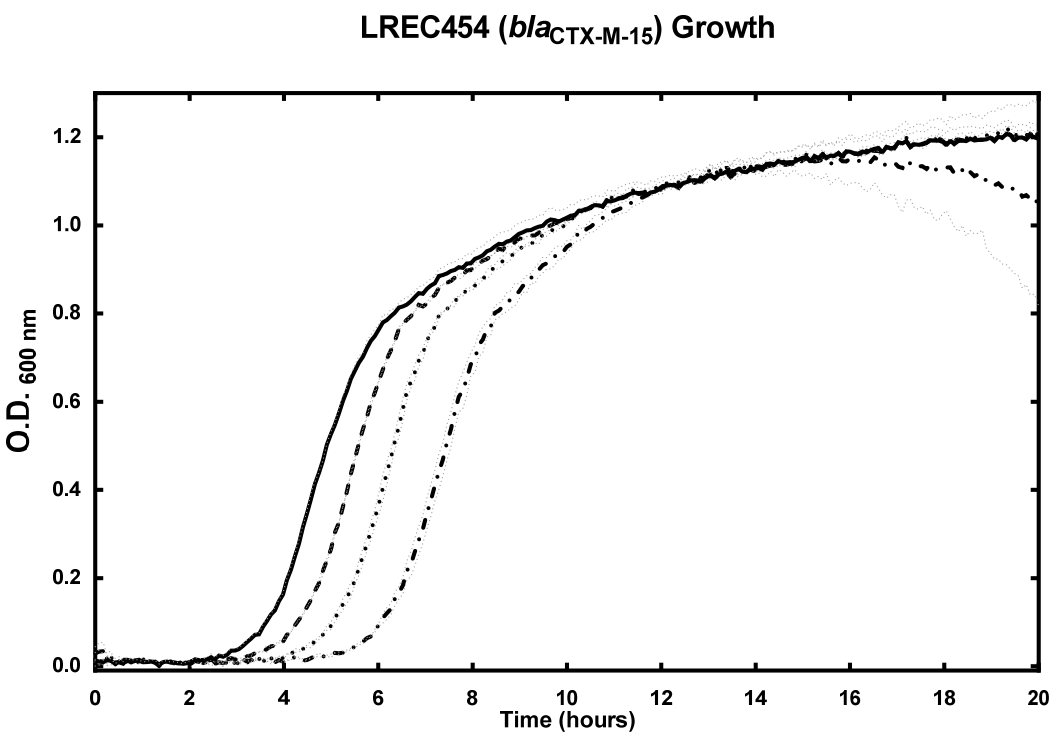


Figure 5-11. Growth curves showing effect of P-PMO1 (10 - 30 μM) in the absence of CTX on field isolate LREC454 harbouring *bla*$_{CTX-M-15}$.

LREC454 incubated with P-PMO1 (10 - 30 μM). Solid line: control, dashed line: P-PMO1 (10 μM), dotted line: P-PMO1 (20 μM), dash-dot line: P-PMO1 (30 μM). Error bars indicate ± 1 standard deviation (n=2).

To isolate non-specific effects of P-PMO1 or effects of peptide portion of the P-PMO1 conjugate, field isolate LREC90 harbouring *bla*$_{\text{CTX-M-14}}$, a member of CTX-M-group 9, was cultured in the presence and absence of CTX and in the presence of P-PMO1. PMO1 shared 56% sequence complementarity (14/25 bases) with *bla*$_{\text{CTX-M-14}}$ (Figure 5-2) making this, as previously noted, an equivalent control to a non-specific scrambled antisense oligomer with *bla*$_{\text{CTX-M-15}}$. A dose-dependent inhibitory effect of similar size to that previously observed in the growth of LREC454 (Figure 5-11) was observed when LREC90 was cultured in the presence of P-PMO1 alone (Figure 5-12).

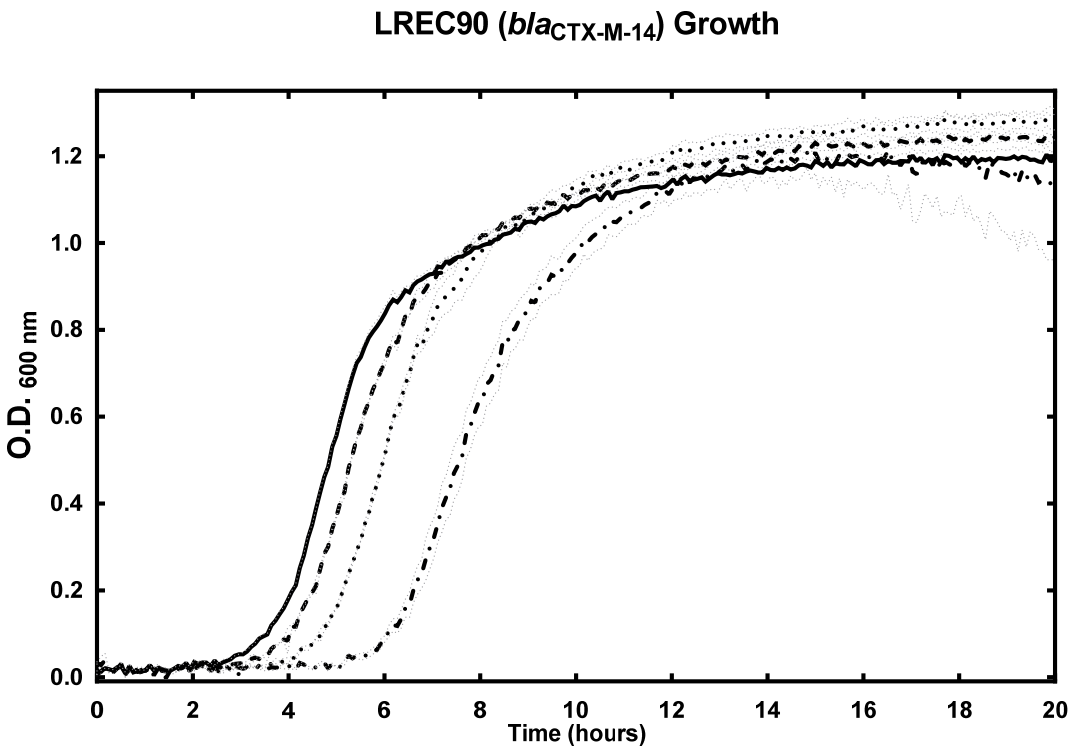


Figure 5-12. Growth curves showing effect of P-PMO1 (10 - 30 µM) in the absence of CTX on field isolate LREC90 harbouring *bla*$_{\text{CTX-M-14}}$.
LREC90 incubated with P-PMO1 (10 - 30 µM). Solid line: control, dashed line: P-PMO1 (10 µM), dotted line: P-PMO1 (20 µM), dash-dot line: P-PMO1 (30 µM). Error bars indicate ± 1 standard deviation (n=2).

Control strain LREC90 was cultured in the presence of P-PMO1 and CTX (3 µg/ml; Figure 5-13) and an effect greater than that observed when LREC90 was cultured in the presence of P-PMO1 alone (Figure 5-12), was observed. This was potentially attributable to the combined additive effects of CTX and the peptide portion of the P-PMO1 conjugate previously observed.

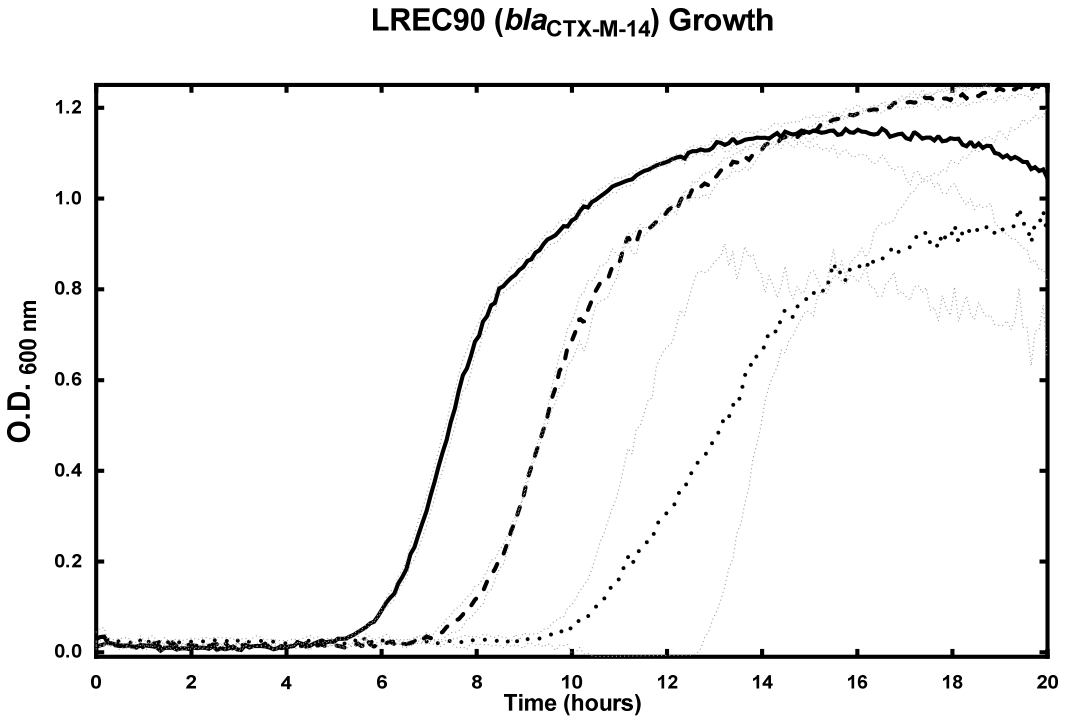


Figure 5-13. Growth curves showing effect of P-PMO1 (10 - 30 µM) in the presence of CTX (3 µg/ml) on field isolate LREC90 harbouring *bla*CTX-M-14.
LREC90 incubated with CTX (3 µg/ml) and P-PMO1 (10 - 30 µM). Solid line: CTX (3 µg/ml), dashed line: CTX (3 µg/ml) + P-PMO1 (10 µM), dotted line: CTX (3 µg/ml) + P-PMO1 (30 µM). Error bars indicate ± 1 standard deviation (n=2).

To evaluate specific effects of P-PNA4, *E. coli* field isolate LREC90 (control strain), harbouring *bla*$_{\text{CTX-M-14}}$ was incubated in the presence of CTX (2 – 20 µg/ml) and minimum inhibitory concentrations established (Figure 5-14). In the presence of CTX (2 – 20 µg/ml) and P-PNA4 (3.2 µM), the MIC (to CTX) was not reduced (Figure 5-15).

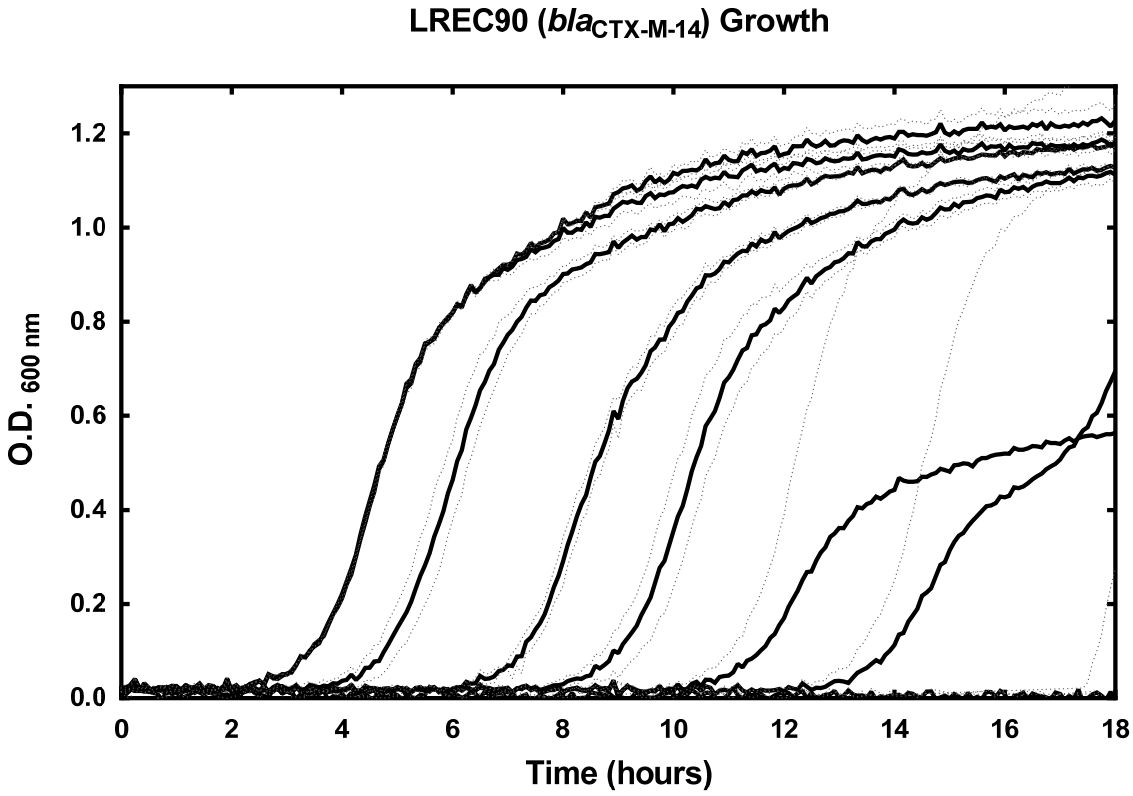


Figure 5-14. Growth curves showing effect of CTX (2 - 20 µg/ml) on growth of control strain LREC90 harbouring *bla*$_{\text{CTX-M-14}}$.
Bacterial growth curves from left to right: CTX (0 µg/ml), CTX (2 µg/ml), CTX (5 µg/ml), CTX (8 µg/ml), CTX (11 µg/ml), CTX (14 µg/ml), CTX (17 µg/ml), CTX (20 µg/ml; no growth). Error bars indicate ± 1 standard deviation (n=2).

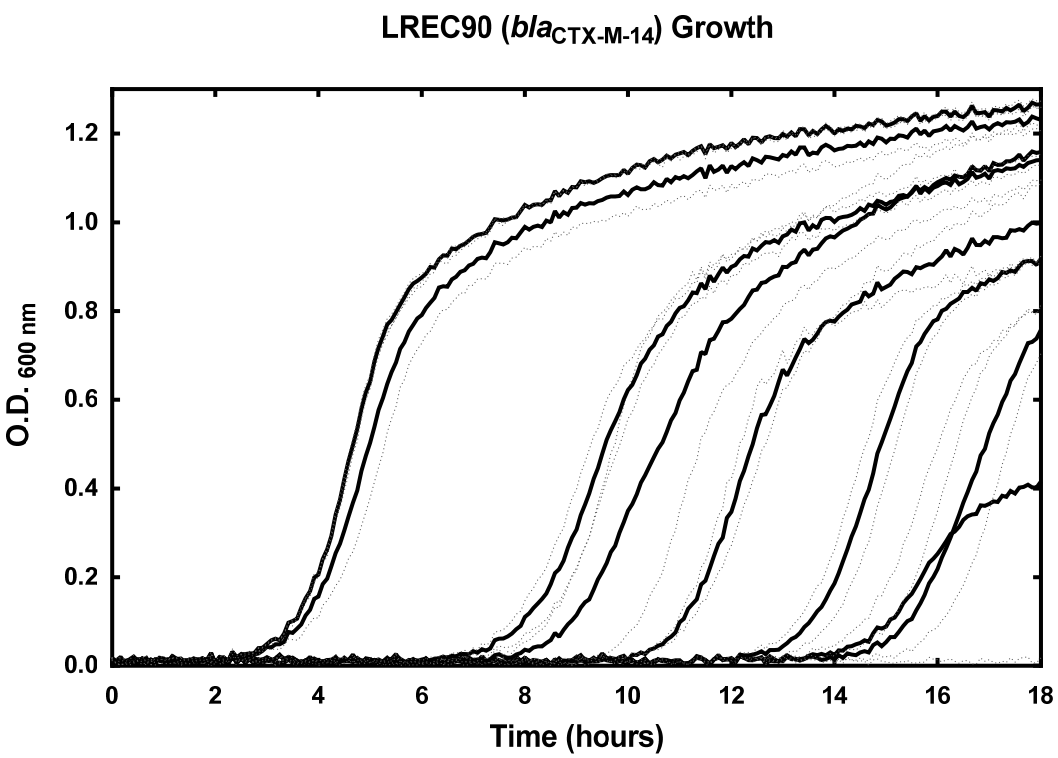


Figure 5-15. Growth curves showing effect of CTX (2 - 20 µg/ml) and P-PNA4 (3.2 µM) on growth of control strain LREC90 harbouring *bla*CTX-M-14.
Curves from left to right: CTX (0 µg/ml) + P-PNA4 (3.2 µM), CTX (2 µg/ml) + P-PNA4 (3.2 µM), CTX (5 µg/ml) + P-PNA4 (3.2 µM), CTX (8 µg/ml) + P-PNA4 (3.2 µM), CTX (11 µg/ml) + P-PNA4 (3.2 µM), CTX (14 µg/ml) + P-PNA4 (3.2 µM), CTX (17 µg/ml) + P-PNA4 (3.2 µM), CTX (20 µg/ml) + P-PNA4 (3.2 µM). Error bars indicate ± 1 standard deviation (n=2).

*E. coli* field isolate LREC90 (control strain), harbouring *bla*CTX-M-14 was treated with P-PNA4 (1.6 - 5 µM) in the absence of CTX (Figure 5-16) and treated with P-PNA4 (1.6 - 5 µM) in combination with CTX (2 µg/ml; Figure 5-17). No significant differences were observed between the cultures incubated in the presence of P-PNA4 and CTX and the cultures incubated in the presence of P-PNA4 alone.

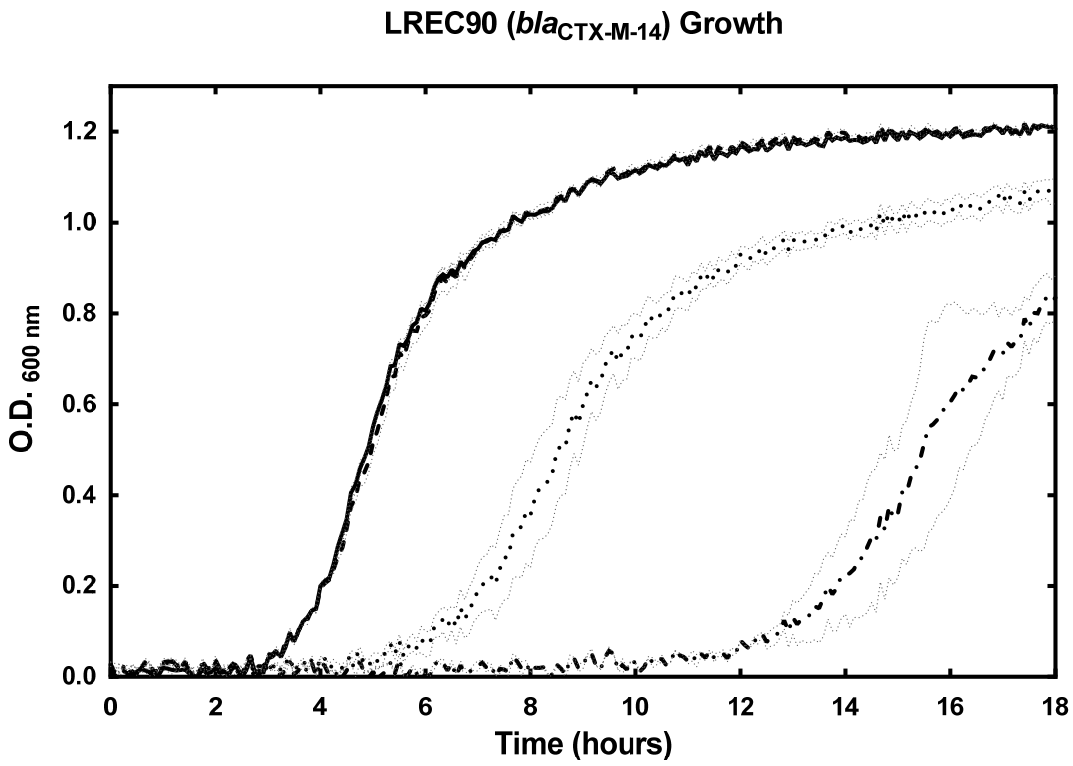


Figure 5-16. Growth curves showing effect of P-PNA4 (1.6 - 5 μM) on growth of control strain LREC90 harbouring *bla*CTX-M-14.

Solid line: control, dashed line: P-PNA4 (1.6 μM), dotted line: P-PNA4 (3.2 μM), dash-dot line: P-PNA4 (5 μM). Error bars indicate ± 1 standard deviation (n=2).

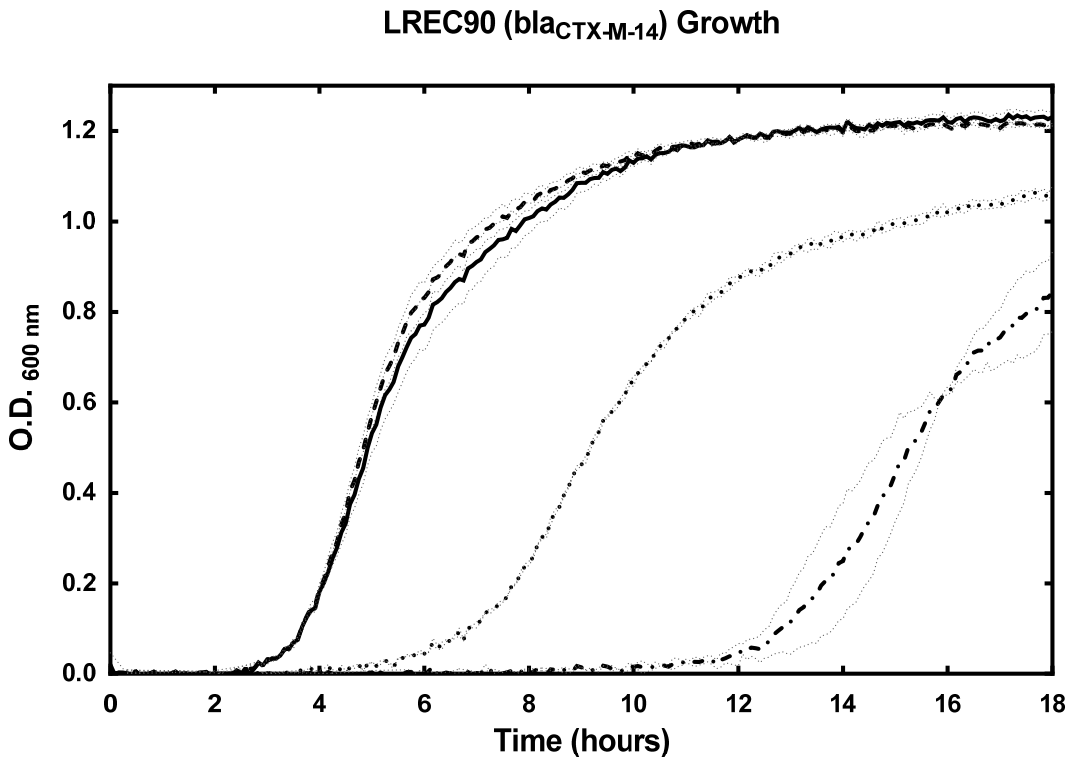


Figure 5-17. Growth curves showing effect of P-PNA4 (1.6 - 5 µM) and CTX (2 µg/ml) on growth of control strain LREC90 harbouring *bla*$_{\text{CTX-M-14}}$.
Solid line: CTX (2 µg/ml), dashed line: CTX (2 µg/ml) + P-PNA4 (1.6 µM), dotted line: CTX (2 µg/ml) + P-PNA4 (3.2 µM), dash-dot line: CTX (2 µg/ml) + P-PNA4 (5 µM). Error bars indicate ± 1 standard deviation (n=2).

For a direct comparative study of specificity of anti-*bla*$_{\text{CTX-M-15}}$ P-PNA4, *E. coli* field isolate LREC454 harbouring *bla*$_{\text{CTX-M-15}}$ was incubated under the same conditions as the previous control study with strain LREC90, in the presence of P-PNA4 (1.6 - 5 µM) and in the absence and presence of CTX (2 µg/ml). A comparable effect on growth to that observed with LREC90 incubated in the presence of P-PNA4 alone (1.6 - 5 µM; Figure 5-16) was observed with strain LREC454 incubated in the presence of P-PNA4 alone (1.6 – 5 µM; Figure 5-18). However, in contrast with the control study using strain LREC90, when LREC454 was cultured in the presence of CTX (2 µg/ml) and P-PNA4

(1.6 - 5 μM) a greater negative effect on growth was observed (Figure 5-19), suggesting a CTX potentiating effect of P-PNA4.

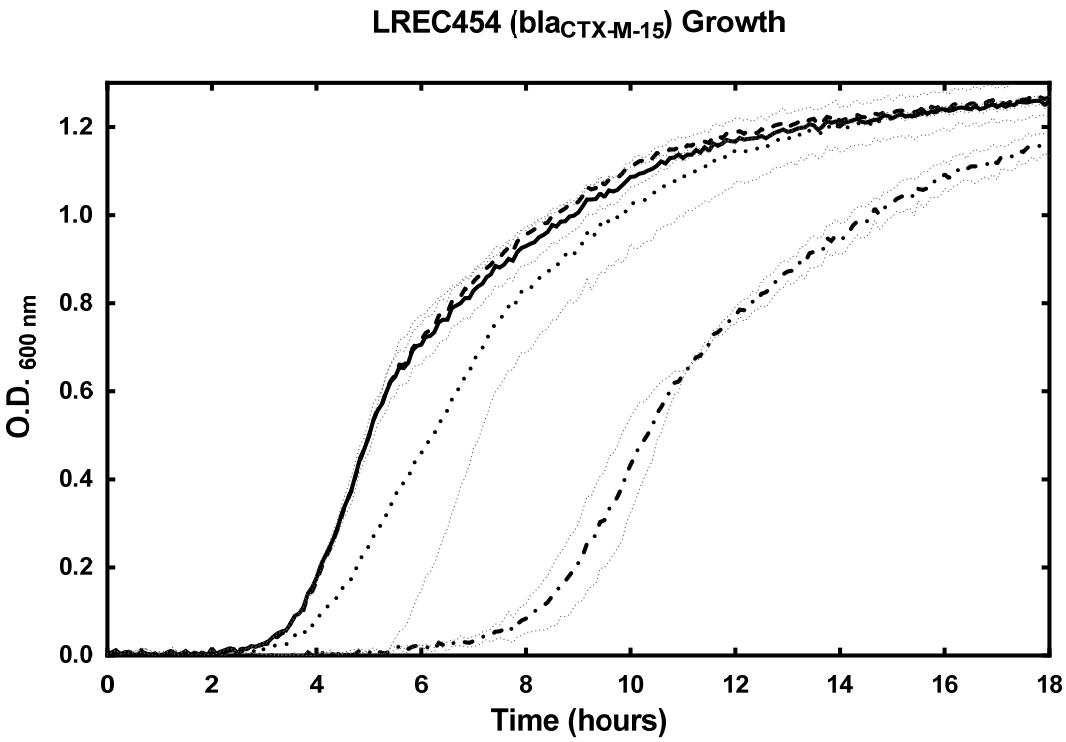


Figure 5-18. Growth curves showing effect of P-PNA4 (1.6 - 5 μM) on growth of control strain LREC454 harbouring *bla*$_{\text{CTX-M-15}}$.
Solid line: control, dashed line: P-PNA4 (1.6 μM), dotted line: P-PNA4 (3.2 μM), dash-dot line: P-PNA4 (5 μM). Error bars indicate ± 1 standard deviation (n=2).

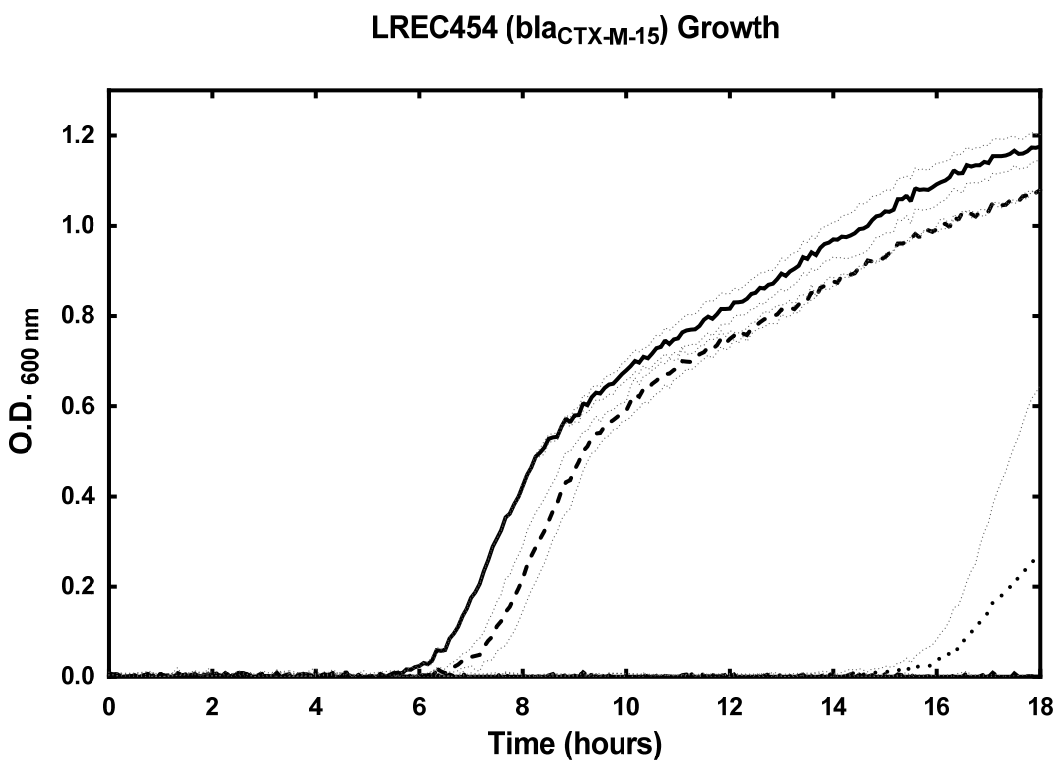


Figure 5-19. Growth curves showing effect of P-PNA4 (1.6 - 5 μM) and CTX (2 μg/ml) on growth of control strain LREC454 harbouring *bla*CTX-M-15.
Solid line: CTX (2 μg/ml), dashed line: CTX (2 μg/ml) + P-PNA4 (1.6 μM), dotted line: CTX (2 μg/ml) + P-PNA4 (3.2 μM), dash-dot line: CTX (2 μg/ml) + P-PNA4 (5 μM). Error bars indicate ± 1 standard deviation (n=2).

### 5.2.4. Effects of the combination of P-PNA4 and CTX on *E. coli* field isolate LREC525 cultures

Previous studies had demonstrated the growth-inhibitory properties of the CTX / peptide-conjugated antisense oligomer combination in field and clinical isolates. To observe any effects of P-PNA4 on established cultures, field isolate LREC525 harbouring *bla*$_{\text{CTX-M-15}}$ was cultured until early-mid log phase (O.D. $_{600\ \text{nm}}$ 0.2 - 0.3) was achieved, and then split into 4 aliquots and treated as follows: control; CTX (48 µg/ml); P-PNA4 (3.2 µM), and P-PNA4 (3.2 µM) and CTX (48 µg/ml). The aliquots were incubated and samples removed approximately every 10 minutes. The samples were diluted and spread onto LB agar plates and cultured overnight. The next day, visible colonies from each time point were counted. Colony counts indicated the cultures exposed to P-PNA4 / CTX combination declined between 13 and 94 minutes, from $1.04 \times 10^5$ CFU/µl to $2.9 \times 10^4$ CFU/µl, but were then able to recover and achieve logarithmic growth. The samples treated with P-PNA4 alone showed an overall increase in the colony forming units, although a static period of no growth was observed between 40 and 70 minutes. The culture sample not treated with any antibiotic or P-PNA4 increased steadily in number over 90 minutes. The aliquot treated with cefotaxime alone showed a slight decline in colony forming units between 10 and 70 minutes after exposure, before increasing in number (Figure 5-20).

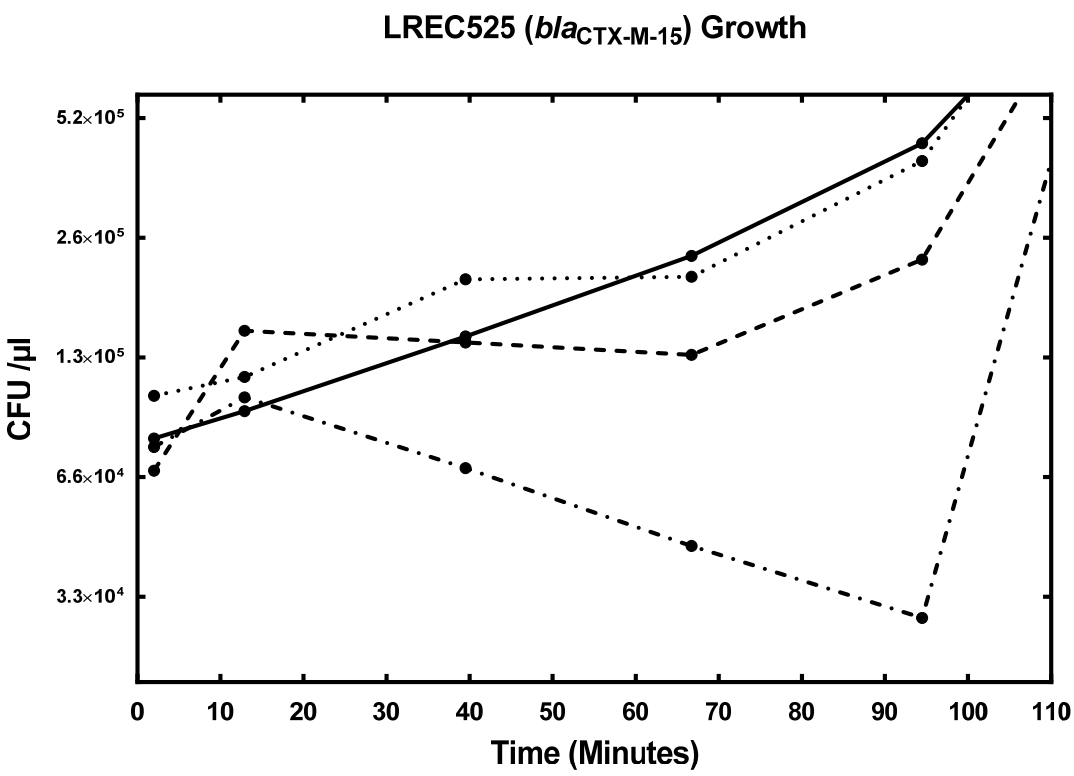


Figure 5-20. Results of treating an established early log-phase culture with CTX/P-PNA4 combinations.

Cultures were grown until culture turbidity reached a level indicating early log phase (O.D. $_{600\ nm}$ = 0.2). The culture was split and aliquots were treated with CTX, P-PNA4 or both, at the concentrations specified. Solid line: control, dashed line: CTX (48 µg/ml), dotted line: P-PNA4 (3.2 µM), dash-dot line: CTX (48 µg/ml) + P-PNA4 (3.2 µM).

### 5.2.5. Effects of β-lactamase inhibitors clavulanic acid, tazobactam and sulbactam on *E. coli* field isolate growth

For comparative evaluation of the efficacy of P-PNA4 and P-PMO1, field isolates were exposed to the β-lactamase inhibitors clavulanic acid, tazobactam and sulbactam in the presence and absence of cefotaxime.

Clavulanic acid (64 – 444 μg/ml) was found to be a weak inhibitor of β-lactamase when evaluated in combination with cefotaxime (48 μg/ml) in cultures of field isolate LREC454 (the concentration of 48 μg/ml was selected as a CTX concentration that was sub-inhibitory, but which had an observable negative growth effect to enable any inhibitory effects to be readily apparent). At a CTX concentration of 48 μg/ml, a dose dependent response to clavulanic acid was observed, although there was no concentration of clavulanic acid tested (64 - 444 μg/ml) sufficient for the combination of antibiotic and clavulanic acid to completely inhibit growth (Figure 5-21).

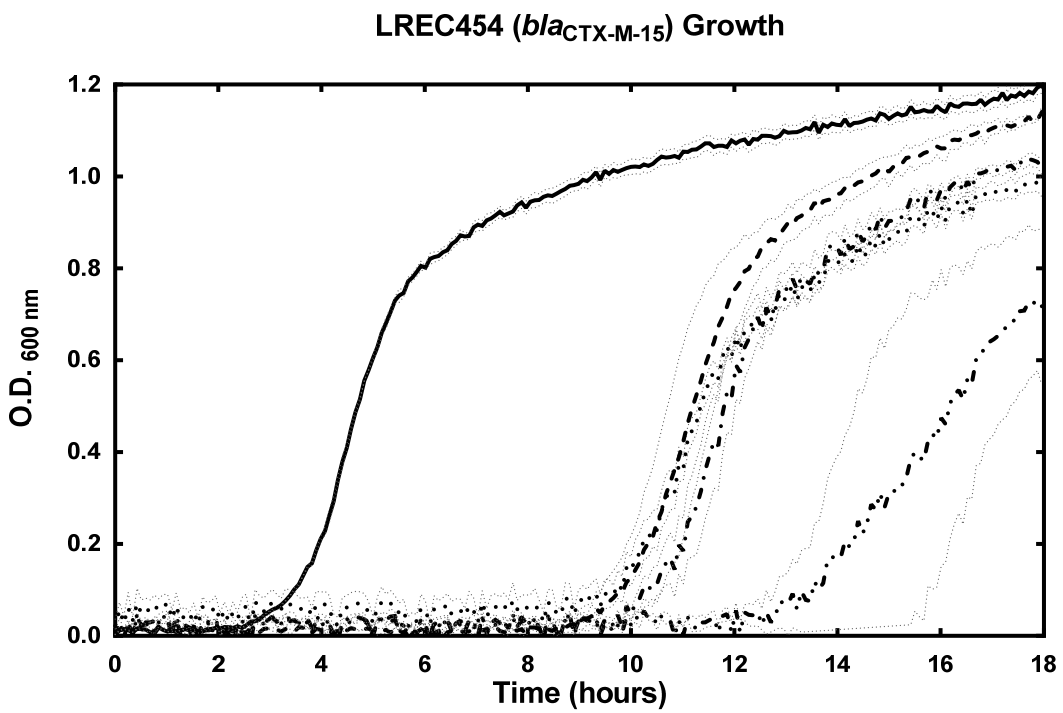


Figure 5-21. Effects of CTX (48 µg/ml) and clavulanic acid (0 – 444 µg/ml) on LREC454 harbouring *bla*$_{\text{CTX-M-15}}$.

LREC454 incubated with CTX (48 µg/ml) and/or clavulanic acid. Solid line: control, dashed line: CTX (48 µg/ml), dotted line: CTX (48 µg/ml) + clavulanic acid (64 µg/ml), dash-dot line: CTX (48 µg/ml) + clavulanic acid (256 µg/ml), dash-dot-dot line: CTX (48 µg/ml) + clavulanic acid (444 µg/ml). Error bars indicate ± 1 standard deviation (n=2).

In contrast, all concentrations of sulbactam of 1 µg/ml and above were found to be inhibitory when co-administered with CTX (48 µg/ml) in *E. coli* field isolate LREC525, harbouring *bla*$_{\text{CTX-M-15}}$ (Figure 5-22). Aliquots of the same culture were treated with sulbactam alone, and sulbactam was observed to exhibit inherent antimicrobial properties; concentrations of 32 µg/ml and higher were sufficient to completely inhibit growth (Figure 5-23).

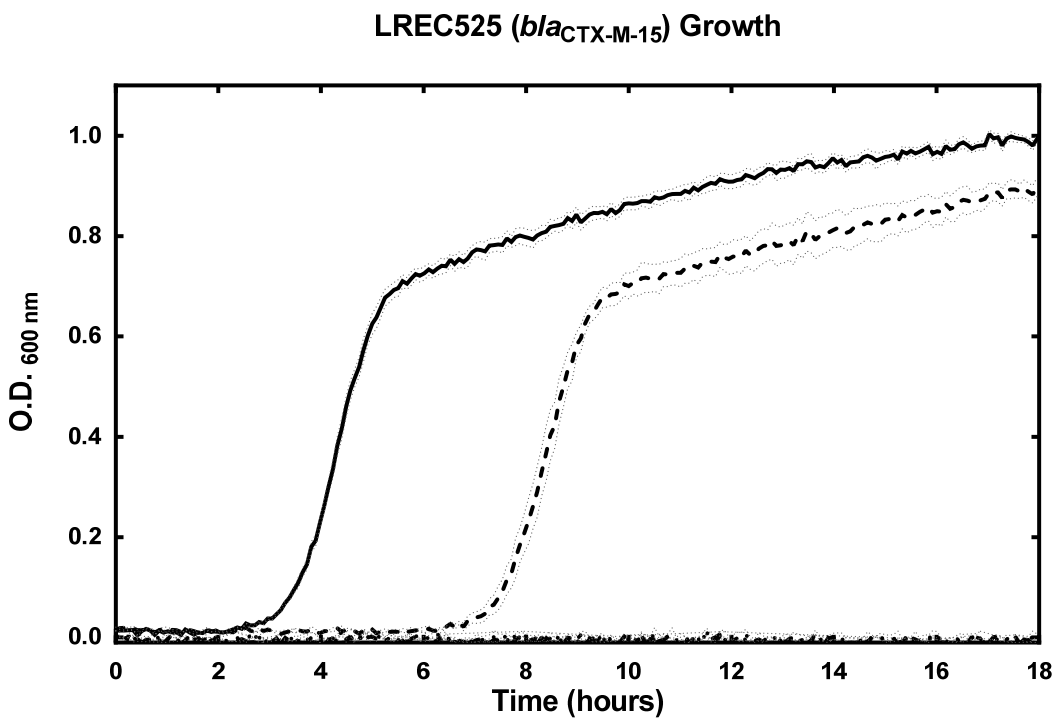


Figure 5-22. Effects of CTX (48 µg/ml) and sulbactam (1 – 4 µg/ml) on LREC525 harbouring *bla*CTX-M-15.

LREC525 incubated with CTX (48 µg/ml) and/or sulbactam (1 – 4 µg/ml). Solid line: control, dashed line: CTX (48 µg/ml), dotted line (no growth): CTX (48 µg/ml) + sulbactam (1 µg/ml), dash-dot line (no growth): CTX (48 µg/ml) + sulbactam (2 µg/ml), dash-dot-dot line (no growth): CTX (48 µg/ml) + sulbactam (4 µg/ml). Error bars indicate ± 1 standard deviation (n=3).

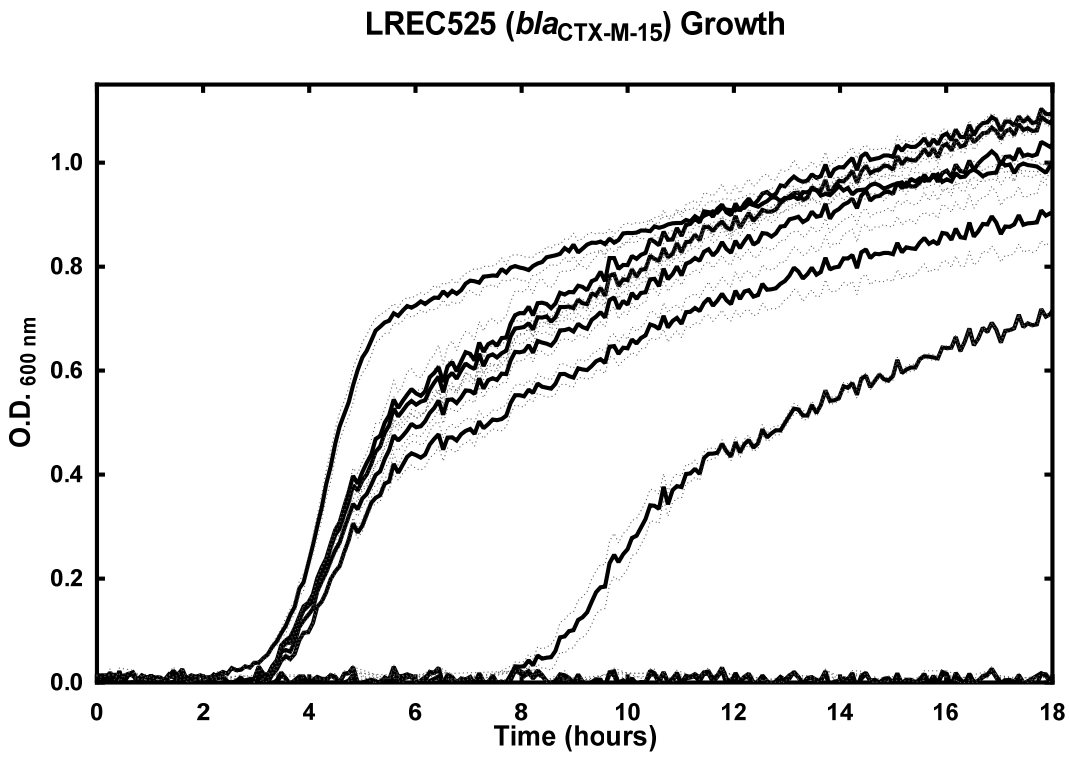


Figure 5-23. Effects of sulbactam (1 – 64 µg/ml) on growth of LREC525 harbouring *bla*CTX-M-15.

LREC525 incubated with sulbactam (1 – 64 µg/ml). Curves from left to right: sulbactam (1 µg/ml), sulbactam (2 µg/ml), sulbactam (4 µg/ml), sulbactam (8 µg/ml), sulbactam (16 µg/ml), sulbactam (32 µg/ml; no growth), sulbactam (64 µg/ml; no growth). Error bars indicate ± 1 standard deviation (n=3).

Tazobactam was found to be effective in inhibiting growth of field isolate LREC525 when co-administered with CTX (Figure 5-24), but weak antimicrobial activity was observed when administered in the absence of CTX (Figure 5-25).

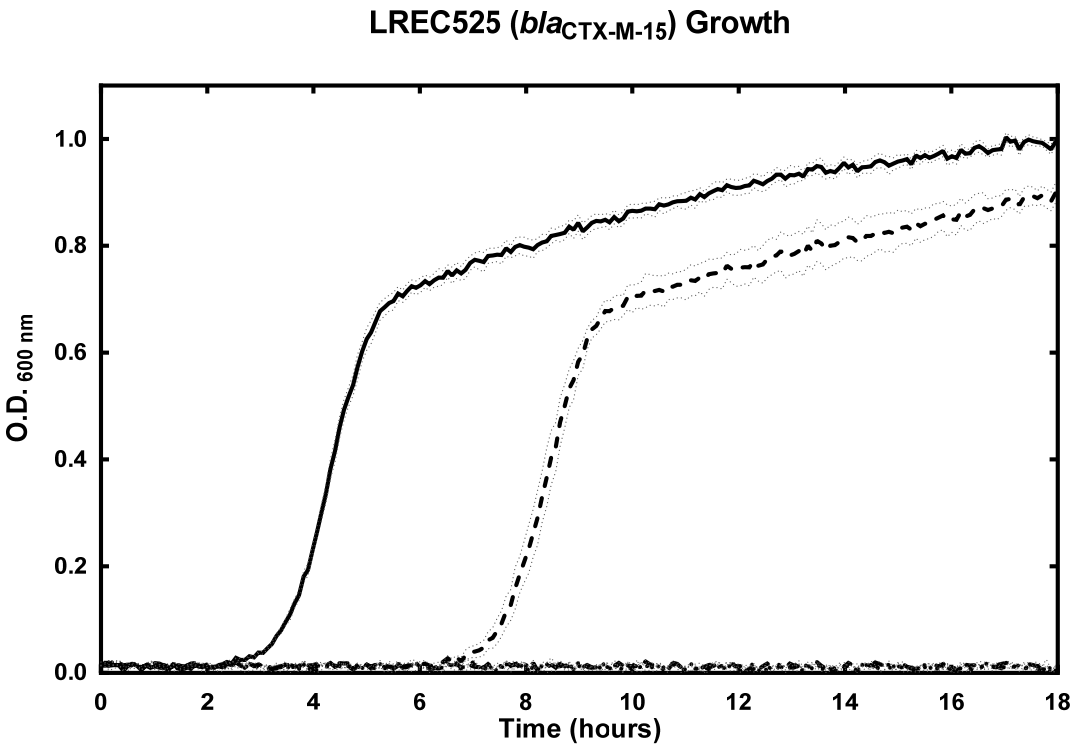


Figure 5-24. Effects of CTX (48 µg/ml) and tazobactam (1 – 4 µg/ml) on the growth of field isolate LREC525.

Solid line: control, dashed line: CTX (48 µg/ml), dotted line: CTX (48 µg/ml) + tazobactam (1 µg/ml), dash-dot line: CTX (48 µg/ml) + tazobactam (2 µg/ml), dash-dot-dot line: CTX (48 µg/ml) + tazobactam (4 µg/ml). Error bars indicate ± 1 standard deviation (n=3).

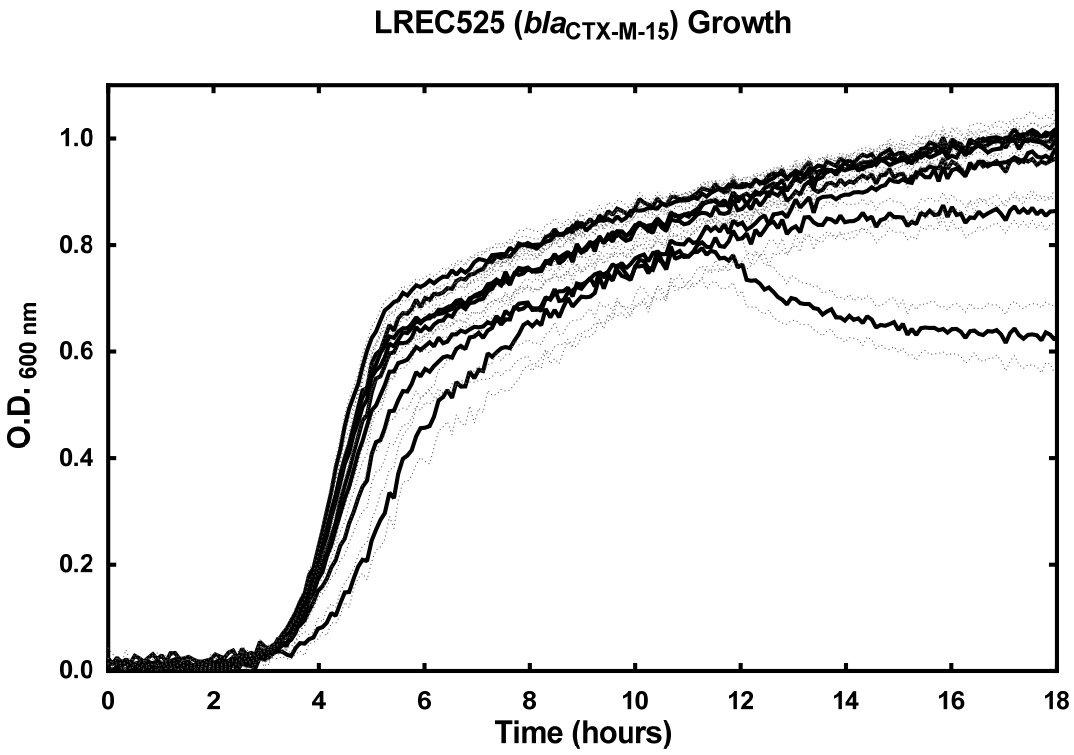


Figure 5-25. Effects of tazobactam (1 – 64 µg/ml) alone on the growth of field isolate LREC525 harbouring *bla*$_{\text{CTX-M-15}}$.

Curves from left to right: tazobactam (1 µg/ml), tazobactam (2 µg/ml), tazobactam (4 µg/ml), tazobactam (8 µg/ml), tazobactam (16 µg/ml), tazobactam (32 µg/ml), tazobactam (64 µg/ml). Error bars indicate ± 1 standard deviation (n=3).

## 5.3. Discussion

### 5.3.1. Observed increase in CTX sensitivity in AS19/pJBRCTX516 cultured in the presence of unmodified antisense oligomers PMO1 and PNA4

Transformation of atypically permeable mutant *E. coli* strain AS19 with plasmid pJBRCTX516 harbouring *bla*$_{\text{CTX-M-15}}$ enabled the evaluation of PMO1 and PNA4 β-lactamase expression inhibition without the necessity of cell penetration strategies. Studies revealed an increase in CTX susceptibility in AS19/pJBRCTX516 when treated with CTX (4 μg/ml) in the presence of PMO1 and PNA4. PNA4 (20 μM) was found to reduce the MIC (to CTX) of AS19/pJBRCTX516 from 80 μg/ml to 4 μg/ml whereas a PMO1 concentration of 40 μM was required to achieve the same reduction in MIC (to CTX). This contrasted with cell-free inhibition studies which demonstrated a slightly higher cefotaximase inhibitory effect of PMO1 over PNA4. The observation that PNA4 was 2-fold more effective over PMO1 in increasing CTX susceptibility in AS19/pJBRCTX516 was potentially attributable to multiple factors. Previous bacterial experimental studies appear to indicate that the optimum size of synthetic antisense agents would be between 9 and 15 bases in length [134]. PNA4 at 13 nt in length fell within this range whereas PMO1 at 25 nt in length was larger. Additionally, the uptake efficiency of PMO1 and PNA4 by the partially permeable strain AS19/pJBRCTX516 is unknown, and likely to contribute to the differences observed in CTX re-sensitisation by antisense oligomer gene expression inhibition. The shorter length of the PNA potentially facilitates greater cell wall penetration efficiency; it would not be an unreasonable assumption that a much smaller molecule would be able to cross the partially permeable cell wall with greater ease. Differences in PNA/PMO chemistries may also have potentially contributed to differences in cell wall penetration efficiency,

as well as cellular efflux efficiency relative to the differences (size and structure) of the two different antisense agent types.

AS19/pJBRCTX516 was treated with PMO1 in the absence of CTX and no effects on cell growth were observed. However, when treating AS19/pJBRCTX516 with PNA4 alone, a dose-dependent growth inhibitory effect was noted. The deleterious effect of PNA4 alone can potentially be ascribed to off-target gene transcript matches: the target sequence was checked by BLAST searching and found to be to have four bacterial off-target matches with 92.3% (12 out of 13 bases) sequence complementarity. PNA4 was found by a BLAST search to share 92.3% complementarity to the SD region upstream of one of these off-target matches, the universal stress protein UspC. This is potentially significant, being an mRNA region sensitive to expression inhibition by antisense agents. To extenuate this, PNA4 was subsequently administered at a maximum concentration (5 μM) shown to have an insignificant effect on the growth of AS19/pJBRCTX516 in the absence of CTX.

### 5.3.2. Observed increase in CTX sensitivity in field isolates cultured in the presence of peptide-conjugated antisense oligomers P-PMO1 and P-PNA4

Unmodified antisense agents PNA4 and PMO1 were shown to have no significant effect on the susceptibility to cefotaxime, or to the growth characteristics of field isolates with intact cell walls. This was not unexpected as previous studies have shown that unmodified antisense oligomers do not efficiently penetrate *E. coli* strains with intact cell walls [119]. To overcome this barrier, the anti-*bla*$_{\text{CTX-M}}$ oligomers PMO1 and PNA4 were covalently attached to the cell-penetrating peptide, $(KFF)_3K$, which has been shown to be effective in promoting uptake across the bacterial cell wall and delivering a cargo molecule to the cytoplasm [121, 141].

Peptide conjugated PNA4 (P-PNA4) and PMO1 (P-PMO1) both increased the effects of CTX as evidenced by the effects on growth of a range of field and clinical isolates harbouring β-lactamase genes from CTXM group 1. The amount of observed increase in sensitivity to CTX varied in each strain, and between the effects observed with P-PMO1 and P-PNA4 antisense oligomers. P-PNA4 was found to be between 9 and 56-fold more effective in decreasing minimum inhibitory concentrations to CTX than P-PMO1 (Table 5-3) which could be attributable to two potential explanations:

1. The shorter length of the PNA potentially contributes to greater cell penetration efficiency which would be of interest to investigate further. Methods of evaluating this would necessitate labelling of the molecules with a quantifiable reporter molecule, and determining the amount that gained access to the bacterial cytoplasm. The disadvantage of labelling with a reporter is that the reporter molecule itself increases the overall size of the labelled complex, affecting cell penetration efficiency. Attempts were made in the course of the current study to visualise internalised PMO molecules labelled with a fluorescent marker (fluorescein), however fluorescence microscopic outcomes were of insufficient intensity to be distinguishable from the background.
2. PNA4 was found to have some inherent toxicity, as previously discussed, and not observed with PMO1. This is likely due to the shorter length of the PNA resulting in unwanted sequence complementarity and the target region - PNA4, 13 nucleotides in length, and targeting an extragenic downstream region, was found to share some sequence identity with other genes not intentionally targeted. It is likely that these off target matches are the reason for the inherent toxicity of PNA4. However, the growth inhibitory effects of PNA4 alone were relatively small in comparison with the effect in combination with cefotaxime –

at concentrations required to significantly increase sensitivity to cefotaxime (2 - 5 μM), PNA4 alone typically had no significant effect on culture growth. This would suggest a potentiating effect on CTX of P-PNA4, and that the primary and preferential target of P-PNA4 was *bla*$_{\text{CTX-M}}$ of group 1.

### 5.3.3. Control studies to isolate non-specific effects of anti-*bla*$_{\text{CTX-M-15}}$ P-PMO1 and P-PNA4 in field isolates

Previous studies have shown limited or no effect of scrambled or mismatch control peptide-conjugated PNAs on bacterial growth, including mismatch controls containing as few as two base substitutions [120]. Studies with the peptide $(KFF)_3K$ attached to PNA oligomers have demonstrated the efficacy of synthetic antigene oligomers in bacteria, and their specificity by demonstrating low inhibition of target and reporter genes when challenged with scrambled non-specific peptide-conjugated PNAs [121].

Specific anti-*bla*$_{\text{CTX-M-15}}$ activity was demonstrated in this study, in the first instance by studies in a cell-free environment using *bla*$_{\text{CTX-M-15}}$–harbouring recombinant plasmid pJBRCTX516. Cefotaximase activity was inhibited by the presence of PNA4 and PMO1. There was no observed increase in CTX sensitivity when atypically permeable strain AS19/pJBRCTX516 was challenged with the combination of non-*bla*$_{\text{CTX-M}}$ specific control PMO and CTX. In the absence of CTX, no effects on growth were observed when AS19/pJBRCTX516 was challenged with PMO1 alone (10 – 30 μM; Figure 5-6). In the absence of CTX, significant effects on growth were observed when AS19/pJBRCTX516 was challenged with PNA4 alone at concentrations higher than 5 μM (Figure 5-8). This was potentially attributable to unintended off-target partial complementarity with other bacterial genes. Consequently, PNA4 concentrations in

subsequent studies did not exceed a concentration of 5 μM, typically cultures were treated with 3.2 μM P-PNA4 and controls in the absence of CTX were included.

Additional control studies, equivalent to the use of a scrambled non-specific P-PNA or P-PMO1, were undertaken in *E. coli* strain LREC90 harbouring *bla*$_{\text{CTX-M-14}}$. PMO1 and PNA4, having only 56% and 15% complementarity with the *bla*$_{\text{CTX-M-14}}$ target region respectively, were regarded as non-specific to *bla*$_{\text{CTX-M-14}}$ expressed by LREC90.

A comparable effect on the growth of LREC90 (*bla*$_{\text{CTX-M-14}}$) and LREC454 (*bla*$_{\text{CTX-M-15}}$) was observed when each strain was cultured in the presence of P-PMO1 (10 – 30 μM) alone. As PMO1 (unmodified; 10 – 30 μM) previously been shown to have no significant effect on the growth of AS19/pJBRCTX516, it would be reasonable to attribute the effects on growth of LREC454 and LREC90 in the presence of P-PMO1 alone to either non-specific toxic effects of the peptide portion of the conjugate, or a result of cell wall perturbation. The cell-penetrating peptide $(KFF)_3K$ alone has been previously shown to have a synergistic effect with certain antibiotics [147].

The negative effect of P-PMO1 on the growth of control strain LREC90 was increased in an additive manner (estimated fractional inhibitory concentration index (FICI) between 0.5 and 1) when LREC90 was cultured in the presence of P-PMO1 (10 - 30 μM) and CTX (3 μg/ml; Figure 5-13). In contrast, the negative effect on growth of P-PMO1 on the growth of field isolate LREC454 was increased in a synergistic manner (estimated FICI < 0.5) when LREC454 was cultured in the presence of P-PMO1 and CTX (24 μg/ml; Figure A-1). A similar, comparable effect was observed on the growth of both LREC454 (*bla*$_{\text{CTX-M-15}}$) and LREC90 (*bla*$_{\text{CTX-M-14}}$) when cultured in the presence of P-PNA4 (1.6 - 5 μM; Figure 5-17; Figure 5-18). No significant differences were observed between the effects on growth of LREC90

cultured in the presence of P-PNA4 alone (1.6 – 5 μM), and P-PNA4 (1.6 – 5 μM) co-administered with CTX (2 μg/ml). A significant difference, however, was noted in LREC454 cultured in the presence of P-PNA4 (1.6 - 5 μM) alone (Figure 5-18) and LREC454 cultured in the presence of P-PNA4 (1.6 - 5 μM) in combination with CTX (2 μg/ml; Figure 5-19). Additionally, minimum inhibitory concentrations (to CTX) of LREC90 were not reduced in the presence of P-PNA4 (Figure 5-14; Figure 5-15).

These data would strongly indicate specific anti-*bla*$_{\text{CTX-M-15}}$ activity of P-PNA4 and P-PMO1.

### 5.3.4. Cefotaxime potentiating effect of peptide-conjugated antisense oligomers in field isolates expressing *bla*$_{\text{CTX-M-15}}$

Peptide conjugated PNA4, as previously noted, exhibited some inherent inhibitory effects when cultures were treated in the absence of cefotaxime. To determine that the combined effect of the antibiotic and P-PNA4 was greater than the effects of the sum of its constituent parts, i.e. to establish that there was a CTX potentiating effect, two methods were employed:

i) A concentration of cefotaxime was established that yielded a similar inhibition profile (an equivalent amount of time taken to achieve logarithmic growth phase), as P-PNA4 (3 μM) alone, in *E. coli* strain LREC525. A doubling of the CTX concentration enabled a visual estimation of the additive or synergistic nature of the P-PNA4/CTX combination.

A starter culture was grown until an appropriate cell density (O.D. $_{600\ nm}$ = 0.1-0.2) was reached, diluted to yield 50,000 CFU/ml, and split into equal aliquots. One aliquot was cultured in the presence of the concentration of cefotaxime required to yield an

equivalent growth inhibitory effect as P-PNA4 (3 μM). Another aliquot was cultured in the presence of P-PNA4, a third aliquot was cultured in the presence of double the concentration of cefotaxime, and the final aliquot in the presence of cefotaxime and P-PNA4. The effect of the P-PNA4-cefotaxime combination was visibly greater than the effect of the double cefotaxime dose aliquot suggesting a CTX potentiating effect.

ii) The fractional inhibitory concentration index (FICI) was evaluated for cefotaxime and P-PNA4. Maximum tested concentrations of P-PNA4 and P-PMO1 administered in the absence of CTX were insufficient to completely inhibit the growth of field isolates, and so a conservative estimation of an inhibitory concentration based on a visual extrapolation from dose-response growth curves was used to calculate an estimated fractional inhibitory concentration index value. In all cases a strong synergistic relationship was indicated (FICI < 0.05).

### 5.3.5. Comparative evaluation of the effects of clavulanic acid, sulbactam and tazobactam with P-PNA4 and P-PMO1 in increasing sensitivity to CTX in field isolates

For comparison with the efficacy of antisense oligomers, field isolates were treated with a combination of CTX and the β-lactamase inhibitors clavulanic acid, sulbactam and tazobactam. There was no concentration of clavulanic acid tested (269 μM – 1.9 mM) that was found to completely inhibit growth of LREC454 cultures co-treated with CTX (48 μg/ml). In contrast, CTX (2 μg/ml) was sufficient to inhibit growth of LREC454 cultures co-treated with P-PNA4 (3.2 μM), and CTX at a concentration of 24 μg/ml was found to be inhibitory when co-administered with P-PMO1 (30 μM).

The MIC (to CTX) of LREC525 was reduced in the presence of tazobactam (3.1 μM) from 260 μg/ml to 48 μg/ml. In the presence of sulbactam (4.3 μM) the MIC (to CTX) of LREC525 was also reduced from 260 μg/ml to 48 μg/ml.

This compared with an equivalent MIC (to CTX) reduction (from 260 μg/ml to 48 μg/ml) in the presence of P-PNA4 (3.2 μM). A co-treatment of P-PMO1 (30 μM) and CTX (96 μg/ml) was observed to be inhibitory in LREC525 cultures under the same conditions.

These data suggest that the efficacy of P-PNA4 was comparable to tazobactam and sulbactam, and superior to clavulanic acid in partially restoring CTX sensitivity in a strain expressing *bla*$_{\text{CTX-M-15}}$. The efficacy of P-PMO1 in increasing CTX sensitivity in a strain expressing *bla*$_{\text{CTX-M-15}}$ was observed to be lower than that of either tazobactam or sulbactam, but greater than clavulanic acid.

# Chapter 6.

# Exposure to cephalosporins stimulates an increase of β-lactamase activity in *E. coli* strains AS19/pJBRCTX516 and LREC460

## 6.1. Introduction

In comparison with the observed effects of anti-*bla*$_{\text{CTX-M}}$ antisense agents in a cell-free translation/transcription coupled system, results obtained from inhibition of cefotaximase activity studies in whole cells appeared to show a markedly lower effect size than expected. At relatively low concentrations of PNA/PMO (500-1000 nM) near complete inhibition of *bla*$_{\text{CTX-M-15}}$ was observed in such a cell-free system. However, when attempting to inhibit the activity of *bla*$_{\text{CTX-M-15}}$ in whole, biologically active cells a much lower efficiency was observed. This was hypothesised to relate to a number of factors including, but not limited to: the inherent difficulties of delivering the antisense agents into the bacterial cell, efflux mechanisms responsible for pumping agents out of the cell, a high level of constitutive expression or an inducible β-lactamase upregulation mechanism. The apparent difficulties in achieving complete inhibition of the cefotaximase activity, contrasted with high levels of expression inhibition reported by other studies targeting different genes in the same species with the same or equivalent synthetic antisense agents. This may suggest *bla*$_{\text{CTX-M-15}}$ is either a constitutively strongly expressed gene, or a differentially expressed inducible gene, under the control of one or more regulation mechanisms.

Regulatory mechanisms that induce increased expression in other β-lactamases such as AmpC β-lactamases are known to exist [66]. Jacoby *et al.* showed that genes *ampG* and *ampD* essential for β-lactamase induction were also required for peptidoglycan recycling, suggesting a mechanism of cell-wall integrity monitoring, in which

β-lactamase induction was related to the levels of muropeptides (resulting from enzymatic digestion of glycan strands [180]) in the cytoplasm [181]. Lindberg *et al.* found that AmpC β-lactamase is inducible in the presence of the regulatory gene *ampR* [182]. The cytoplasmic protein, AmpD, and the membrane-bound protein AmpE have been linked to the detection of the activity of β-lactam antibiotics and the relaying of this signal to AmpR [183]. In the gram-negative pathogen *Vibrio parahaemolyticus,* a receptor which directly recognised β-lactam antibiotics was identified which controlled β-lactamase expression – mutants lacking the receptor were found to not produce β-lactamase and were re-sensitised to β-lactam antibiotics [184].

To investigate evidence of increased levels of *bla*$_{\text{CTX-M}}$ expression in the presence of 3$^{rd}$ generation cephalosporins, 3 different methods were employed:

1. Supernatant extracts from AS19/pJBRCTX516 obtained from cultures incubated in the presence of increasing concentrations of CTX were incubated with nitrocefin and the rate of degradation by β-lactamase monitored by spectrophotometry.
2. AS19/pJBRCTX516 cultures were exposed to varying concentrations of CTX and samples taken at regular intervals. Remaining CTX was quantified from each sample by HPLC.
3. AS19/pJBRCTX516 and LREC460 cultures were incubated with varying concentrations of the 3$^{rd}$ generation cephalosporin ceftriaxone (CRO) for 30 and 45 minutes to differentially induce β-lactamase activity. Cells were disrupted and supernatant samples from each culture were transferred to a CTX solution. CTX degradation was quantified by an HPLC time-course assay.

## 6.2. Results

### 6.2.1. Quantification of CTX induced β-lactamase expression upregulation by colourimetric nitrocefin based assay

*E. coli* strain AS19/pJBRCTX516 was cultured from frozen glycerol stocks in MHB supplemented with CTX (final concentration of 2 μg/ml) and KAN (final concentration of 40 μg/ml) until early log phase (O.D. $_{600\ nm}$ = 0.1) was reached. The culture was diluted 1:500 and split into five equal (7.5 ml) aliquots. Each aliquot was cultured in the presence of final CTX concentrations of 0, 2, 16, 32 and 64 μg/ml and cultured at 37° C. Aliquots (2 ml) were removed at time intervals 0, 1 and 2 hours and growth measured by spectrophotometry (O.D. $_{600\ nm}$) to normalise results. Bacterial cells were separated by centrifugation and the supernatant removed. Aliquots (20 μl) of each supernatant were added to wells in a 96-well microtiter plate, pre-prepared with nitrocefin solution (final concentration of 200 μM), and β-lactamase activity monitored by spectrophotometry (O.D. $_{492\ nm}$). The results indicated a more rapid reaction occurred with supernatant aliquots obtained from cultures exposed to higher CTX concentrations (Figure 6-1). The samples taken at the time of initial CTX exposure revealed no significant differences in the rate of nitrocefin reaction (Figure 6-1a). After 1 and 2 hours of CTX pre-exposure, the subsequent nitrocefin colour change reaction proceeded more rapidly and in a dose dependant manner with supernatant aliquots obtained from cultures exposed to higher CTX concentrations (Figure 6-1b-c). The nitrocefin colour change reaction had been previously shown to have direct proportional relationship with β-lactamase quantity, and as such was a suitable marker for the quantification of β-lactamase present in solution.

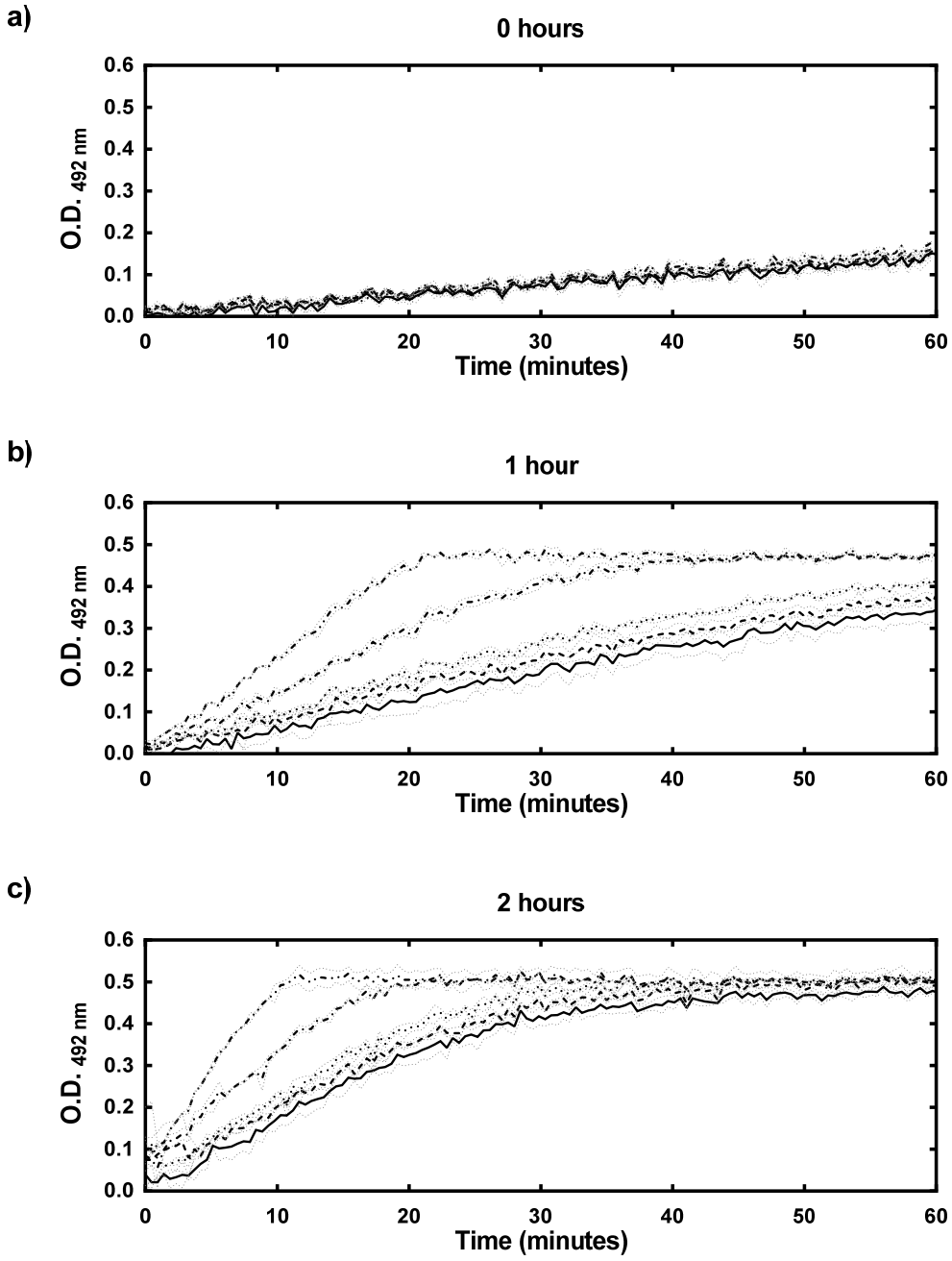


Figure 6-1. Nitrocefin assay to measure the effects of CTX (0 - 64 µg/ml) on inducing β-lactamase activity in AS19/pJBRCTX516.

Supernatant extracts from AS19/pJBRCTX516 incubated with CTX (0 - 64 µg/ml), **a)** nitrocefin reaction at the time of initial CTX exposure. **b)** Nitrocefin reaction after 1 hour CTX incubation; **c)** nitrocefin reaction after 2 hours CTX incubation. Error bars indicate ± 1 standard deviation (n=2). Solid line: control, dashed line: CTX (2 µg/ml), dotted line: CTX (16 µg/ml), dash-dot line: CTX (32 µg/ml), dash-dot-dot line: CTX (64 µg/ml).

### 6.2.2. Quantification of CTX degradation in AS19/pJBRCTX516 cultures exposed to differing levels of CTX concentrations

*E. coli* strain AS19/pJBRCTX516 was cultured from frozen glycerol stocks until early log phase (O.D. $_{600\ nm}$ = 0.1 - 0.2) was reached. The culture was diluted 1:500 and split into 5 equal (20 ml) aliquots. Each aliquot was supplemented with CTX, or carrier medium, to achieve the following final concentrations: 0, 2, 16, 32 and 64 µg/ml and incubated at 37° C. At approximately 1 hour intervals culture growth was quantified by spectrophotometry (O.D. $_{600\ nm}$) for each time interval, and aliquots (1 ml) were taken from each culture. HCl (1M, 85 µl) was added to halt enzymatic reactions of each aliquot by increasing acidity to pH 2.2. Remaining CTX in solution was quantified by HPLC for each time point in duplicate. The rate of CTX degradation increased proportionally with the increase in CTX exposure (Figure 6-2, Table 6-1). Culture growth was monitored by spectrophotometry for the purposes of normalising results, however, culture turbidity remained lower than the resolution of the spectrophotometer to accurately estimate CFU number – optical density readings for all samples remained below 0.002 (O.D. $_{600\ nm}$) for the period of time that cefotaxime was still of quantifiable amounts in solution. β-Lactamase activity was regarded as having been produced from an approximately equivalent amount of cells. Maximum rates of CTX degradation were calculated from the linear section of the CTX degradation curve and are shown in Table 6-1.

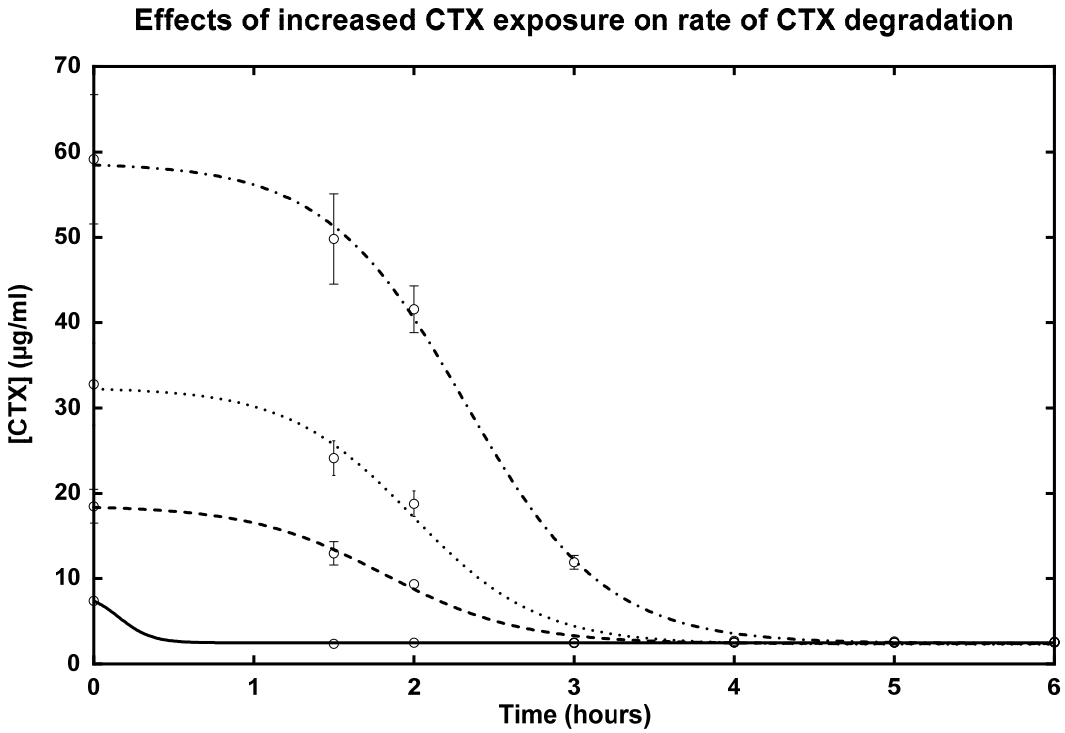


Figure 6-2. Effects of CTX exposure on β-lactamase activity in AS19/pJBRCTX516. AS19/pJBRCTX516 incubated with CTX (2 - 64 µg/ml), Error bars indicate ± 1 standard deviation (n=2). Solid line: CTX (2 µg/ml), dashed line: CTX (16 µg/ml), dotted line: CTX (32 µg/ml), dash-dot line: CTX (64 µg/ml).

Table 6-1. Rates of CTX degradation in AS19/pJBRCTX516 exposed to different concentrations of CTX.

| CTX Concentration | Maximum rate of CTX degradation (µg/ml/min) |
|---|---|
| 64 | 29.7 |
| 32 | 10.7 |
| 16 | 7.2 |
| 2 | 3.4 |
| 0 | 0 |

### 6.2.3. Quantification of CTX degradation by supernatant extracts from *E. coli* cultures exposed to differing levels of ceftriaxone

*E. coli* strain AS19/pJBRCTX516 and field isolate LREC460, both harbouring *bla*$_{\text{CTX-M-15,}}$ was cultured from frozen glycerol stocks until early log phase (O.D. $_{600\ nm}$ = 0.1 - 0.2) was reached. The culture was diluted 1:500 and split into 5 equal (2 ml) aliquots. Each aliquot was supplemented with CRO (final concentrations 0 - 384 µg/ml) and incubated at 37° C for 30 minutes. Culture turbidity was measured (O. D. $_{600\ nm}$) to normalise cell culture growth. Cell aggregates were disrupted by bead milling and separated by centrifugation. Supernatant aliquots (700 µl) were removed, added to 700 µl CTX solution (800 µg/ml) and incubated at 37° C. 125 µl aliquots were removed at regular time intervals and added to pre-prepared HPLC vials containing 125 µl phosphate buffer/ HCl, pH2.2. The degradation of CTX over time (80 minutes) was quantified by HPLC. All studies were performed using independent cultures.

AS19/pJBRCTX516 cultures were pre-exposed to CRO (0, 2, 32 and 64 µg/ml) for 30 minutes. A dose dependant increase in the amount of CTX degradation was observed, with the exception of cultures exposed to CRO 0 and 2 µg/ml (Figure 6-3). The rate of CTX degradation for each concentration of ceftriaxone is shown in Figure 6-4.

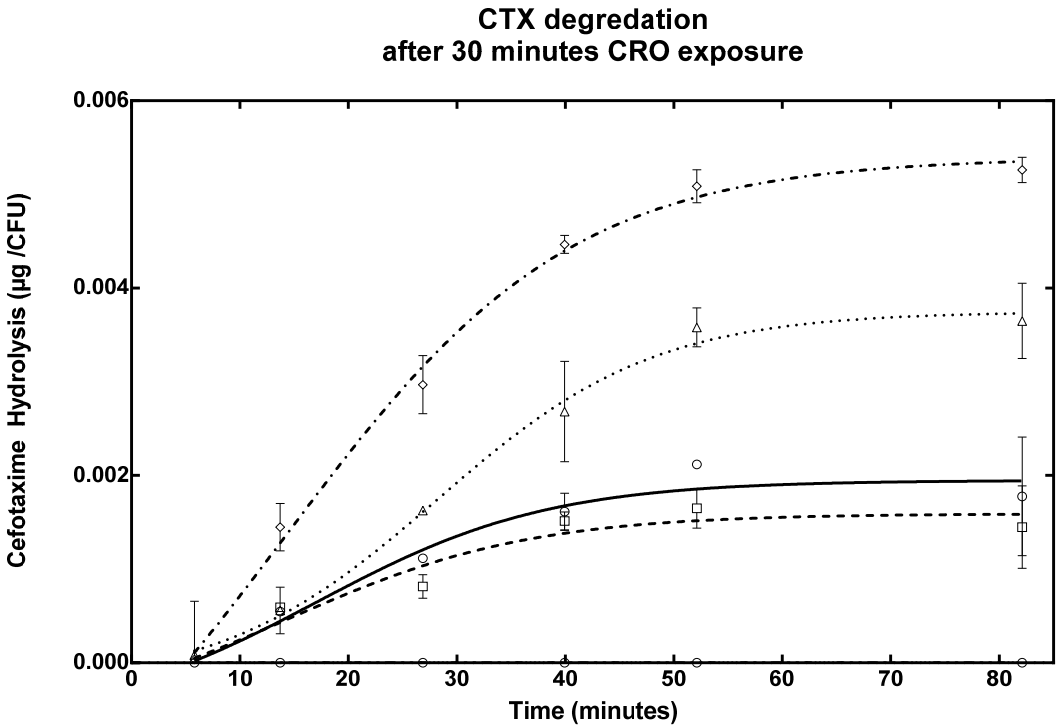


Figure 6-3. Effects of exposure to ceftriaxone on the upregulation of cefotaximase activity in recombinant *E. coli* strain AS19/pJBRCTX516.

*E. coli* cultures of strain AS19 harbouring the plasmid pJBRCTX516, were incubated with concentrations of CRO (2 - 64 µg/ml) for 30 minutes. Supernatants were collected, and incubated with CTX. A quantification of CTX degradation was established by HPLC in aliquots collected at regular intervals over 50 minutes. Solid line: CRO (0 µg/ml), dashed line: CRO (2 µg/ml), dotted line: CRO (32 µg/ml), dash-dot line: CRO (64 µg/ml), dash-dot-dot line: blank (HPLC control). Error bars indicate ± 1 standard deviation (n=2).

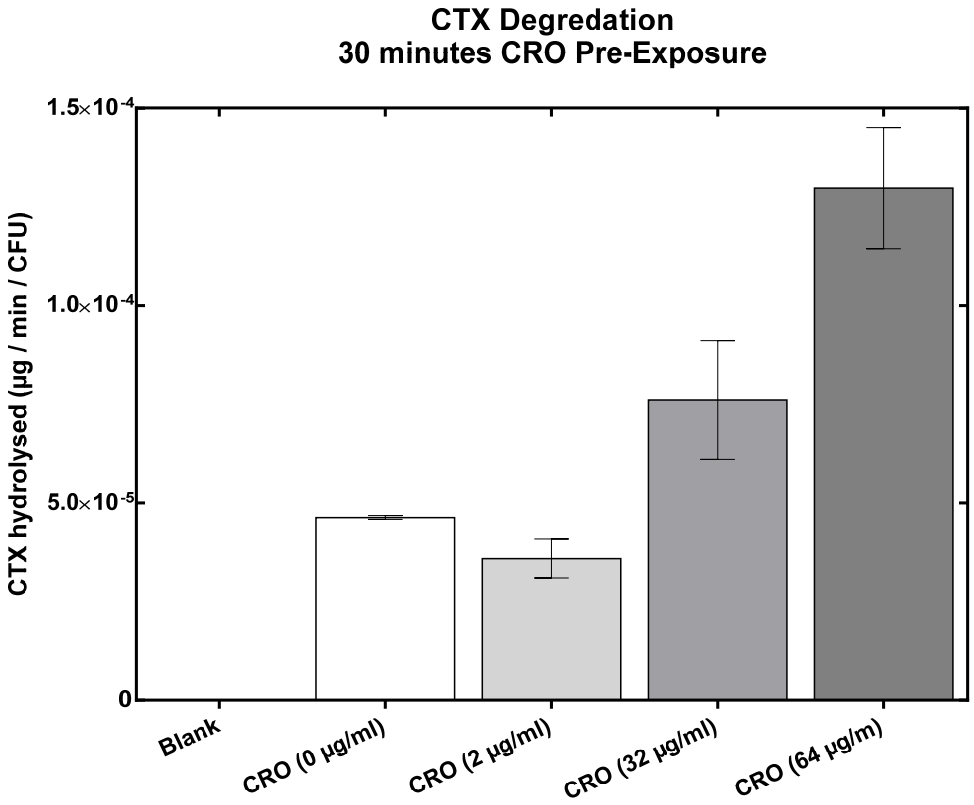


Figure 6-4. Effects of pre-exposure to ceftriaxone (0 – 64 µg/ml) of *E. coli* strain AS19/pJBRCTX516 on the rate of cefotaxime degradation.
Rate of degradation of CTX (µg/min/CFU) incubated with supernatant extracts from *E. coli* strain LREC460 was measured by HPLC. AS19/pJBRCTX516 was incubated with CRO (0 - 64 µg/ml) for 30 minutes prior to the supernatant incubation with CTX. Error bars indicate ± 1 standard deviation (n=2).

LREC460 cultures were exposed to CRO (0, 2, 64, 128 and 384 µg/ml) for 45 minutes. Supernatant aliquots (700 µl) were removed, added to 700 µl CTX solution (800 µg/ml) and incubated at 37° C. 125 µl aliquots were removed at regular time intervals and added to pre-prepared HPLC vials containing 125 µl phosphate buffer/ HCl, pH2.2. The degradation of CTX over time (110 minutes) was quantified by HPLC. A dose dependant increase in the amount of CTX degradation was observed, with the exception of cultures exposed to 0 and 2 µg/ml CRO (Figure 6-5). The rate of CTX degradation for each concentration of ceftriaxone is shown in Figure 6-6.

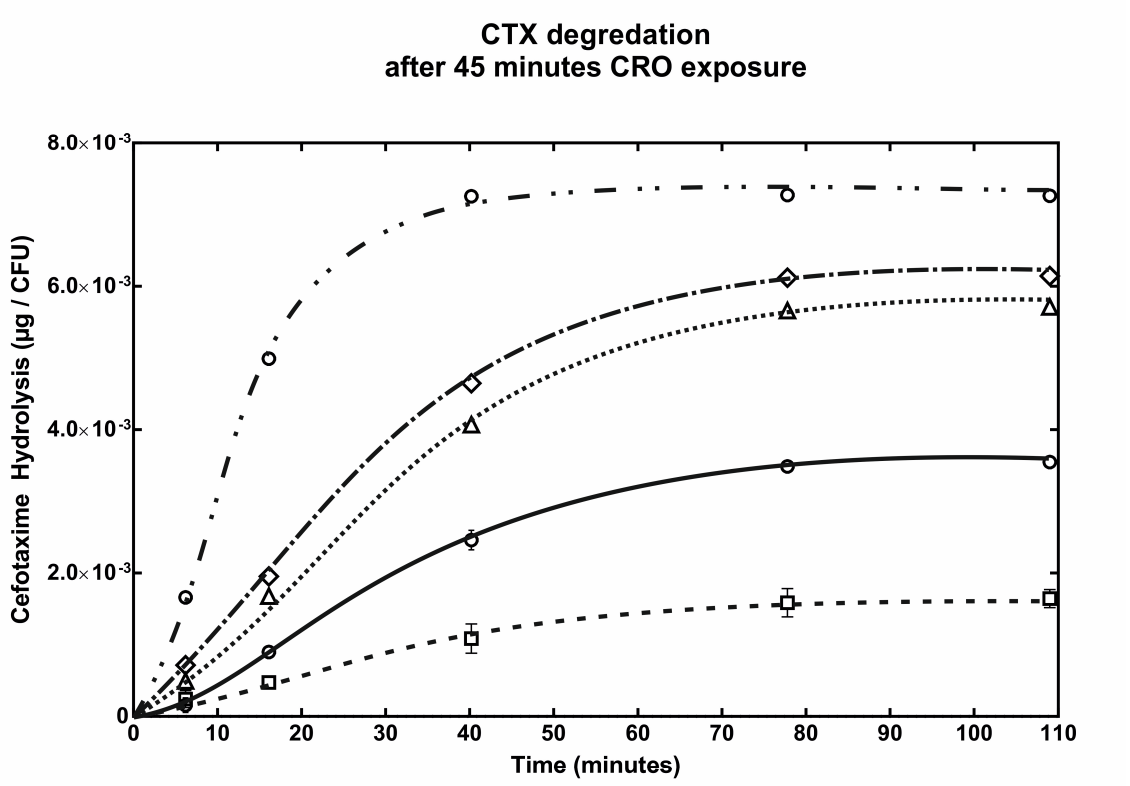


Figure 6-5. Effect of exposure of *E. coli* strain LREC460 to ceftriaxone (0 – 384 µg/ml) on cefotaximase activity.

LREC460 incubated with CRO (0 - 384 µg/ml) for 45 minutes prior to the supernatant incubation with CTX. Error bars indicate ± 1 standard deviation (n=4). Solid line: CRO (0 µg/ml), dashed line: CRO (2 µg/ml), dotted line: CRO (64 µg/ml), dash-dot line: CRO (128 µg/ml), dash-dot-dot line: CRO (384 µg/ml). HPLC blank not shown (no hydrolysis over the time course was observed).

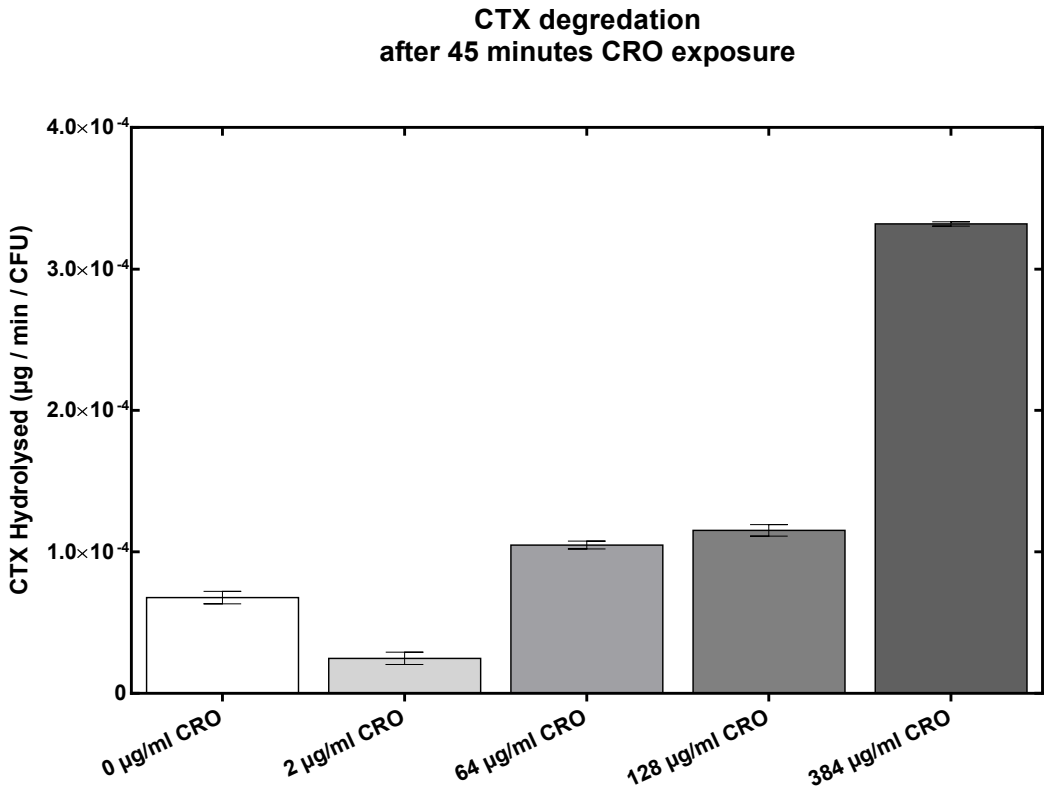


Figure 6-6. Effect of exposure of *E. coli* strain LREC460 to ceftriaxone (0 – 384 µg/ml) on the rate of cefotaxime degradation.
LREC460 was incubated with CRO (0 - 384 µg/ml) for 45 minutes prior to the supernatant incubation with CTX. Error bars indicate ± 1 standard deviation (n=4).

## 6.3. Discussion

The current study demonstrated, by three different techniques, increased CTX degradation induced by the exposure to the 3rd generation cephalosporins, cefotaxime and ceftriaxone in field isolate LREC460 and lab strain AS19 transformed with recombinant plasmid pJBRCTX516. Cultures not exposed to β-lactams were shown to express β-lactamase, indicating a level of constitutive expression. A proportional, dose-dependent upregulation of β-lactamase was indicated by the quantification of the markers of β-lactamase CTX-M activity: nitrocefin degradation and cefotaxime degradation. This induced upregulation of *bla*$_{\text{CTX-M-15}}$ was observed in both field isolate LREC460 and in AS19 transformed with recombinant plasmid pJBRCTX516, which

may suggest that the regulatory mechanism was not plasmid-borne. Further studies would be required to elucidate the nature of this inducible upregulation.

Further information relating to the nature of such a regulatory mechanism could be obtained by investigation of *bla*$_{\text{CTX-M-15}}$ transcripts with such methods as quantitative PCR, RNA-seq or micro-arrays in cultures exposed to a range of antibiotic conditions. Transcript data obtained, and combined with data obtained from β-lactamase protein quantification assays would potentially add to the understanding of this phenomenon.

The likelihood of the presence of a regulation mechanism controlling differential expression of *bla*$_{\text{CTX-M-15}}$ also presents a possibility of one or more attractive additional or alternative translational inhibition targets to increase sensitivity to CTX in resistant bacteria.

# Chapter 7.

# Molecular 3D tetrahedral nanostructure vectors for targeted intracellular delivery of synthetic antisense/antigene agents in bacteria

## 7.1. Introduction

As previously discussed, one of the greatest obstacles to the inhibition of bacterial gene expression via synthetic antisense oligomers is the efficient intracellular delivery of inhibitory agents. The bacterial cell wall complex presents a major obstacle to delivery of antisense oligomers into field and clinical isolates [119, 136] which necessitates an efficient delivery strategy. Currently, a commonly used and effective delivery method is conjugation of a synthetic antisense molecule to a cell-penetrating peptide. However, the use of cell-penetrating peptides has certain significant associated problems such as their inherent toxicity to bacterial and mammalian cells. Additionally, the synthesis of the peptides and conjugation to antisense agents is presently an expensive and time consuming procedure, making it unlikely to be able to transition into a viable therapeutic option unless bulk production methods were able to significantly reduce costs. Resistance to cell-penetrating peptides have also been observed to arise, for example linked to mutations in a gene coding for the active transporter SbmA [143]. Most cell-penetrating peptides have also been shown to lack discriminatory ability with no specificity to any cell type having been shown [145], hindering its application as a carrier for therapeutic molecules. This is potentially a significant hindrance to the implementation of CPPs as a delivery mechanism for therapeutic cargo molecules to treat bacterial infections – antisense oligomers bound to cell-penetrating peptides will be delivered into any cell type, including those of the host organism, reducing the bioavailability of therapeutic agents available to the target bacteria, and potentially

causing unwanted negative effects on host organisms own cells. Previous studies have found a synergistic effect of certain antibiotics with cell-penetrating peptides [147] and an increase in bacterial cell wall permeability [158]. These studies may suggest cell wall disruption is a likely mechanism of cell penetration and would be a disadvantageous characteristic for the development of target-specific therapeutic agents.

The current study developed a potential alternative delivery vehicle for synthetic antisense oligomers; a novel delivery mechanism based on self-assembling 3D DNA tetrahedral structures. Setyawati *et al.* (2014) reported that a tetrahedral DNA structure was able to traverse the bacterial gram-negative cell wall and enter the cytoplasm [185]. The DNA tetrahedron designed and assembled by Setyawati *et al.* (2014) was based on the assembly methods described by Pei *et al.* (2010) and was designed to be self-assembling based on regions of complementarity between single-stranded DNA (ssDNA) [168]. This DNA tetrahedron consisted of four 55-base ssDNA strands, each strand incorporating unique regions of complementarity with other strands resulting in, by Watson-Crick base pairing, the folding of the strands to form a stable 3-dimensional equilateral tetrahedron.

Adapting this approach to the design and construction of 3D structures based on ssDNA, the current study designed one DNA tetrahedron to incorporate PNA4 (13-mer), and two tetrahedrons of differing sizes to incorporate PMO1 (25-mer) as part of their intrinsic structures. The delivery of the synthetic antisense component of the tetrahedron after translocation across the bacterial cell wall relied upon the DNA components of the structure being degraded either wholly or partially by endonucleases upon entering the bacterial cytoplasm, releasing the synthetic antisense agent from the DNA tetrahedron. Assembled tetrahedral vector sizes are defined by their constituent

total numbers of base-pairs – for example a tetrahedron assembled from three ssDNA oligomers and one 25 nucleotide PMO was identified as a 50 bp tetrahedron.

### 7.1.1. Design of ssDNA sequences to self-assemble into 3D tetrahedron nanoparticles carrying antisense oligomers

#### 7.1.1.1. Design of a 50 bp tetrahedron nanoparticle to carry a single 25-mer PMO

A DNA/PMO tetrahedron was designed to self-assemble from three 25-base ssDNA strands and unmodified PMO1 (Figure 7-1). After self-assembly, this was designed to result in a tetrahedron of a total size of 50 bp, with each edge being 8-9 bp in length, and PMO1 forming one face. Each DNA strand was designed with unique complementary regions to regions on the other strands and to PMO1 to facilitate the formation of the 3D structure. ssDNA strands were checked for unwanted hetero and homo dimerisation with Multiple Primer Analyzer (ThermoFisher Scientific).

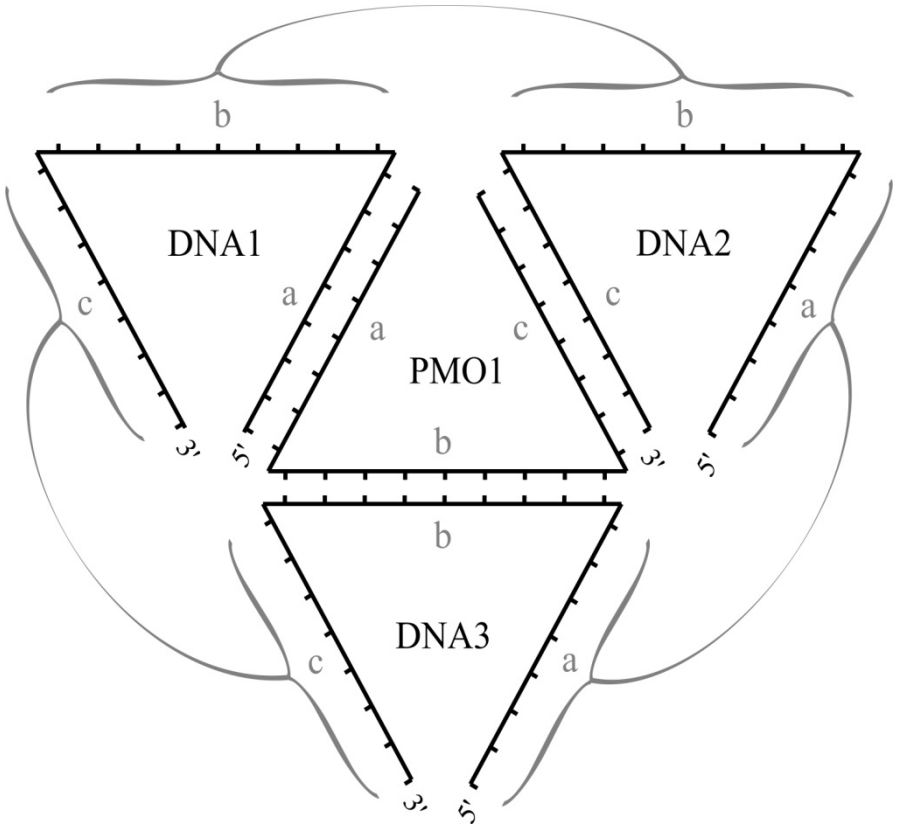


Figure 7-1. Design of a 50 bp tetrahedron nanoparticle to carry a single 25-mer PMO. Single-stranded DNA strands, DNA1, DNA2 and DNA3 were designed with unique regions of complementarity with each other ssDNA strand and PMO1 to form a 3D tetrahedron. Paired regions of 100% complementarity are shown in grey. Tick marks represent approximate positions of individual DNA/PMO bases.

#### 7.1.1.2. Design of a 108 bp tetrahedron nanoparticle to carry a single 25-mer PMO

A DNA/PMO tetrahedron was designed to self-assemble from three 54 nt ssDNA oligonucleotides, one 29 nt ssDNA oligonucleotide and unmodified PMO1. After self-assembly, this was designed to form a tetrahedron of a total size of 108 bp, with each edge being 18 bp in length, and PMO1 forming a portion of two faces (Figure 7-2). ssDNA oligonucleotides were checked for unwanted hetero and homo dimerisation with Multiple Primer Analyzer (ThermoFisher Scientific).

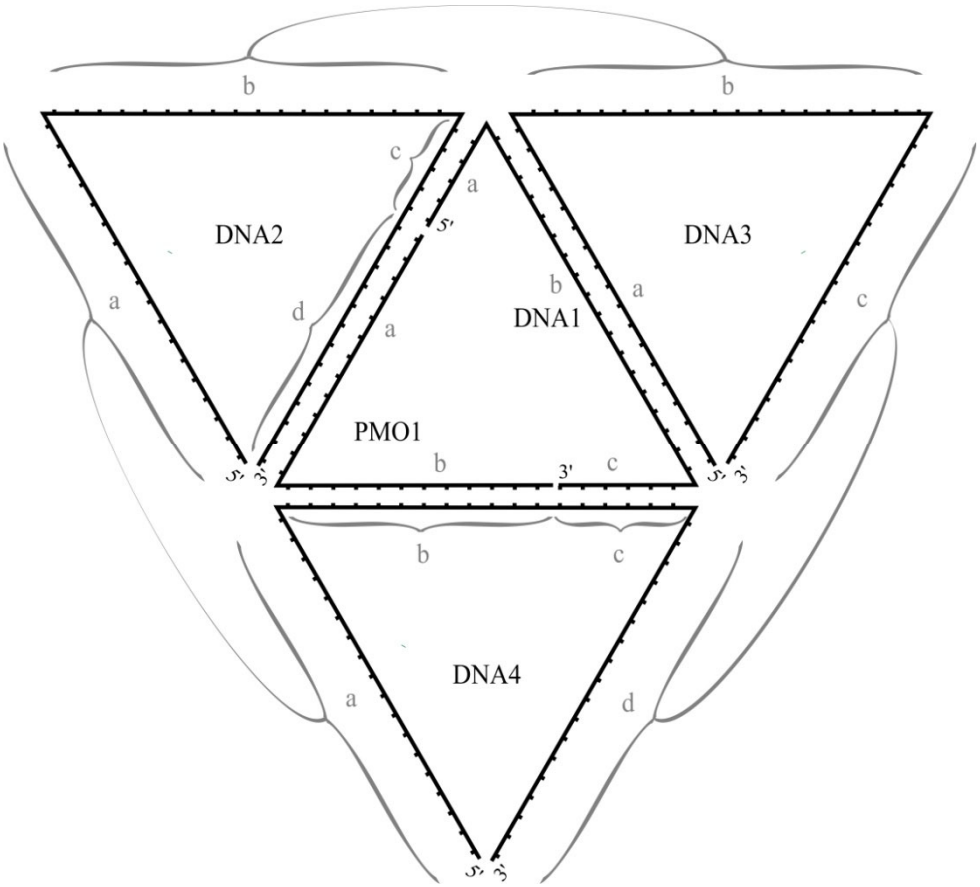


Figure 7-2. 108 bp tetrahedron design to carry one 25-mer PMO (PMO1).
ssDNA strands, DNA1, DNA2, DNA3 and DNA4 were designed with unique regions of complementarity with each other ssDNA strand and PMO1 to form a 3D tetrahedron. Paired regions of 100% complementarity are shown in grey: DNA1 region ‘a’ pairs with DNA2 region ‘c’, DNA1 region ‘b’ pairs with DNA3 region ‘a’, DNA1 region ‘c’ pairs with DNA4 region ‘c’, PMO1 region ‘a’ pairs with DNA2 region ‘d’, PMO1 region ‘b’ pairs with DNA4 region ‘b’, DNA2 region ‘a’ pairs with DNA4 region ‘a’, DNA2 region ‘b’ pairs with DNA3 region ‘b’, DNA3 region ‘c’ pairs with DNA4 region ‘d’. Tick marks represent approximate positions of individual DNA/PMO1 bases.

#### 7.1.1.3. Design of a 108 bp tetrahedron nanoparticle to carry a single 13-mer PNA (PNA4)

A DNA/PNA tetrahedron was designed to self-assemble from three 54 nt ssDNA oligonucleotides, one 41 nt ssDNA oligonucleotide and one 13-mer PNA (unmodified PNA4). After self-assembly, this was designed to result in a tetrahedron with a total size of 108 bp, each edge being 18 bp in length, and PNA4 carried by a region of complementarity with DNA3 (Figure 7-3). ssDNA strands were checked for unwanted hetero and homo dimerisation with Multiple Primer Analyzer (ThermoFisher Scientific). Of the three tetrahedron designs evaluated in the current study, this uniquely did not require the antisense oligomer to bend to form the 3D structure (Figure 7-3; Figure 7-4).

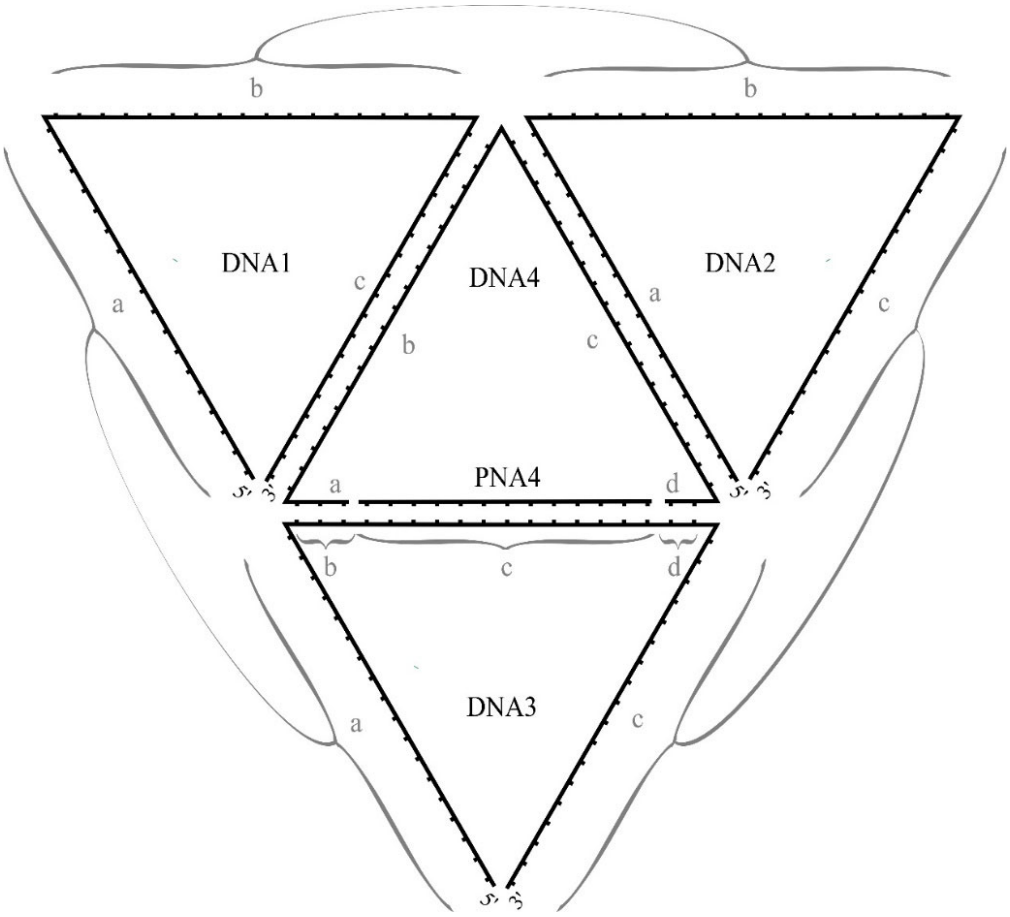


Figure 7-3. 108 bp tetrahedron design to carry one 13-mer PNA (PNA4).
ssDNA strands, DNA1, DNA2, DNA3 and DNA4 were designed with unique regions of complementarity with each other ssDNA strand and PNA4 to form a 3D tetrahedron. Paired regions of 100% complementarity are shown in grey. PNA4 was complementary to region C of DNA3. Tick marks represent approximate positions of individual DNA/PNA bases.

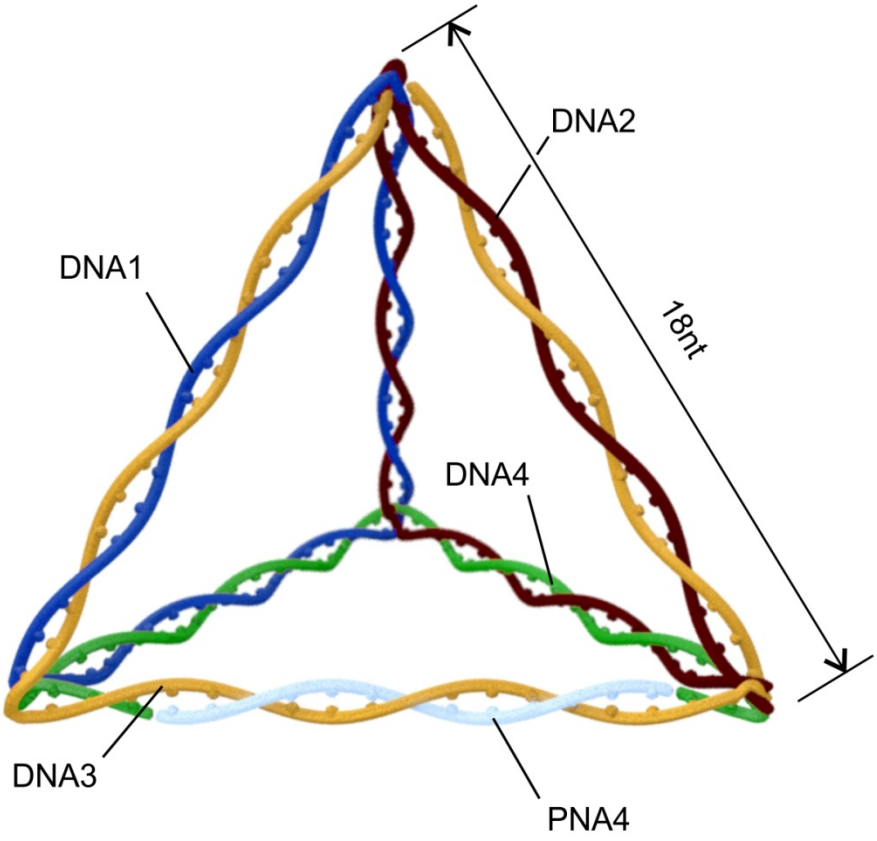


Figure 7-4. 3D diagram representing assembled PNA4-carrying DNA tetrahedron. Regions of each strand of ssDNA are complementary to a unique region on another DNA strand. The strands fold to form a rigid 3D structure. Unmodified PNA4 is carried by complementarity with DNA3 over the region shown.

### 7.1.2. Tetrahedron designations

Three tetrahedron designs carrying anti-*bla*$_{\text{CTX-M-15}}$ oligomers were designed and constructed, as discussed, and are summarised in Table 7-1.

Table 7-1. Antisense oligomer-carrying DNA tetrahedron designs.

| Designation | Antisense oligomer cargo | Antisense oligomer length (nt) | Tetrahedron Size (bp) |
|---|---|---|---|
| PMOP | PMO1 | 25 | 50 |
| CPMOP | PMO1 | 25 | 108 |
| SPNAP | PNA4 | 13 | 108 |

## 7.2. Results

### 7.2.1. Verification of assembly of tetrahedron by agarose gel electrophoresis

Assembly of the tetrahedrons were verified by visualisation of DNA by agarose gel electrophoresis. Component ssDNA strands, and combinations of strands annealed under the same conditions as described in the tetrahedron assembly protocol, were loaded in separate lanes, e.g. DNA1 + DNA2, DNA1 + DNA2 + DNA3, DNA1 + DNA2 + DNA3 + DNA4 + PNA4, and analysed for size by gel electrophoresis. The results suggested that the strands annealed to form progressively larger DNA complexes with the additional tetrahedron components; when visualised by gel electrophoresis, the reaction mixture comprising of all components necessary for tetrahedron formation yielded a single discreet band, in a position on the gel to indicate a larger DNA molecule than the component parts, and of approximately the expected size (Figure 7-5).

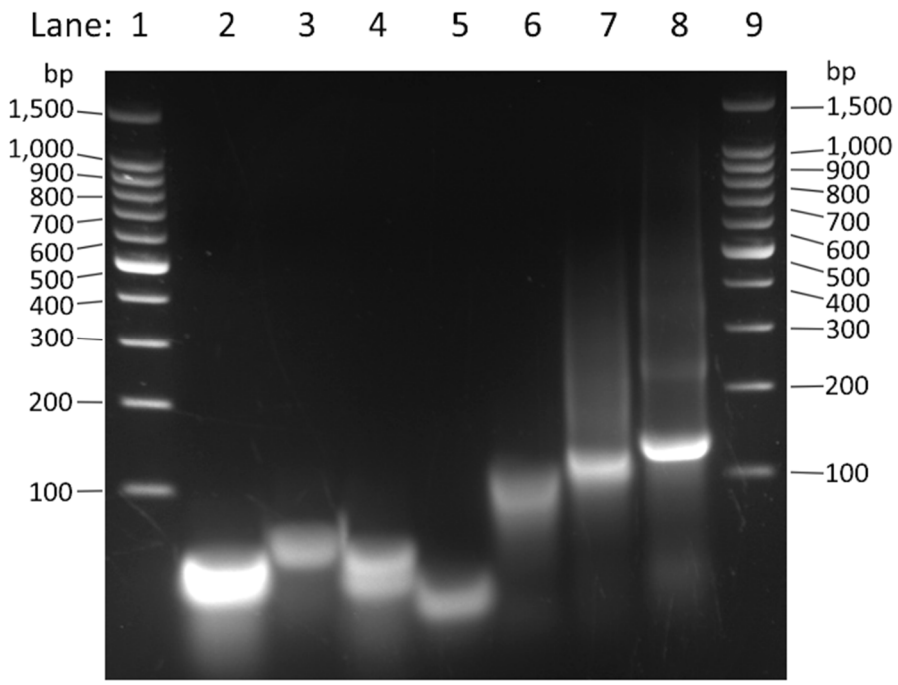


Figure 7-5. Gel showing relative sizes of tetrahedron (SPNAP; 108 bp) component parts, partial assembly, and full assembly.

Lane 1: Promega 100bp DNA ladder. Lane 2: DNA1. Lane 3: DNA2. Lane 4: DNA3. Lane 5: DNA4. Lane 6: DNA1 + DNA2. Lane 7: DNA1 + DNA2 + DNA3. Lane 8: DNA1 + DNA2 + DNA3 + DNA4 + PNA4 (complete tetrahedron (SPNAP) assembly). Lane 9: Promega 100 bp DNA ladder.

### 7.2.2. Increase in sensitivity of *E. coli* strains to CTX when co-administered with 50 bp PMO1-carrying tetrahedron PMOP

*E. coli* strains AS19/pJBRCTX516 and field isolate LREC460 were challenged with CTX, 50 bp PMO1-carrying tetrahedron PMOP, and both in combination. No significant effects of PMOP were observed on LREC460 growth when treated in combination with CTX (not shown). Atypically permeable strain AS19, transformed with pJBRCTX516 was challenged with PMOP alone, CTX alone and PMOP and CTX in combination. No significant effects were observed in cultures incubated with PMOP or PMO1 alone (10-20 μM; Figure 7-6; Figure 7-7). Cultures incubated with CTX concentrations of 32 μg/ml and 64 μg/ml had a significant ($p < 0.05$) negative effect on growth - the lag phase was observed to be significantly longer in duration than that of the sample with no antibiotic – early log phase (O.D. $_{600\ nm} > 0.1$) was reached in the culture with no antibiotic in 4.6 - 5.25 hours, when cultured in the presence of 32 μg/ml CTX this increased to 10.8 hours, when cultured in the presence of 64 μg/ml CTX this increased to 12.4 hours. This effect was further increased in cultures incubated in the presence of both CTX (64 μg/ml) and PMOP (10 μM; Figure 7-6), and the combination of CTX concentration of 32 μg/ml and PMOP of 20 μM was sufficient to completely inhibit growth (Figure 7-7). The inhibitory effect of CTX (32 μg/ml and 64 μg/ml) in the presence of PMOP was greater than that of PMO1.

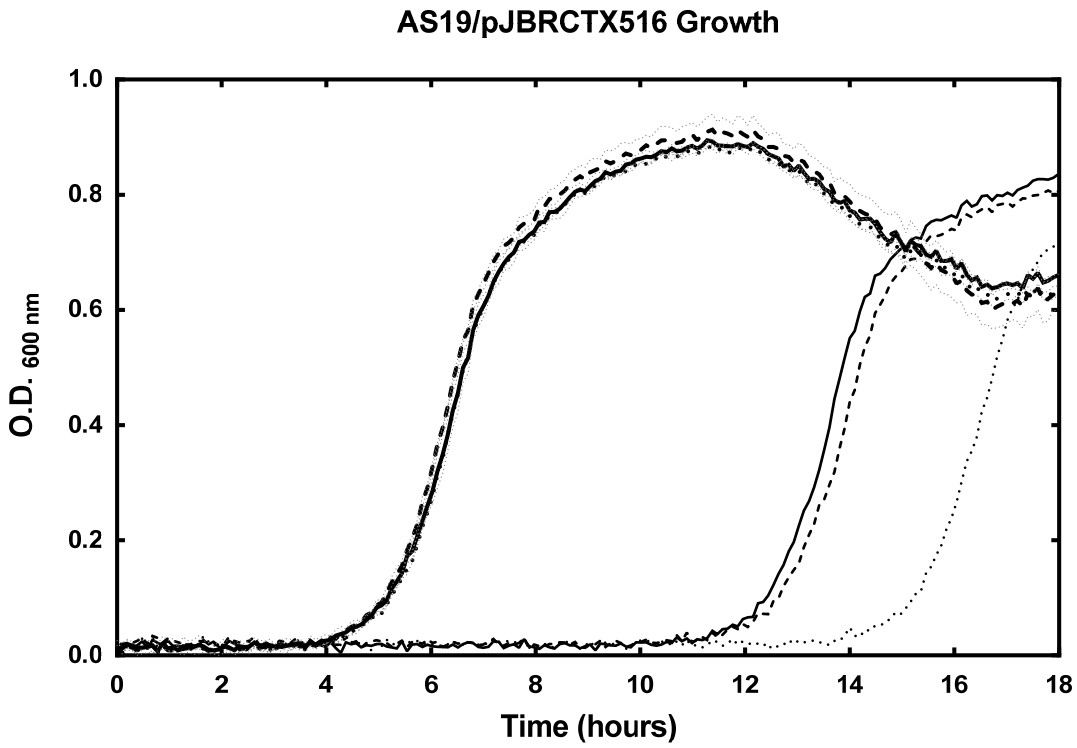


Figure 7-6. Effects of CTX, PMO1 and PMOP on AS19/pJBRCTX516 growth. Growth curves showing effect on growth of atypically permeable *E. coli* strain AS19 harbouring *bla*$_{\text{CTX-M-15}}$-carrying plasmid pJBRCTX516 incubated with CTX, PMO1 and PMO1 carried by tetrahedron PMOP. Solid line: CTX (0 μg/ml), dashed line: CTX (0 μg/ml) + PMOP (10 μM), dotted line (partially obscured by thick solid line): CTX (0 μg/ml) + PMO1 (10 μM), thin solid line: CTX (64 μg/ml), thin dashed line: CTX (64 μg/ml) + PMO1 (10 μM), thin dotted line: CTX (64 μg/ml) + PMOP (10 μM). Error bars indicate +/- 1 standard deviation (n=2).

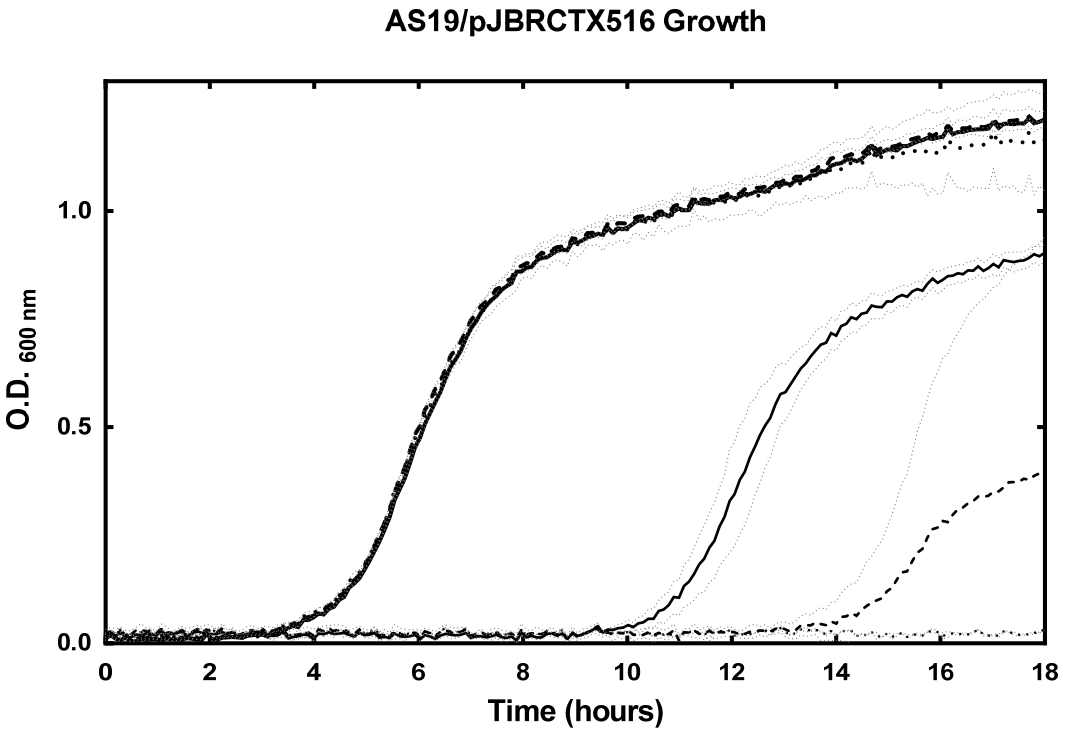


Figure 7-7. Effects of CTX, PMO1 and PMOP on AS19/pJBRCTX516 growth. Growth curves showing effect on growth of atypically permeable *E. coli* strain harbouring *bla*$_{\text{CTX-M-15}}$-carrying plasmid incubated with CTX, PMO1 and PMO1 carried by tetrahedron PMOP. Solid line: CTX (0 μg/ml), dashed line: CTX (0 μg/ml) + PMOP (20 μM), dotted line: CTX (0 μg/ml) + PMO1 (20 μM), thin solid line: CTX (32 μg/ml), thin dashed line: CTX (32 μg/ml) + PMO1 (20 μM), thin dotted line (no growth): CTX (32 μg/ml) + PMOP (20 μM). Error bars indicate +/- 1 standard deviation (n=3).

### 7.2.3. Increase in sensitivity of *E. coli* field isolate LREC461 to CTX when co-administered with 108 bp PMO-carrying tetrahedron CPMOP

*E. coli* field isolate LREC461 carrying plasmid pEK204 which harboured *bla*$_{\text{CTX-M-3,}}$ was incubated in MHB supplemented with 108 bp DNA tetrahedron, CPMOP, carrying 25-mer PMO1 (10 - 30 μM), and CTX (16 μg/ml). Growth was inhibited in a dose dependant manner (10 - 30 μM), completely inhibited at 30 μM (Figure 7-8). There were no observable inhibitory effects on growth when treated with CPMOP alone.

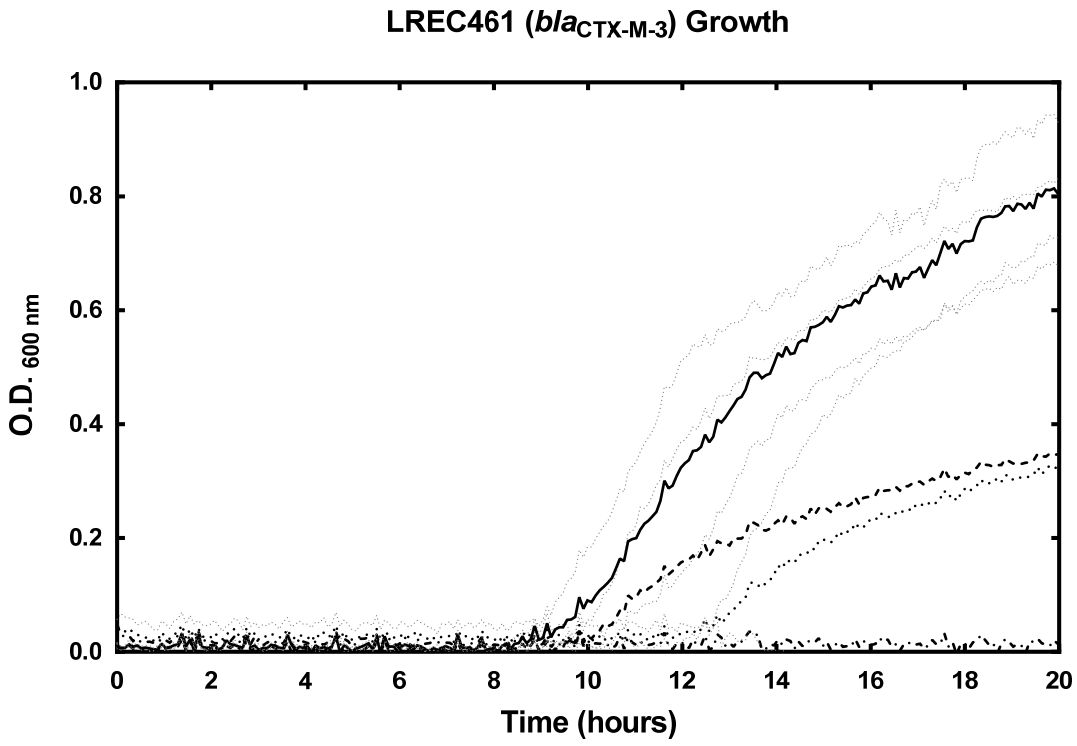


Figure 7-8. Effects of the combination of CTX and CPMOP on the growth of field isolate LREC461.

Growth curves showing effect on growth of field isolate LREC461 incubated with CTX and PMO1 carried by tetrahedron CPMOP. Solid line: CTX (16 µg/ml), dashed line: CTX (16 µg/ml) + CPMOP (10 µM), dotted line: CTX (16 µg/ml) + CPMOP (20 µM), dash-dot line (no growth): CTX (16 µg/ml) + CPMOP (30 µM). Error bars indicate +/- 1 standard deviation (n=2).

### 7.2.4. Increase in sensitivity of *E. coli* field isolate LREC461 to CTX when co-administered with 108 bp PNA-carrying tetrahedron SPNAP

Field isolate LREC461 was challenged with a combination of CTX (16 μg/ml) and SPNAP (0 – 40 μM), and a synergistic (FICI < 0.5) dose dependant effect was observed, evidenced by the increasing the amount of time taken for cells to achieve logarithmic growth (Figure 7-9).

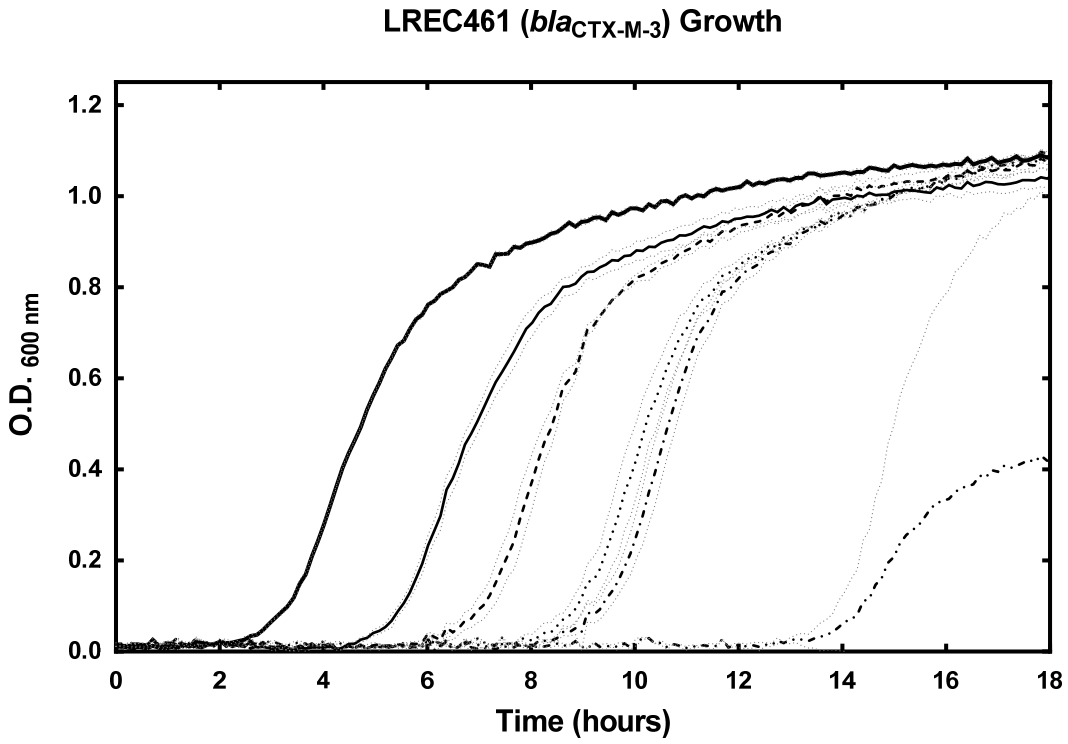


Figure 7-9. Effects of CTX and SPNAP on growth of field isolate LREC461.
Growth curves showing effect on growth of field isolate LREC461 incubated with CTX and PNA4 carried by tetrahedron SPNAP. Thick solid line: CTX (0 μg/ml), thin solid line: CTX (16 μg/ml), dashed line: CTX (16 μg/ml) + SPNAP (10 μM), dotted line: CTX (16 μg/ml) + SPNAP (20 μM), dash-dot line: CTX (16 μg/ml) + SPNAP (30 μM), dash-dot-dot line: CTX (16 μg/ml) + SPNAP (40 μM). Error bars indicate +/- 1 standard deviation (n=2).

LREC461 was cultured in the absence of CTX, and in the presence of 108 bp PNA4-carrying tetrahedron, SPNAP (10 – 30 μM), no significant effects were observed (Figure 7-10).

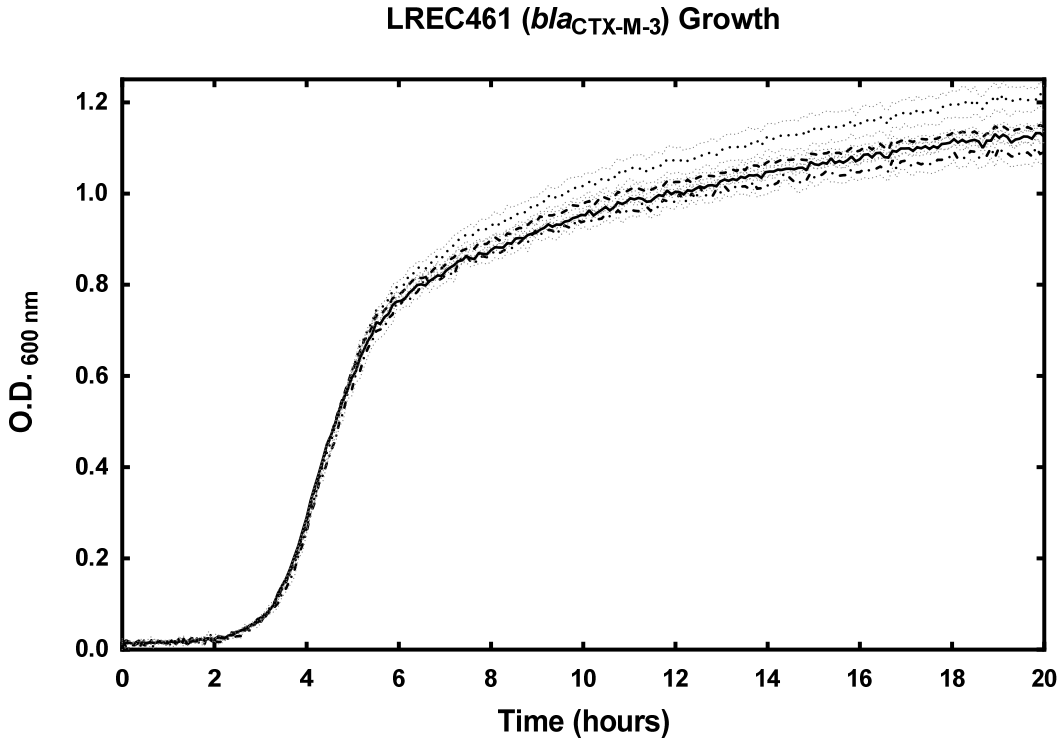


Figure 7-10. Effect of SPNAP on growth of field isolate LREC461 in the absence of CTX.

Growth curves showing lack of effect on growth of field isolate LREC461 incubated with PNA4-carrying tetrahedron SPNAP. Solid line: no culture supplements, dashed line: SPNAP (10 μM), dotted line: SPNAP tetrahedron (20 μM), dash-dot line: SPNAP tetrahedron (30 μM). Error bars indicate +/- 1 standard deviation (n=2).

A control DNA tetrahedron was assembled substituting a 13 nt ssDNA oligonucleotide for PNA4. The 13 nt ssDNA strand shared 100% sequence identity with PNA4 and the DNA tetrahedron was assembled using the components DNA1-DNA4 (Figure 7-3). No significant negative effects on growth were observed when field isolate LREC461 was cultured in the presence of the DNA control tetrahedron (10 – 30 μM; Figure 7-11).

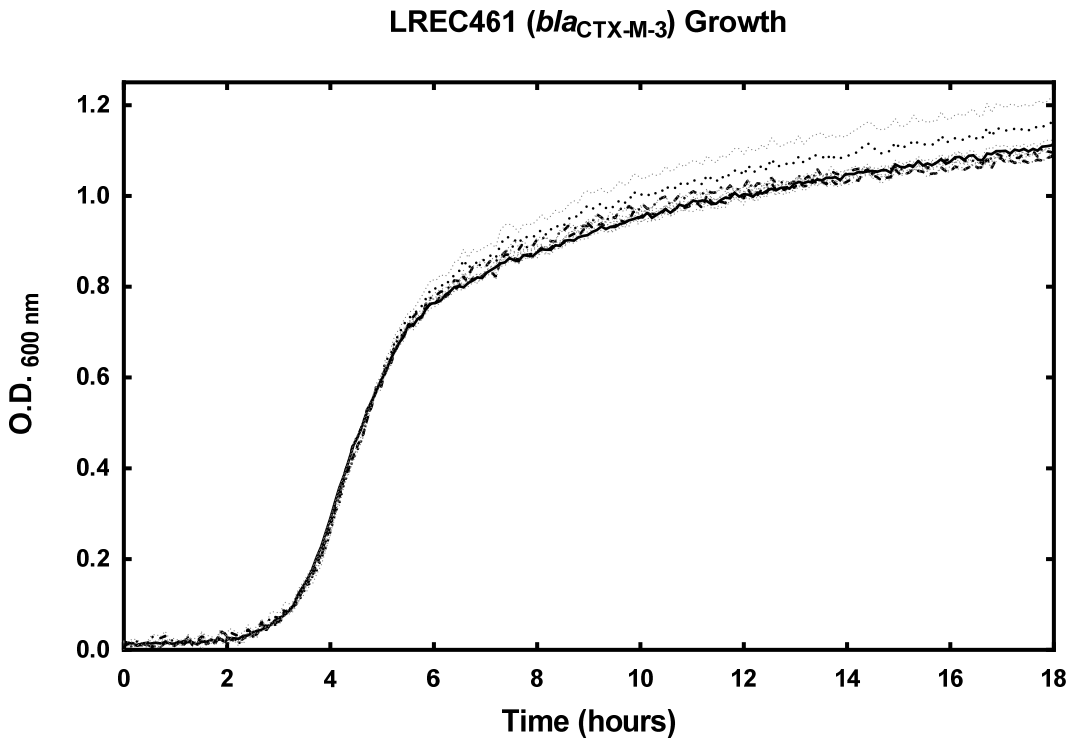


Figure 7-11. Effect of DNA control tetrahedron on growth of field isolate LREC461. Growth curves showing effect on growth of field isolate LREC461 incubated with control DNA tetrahedron. Solid line: no culture supplements, dashed line: DNA control tetrahedron (10 μM), dotted line: DNA control tetrahedron (20 μM), dash-dot line: DNA control tetrahedron (30 μM). Error bars indicate ± 1 standard deviation (n=2).

Small but significant negative effects on growth were observed when field isolate LREC461 was cultured in the presence of the DNA control tetrahedron (10 μM) and CTX (16 μg/ml) (Figure 7-12). An atypically high sensitivity to CTX (16 μg/ml) alone was observed in this instance, potentially as a result of a low bacterial cell count present in the culture. Attempts were made with each experiment to normalise the number of colony-forming units to 100,000 CFU/ml; colony counts after overnight incubation on LB agar revealed the amount present on this occasion to be 40,000 CFU/ml.

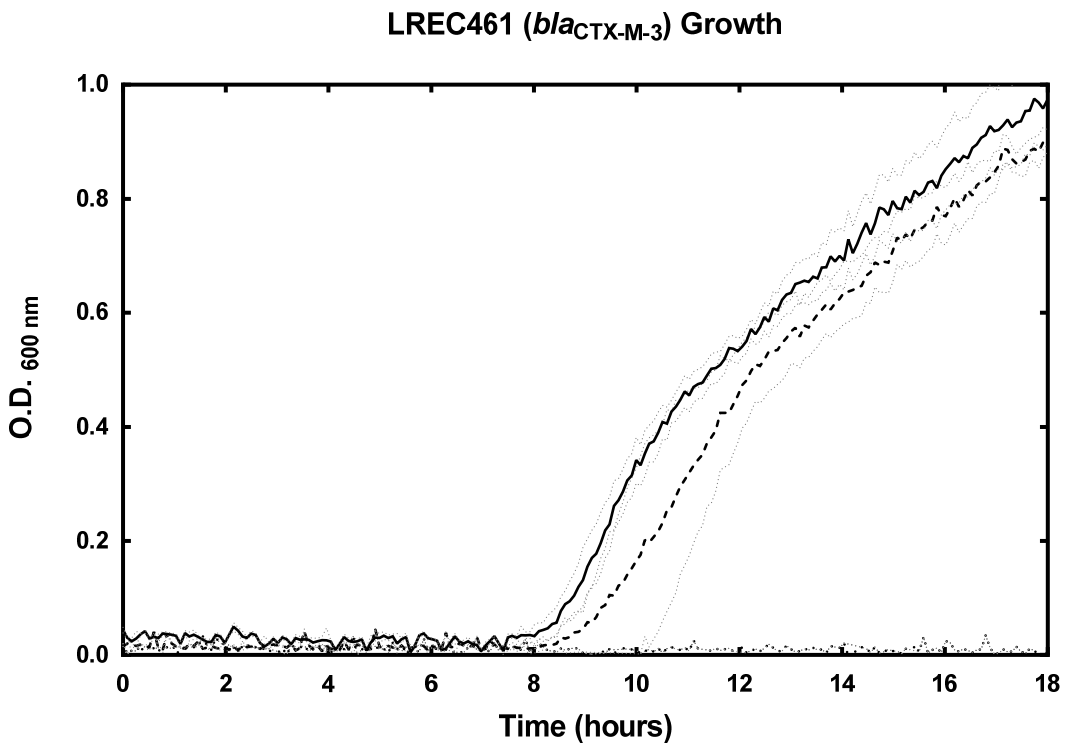


Figure 7-12. Effects of DNA control tetrahedron and SPNAP on LREC461 growth in the presence of CTX.

Growth curves showing effect on growth of field isolate LREC461 incubated with control DNA tetrahedron and SPNAP. Solid line: CTX (16 µg/ml), dashed line: DNA control tetrahedron (10 µM) + CTX (16 µg/ml), dotted line (no growth): SPNAP (10 µM) + CTX (16 µg/ml). Error bars indicate ± 1 standard deviation (n=2).

## 7.3. Discussion

The current study demonstrated the potential application of three variations of a DNA tetrahedron to deliver antisense agents within a bacterial cell using complementary base pairing approach. The antisense oligomers available for initial evaluation of delivery vehicle efficacy were the unmodified anti-*bla*$_{\text{CTX-M}}$ PMO1 and PNA4 used throughout the current study (see Table 2-3 for sequences). The use of these antisense oligomers also provided direct comparison of *bla*$_{\text{CTX-M-15}}$ expression inhibition by antisense oligomers carried by a DNA tetrahedron with the more conventional cell-penetrating peptide conjugate delivery strategy.

A CTX potentiating effect was observed when AS19/pJBRCTX516 was incubated in the presence of CTX (32 μg/ml and 64 μg/ml) and 50 bp DNA/PMO1 tetrahedron, PMOP (10 μM and 20 μM). The effect size of the combination of CTX and tetrahedron was greater than that of the combination of CTX and PMO1 under the same conditions, suggesting that although AS19/pJBRCTX516 exhibited an atypically permeable phenotype, PMO1 carried in a tetrahedron structure achieved a greater level of cell wall penetration and cytoplasmic accumulation, resulting in a higher level of *bla*$_{\text{CTX-M-15}}$ expression inhibition and CTX re-sensitisation. A small inhibitory effect was observed (not shown) under similar conditions in isolates with typically permeable cell walls.

Potentiation of CTX, in a dose dependent manner, was observed when field isolate LREC461, harbouring *bla*$_{\text{CTX-M-3}}$, was incubated in the presence of CTX and the 108 bp tetrahedron, CPOMP, carrying PMO1. A dose dependent effect of greater size was observed when field isolate LREC461 was incubated in the presence of the combination of CTX and SPNAP; LREC461 was significantly more sensitive to CTX in the presence of SPNAP than CPMOP.

A control DNA tetrahedron was constructed, substituting ssDNA, of the same sequence, for the antisense oligomer. There were no observable effects in field isolates incubated in the presence of a DNA control tetrahedron in the absence of CTX. In the presence of CTX and DNA control tetrahedron combination, a small increase in CTX sensitivity was observed, possibly due to opportunistic co-translocation of CTX with the control DNA tetrahedron. Control data suggests no inherent antimicrobial properties of the structure and may indicate that membrane perturbation was not the primary mechanism of cell penetration.

The observed re-sensitisation of field isolates to previously sub-lethal concentrations of CTX suggest that this DNA tetrahedron design penetrates a bacterial cell wall and delivers its cargo, which is able to specifically bind to its target and inhibit protein expression. Tetrahedron CPMOP had no observable inhibitory effects on cell growth when cells were treated in the absence of antibiotics. No significant inhibitory effects were observed when field isolate LREC461 was treated with PNA4-carrying tetrahedron SPNAP in the absence of CTX. This was not expected as PNA4 had been previously observed to exhibit dose-dependent inhibitory effects. Further studies are required to verify and elucidate this initial observation.

The CTX-sensitising effects of both CPMOP and SPNAP were smaller than the equivalent peptide-conjugated antisense oligomers, potentially suggesting a less efficient penetration ability of the tetrahedron. However, the cell-penetrating peptide portion of the CPP-antisense oligomer conjugate, $(KFF)_3K$, has been previously shown to have a synergistic effect with certain antibiotics [147, 158], and some potential inherent toxicity (this study). In addition, *E. coli* cell permeabilisation has been shown to be reduced in the presence of $MgCl_2$ [158]. As the current study annealed the

tetrahedron components in an $MgCl_2$-rich (50 mM) buffer, further studies are required to determine any significant increased cell penetrating efficacy of antisense agent-carrying tetrahedral structures either annealed in the absence of $MgCl_2$, or of tetrahedrons purified after assembly.

Further studies are required to determine the range of bacterial strains susceptible to antisense oligomer mediated protein expression inhibition carried by DNA tetrahedrons. The mechanism of cellular uptake of DNA tetrahedrons in bacteria is presently unclear, although the lack of effect on cell growth of isolates challenged with a tetrahedron alone may suggest that the mechanism of penetration does not involve the disruption of the cell wall. A range of influx mutants could be generated and employed to investigate an active transport mechanism.

The size of the tetrahedron would appear to have a large effect on penetration efficacy – a marked increase in the inhibitory ability of the PMO was observed when increasing the length of each edge from 8 to 18 bp. This would suggest further optimisation potential. Both size and shape of 3D DNA structures would appear to be of great importance in their ability to enter a bacterial cell. It may be advantageous to design and construct a range of DNA 3D structures of differing dimensions and shape, incorporating quantifiable and observable markers, to determine the optimal structure for use as a synthetic antisense oligomer delivery vehicle.

In addition, the design of the DNA tetrahedron allows for the incorporation of multiple antisense molecules, potentially up to three 15-mer PNAs could be incorporated into a single 108 bp tetrahedron without significant reduction of structural integrity. Each PNA could potentially target a different gene transcript, allowing for inhibition of the expression of multiple genes with a single therapeutic molecule.

Studies to investigate the discriminatory potential of tetrahedral delivery vehicles would also be advantageous – cell-penetrating peptides commonly lack specificity for any cell types. A 108 bp 25-mer PMO-carrying tetrahedron was designed and constructed to carry an anti-dystrophin PMO, and found to have no observable effects in murine cell lines (L. Popplewell, pers. comm.). Although more data is required, this could suggest a degree of specificity to bacterial cells. This lack of observable effect in murine cells, combined with the lack of effect observed with control tetrahedrons in *E. coli* field isolates could implicate a non-membrane disruptive mechanism of cell penetration. A delivery vector that was specific to bacterial cells and did not have inherent negative effects on cell growth would be highly desirable characteristics for a targeted vector.

With a demonstrated ability to both penetrate a bacterial cell wall and deliver an active synthetic antisense oligomer, this approach has a large range of optimisation options, and a variety of potential applications. The low cost, simplicity and speed of assembly would appear to make this a potentially viable alternative antisense oligomer delivery vehicle.

# Chapter 8.

# Discussion, future work and conclusions

## 8.1. Discussion

The application of antisense oligomers for the targeted inhibition of the expression of specific genes that confer resistance to extended-spectrum β-lactam antibiotics is an attractive strategy for the restoration of antimicrobial sensitivity. PMO and PNA chemistries have both been successfully employed previously to inhibit bacterial protein expression in a targeted, sequence-specific manner [186]. A wide range of bacterial gene transcripts have been targeted and inhibited by synthetic antisense oligomers. For example, a 17-mer PNA was reported by Lecosnier *et al.* in 2011 to inhibit anti-insulin-like growth factor 1 receptor (IGF-1R) by 70-80% [118]. Geller *et al.* found that an 11-mer PMO significantly inhibited the viability *E. coli* through targeted inhibition of an essential gene (*acpP*) for phospholipid biosynthesis [127].

The current study designed and evaluated PMO and PNA antisense/antigene oligomers for effective reduction of a range of CTX-M group 1 β-lactamases. Anti-*bla*$_{\text{CTX-M}}$ antisense oligomers, three 13-mer PNAs and one 25-mer PMO, were designed and synthesised to target mRNA Shine-Dalgarno and start codon regions, having previously been shown to be the regions most susceptible for protein expression inhibition. β-Lactamase activity inhibition was demonstrated by the quantification cefotaxime degradation in a variety of systems including: a cell free transcription/translation assay using recombinant plasmids (pJBRCTX499 and pJBRCTX516) with a high amplitude promoter harbouring a CTX-M-15 gene, in a cell wall compromised mutant *E. coli* strain (AS19/pJBRCTX516) also containing this recombinant plasmid, and in a panel of

field isolates whose group 1 CTX-M plasmids had been previously sequenced (Table 2-1).

Bacterial cell wall penetration and delivery of antisense oligomers into field and clinical isolates with intact cell walls was accomplished by the use of the cell-penetrating peptide $(KFF)_3K$ as a carrier molecule, and by the development of a novel delivery vector.

### 8.1.1. Inhibition of β-lactamase expression in a cell-free translation/transcription coupled system

In cell-free studies using constructed plasmid pJBRCTX516, harbouring a single copy of *bla*$_{CTX\text{-}M\text{-}15}$, as the DNA template, PMO1 was observed to inhibit the expression of β-lactamase in a dose-dependent (50 - 1000 nM) manner. Neither a 25 nt scrambled control PMO, nor a 25 nt control PMO targeting an unrelated human (dystrophin) mRNA, was observed to have any inhibitory effects on β-lactamase expression. The control PMOs shared no sequence identity with any bacterial gene or transcript sequence. These data suggested high sequence specific inhibitory properties of anti-*bla*$_{CTX\text{-}M}$ PMO1.

The inhibition of β-lactamase expression was also observed in a translation/transcription coupled system when pJBRCTX516 was incubated in the presence of PNAs 1, 3 and 4. Maximum observed β-lactamase activity inhibition amounts were: PNA1 (1000 nM) – 96%, PNA3 (1000 nM) – 84% and PNA4 (1000 nM) – 89% (Figure 8-1). As previously discussed herein, PMO1 and PNA4 were selected as the antisense oligomers of maximum interest for subsequent studies (Chapter 5).

### 8.1.2. Increase in sensitivity of cell wall compromised mutant strain AS19/pJBRCTX516 to CTX when co-administered with PMO1

In live cells, the β-lactamase expression inhibition properties of PMO1 were first evaluated using the atypically permeable cell-wall mutant *E. coli* strain AS19 transformed with pJBRCTX516 harbouring *bla*$_{\text{CTX-M-15}}$. Specific anti-*bla*$_{\text{CTX-M-15}}$ activity was demonstrated by the combination of an observation of a cefotaxime potentiating effect of PMO1, a lack of effect on growth of control PMOs, and of an observation of no effect on growth when cultures were incubated in the presence of PMO1 and in the absence of cefotaxime. When cultured in the presence of both cefotaxime and PMO1, increased antibiotic sensitivity was observed in a dose-dependent manner (5 – 40 nM). The typical minimum inhibitory concentration of cefotaxime for this transformant was 80 μg/ml. In the presence of PMO1 (40 μM), the minimum inhibitory concentration was reduced to 4 μg/ml. These data demonstrated the lack of any inherent toxicity of PMO1 at the concentrations used, and the specific activity of PMO1 against *bla*$_{\text{CTX-M-15}}$.

### 8.1.3. Increase in sensitivity of cell wall compromised mutant strain AS19/pJBRCTX516 to CTX when co-administered with PNA4

A dose-dependent effect of increasing the CTX sensitivity of AS19/pJBRCTX516 was observed when cultured in the presence of PNA4. This effect was greater than that of PMO1, with a PNA concentration of 20 μM required to reduce the MIC (to CTX) of AS19/pJBRCTX516 from 80 μg/ml to 4 μg/ml. However, a significant ($p < 0.0001$) negative effect on growth was observed when AS19/pJBRCTX516 was cultured in the presence of PNA4 alone (> 10 μM) suggesting either inherent toxicity of PNA4 or the effect of off-target sequence similarity.

As previously noted, a smaller antisense molecule with fewer bases naturally leads to a greater risk of a lack of specificity, with more sequences likely to share partial sequence identity. This risk is increased when the target area is extra-genic, as is the case with PNA4, where regions are likely to be conserved. A BLAST search revealed that the region targeted by PNA4 shared 11 and 12 consecutive bases of the total 13, of genes coding for condesin subunit F, and NADH:ubiquinone oxidoreductase respectively. Both of these genes play essential roles in *E. coli*, and this is a likely explanation of the observed negative effect on growth when field isolates were challenged with PNA4 alone. The negative effects of putative off-target sequence identity were insufficient to inhibit growth in any field isolate tested up to 40 μM, and the effects of cefotaxime and PNA4 were shown to be strongly synergistic suggesting that β-lactamase was the primary and preferential target of PNA4. The negative effects of growth of cultures incubated in the presence of PNA4 alone at concentrations of 5 μM and lower, were not significantly ($p = 0.2524$) different from control cultures grown in the absence of PNA4.

### 8.1.4. Increase in sensitivity of field and clinical isolates to CTX when co-administered with peptide conjugated PMO1 and PNA4

No effect on cefotaxime sensitivity was observed when field isolate LREC461 carrying resistance plasmid pEK204 harbouring *bla*$_{\text{CTX-M-3}}$ was cultured in the presence of the PMO1 (5 – 20 μM) or PNA4 (5 – 40 μM). This was not unexpected as previous studies have shown that *E. coli* with an intact cell wall do not efficiently take up PMOs [119]. To overcome this barrier, anti-*bla*$_{\text{CTX-M}}$ PMO1 and PNA4 were covalently bound to the cell-penetrating peptide, $(KFF)_3K$, which has been shown to be effective in promoting uptake across the bacterial cell wall and delivering a cargo molecule into the cytoplasm [121, 158].

A panel of field isolates and clinical *E. coli* strains, each harbouring a β-lactamase-producing gene from CTX-M-group 1 was challenged with a combination of peptide-conjugated antisense agent and cefotaxime. All isolates tested showed an increased sensitivity to CTX when treated with P-PMO1 or P-PNA4 ranging from a reduction in the MIC (to CTX) of *bla*$_{\text{CTX-M-3}}$-harbouring *E. coli* strain LREC461 from 35 μg/ml to 16 μg/ml (P-PMO1, 30 μM), to *E. coli* strain LREC454 harbouring *bla*$_{\text{CTX-M-15}}$ from 110 μg/ml to 2 μg/ml (P-PNA4, 3.2 μM; Table 5-3).

The CTX re-sensitising effectiveness of P-PNA4 ranged from 9 to 56-fold greater than that of P-PMO1. There were no significant effects of P-PNA4 alone at concentrations of less than 5 μM although at higher concentrations (> 10 μM), in the absence of cefotaxime, P-PNA4 significantly inhibited the growth of field isolates. The reason for the greater effect of P-PNA4 over P-PMO1 remains unclear, although the higher binding strength of PNAs enables a smaller molecule, potentially facilitating more efficient cell penetration. It would be reasonable to suggest that a smaller molecule is able to penetrate the bacterial cell wall more efficiently than a larger molecule, and further studies would be useful to clarify if this is indeed the case. The data obtained from cell-free studies in a translation/transcription coupled system, thus removing the cell wall penetration obstacles, demonstrated that PMO1 inhibited β-lactamase expression more efficiently than any PNA tested. This may suggest that size, and thus penetration efficiency in live cells, is a significant contributory factor to the efficacy of bacterial gene expression inhibition with antisense oligomers. The ability of PNAs to form complexes with double-stranded DNA has been previously described and demonstrated [117], potentially also contributing to the overall larger observed effect of P-PNA4 over P-PMO1. Further studies would be needed to elucidate this situation further.

Control studies using P-PMO1 and P-PNA4 in the presence and absence of CTX in strain LREC90 harbouring *bla*$_{\text{CTX-M-14}}$, to which anti-*bla*$_{\text{CTX-M-15}}$ P-PMO1 and P-PNA4 had only partial sequence complementarity, revealed no synergistic relationship with CTX. In addition, when strains harbouring *bla*$_{\text{CTX-M-15}}$ were challenged with P-PMO1 and P-PNA4 alone, a comparable effect size to that shown in LREC90 was observed. Previously sub-lethal concentrations of CTX were sufficient to completely inhibit growth of these group 1 strains when in the presence of P-PMO1 or P-PNA4 at concentrations observed to have small or insignificant effects alone.

### 8.2. β-Lactam induced upregulation of β-lactamase activity in AS19/pJBRCTX516 and field isolates

Studies in a cell-free environment demonstrated the abilities of antisense oligomers to completely inhibit the expression of *bla*$_{\text{CTX-M-15}}$ (100% at a PMO1 concentration of 1000 nM) under certain conditions. It was therefore unexpected that a restoration of CTX sensitivity to a comparable level to that of the CTX sensitive host parental strain (AS19; 1- 2 μg/ml) was not observed in *E. coli* strain AS19/pJBRCTX516 when treated with relatively high concentrations of PMO1 (40 μM) or PNA4 (20 μM).

The current study provided experimental evidence to suggest that in conditions of increasing concentrations of CTX, in both field isolates and AS19/pJBRCTX516 there is a proportional upregulation of β-lactamase activity. This would appear to present an obstacle to be overcome in the goal of the restoration of sensitivity to 3$^{rd}$ generation cephalosporin antibiotics in bacteria with a phenotype of reduced susceptibility. The differential expression mechanism is presently unclear and requires further study.

### 8.3. Molecular bacterial intracellular delivery vectors for targeted synthetic antisense/antigene agents

The current study designed and developed a self-assembling 3D tetrahedral novel vector for the transportation of antisense oligomers across the cell wall of *E .coli* field isolate LREC461. This vector had the advantages of being quick, inexpensive and simple to assemble, and had no observable inherent toxic properties in the field isolates tested. A dose-dependent effect (10 – 30 μM) of increasing CTX sensitivity was observed, and there was no effect on growth when field isolates were treated with a control tetrahedron. The data presented in the current study (the combined effects of CTX and SPNAP on culture growth of field isolate LREC461, and the lack of any significant effects of SPNAP alone) suggest that the tetrahedral vector was successful in delivering its cargo to the bacterial cytoplasm. Further studies, such as the labelling of the tetrahedron with a quantifiable reporter molecule, are required to verify this.

The use of the tetrahedral DNA vector as a carrier for the antisense oligomers PMO1 and PNA4 provided a comparison of efficacy with the same antisense oligomers conjugated to the cell-penetrating peptide $(KFF)_3K$. The smaller effect of the PNA or PMO carried by the tetrahedron compared with the same PNA or PMO carried by a cell-penetrating peptide, suggest that further optimisation of the tetrahedron is required. However, the cell-penetrating peptide, $(KFF)_3K$, has been shown to have some inherent bacterial toxicity, and also have a synergistic effect with certain antibiotics [147]. The contribution of the peptide portion of the P-PMO1 and P-PNA4 conjugates to the overall negative effects on bacterial growth in the current study make a direct comparison between antisense oligomers carried by a tetrahedron (which in the absence of CTX had no observable effects on growth) and those carried by $(KFF)_3K$ difficult, and further studies would be required to separate the effect sizes of the component parts.

## 8.4. Future Work

### 8.4.1. Optimisation of anti-*bla*$_{CTX\text{-}M\text{-}15}$ synthetic antisense sequences

There would appear to be scope for optimisation and enhancements of the effects of the anti-*bla*$_{CTX\text{-}M}$ PMO and PNAs by alterations to the mRNA target area and lengths of antisense oligomers. Due to operational constraints, it was not possible to design and synthesise a series of tiled PNAs and PMOs to span a larger region of *bla*$_{CTX\text{-}M}$ mRNA. As previous studies had indicated that the most effective areas to target for efficient protein inhibition were the start codon region and the SD region, three PNAs and one PMO were targeted to that region. The results from the current study demonstrated a greater effect size of PNA over PMO in inhibiting the expression of β-lactamase in field isolates and the atypically permeable strain AS19, although as they differed in both length and target region they were not directly comparable.

In cell-free studies, the β-lactamase inhibitory effect of the three PNAs varied from 84% inhibition (PNA3, 1000 nM) to 96% inhibition (PNA1; 1000 nM; Figure 8-1). This suggests that small changes in the PNA sequence and hence the region result in a large effect on the ultimate effect of the inhibitory agents.

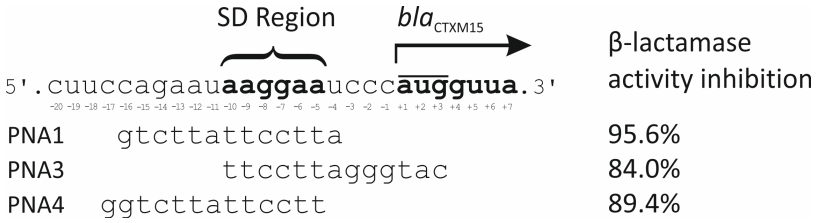


Figure 8-1. β-Lactamase activity inhibition by PNA1 (1000 nM), PNA3 (1000 nM) and PNA4 (1000 nM) in a cell-free translation/transcription coupled system.

It is possible that a refinement of the PNA target region design and size would yield greater inhibitory efficiency. Further PNA designs targeting the start codon and extending downstream would also be likely to yield greater specificity and reduce off-target hybridisation.

### 8.4.2. Potential complementary/additional genetic targets in addition to *bla*$_{\text{CTX-M}}$ for translational inhibition by antisense oligomers to increase sensitivity to CTX in resistant *E. coli* strains

Having demonstrated the β-lactam induced upregulation of β-lactamase, the potential exists to enhance and complement the effect of re-sensitising *E. coli* strains to CTX by inhibiting the expression of other related genes. The mechanism by which *bla*$_{\text{CTX-M}}$ is upregulated in the presence of 3$^{rd}$ generation cephalosporins is currently unclear, however, a similar mechanism to the previously described ampicillin peptide dependent repressor release system may be a potential candidate for investigation [181]. The gene for a muro-peptide permease (*ampG*) or, potentially, the regulatory gene *ampR* [182] may thus be an attractive potential target for additional inhibition by antisense oligomers, which could potentially complement and enhance the effects of *bla*$_{\text{CTX-M}}$ inhibition.

β-Lactam antibiotics, inhibiting the formation of cross-links between components of the peptidoglycan layer, and thus inhibiting the formation of the cell wall, have a bactericidal effect on dividing cells only. In the presence of a β-lactam antibiotic, upon detection of an inhibition of cell wall synthesis, the SOS response is induced [187, 188], extending the static non-dividing phase and arresting the growth phase of the cell cycle as part of its defensive mechanism. An antisense inhibition strategy targeting genes responsible for the detection of cell-wall damage, such as muropeptide transporters for

example, co-administered with a β-lactamase antisense inhibition agent could potentially greatly increase the effect of a β-lactamase inhibitor/β-lactam antibiotic combination.

A receptor identified as directly recognising β-lactam antibiotics and inducing the expression of β-lactamase in *Vibrio parahaemolyticus* [184] may suggest the possibility of a related receptor in other species, which could also prove an attractive target for expression inhibition with a goal of restoring antibiotic sensitivity.

### 8.4.3. Further development of self-assembling DNA based delivery vehicles for synthetic antisense agents

Initial studies with a DNA tetrahedron as a carrier for antisense agents were successful in increasing sensitivity of field isolates to CTX in field isolates, and there is potential for further development. As previously noted, *E. coli* cell permeabilisation has been shown to be reduced in the presence of $MgCl_2$ [158], which is a component of the tetrahedron annealing buffer (50 mM). An alternative annealing buffer or a tetrahedron purification step may yield higher cell penetration efficacy.

The tetrahedron observed to be most efficacious in increasing CTX sensitivity in field isolate LREC461, was the 13-mer PNA-carrying 108 bp tetrahedron SPNAP. This tetrahedron could potentially incorporate an additional PNA into its design whilst still maintaining structural integrity and rigidity (Figure 8-2). This structure could incorporate either two PNAs of the same design to increase its overall PNA concentration, or two different PNAs with separate targets. In the case of restoring β-lactam sensitivity, for example, this tetrahedron design could incorporate one PNA to target and inhibit the expression of β-lactamase and another to inhibit the expression of a muro-peptide transporter. This approach could potentially result in a single therapeutic

agent with dual complementary targets to achieve an enhanced effect on the inhibition of the expression of β-lactamase.

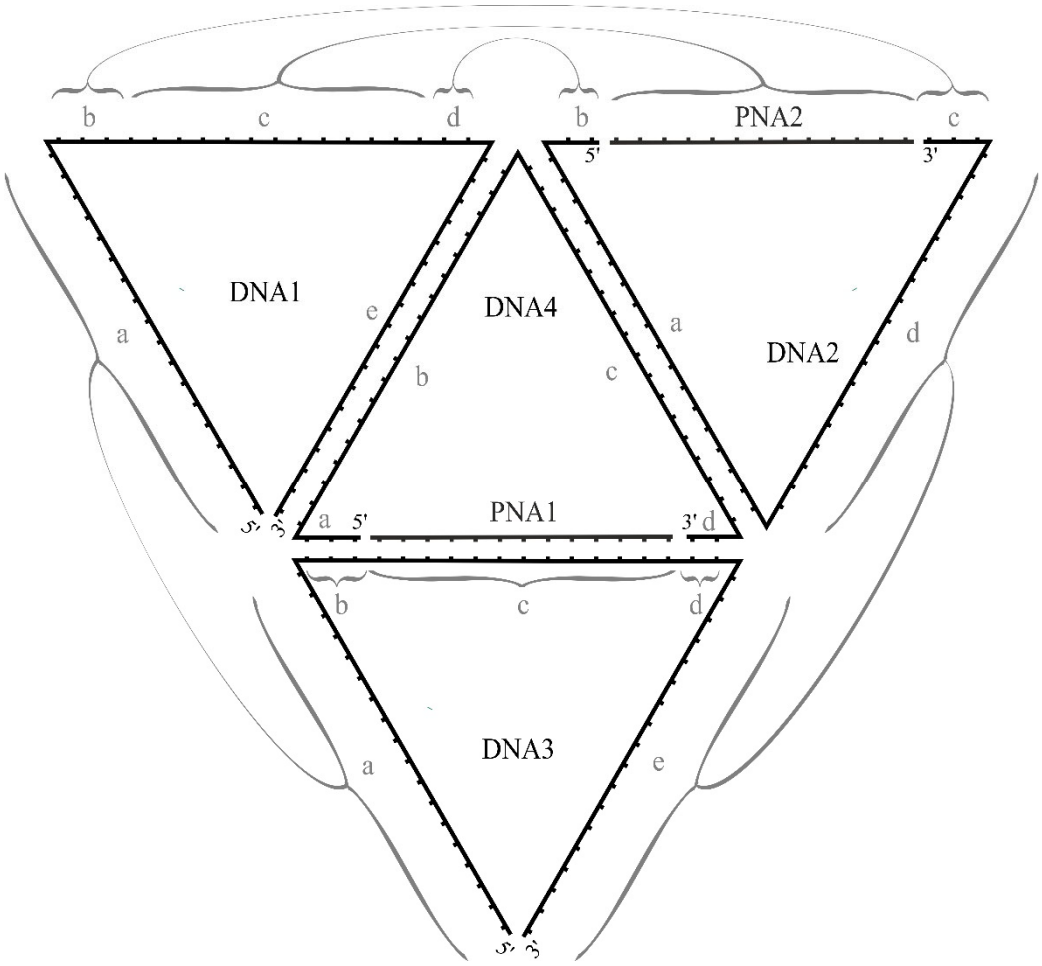


Figure 8-2. Illustrative structural design diagram of DNA tetrahedron to carry two 13-mer PNA antisense oligomers.

Proposed design of tetrahedron incorporating two PNA oligomers to target two genes/transcripts simultaneously. Complementary base-pairing regions are shown in grey (refer to Table 8-1). Tick marks represent approximate positions of individual DNA/PNA bases.

Table 8-1. Regions of complementarity between regions of proposed 2-PNA DNA tetrahedron before self-assembly.
This table provides a key to the regions of complementarity shown in Figure 8-2.

| | | Regions of complementarity | | | | |
|---|---|---|---|---|---|---|
| | | **DNA2** | **DNA3** | **DNA4** | **PNA1** | **PNA2** |
| **DNA1** | **a** | | a | | | |
| | **b** | c | | | | |
| | **c** | | | | | All |
| | **d** | b | | | | |
| | **e** | | | b | | |
| **DNA2** | **a** | | | c | | |
| | **d** | | e | | | |
| **DNA3** | **b** | | | a | | |
| | **c** | | | | All | |
| | **d** | | | d | | |

Further optimisation of the tetrahedral antisense oligomer vehicle could include studies into relative penetration efficiencies of varying sizes and shapes. The current study constructed two size variations of an equilateral tetrahedron. Further investigation would be required to ascertain the optimum size and shape for maximum penetration efficiency.

The penetration mechanism of the tetrahedron is currently unclear, and it is not yet known if it is discriminatory, again, further studies are required to elucidate this. Initial studies with mammalian cells suggested that a 108 bp PMO-carrying tetrahedron was unable to cross the cell membrane. This may suggest bacterial discriminatory potential, and could implicate a specific bacterial receptor-mediated uptake mechanism. Further studies are required.

## 8.5. Conclusions

The current study designed and developed synthetic antisense oligomers to inhibit the expression of β-lactamase and restore sensitivity in *E. coli* strains with a phenotype of reduced-susceptibility. Sensitivity was increased in field and clinical isolates, and these are the first studies to show a re-sensitisation to third generation cephalosporins of these strains.

The data obtained from inhibition studies of *bla*$_{\text{CTX-M}}$ in field isolates, and the potential for further optimisation and enhancement, demonstrated the potential for therapeutic use of P-PMOs and P-PNAs in re-sensitising resistant bacteria to CTX.

The development of a tetrahedral nucleic acid nanoparticle vector for the delivery of PNAs and PMOs further increases the potential of antisense biotechnology for diagnostic, research and therapeutic applications.

## References


1. Javaux, E.J., Marshall, C.P., and Bekker, A., *Organic-walled microfossils in 3.2-billion-year-old shallow-marine siliciclastic deposits.* Nature, 2010. **463**(7283): p. 934-8.
2. Wacey, D., Kilburn, M.R., Saunders, M., Cliff, J., and Brasier, M.D., *Microfossils of sulphur-metabolizing cells in 3.4-billion-year-old rocks of Western Australia.* Nature Geoscience, 2011. **4**(10): p. 698-702.
3. Ackerman, J., *How Bacteria in Our Bodies Protect Our Health* in *Scientific American* 2012.
4. Sussman, M., *Escherichia coli: Mechanisms of Virulence*. 1997, University Press, Cambridge: Cambridge University Press.
5. Singleton, P., *Bacteria in Biology, Biotechnology and Medicine*. 5th ed. 1999: Wiley.
6. Lukjancenko, O., Wassenaar, T.M., and Ussery, D.W., *Comparison of 61 sequenced Escherichia coli genomes.* Microb Ecol, 2010. **60**(4): p. 708-20.
7. Reid, G., Howard, J., and Gan, B.S., *Can bacterial interference prevent infection?* Trends in Microbiology. **9**(9): p. 424-428.
8. Vashakidze, E., Megrelishvili, T., Pachkoria, E., Tevzadze, L., and Lashkarashvili, M., *Enterohemorrhagic E. coli and hemolytic uremic syndrome in Georgia.* Georgian Med News, 2010(186): p. 38-41.
9. Kumar, P. and Libchaber, A., *Pressure and temperature dependence of growth and morphology of Escherichia coli: experiments and stochastic model.* Biophys J, 2013. **105**(3): p. 783-93.

10. Bassett, E., Keith, M., Armelagos, G., Martin, D., and Villanueva, A., *Tetracycline-labeled human bone from ancient Sudanese Nubia (A.D. 350).* Science, 1980. **209**(4464): p. 1532-1534.

11. Cook, M., Molto, E., and Anderson, C., *Fluorochrome labelling in Roman period skeletons from Dakhleh Oasis, Egypt.* Am J Phys Anthropol, 1989. **80**(2): p. 137-43.

12. Domagk, G.J., *Ein Beitrag zur Chemotherapie der bakteriellen infektionen.* Dtsch. med. Wochenschr, 1935. **61**: p. 250 - 253.

13. Aminov, R.I., *A brief history of the antibiotic era: lessons learned and challenges for the future.* Front Microbiol, 2010. **1**: p. 134.

14. Fleming, A., *On the Antibacterial Action of Cultures of a Penicillium, with Special Reference to their Use in the Isolation of B. influenzæ.* British journal of experimental pathology, 1929. **10**(3): p. 226-236.

15. Burdon-Sanderson, J., *Appendix No. 5—Further report of researches concerning the intimate pathology of contagion. The origin and distribution of microzymes (bacteria) in water, and the circumstances which determine their existence in the tissue and liquids of the living body.* 13th Report of the Medical Officer of the Privy Council [John Simon], with Appendix, 1870 (Her Majesty's Stationery Office, London), 1871: p. 10.

16. Bucci, R. and Gallì, P., *Vincenzo Tiberio: a misunderstood researcher.* Italian Journal of Public Health, 2011. **8**(4): p. 3.

17. Gratia, J.-P., *André Gratia: a forerunner in microbial and viral genetics.* Genetics, 2000. **156**: p. 471-476.

18. Lewis, K., *Platforms for antibiotic discovery.* Nat Rev Drug Discov, 2013. **12**(5): p. 371-387.

19. Butler, M.S., Blaskovich, M.A., and Cooper, M.A., *Antibiotics in the clinical pipeline in 2013.* J Antibiot, 2013. **66**(10): p. 571-591.

20. Ling, L.L., Schneider, T., Peoples, A.J., Spoering, A.L., Engels, I., Conlon, B.P., Mueller, A., Schaberle, T.F., Hughes, D.E., Epstein, S., Jones, M., Lazarides, L., Steadman, V.A., Cohen, D.R., Felix, C.R., Fetterman, K.A., Millett, W.P., Nitti, A.G., Zullo, A.M., Chen, C., and Lewis, K., *A new antibiotic kills pathogens without detectable resistance.* Nature, 2015. **517**(7535): p. 455-9.

21. Elander, R.P., *Industrial production of beta-lactam antibiotics.* Appl Microbiol Biotechnol, 2003. **61**(5-6): p. 385-92.

22. McGeary, R. *Medicinal Chemistry*. 2008 [cited 2014 30/06/14]; Available from: http://www.scmb.uq.edu.au/academicstaff/mcgeary/medicinal_chemistry.htm.

23. Pascual, A., Perez, M.H., Jaton, K., Hafen, G., Di Bernardo, S., Cotting, J., Greub, G., and Vaudaux, B., *Mycoplasma hominis necrotizing pleuropneumonia in a previously healthy adolescent.* BMC Infect Dis, 2010. **10**: p. 335.

24. Vollmer, W. and Holtje, J.V., *The Architecture of the Murein (Peptidoglycan) in Gram-Negative Bacteria: Vertical Scaffold or Horizontal Layer(s)?* J Bacteriol, 2004. **186**(18): p. 5978-87.

25. Rawat, D. and Nair, D., *Extended-spectrum β-lactamases in Gram Negative Bacteria.* J Glob Infect Dis. , 2010. **2**(3): p. 263 - 274.

26. Demain, A.L. and Elander, R.P., *The β-lactam antibiotics: past, present, and future.* Antonie van Leeuwenhoek, 1998. **75**(1-2): p. 5-19.

27. Crawford, K., Heatley, N.G., Boyd, P.F., Hale, C.W., Kelly, B.K., Miller, G.A., and Smith, N., *Antibiotic Production by a Species of Cephalosporium.* Journal of General Microbiology, 1952. **6**(1 & 2): p. 47-59.

28. Marino, P.L., *ICU Book, The, 3rd Edition*. 2007: Lippincott Williams & Wilkins.

29. Chan, M. *Antimicrobial resistance in the European Union and the world*. in *Combating antimicrobial resistance: time for action*. 2012. Copenhagen, Denmark.

30. HM Government, *Review on Antimicrobial Resistance. Antimicrobial Resistance: Tackling a Crisis for the Health and Wealth of Nations*. 2014.

31. CDC, *Antibiotic Resistance Threats in the United States*. 2013, Centres for Disease Control and Prevention.

32. Hodgekiss, A., *Antibiotic resistance is now as serious a threat as terrorism and could trigger an 'apocalyptic scenario', warns UK's top doctor*, in *Mail Online*. 2013, Associated Newspapers Ltd: http://www.dailymail.co.uk/health/article-2267567/Antibiotic-resistance-terrorism-trigger-apocalyptic-scenario-warns-UKs-doctor.html.

33. Hopkins, J.M. and Towner, K.J., *Enhanced resistance to cefotaxime and imipenem associated with outer membrane protein alterations in Enterobacter aerogenes.* Journal of Antimicrobial Chemotherapy. **25**: p. 49-55.

34. ESCMID, *Antibiotic Armageddon in UK and Europe by 2025*. 2015. p. 1-3.

35. Liu, Y.-Y., Wang, Y., Walsh, T.R., Yi, L.-X., Zhang, R., Spencer, J., Doi, Y., Tian, G., Dong, B., Huang, X., Yu, L.-F., Gu, D., Ren, H., Chen, X., Lv, L., He, D., Zhou, H., Liang, Z., Liu, J.-H., and Shen, J., *Emergence of plasmid-mediated colistin resistance mechanism MCR-1 in animals and human beings in China: a microbiological and molecular biological study.* The Lancet Infectious Diseases, 2015.

36. Gallagher, J., *Bacteria that resist 'last antibiotic' found in UK*, in *BBC*. 2015.

37. Smith, R. and Coast, J., *The true cost of antimicrobial resistance.* BMJ, 2013. **346**: p. f1493.

38. Centers for Disease Control and Prevention, *World Health Day: Media Fact Sheet*. 2011.

39. Taylor, J., Hafner, M., Yerushalmi, E., Smith, R., Bellasio, J., Vardavas, R., Bienkowska-Gibbs, T., and Rubin, J., *Estimating the economic costs of antimicrobial resistance: Model and Results*. 2014, RAND Corporation: Santa Monica, CA.

40. Walsh, F. *BBC News - Antibiotic resistance: Cameron warns of medical 'dark ages'*. 2014; Available from: http://www.bbc.co.uk/news/health-28098838.

41. Bonnet, R., *Growing Group of Extended-Spectrum β-Lactamases: the CTX-M Enzymes.* Antimicrobial Agents and Chemotherapy, 2003. **48**(1): p. 1-14.

42. Yezli, S. and Li, H., *Antibiotic resistance amongst healthcare-associated pathogens in China.* Int J Antimicrob Agents, 2012. **40**(5): p. 389-397.

43. Yang, Y.H., Fu, S.G., Peng, H., Shen, A.D., Yue, S.J., and Go, Y.F., *Abuse of antibiotics in China and its potential interference in determining the etiology of pediatric bacterial diseases.* Pediatr Infect Dis J, 1993. **12**: p. 986-989.

44. Bate, R., *Antimicrobial resistance: How substandard medicines contribute.* AEI Economic Perspectives, 2015(4).

45. *Regulation (EC) No 1831/2003 of the European Parliament and of the Council of 22 September 2003 on additives for use in animal nutrition (Text with EEA relevance)* Official Journal L 268, 2003. **46**: p. 0029 - 0043.

46. Livermore, D.M., *Current epidemiology and growing resistance of gram-negative pathogens.* Korean J Intern Med, 2012. **27**(2): p. 128-42.

47. Davies, J., *Inactivation of Antibiotics and the Dissemination of Resistance Genes.* Science, 1994. **264**: p. 375-382.

48. Woodford, N. and Wareham, D.W., *Tackling antibiotic resistance: a dose of common antisense?* J Antimicrob Chemother, 2009. **63**(2): p. 225-229.

49. Poole, K., *Mechanisms of bacterial biocide and antibiotic resistance.* J Appl Microbiol, 2002. **92 Suppl**: p. 55s-64s.

50. Dever, L.A. and Dermody, T.S., *Mechanisms of bacterial resistance to antibiotics.* Arch Intern Med, 1991. **151**(5): p. 886-95.

51. McDermott, P.F., Walker, R.D., and White, D.G., *Antimicrobials: modes of action and mechanisms of resistance.* Int J Toxicol, 2003. **22**(2): p. 135-43.

52. Poole, K., *Efflux-mediated antimicrobial resistance.* J Antimicrob Chemother, 2005. **56**(1): p. 20-51.

53. Blair, J.M., Webber, M.A., Baylay, A.J., Ogbolu, D.O., and Piddock, L.J., *Molecular mechanisms of antibiotic resistance.* Nat Rev Microbiol, 2015. **13**(1): p. 42-51.

54. Ramirez, M.S. and Tolmasky, M.E., *Aminoglycoside modifying enzymes.* Drug Resist Updat, 2010. **13**(6): p. 151-71.

55. Spratt, B.G., *Resistance to antibiotics mediated by target alterations.* Science, 1994. **264**(5157): p. 388-93.

56. Lambert, P.A., *Bacterial resistance to antibiotics: modified target sites.* Adv Drug Deliv Rev, 2005. **57**(10): p. 1471-85.

57. Telenti, A., Imboden, P., Marchesi, F., Schmidheini, T., and Bodmer, T., *Direct, automated detection of rifampin-resistant Mycobacterium tuberculosis by polymerase chain reaction and single-strand conformation polymorphism analysis.* Antimicrob Agents Chemother, 1993. **37**(10): p. 2054-8.

58. Honore, N. and Cole, S.T., *Molecular basis of rifampin resistance in Mycobacterium leprae.* Antimicrob Agents Chemother, 1993. **37**(3): p. 414-8.

59. McMurry, L., Petrucci, R.E., Jr., and Levy, S.B., *Active efflux of tetracycline encoded by four genetically different tetracycline resistance determinants in Escherichia coli.* Proc Natl Acad Sci U S A, 1980. **77**(7): p. 3974-7.

60. Nguyen Van, J.C. and Gutmann, L., *Resistance to antibiotics caused by decrease of the permeability in gram-negative bacteria.* Presse Med, 1994. **23**(11): p. 522, 527-31.

61. Delcour, A.H., *Outer Membrane Permeability and Antibiotic Resistance.* Biochimica et biophysica acta, 2009. **1794**(5): p. 808-816.

62. Charrel, R.N., Pagès, J.M., De Micco, P., and Mallea, M., *Prevalence of outer membrane porin alteration in beta-lactam-antibiotic-resistant Enterobacter aerogenes.* Antimicrobial Agents and Chemotherapy, 1996. **40**(12): p. 2854-2858.

63. Hawkey, P.M. and Jones, A.M., *The changing epidemiology of resistance.* J Antimicrob Chemother, 2009. **64 Suppl 1**: p. i3-10.

64. Abraham, E.P. and Chain, E., *An Enzyme from Bacteria able to Destroy Penicillin : Abstract : Nature.* Nature, 1940. **146**: p. 837-838.

65. Hall, B.G. and Barlow, M., *Evolution of the serine beta-lactamases: past, present and future.* Drug Resist Updat, 2004. **7**(2): p. 111-23.

66. Jacoby, G.A., *AmpC beta-lactamases.* Clin Microbiol Rev, 2009. **22**(1): p. 161-182.

67. Ambler, R.P., *The Structure of β-Lactamases.* Philosophical Transactions of the Royal Society B: Biological Sciences, 1980. **289**(1036): p. 321-331.

68. Hall, B.G. and Barlow, M., *Revised Ambler classification of {beta}-lactamases.* J Antimicrob Chemother, 2005. **55**(6): p. 1050-1051.

69. Bush, K., Jacoby, G.A., and Medeiros, A.A., *A functional classification scheme for β-lactamases and its correlation with molecular structure.* 1995. **36**(6): p. 1211-1233.

70. Bush, K. and Jacoby, G.A., *Updated functional classification of beta-lactamases.* Antimicrob Agents Chemother, 2010. **54**(3): p. 969-76.

71. Knothe, H., Shah, P., Krcmery, V., Antal, M., and Mitsuhashi, S., *Transferable resistance to cefotaxime, cefoxitin, cefamandole and cefuroxime in clinical isolates of Klebsiella pneumoniae and Serratia marcescens.* Infection, 1983. **11**: p. 315-7.

72. Rossolini, G.M., D'Andrea, M.M., and Mugnaioli, C., *The spread of CTX-M-type extended-spectrum β-lactamases.* Clin Microbiol Infect, 2008. **14**(1): p. 33-41.

73. Navarro, F. and Miro, E., *Update on CTX-M-type β-lactamases.* Reviews in Medical Microbiology, 2002. **13**: p. 63-73.

74. Woodford, N., Carattoli, A., Karisik, E., Underwood, A., Ellington, M.J., and Livermore, D.M., *Complete nucleotide sequences of plasmids pEK204, pEK499, and pEK516, encoding CTX-M enzymes in three major Escherichia coli lineages from the United Kingdom, all belonging to the international O25:H4-ST131 clone.* Antimicrob Agents Chemother, 2009. **53**(10): p. 4472-4482.

75. Karim, A., Poirel, L., Nagarajan, S., and Nordmann, P., *Plasmid-mediated extended-spectrum β-lactamase (CTX-M-3 like) from India and gene association with insertion sequence ISEcp1.* FEMS Microbiology Letters, 2001. **201**: p. 237-241.

76. Poirel, L., Decousser, J.W., and Nordmann, P., *Insertion Sequence ISEcp1 Is Involved in Expression and Mobilization of a bla$_{CTX-M}$ β-lactamase Gene.* Antimicrobial Agents and Chemotherapy, 2003. **47**(9): p. 2938-2945.

77. Conceicao, T., Brizio, A., Duarte, A., Lito, L.M., Cristino, J.M., and Salgado, M.J., *First description of CTX-M-15-producing Klebsiella pneumoniae in Portugal.* Antimicrob Agents Chemother, 2005. **49**(1): p. 477-8.

78. Eckert, C., Gautier, V., and Arlet, G., *DNA sequence analysis of the genetic environment of various blaCTX-M genes.* J Antimicrob Chemother, 2006. **57**(1): p. 14-23.

79. Hirai, I., Fukui, N., Taguchi, M., Yamauchi, K., Nakamura, T., Okano, S., and Yamamoto, Y., *Detection of chromosomal blaCTX-M-15 in Escherichia coli O25b-B2-ST131 isolates from the Kinki region of Japan.* International Journal of Antimicrobial Agents. **42**(6): p. 500-506.

80. Lartigue, M.F., Poirel, L., and Nordmann, P., *Diversity of genetic environment of bla(CTX-M) genes.* FEMS Microbiol Lett, 2004. **234**(2): p. 201-7.

81. Dhanji, H., Patel, R., Wall, R., Doumith, M., Patel, B., Hope, R., Livermore, D.M., and Woodford, N., *Variation in the genetic environments of bla(CTX-M-15) in Escherichia coli from the faeces of travellers returning to the United Kingdom.* J Antimicrob Chemother, 2011. **66**(5): p. 1005-12.

82. Kamruzzaman, M., Patterson, J.D., Shoma, S., Ginn, A.N., Partridge, S.R., and Iredell, J.R., *Relative Strengths of Promoters Provided by Common Mobile Genetic Elements Associated with Resistance Gene Expression in Gram-Negative Bacteria.* Antimicrob Agents Chemother, 2015. **59**(8): p. 5088-91.

83. Bonnet, R., Sampaio, J.L.M., Labia, R., Champs, C.D., Sirot, D., Chanal, C., and Sirot, J., *A Novel CTX-M β-lactamase (CTX-M-8) in Cefotaxime-Resistant*

*Enterobacteriaceace Isolated in Brazil.* Antimicrobial Agents And Chemotherapy, 2000. **44**(7): p. 1936-1942.

84. Williams, J.D., *Beta-lactamases and beta-lactamase inhibitors.* Int J Antimicrob Agents, 1999. **12 Suppl 1**: p. S3-7; discussion S26-7.

85. Zhanel, G., Lawson, C., Adam, H., Schweizer, F., Zelenitsky, S., Lagacé-Wiens, P.S., Denisuik, A., Rubinstein, E., Gin, A., Hoban, D., Lynch, J., 3rd, and Karlowsky, J., *Ceftazidime-Avibactam: a Novel Cephalosporin/β-lactamase Inhibitor Combination.* Drugs, 2013. **73**(2): p. 159-177.

86. Zhang, J., Chen, Y.P., Miller, K.P., Ganewatta, M.S., Bam, M., Yan, Y., Nagarkatti, M., Decho, A.W., and Tang, C., *Antimicrobial metallopolymers and their bioconjugates with conventional antibiotics against multidrug-resistant bacteria.* J Am Chem Soc, 2014. **136**(13): p. 4873-6.

87. Ahmed F. Abdel-Magid, *Combatting resistant bacteria with the help of Beta-lactamase inhibitors.* ACS Med Chem Lett, 2014. **5**(1): p. 6-7.

88. Kenilworth, N.J., *Results of Phase 2 Study of Merck's Investigational Beta-Lactamase Inhibitor Relebactam Presented at ICAAC/ICC 2015*. 2015: Business Wire.

89. Reading, C. and Cole, M., *Clavulanic Acid: a Beta-Lactamase-Inhibiting Beta-Lactam from Streptomyces clavuligerus.* Antimicrob. Agents Chemother. , 1977. **11**(5): p. 852-857.

90. Neu, H.C. and Fu, K.P., *Clavulanic Acid, a Novel Inhibitor of β-Lactamases.* Antimicrobial Agents and Chemotherapy, 1978. **14**(5): p. 650-655.

91. Drawz, S.M. and Bonomo, R.A., *Three decades of beta-lactamase inhibitors.* Clin Microbiol Rev, 2010. **23**(1): p. 160-201.

92. Brown, A.G., *Clavulanic acid, a novel β-lactamase inhibitor: a case-study in drug discovery and development.* Drug design and delivery 1986. **1**(1): p. 1-21.

93. Salvo, F., Polimeni, G., Moretti, U., Conforti, A., Leone, R., Leoni, O., Motola, D., Dusi, G., and Caputi, A.P., *Adverse drug reactions related to amoxicillin alone and in association with clavulanic acid: data from spontaneous reporting in Italy.* J Antimicrob Chemother, 2007. **60**(1): p. 121-6.

94. Brumfitt, W., Hamilton-Miller, J.M.T., Dixson, S., Gargan, R.A., and Gooding, A., *Phenomenon of resistance to Augmentin associated with sensitivity to ampicillin: occurrence and explanation.* J Clin Pathol, 1983. **36**: p. 4.

95. Williams, J.D., *Beta-Lactamase inhibition and in vitro activity of sulbactam and sulbactam/cefoperazone.* Clin Infect Dis, 1997. **24**(3): p. 494-7.

96. Aronoff, S.C., Jacobs, M.R., Johenning, S., and Yamabe, S., *Comparative activities of the beta-lactamase inhibitors YTR 830, sodium clavulanate, and sulbactam combined with amoxicillin or ampicillin.* Antimicrobial Agents and Chemotherapy, 1984. **26**(4): p. 580-582.

97. Singh, J., Petter, R.C., Baillie, T.A., and Whitty, A., *The resurgence of covalent drugs.* Nat Rev Drug Discov, 2011. **10**(4): p. 307-17.

98. Kalp, M., Totir, M.A., Buynak, J.D., and Carey, P.R., *Different intermediate populations formed by tazobactam, sulbactam, and clavulanate reacting with SHV-1 beta-lactamases: Raman crystallographic evidence.* J Am Chem Soc, 2009. **131**(6): p. 2338-47.

99. Yang, Y., Rasmussen, B.A., and Shlaes, D.M., *Class A beta-lactamases--enzyme-inhibitor interactions and resistance.* Pharmacol Ther, 1999. **83**(2): p. 141-51.

100. Vedel, G., Belaaouaj, A., Gilly, L., Labia, R., Philippon, A., Nevot, P., and Paul, G., *Clinical isolates of Escherichia coli producing TRI beta-lactamases: novel TEM-enzymes conferring resistance to beta-lactamase inhibitors.* J Antimicrob Chemother, 1992. **30**(4): p. 449-62.

101. Speldooren, V., Heym, B., Labia, R., and Nicolas-Chanoine, M.H., *Discriminatory detection of inhibitor-resistant beta-lactamases in Escherichia coli by single-strand conformation polymorphism-PCR.* Antimicrob Agents Chemother, 1998. **42**(4): p. 879-84.

102. Lemozy, J., Sirot, D., Chanal, C., Huc, C., Labia, R., Dabernat, H., and Sirot, J., *First characterization of inhibitor-resistant TEM (IRT) beta-lactamases in Klebsiella pneumoniae strains.* Antimicrob Agents Chemother, 1995. **39**(11): p. 2580-2.

103. Cundiff, J. and Joe, S., *Amoxicillin-clavulanic acid–induced hepatitis.* American Journal of Otolaryngology, 2007. **28**(1): p. 28-30.

104. Ersoz, G., Karasu, Z., Yildiz, C., Akarca, U.S., Yuce, G., and Batur, Y., *Severe toxic hepatitis associated with amoxycillin and clavulanic acid.* J Clin Pharm Ther, 2001. **26**(3): p. 225-9.

105. South Dakota State University. *Pharmacists' study helps prevent antibiotic-induced kidney failure*. 2015 [cited 2015 30/10]; Available from: http://www.sdstate.edu/news/articles/pharmacy-study-helps-prevent-antibiotic-induced-kidney-failure.cfm.

106. Stephenson, M.L. and Zamecnik, P.C., *Inhibition of Rous sarcoma viral RNA translation by a specific oligodeoxyribonucleotide.* Proceedings of the National Academy of Sciences of the United States of America, 1978. **75**(1): p. 285-288.

107. Pestka, S., *Antisense RNA. History and perspective.* Ann N Y Acad Sci, 1992. **660**: p. 251-62.

108. Zamecnik, P.C., *History of Antisense Oligonucleotides*, in *Antisense Therapeutics*, S. Agrawal, Editor. 1996, Humana Press: Totowa, NJ. p. 1-11.

109. Good, L., *Translation repression by antisense sequences.* Cell Mol Life Sci, 2003. **60**(5): p. 854-61.

110. Gottesman, S., McCullen, C.A., Guillier, M., Vanderpool, C.K., Majdalani, N., Benhammou, J., Thompson, K.M., FitzGerald, P.C., Sowa, N.A., and FitzGerald, D.J., *Small RNA regulators and the bacterial response to stress.* Cold Spring Harb Symp Quant Biol, 2006. **71**: p. 1-11.

111. Gottesman, S. and Storz, G., *Bacterial small RNA regulators: versatile roles and rapidly evolving variations.* Cold Spring Harb Perspect Biol, 2011. **3**(12).

112. Coleman, J., Green, P.J., and lnouye, M., *The Use of RNAs Complementary to Specific mRNAs to Regulate the Expression of Individual Bacterial Genes.* Cell, 1984. **37**(2): p. 8.

113. K.H. Altmann, D. Fabbrot, N. M. Dean, T. Geigert, P. Mania, M. Mullert, and P. Nickling, *Second-generation antisense oligonucleotides: structure-activity relationships and the design of improved signal-transduction inhibitors* Biochemical Society Transactions, 1996. **24**: p. 630-637.

114. Dias, N. and Stein, C.A., *Antisense Oligonucleotides: Basic Concepts and Mechanisms.* American Association for Cancer Research, 2002. **1**(5): p. 347-355.

115. Nielsen, P.E., Egholm, M., Berg, R.H., and Buchardt, O., *Sequence-selective recognition of DNA by strand displacement with a thymine-substituted polyamide.* Science, 1991. **254**(5037): p. 1497-500.

116. Watson, J.D. and Crick, F.H.C., *Molecular Structure of Nucleic Acids: A Structure for Deoxyribose Nucleic Acid.* Nature, 1953. **171**(4356): p. 737-738.

117. Armitage, B.A., *The impact of nucleic acid secondary structure on PNA hybridization.* Drug Discovery Today, 2003. **8**(5): p. 222-228.

118. Lecosnier, S., Cordier, C., Simon, P., Francois, J.C., and Saison-Behmoaras, T.E., *A steric blocker of translation elongation inhibits IGF-1R expression and cell transformation.* FASEB J, 2011. **25**(7): p. 2201-10.

119. Good, L., Sandberg, R., Larsson, O., Nielsen, P.E., and Wahlestedt, C., *Antisense PNA effects in Escherichia coli are limited by the outer-membrane LPS layer.* Microbiology, 2000. **146**: p. 2556-2561.

120. Ghosal, A. and Nielsen, P.E., *Potent antibacterial antisense peptide-peptide nucleic acid conjugates against Pseudomonas aeruginosa.* Nucleic Acid Ther, 2012. **22**(5): p. 323-34.

121. Good, L., Awasthi, S.K., Dryselius, R., Larsson, O., and Nielsen, P.E., *Bactericidal antisense effects of peptide–PNA conjugates.* nature biotechnology, 2001. **19**: p. 7.

122. Good, L. and Nielsen, P.E., *Inhibition of translation and bacterial growth by peptide nucleic acid targeted to ribosomal RNA.* Proceedings of the National Academy of Sciences, 1998. **95**: p. 4.

123. Kurupati, P., Tan, K.S., Kumarasinghe, G., and Poh, C.L., *Inhibition of gene expression and growth by antisense peptide nucleic acids in a multiresistant beta-lactamase-producing Klebsiella pneumoniae strain.* Antimicrob Agents Chemother, 2007. **51**(3): p. 805-11.

124. Nekhotiaeva, N., Awasthi, S.K., Nielsen, P.E., and Good, L., *Inhibition of Staphylococcus aureus gene expression and growth using antisense peptide nucleic acids.* Mol Ther, 2004. **10**(4): p. 652-659.

125. Soofi, M.A. and Seleem, M.N., *Targeting essential genes in Salmonella enterica serovar typhimurium with antisense peptide nucleic acid.* Antimicrob Agents Chemother, 2012. **56**(12): p. 6407-9.

126. Geller, B.L., Deere, J.D., Stein, D.A., Kroeker, A.D., Moulton, H.M., and Iversen, P.L., *Inhibition of Gene Expression in Escherichia coli by Antisense Phosphorodiamidate Morpholino Oligomers.* Antimicrobial Agents and Chemotherapy, 2003. **47**(10): p. 3233-3239.

127. Geller, B.L., Deere, J., Tilley, L., and Iversen, P.L., *Antisense phosphorodiamidate morpholino oligomer inhibits viability of Escherichia coli in pure culture and in mouse peritonitis.* J Antimicrob Chemother, 2005. **55**(6): p. 983-8.

128. Mitev, G.M., Mellbye, B.L., Iversen, P.L., and Geller, B.L., *Inhibition of intracellular growth of Salmonella enterica serovar Typhimurium in tissue culture by antisense peptide-phosphorodiamidate morpholino oligomer.* Antimicrob Agents Chemother, 2009. **53**(9): p. 3700-4.

129. Panchal, R.G., Geller, B.L., Mellbye, B., Lane, D., Iversen, P.L., and Bavari, S., *Peptide Conjugated Phosphorodiamidate Morpholino Oligomers Increase Survival of Mice Challenged with Ames Bacillus anthracis.* Nucleic Acid Therapeutics, 2012. **22**(5): p. 305-311.

130. Geller, B.L., Marshall-Batty, K., Schnell, F.J., McKnight, M.M., Iversen, P.L., and Greenberg, D.E., *Gene-Silencing Antisense Oligomers Inhibit Acinetobacter*

*Growth In Vitro and In Vivo.* Journal of Infectious Diseases, 2013. **208**(10): p. 1553-1560.

131. Greenberg, D.E., Marshall-Batty, K.R., Brinster, L.R., Zarember, K.A., Shaw, P.A., Mellbye, B.L., Iversen, P.L., Holland, S.M., and Geller, B.L., *Antisense phosphorodiamidate morpholino oligomers targeted to an essential gene inhibit Burkholderia cepacia complex.* J Infect Dis, 2010. **201**(12): p. 1822-30.

132. Starmer, J., Stomp, A., Vouk, M., and Bitzer, D., *Predicting Shine–Dalgarno Sequence Locations Exposes Genome Annotation Errors.* PLoS Computational Biology. **2**(5): p. 13.

133. Dryselius, R., Aswasti, S.K., Rajarao, G.K., Nielsen, P.E., and Good, L., *The Translation Start Codon Region Is Sensitive to Antisense PNA Inhibition in Escherichia coli.* Oligonucleotides, 2003. **13**: p. 427-433.

134. Deere, J., Iversen, P., and Geller, B.L., *Antisense phosphorodiamidate morpholino oligomer length and target position effects on gene-specific inhibition in Escherichia coli.* Antimicrob Agents Chemother, 2005. **49**(1): p. 249-55.

135. Dryselius, R., Nekhotiaeva, N., and Good, L., *Antimicrobial synergy between mRNA- and protein-level inhibitors.* J Antimicrob Chemother, 2005. **56**(1): p. 97-103.

136. Good, L. and Nielsen, P.E., *Antisense inhibition of gene expression in bacteria by PNA targeted to mRNA.* Nature Biotechnology, 1998. **16**: p. 4.

137. Jeon, B. and Zhang, Q., *Sensitization of Campylobacter jejuni to fluoroquinolone and macrolide antibiotics by antisense inhibition of the CmeABC multidrug efflux transporter.* J Antimicrob Chemother, 2009. **63**(5): p. 946-8.

138. Wang, H., Meng, J., Jia, M., Ma, X., He, G., Yu, J., Wang, R., Bai, H., Hou, Z., and Luo, X., *oprM as a new target for reversion of multidrug resistance in Pseudomonas aeruginosa by antisense phosphorothioate oligodeoxynucleotides.* FEMS Immunol Med Microbiol, 2010. **60**(3): p. 275-82.

139. Goh, S., Loeffler, A., Lloyd, D.H., Nair, S.P., and Good, L., *Oxacillin sensitization of methicillin-resistant Staphylococcus aureus and methicillin-resistant Staphylococcus pseudintermedius by antisense peptide nucleic acids in vitro.* BMC Microbiol, 2015. **15**(1): p. 262.

140. Walker, J.R. and Altman, E., *Biotinylation facilitates the uptake of large peptides by Escherichia coli and other gram-negative bacteria.* Appl Environ Microbiol, 2005. **71**(4): p. 1850-5.

141. Shiraishi, T. and Nielsen, P.E., *Peptide nucleic acid (PNA) cell penetrating peptide (CPP) conjugates as carriers for cellular delivery of antisense oligomers.* Artificial DNA: PNA & XNA, 2011. **2**(3): p. 90-99.

142. Shiraishi, T. and Nielsen, P.E., *Improved cellular uptake of antisense peptide nucleic acids by conjugation to a cell-penetrating peptide and a lipid domain.* Methods Mol Biol, 2011. **751**: p. 209-21.

143. Puckett, S.E., Reese, K.A., Mitev, G.M., Mullen, V., Johnson, R.C., Pomraning, K.R., Mellbye, B.L., Tilley, L.D., Iversen, P.L., Freitag, M., and Geller, B.L., *Bacterial resistance to antisense peptide phosphorodiamidate morpholino oligomers.* Antimicrob Agents Chemother, 2012. **56**(12): p. 6147-53.

144. Herce, H.D. and Garcia, A.E., *Cell penetrating peptides: how do they do it?* J Biol Phys, 2007. **33**(5-6): p. 345-56.

145. Vives, E., *Present and future of cell-penetrating peptide mediated delivery systems: "is the Trojan horse too wild to go only to Troy?".* J Control Release, 2005. **109**(1-3): p. 77-85.

146. Richard, J.P., Melikov, K., Vives, E., Ramos, C., Verbeure, B., Gait, M.J., Chernomordik, L.V., and Lebleu, B., *Cell-penetrating peptides. A reevaluation of the mechanism of cellular uptake.* J Biol Chem, 2003. **278**(1): p. 585-90.

147. Vaara, M. and Porro, M., *Group of peptides that act synergistically with hydrophobic antibiotics against gram-negative enteric bacteria.* Antimicrobial agents and chemotherapy, 1996. **40**: p. 5.

148. Vaara, M., *Agents that increase the permeability of the outer membrane.* Microbiological reviews, 1992. **56**: p. 7.

149. Henriques, S.T., Melo, M.N., and Castanho, M.A., *Cell-penetrating peptides and antimicrobial peptides: how different are they?* Biochem J, 2006. **399**(1): p. 1-7.

150. Reddy, K.V., Yedery, R.D., and Aranha, C., *Antimicrobial peptides: premises and promises.* Int J Antimicrob Agents, 2004. **24**(6): p. 536-47.

151. Hultmark, D., *Drosophila immunity: paths and patterns.* Current Opinion in Immunology, 2003. **15**(1): p. 12-19.

152. Christensen, B., Fink, J., Merrifield, R.B., and Mauzerall, D., *Channel-forming properties of cecropins and related model compounds incorporated into planar lipid membranes.* Proc. Natl. Acad. Sci., 1988. **85**: p. 5072-5076.

153. Takeuchi, K., Takahashi, H., Sugai, M., Iwai, H., Kohno, T., Sekimizu, K., Natori, S., and Shimada, I., *Channel-forming membrane permeabilization by an antibacterial protein, sapecin: determination of membrane-buried and oligomerization surfaces by NMR.* J Biol Chem, 2004. **279**(6): p. 4981-7.

154. Salomon, R.A. and Farias, R.N., *The peptide antibiotic microcin 25 is imported through the TonB pathway and the SbmA protein.* J Bacteriol, 1995. **177**(11): p. 3323-5.

155. Runti, G., Lopez Ruiz Mdel, C., Stoilova, T., Hussain, R., Jennions, M., Choudhury, H.G., Benincasa, M., Gennaro, R., Beis, K., and Scocchi, M., *Functional characterization of SbmA, a bacterial inner membrane transporter required for importing the antimicrobial peptide Bac7(1-35).* J Bacteriol, 2013. **195**(23): p. 5343-51.

156. Mattiuzzo, M., Bandiera, A., Gennaro, R., Benincasa, M., Pacor, S., Antcheva, N., and Scocchi, M., *Role of the Escherichia coli SbmA in the antimicrobial activity of proline-rich peptides.* Mol Microbiol, 2007. **66**(1): p. 151-63.

157. Ghosal, A., Vitali, A., Stach, J.E.M., and Nielsen, P.E., *Role of SbmA in the Uptake of Peptide Nucleic Acid (PNA)-Peptide Conjugates in E. coli.* ACS Chemical Biology, 2013. **8**(2): p. 360-367.

158. Eriksson, M., Nielsen, P.E., and Good, L., *Cell permeabilization and uptake of antisense peptide-peptide nucleic acid (PNA) into Escherichia coli.* J Biol Chem, 2002. **277**(9): p. 7144-7.

159. Canton, R., Gonzalez-Alba, J.M., and Galan, J.C., *CTX-M Enzymes: Origin and Diffusion.* Front Microbiol, 2012. **3**: p. 110.

160. Dai, X., Xiang, S., Li, J., Gao, Q., and Yang, K., *Development of a colorimetric assay for rapid quantitative measurement of clavulanic acid in microbial samples.* Sci China Life Sci, 2012. **55**(2): p. 158-63.

161. Nemutlu, E., Kir, S., Katlan, D., and Beksac, M.S., *Simultaneous multiresponse optimization of an HPLC method to separate seven cephalosporins in plasma*

*and amniotic fluid: application to validation and quantification of cefepime, cefixime and cefoperazone.* Talanta, 2009. **80**(1): p. 117-26.

162. Bethesda Research Laboratories, *BRL pUC host: E. coli DH5αTM competent cells.* Bethesda Res Lab Focus., 1986. **8**: p. 9 - 12.

163. Sekiguchi, M. and Iida, S., *Mutants Of Escherichia Coli Permeable To Actinomycin.* Proceedings of the National Academy of Sciences of the United States of America 1967. **58**(6): p. 2315-2320.

164. Randall, L.P., Clouting, C., Horton, R.A., Coldham, N.G., Wu, G., Clifton-Hadley, F.A., Davies, R.H., and Teale, C.J., *Prevalence of Escherichia coli carrying extended-spectrum beta-lactamases (CTX-M and TEM-52) from broiler chickens and turkeys in Great Britain between 2006 and 2009.* J Antimicrob Chemother, 2011. **66**(1): p. 86-95.

165. Freire Martin, I., AbuOun, M., Reichel, R., La Ragione, R.M., and Woodward, M.J., *Sequence analysis of a CTX-M-1 IncI1 plasmid found in Salmonella 4,5,12:i:-, Escherichia coli and Klebsiella pneumoniae on a UK pig farm.* J Antimicrob Chemother, 2014. **69**(8): p. 2098-101.

166. Thermo Scientific Web Tools. *Multiple Primer Analyzer*. 2015 [cited 2015; Available from: https://www.lifetechnologies.com/uk/en/home/brands/thermo-scientific/molecular-biology/molecular-biology-learning-center/molecular-biology-resource-library/thermo-scientific-web-tools/multiple-primer-analyzer.html.

167. New England BioLabs. *NEBioCalculator™ v1.3.9*. 2015; Available from: http://nebiocalculator.neb.com/#!/ligation.

168. Pei, H., Lu, N., Wen, Y., Song, S., Liu, Y., Yan, H., and Fan, C., *A DNA nanostructure-based biomolecular probe carrier platform for electrochemical biosensing.* Adv Mater, 2010. **22**(42): p. 4754-8.

169. Konaté, K., Mavoungou, J.F., Lepengué, A.N., Aworet-Samseny, R.R., Hilou, A., Souza, A., Dicko, M.H., and M'Batchi, B., *Antibacterial activity against β-lactamase producing Methicillin and Ampicillin-resistants Staphylococcus aureus: fractional Inhibitory Concentration Index (FICI) determination.* Annals of Clinical Microbiology and Antimicrobials, 2012. **11**(18): p. 12.

170. Ghavami, A., Labbé, G., Brem, J., Goodfellow, V.J., Marrone, L., Tanner, C.A., King, D.T., Lam, M., Strynadka, N.C.J., Pillai, D.R., Siemann, S., Spencer, J., Schofield, C.J., and Dmitrienko, G.I., *Assay for drug discovery: Synthesis and testing of nitrocefin analogues for use as β-lactamase substrates.* Analytical Biochemistry, 2015. **486**: p. 75-77.

171. Castillo, M.C.d., Sesma, F., Nader, O.M.d., and Holgado, A.P.d.R., *Properties of β-lactamase from Neisseria gonorrhoeae.* Mem Inst Oswaldo Cruz, 1998. **93**(2): p. 237-241.

172. Zubay, G., *In vitro synthesis of Protein in Microbial Systems.* Annu. Rev. Genet., 1973. **7**: p. 267-287.

173. Kim, D.M., Kigawa, T., Choi, C.Y., and Yokoyama, S., *A Highly Efficient Cell-free Protein Synthesis System from E. coli.* Eur. J. Biochem., 1996. **239**: p. 881-886.

174. Lesley, S.A., Brow, M.A., and Burgess, R.R., *Use of in vitro Protein Synthesis from Polymerase Chain Reaction-generated Templates to Study Interaction of Escherichia coli Transcription Factors with Core RNA Polymerase and for*

*Epitope Mapping of Monoclonal Antibodies.* J. Biol. Chem., 1991. **266**: p. 2632-2638.

175. Studier, F.W., Rosenberg, A.H., Dunn, J.J., and Dubendorff, J.W., *Use of T7 RNA Polymerase to Direct Expression of Cloned Genes.* Meth. Enzymol., 1990. **185**: p. 60-89.

176. Invitrogen. *TOPO® TA Cloning® Kit*. 2014; Available from: http://tools.thermofisher.com/content/sfs/manuals/topota_man.pdf.

177. Qiu, X., Wu, L., Huang, H., McDonel, P.E., Palumbo, A.V., Tiedje, J.M., and Zhou, J., *Evaluation of PCR-generated chimeras, mutations, and heteroduplexes with 16S rRNA gene-based cloning.* Appl Environ Microbiol, 2001. **67**(2): p. 880-7.

178. Stein, C.A. and Krieg, A.M., *Problems in interpretation of data derived from in vitro and in vivo use of antisense oligodeoxynucleotides.* Antisense Research and Development, 1994. **4**: p. 67 - 69.

179. Goh, S., Stach, J., and Good, L., *Antisense effects of PNAs in bacteria.* Methods Mol Biol, 2014. **1050**: p. 223-36.

180. Kuhner, D., Stahl, M., Demircioglu, D.D., and Bertsche, U., *From cells to muropeptide structures in 24 h: peptidoglycan mapping by UPLC-MS.* Sci Rep, 2014. **4**: p. 7494.

181. Jacobs, C., Huang, L.-j., Bartowsky, E., Normark, S., and Park, J.T., *Bacterial cell wall recycling provides cytosolic muropeptides as effectors for β-lactamase induction.* The EMBO Journal, 1994. **13**(19): p. 4684-4694.

182. Lindberg, F., Westman, L., and Normark, S., *Regulatory components in Citrobacter freundii ampC beta-lactamase induction.* Proceedings of the

National Academy of Sciences of the United States of America, 1985. **82**(14): p. 4620-4624.

183. Lindquist, S., Galleni, M., Lindberg, F., and Normark, S., *Signalling proteins in enterobacterial AmpC β-lactamase regulation.* Molecular Microbiology, 1989. **3**(8): p. 1091-1102.

184. Li, L., Wang, Q., Zhang, H., Yang, M., Khan, M.I., and Zhou, X., *Sensor histidine kinase is a β-lactam receptor and induces resistance to β-lactam antibiotics.* Proceedings of the National Academy of Sciences, 2016. **113**(6): p. 1648-1653.

185. Setyawati, M.I., Kutty, R.V., Tay, C.Y., Yuan, X., Xie, J., and Leong, D.T., *Novel theranostic DNA nanoscaffolds for the simultaneous detection and killing of Escherichia coli and Staphylococcus aureus.* ACS Appl Mater Interfaces, 2014. **6**(24): p. 21822-31.

186. Good, L. and Stach, J.E., *Synthetic RNA silencing in bacteria - antimicrobial discovery and resistance breaking.* Front Microbiol, 2011. **2**: p. 185.

187. Perez-Capilla, T., Baquero, M.R., Gomez-Gomez, J.M., Ionel, A., Martin, S., and Blazquez, J., *SOS-independent induction of dinB transcription by β-lactam-mediated inhibition of cell wall synthesis in Escherichia coli.* J Bacteriol, 2005. **187**(4): p. 1515-8.

188. Miller, C., Thomsen, L.E., Gaggero, C., Mosseri, R., Ingmer, H., and Cohen, S.N., *SOS Response Induction by β-Lactams and Bacterial Defense Against Antibiotic Lethality.* Science, 2004. **305**: p. 1629-1631.

## Appendix A

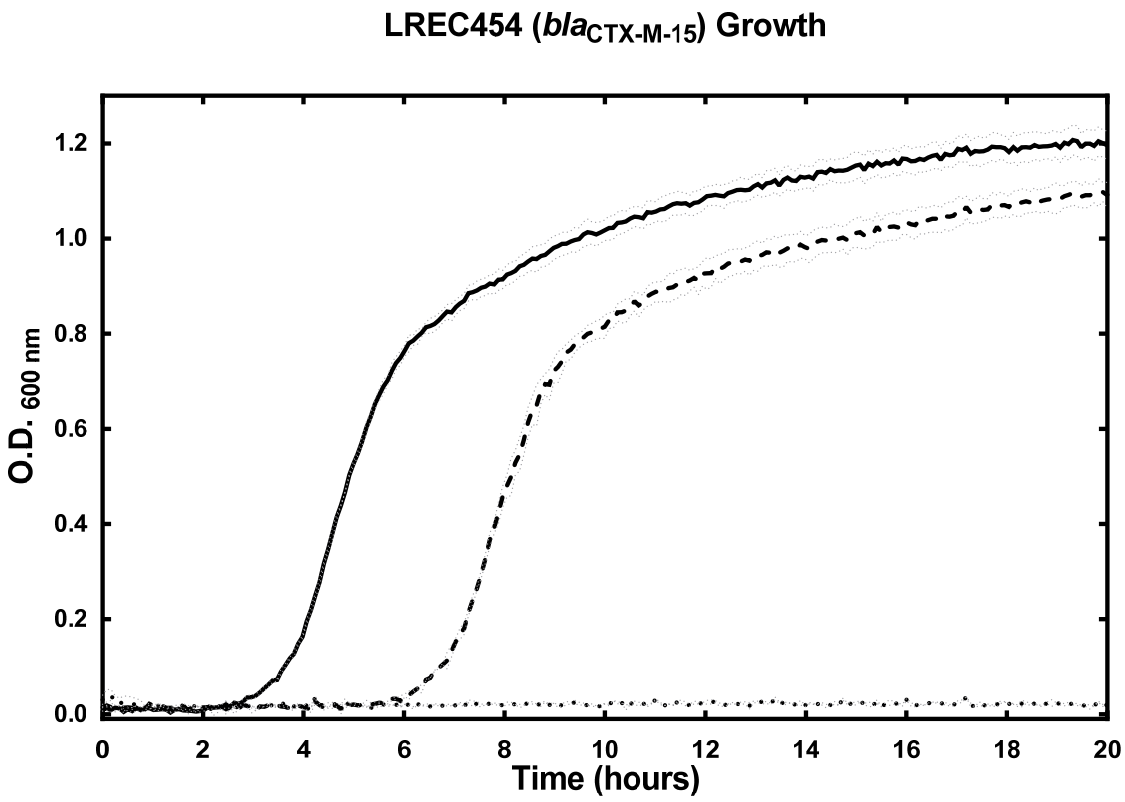


Figure A-1. Growth curves showing effects of P-PMO1 (30 μM) and CTX (24 μg/ml) on field isolate LREC454 harbouring *bla*$_{\text{CTX-M-15}}$.

LREC454 incubated with CTX (24 μg/ml) and P-PMO1 (30 μM). Solid line: control, dashed line: CTX (24 μg/ml), dotted line: CTX (24 μg/ml) + P-PMO1 (30 μM). Error bars indicate ± 1 standard deviation (n=2).

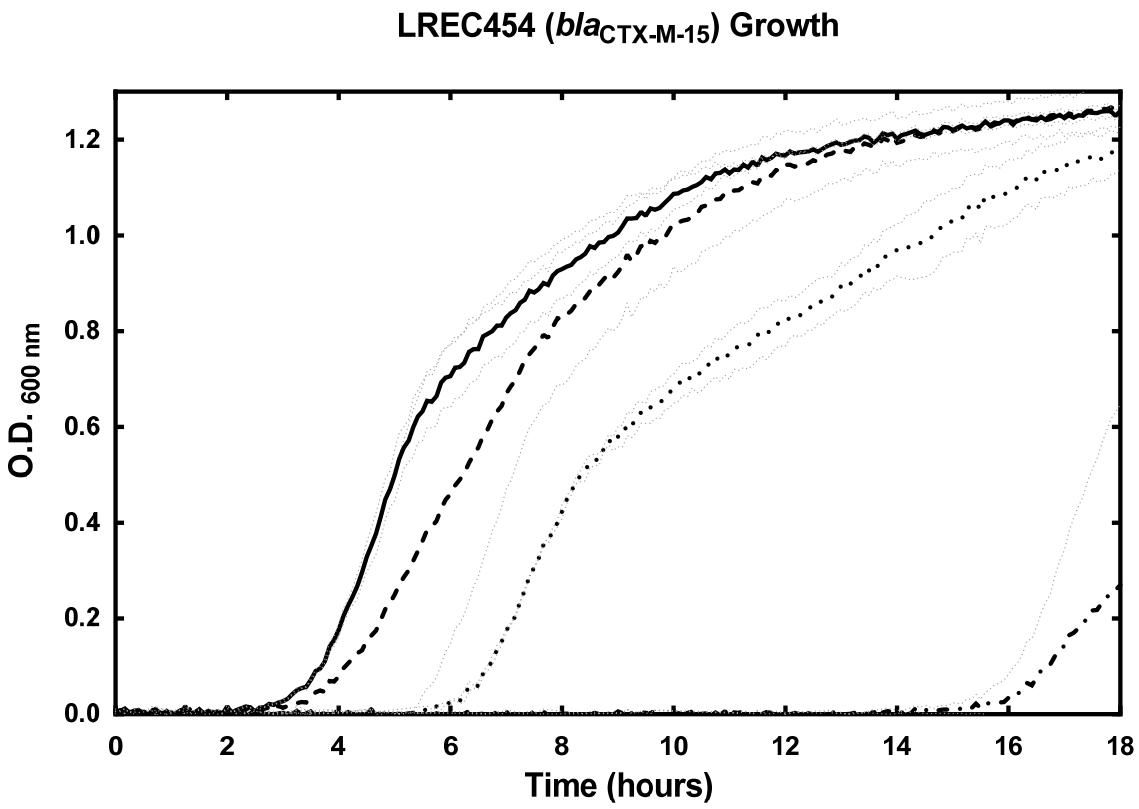


Figure A-2. Growth curves showing effects of P-PNA4 (3.2 μM) and CTX (2 μg/ml) on field isolate LREC454 harbouring *bla*$_{\text{CTX-M-15}}$.

LREC454 incubated with CTX (2 μg/ml) and P-PNA4 (3.2 μM). Solid line: control, dashed line: CTX (2 μg/ml), dotted line: P-PNA4 (3.2 μM), dash-dot line: CTX (2 μg/ml) + P-PNA4 (3.2 μM). Error bars indicate ± 1 standard deviation (n=2).

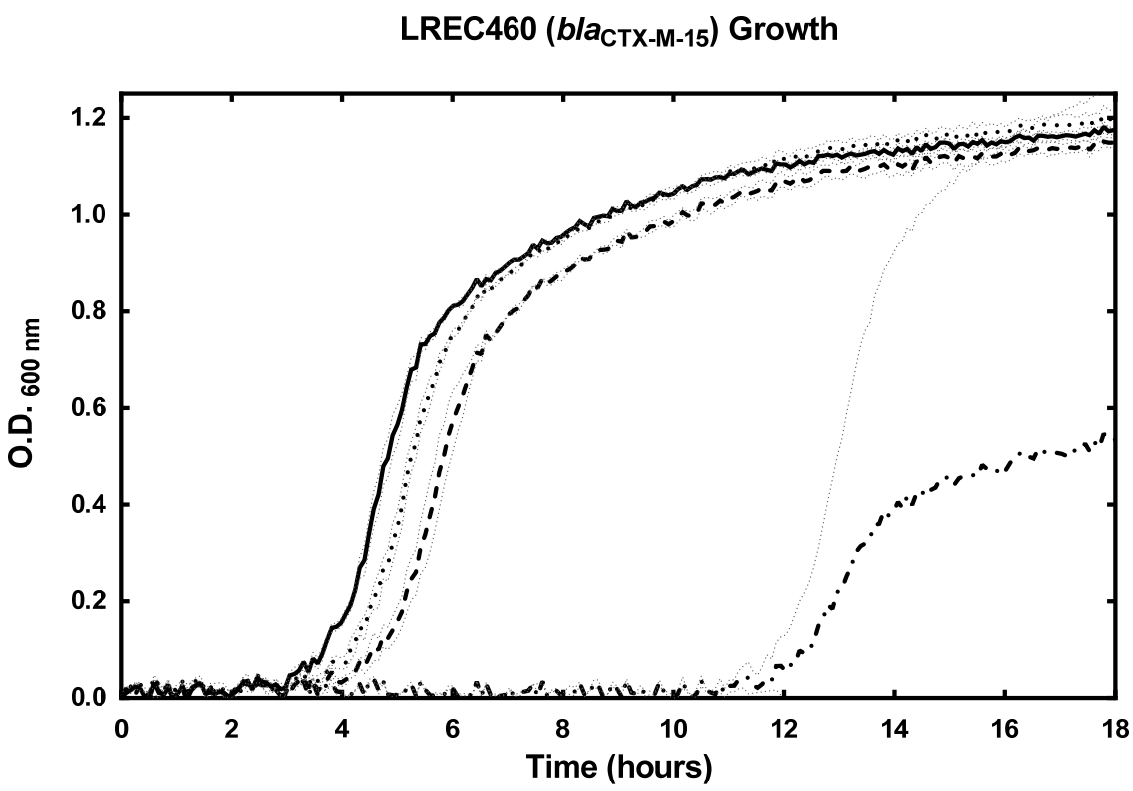


Figure A-3. Growth curves showing effects of P-PNA4 (3.2 µM) and CTX (24 µg/ml) on field isolate LREC460 harbouring *bla*$_{\text{CTX-M-15}}$.

LREC460 incubated with CTX (24 µg/ml) and P-PNA4 (3.2 µM). Solid line: control, dashed line: CTX (24 µg/ml), dotted line: P-PNA4 (3.2 µM), dash-dot line: CTX (24 µg/ml) + P-PNA4 (3.2 µM). Error bars indicate ± 1 standard deviation (n=3).

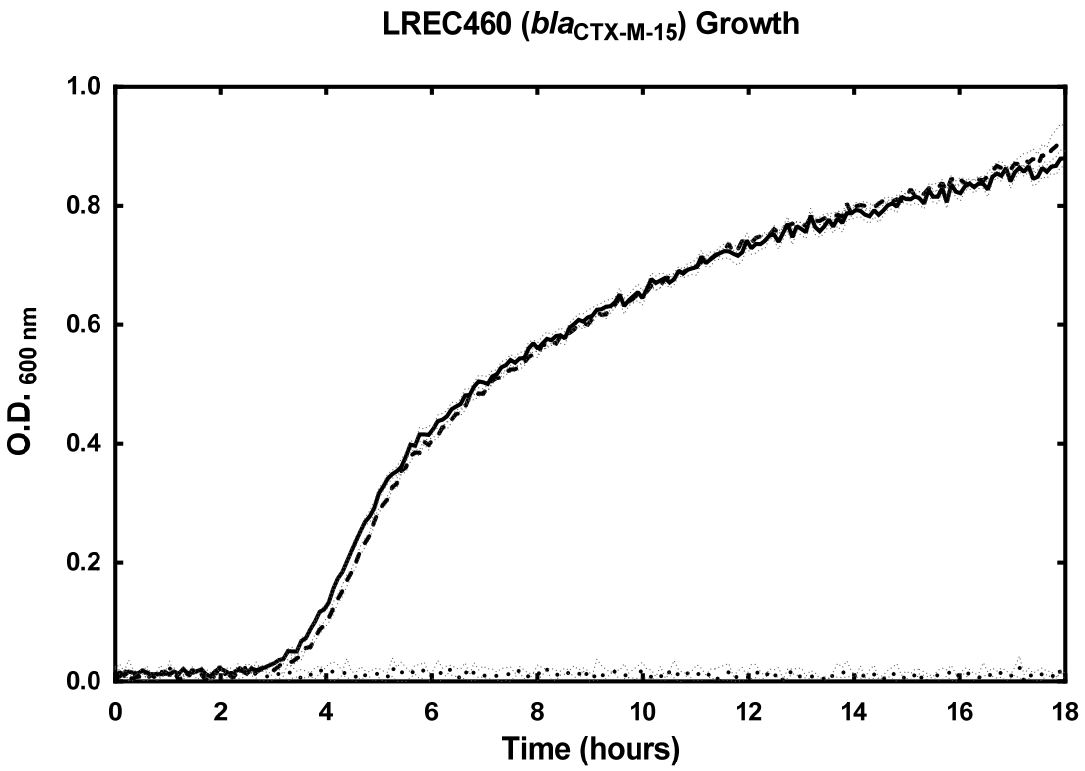


Figure A-4. Growth curves showing effect of P-PMO1 (40 µM) and CTX (32 µg/ml) on field isolate LREC460 harbouring *bla*$_{\text{CTX-M-15}}$.

LREC460 incubated with CTX (32 µg/ml) and P-PMO1 (40 µM). Solid line: control, dashed line: CTX (32 µg/ml), dotted line: CTX (32 µg/ml) + P-PMO1 (40 µM). Error bars indicate ± 1 standard deviation (n=3).

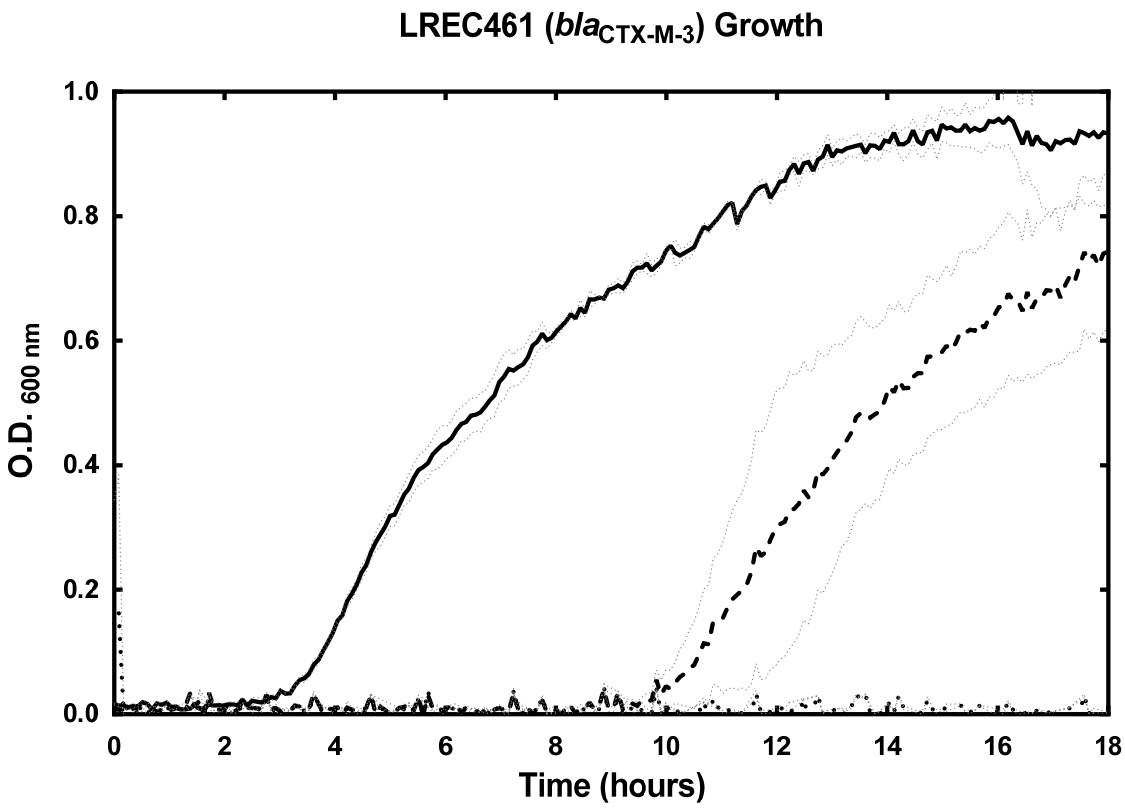


Figure A-5. Growth curves showing effects of P-PMO1 (30 µM) and CTX (16 µg/ml) on field isolate LREC461 harbouring *bla*$_{\text{CTX-M-3}}$.

LREC461 incubated with CTX (16 µg/ml) and P-PMO1 (30 µM). Solid line: control, dashed line: CTX (16 µg/ml), dotted line: CTX (16 µg/ml) + P-PMO1 (30 µM). Error bars indicate ± 1 standard deviation (n=3).

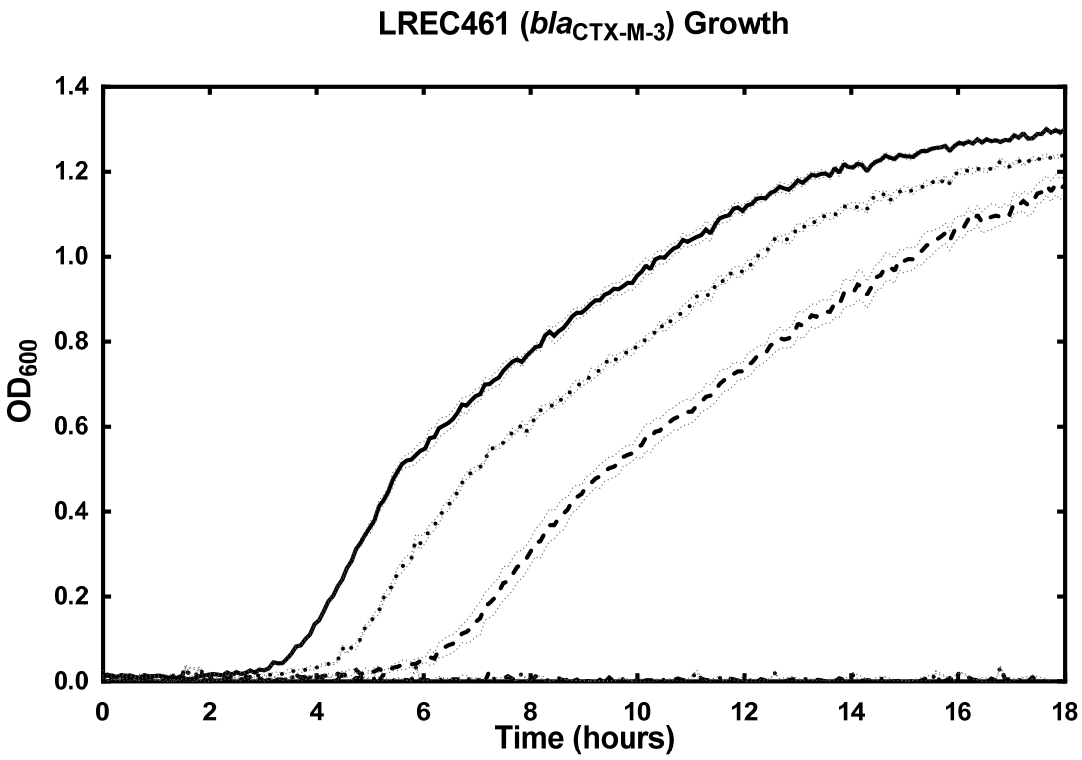


Figure A-6. Growth curves showing effects of P-PNA4 (5 µM) and CTX (8 µg/ml) on field isolate LREC461 harbouring *bla*CTX-M-3.

LREC461 incubated with CTX (8 µg/ml) and P-PNA4 (5 µM). Solid line: control, dotted line: CTX (8 µg/ml), dashed line: P-PNA4 (5 µM), dash-dot line: CTX (8 µg/ml) + P-PNA4 (5 µM). Error bars indicate ± 1 standard deviation (n=2).

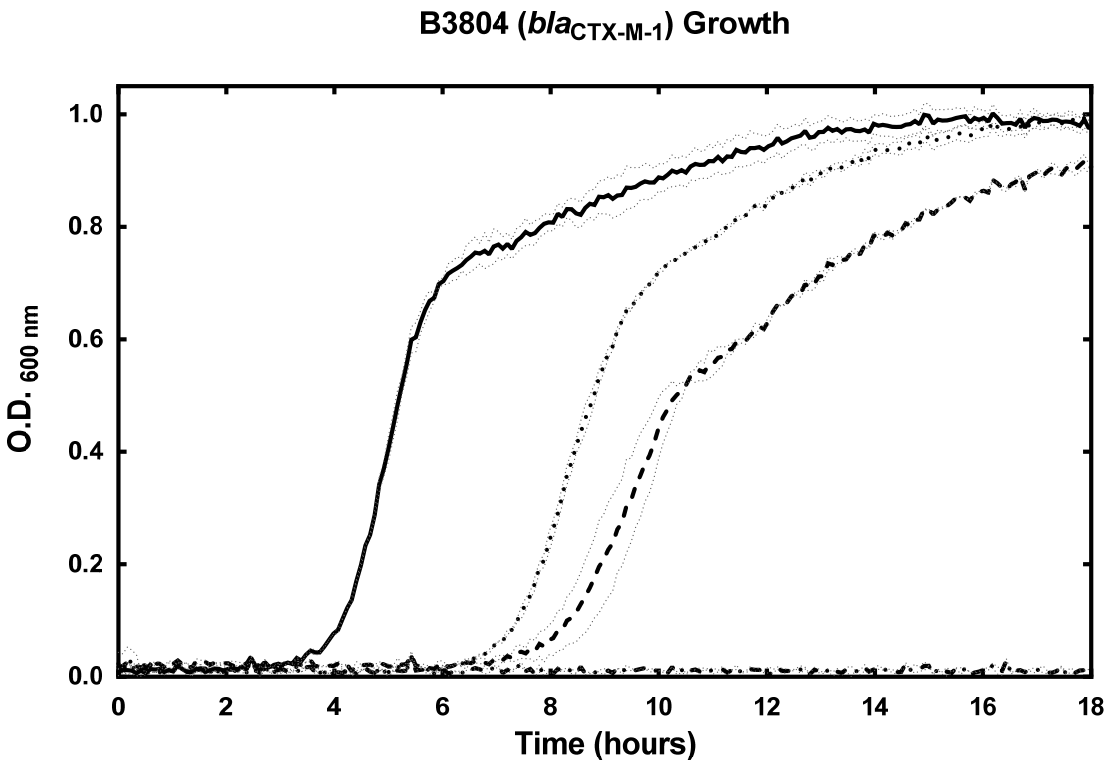


Figure A-7. Growth curves showing effects of P-PMO1 (30 μM) and CTX (10 μg/ml) on field isolate B3804 harbouring *bla*$_{\text{CTX-M-1}}$.

B3804 incubated with CTX (10 μg/ml) and/or P-PMO1 (30 μM). Solid line: control, dashed line: CTX (10 μg/ml), dotted line: P-PMO1 (30 μM), dash-dot line: CTX (10 μg/ml) + P-PMO1 (30 μM). Error bars indicate ± 1 standard deviation (n=2).

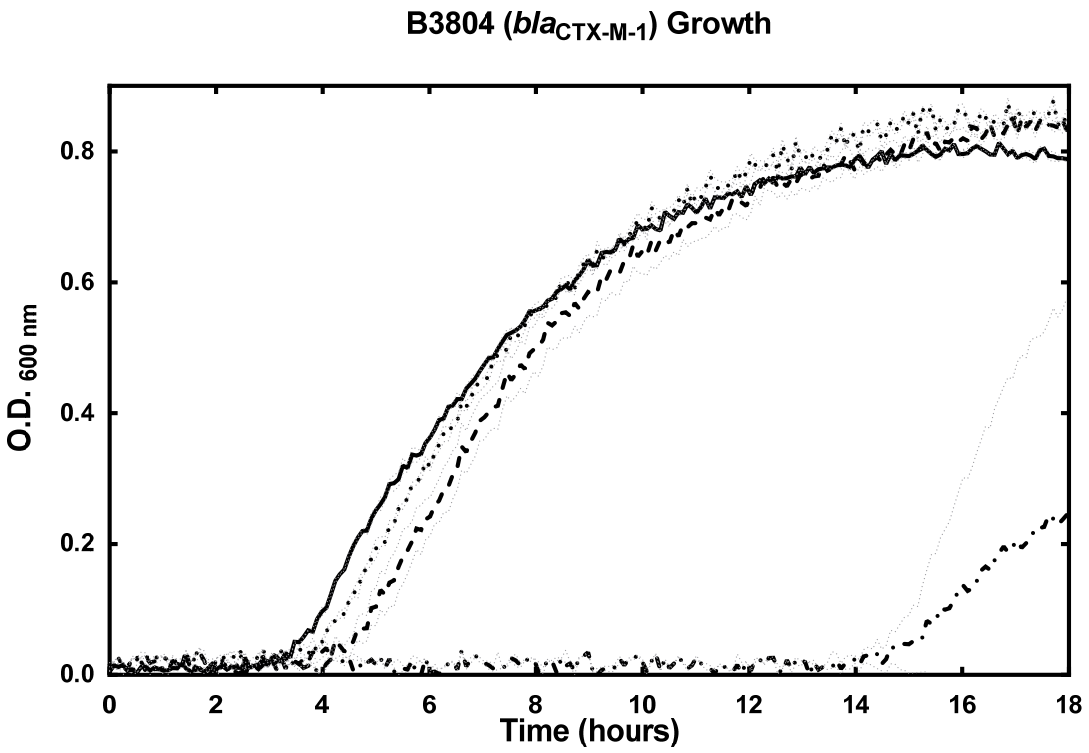


Figure A-8. Growth curves showing effects of P-PNA4 (3.2 µM) and CTX (2 µg/ml) on field isolate B3804 harbouring *bla*$_{\text{CTX-M-1}}$.

B3804 incubated with CTX (2 µg/ml) and/or P-PNA4 (3.2 µM). Solid line: control, dashed line: CTX (2 µg/ml), dotted line: P-PNA4 (3.2 µM), dash-dot line: CTX (2 µg/ml) + P-PNA4 (3.2 µM). Error bars indicate ± 1 standard deviation (n=2).

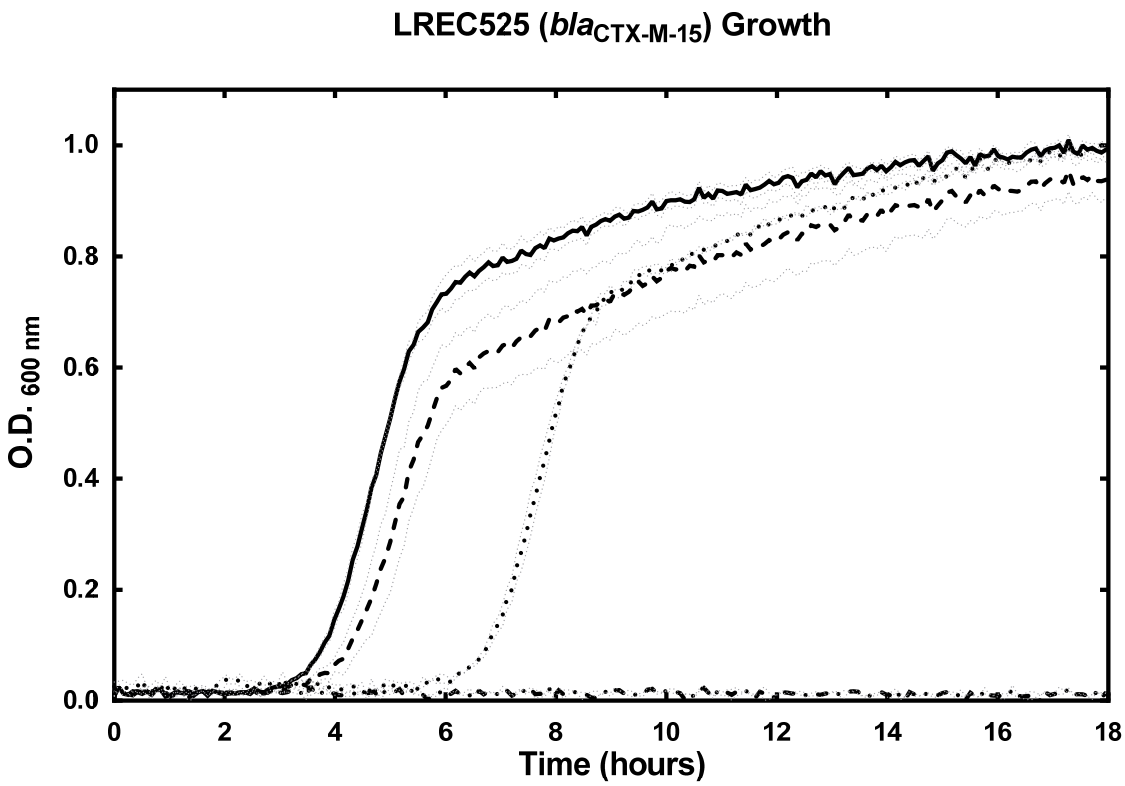


Figure A-9. Growth curves showing effects of P-PNA4 (3.2 µM) and CTX (48 µg/ml) on field isolate LREC525 harbouring *bla*$_{\text{CTX-M-15}}$.
LREC525 incubated with CTX (48 µg/ml) and P-PNA4 (3.2 µM). Solid line: control, dotted line: CTX (48 µg/ml), dashed line: P-PNA4 (3.2 µM), dash-dot line: CTX (48 µg/ml) + P-PNA4 (3.2 µM). Error bars indicate ± 1 standard deviation (n=2).

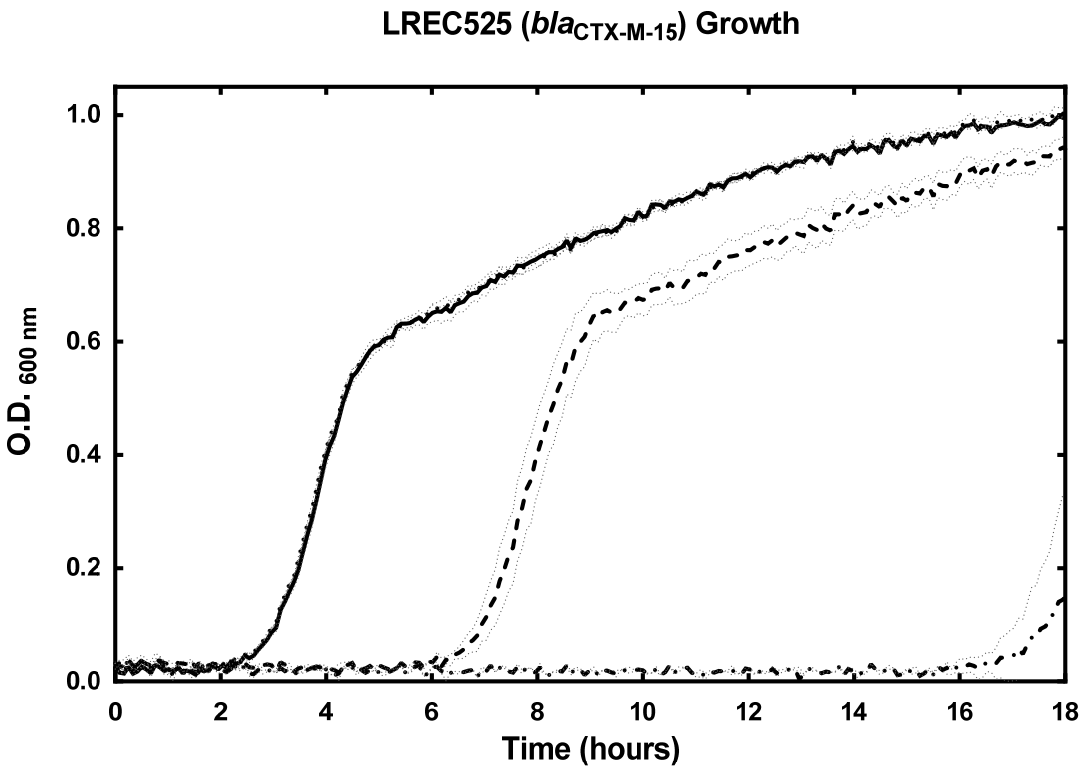


Figure A-10. Growth curves showing effects of P-PMO1 (30 µM) and CTX (96 µg/ml) on field isolate LREC525 harbouring *bla*$_{\text{CTX-M-15}}$.

LREC525 incubated with CTX (96 µg/ml) and/or P-PMO1 (30 µM). Solid line: control, dashed line: CTX (96 µg/ml), dotted line: P-PMO1 (30 µM), dash-dot line: CTX (96 µg/ml) + P-PMO1 (30 µM). Error bars indicate ± 1 standard deviation (n=2).

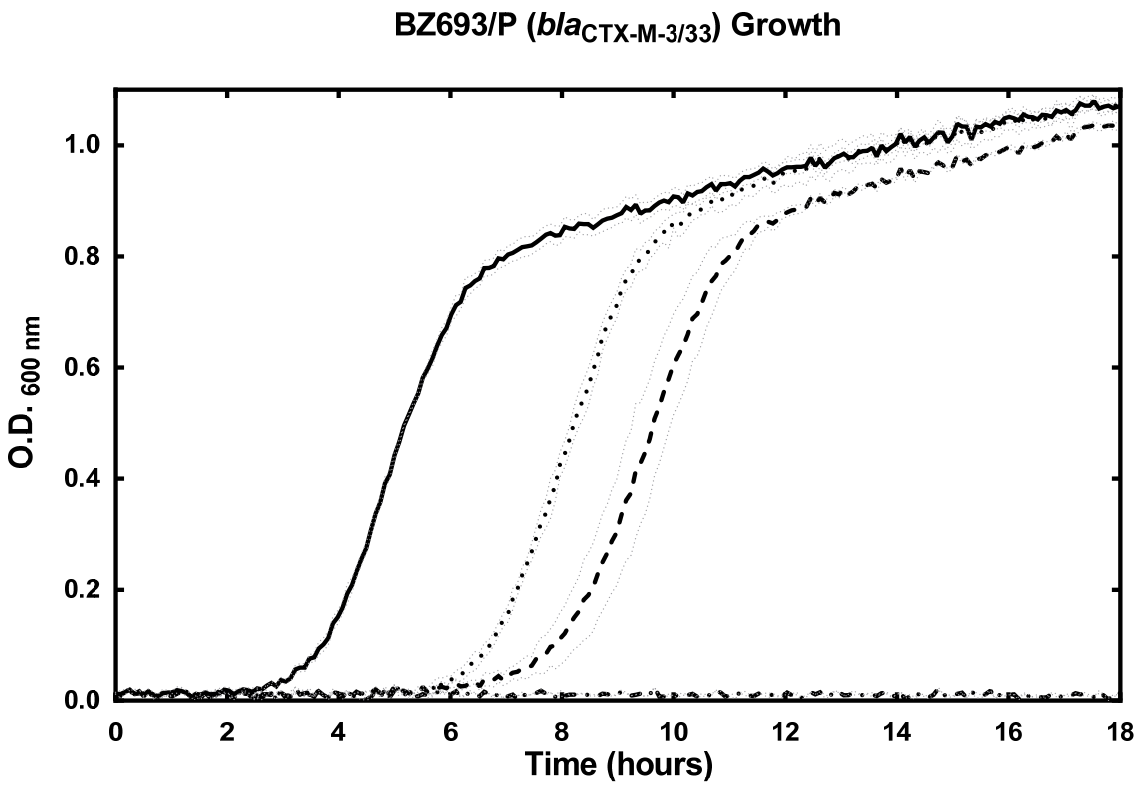


Figure A-11. Growth curves showing effects of P-PNA4 (3.2 µM) and CTX (12 µg/ml) on field isolate BZ693/P harbouring *bla*$_{\text{CTX-M-3/33}}$.

BZ693/P incubated with CTX (12 µg/ml) and P-PNA4 (3.2 µM). Solid line: control, dotted line: CTX (12 µg/ml), dashed line: P-PNA4 (3.2 µM), dash-dot line: CTX (12 µg/ml) + P-PNA4 (3.2 µM). Error bars indicate ± 1 standard deviation (n=2).

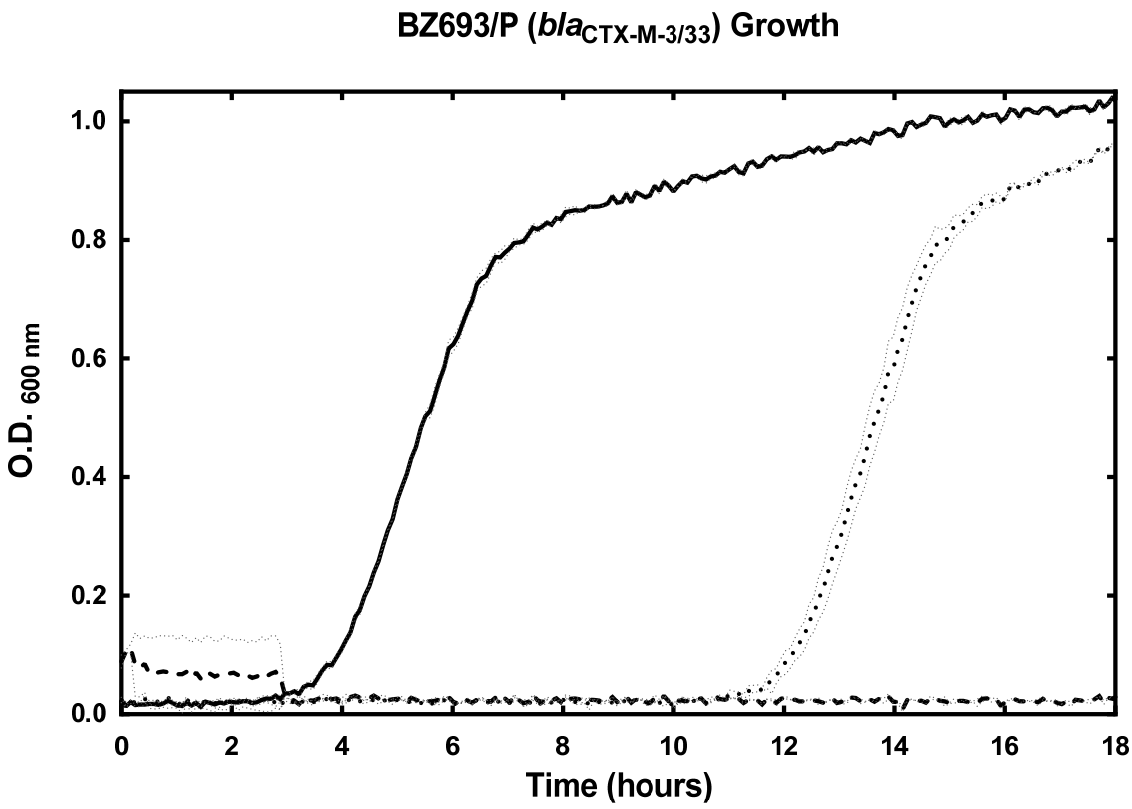


Figure A-12. Growth curves showing effects of P-PMO1 (30 µM) and CTX (15 µg/ml) on field isolate BZ693/P harbouring *bla*$_{\text{CTX-M-3/33}}$.

BZ693/P incubated with CTX (15 µg/ml) and P-PMO1 (30 µM). Solid line: control, dotted line: CTX (15 µg/ml), dashed line: CTX (15 µg/ml) + P-PMO1 (30 µM). Error bars indicate ± 1 standard deviation (n=2).